INDUSTRIAL AND BIOLOGICAL WASTES COMPACTED CEMENT STRUCTURES FOR GREEN CONSTRUCTION

CHALERMPON WUNGSUMPOW

A DISSERTATION SUBMITTED IN PARTIAL FULFILLMENT OF THE REQUIREMENTS
FOR THE DEGREE OF DOCTOR OF PHILOSOPHY IN
CONSTRUCTION ENGINEERING TECHNOLOGY
DEPARTMENT OF CIVIL AND ENVIRONMENTAL ENGINEERING TECHNOLOGY
GRADUATE COLLEGE
KING MONGKUT'S UNIVERSITY OF TECHNOLOGY NORTH BANGKOK
ACADEMIC YEAR 2024

INDUSTRIAL AND BIOLOGICAL WASTES COMPACTED CEMENT STRUCTURES FOR GREEN CONSTRUCTION

CHALERMPON WUNGSUMPOW

A DISSERTATION SUBMITTED IN PARTIAL FULFILLMENT OF THE REQUIREMENTS
FOR THE DEGREE OF DOCTOR OF PHILOSOPHY IN CONSTRUCTION ENGINEERING TECHNOLOGY
DEPARTMENT OF CIVIL AND ENVIRONMENTAL ENGINEERING TECHNOLOGY
GRADUATE COLLEGE
KING MONGKUT'S UNIVERSITY OF TECHNOLOGY NORTH BANGKOK
ACADEMIC YEAR 2024

Dissertation Proposal Certificate

The Graduate College, King Mongkut's University of Technology North Bangkok

Title Industrial and Biological Wastes Compacted Cement Structures for Green Construction

By Chalermpon Wungsumpow

Accepted by the COLLEGE OF INDUSTRIAL TECHNOLOGY, King Mongkut's University of Technology North Bangkok in Partial Fulfillment of the Requirements for the Doctor of Philosophy in Civil and Environmental Engineering Technology

Dean / Head of Department

Dissertation Examination Committee

..... Chairperson

(Assistant Professor Dr. Rattapoohm Parichatprecha)

..... Advisor

(Associate Professor Dr. ir. Keeratikan Piriyakul)

..... Co-Advisor

(Professor Dr.-Ing. habil. Suchart Siengchin)

..... Committee

(Associate Professor Dr. Kittipoom Rodsin)

..... Committee

(Assistant Professor Dr. Rathavoot Ruthankoon)

Name : Chalermpon Wungsumpow
Dissertation Title : Industrial and Biological Wastes Compacted Cement Structures for Green Construction
Major Field : Construction Engineering Technology
King Mongkut's University of Technology North Bangkok
Dissertation Advisor : Associate Professor Dr. ir. Keeratikan Piriyakul
Co-Advisor : Professor Dr.-Ing. habil. Suchart Siengchin
Academic Year : 2024

ABSTRACT

This research aims to enhance the flexural strength and unconfined compressive strength of cement compacted sand using fly ash from municipal solid waste (MSW) with polypropylene fiber and glass fiber. This MSW combustor fly ash by-product and is produced during the combustion of municipal solid waste in solid waste combustor facilities. Incineration has overtaken landfill mining as the most important option for disposal of the increasing volumes of MSW generated in Thailand. The research purposes this new green material and studies its properties which are first peak strength, peak strength, peak strength ratio, toughness, ductility index, equivalent flexural strength and crack behavior. The samples were prepared by adding 5% of cement by weight, varying the fly ash replacement to cement ratio of 0:100, 25:75, 50:50, 75:25 and 100:0 by weight, with varied polypropylene fiber and glass fiber of 0,0.5,1,1.5 and 2% by volume. Then all samples were cured for 28 days to reach their maximum capacity. From the results, the research recommends the fly ash replacement to cement ratio of 25:75 with the polypropylene fiber of 1.5% and glass fiber of 1.0 % by volume showing the maximum flexural strength. The synthetic fiber under investigation has a non-compact interfacial zone that SEM results in only a partial-contact interfacial surface, making them hydrophobic materials. These need to form a strong enough bond with a higher fiber content to produce a hardening-deflection response. The sample has been proven to be sustainable construction material. These support Thailand’s future cement demand while lowering the cement industry’s greenhouse gas emissions.

Keywords: Flexural Strength, Unconfined Compressive Strength, Municipal Solid Waste, Fly Ash, Polypropylene Fiber, Glass Fiber and Cement Compacted Sand

_____ Advisor

ACKNOWLEDGEMENTS

I extend my deepest gratitude to my supervisor, Assoc. Prof. Dr. ir. Keeratikan Piriyakul, for his unwavering support and insightful critiques throughout my research journey. His deep commitment to academic excellence and meticulous attention to detail have significantly shaped this dissertation. I am equally thankful to the members of my Co-advisor, Dr. Prof. Dr.-Ing. habil. Suchart Siengchin, for their constructive feedback and essential suggestions that enhanced the quality of my work, and I would also like to thank the funded by the College of Industrial Technology, King Mongkut's University of Technology North Bangkok, Contract CIT-2022-Grad-23. This thesis is a reflection of the unwavering support and boundless love I received from my family and friends during this challenging academic pursuit. I owe an immense debt of gratitude to my parents, who nurtured my curiosity and supported my educational endeavors from the very beginning. My appreciation also goes to the faculty and staff in the Department of Civil and Environmental Engineering Technology at College of Industrial Technology and KMUTNB Techno Park, King Mongkut's University of Technology North Bangkok, whose resources and assistance have been invaluable. I would also like to acknowledge my peers for their camaraderie and the stimulating discussions that inspired me throughout my academic journey. Their collective wisdom and encouragement have been a cornerstone of my research experience. Finally, this dissertation reflects not only my work but also the collective support of everyone who has touched my life academically and personally. The journey has taught me the value of questioning and the importance of diverse perspectives in enriching our understanding of complex philosophical issues.

Chalermpon Wungsumpow

TABLE OF CONTENTS

Page

TABLE OF CONTENTS (CONTINUED)

Page

LIST OF TABLES

Page

LIST OF FIGURES

Page

LIST OF FIGURES (CONTINUED)

Page

LIST OF FIGURES (CONTINUED)

Page

LIST OF FIGURES (CONTINUED)

Page

LIST OF ABBREVIATIONS

MSW	Municipal Solid Waste
MSWI	Municipal Solid Waste Incinerators
MSWM	Municipal Solid Waste Management
MSWIFA	Fly Ash from Municipal Solid Waste
FA	Fly Ash
BA	Bottom Ash
OPC	Ordinary Portland Cement
RDF	Refuse Derived Fuel
c-RDF	Coarse Refuse Derived
d-RDF	Dense Refuse Derived
PE	Polyethylene
GGBFS	Ground Granulated Blast Furnace Slag
CCFS	Cement Compacted Sand using Fly ash from Municipal Solid Waste
CCFS-PP	Cement Compacted Sand using Fly ash from Municipal Solid Waste and Polypropylene Fiber
CCFS-GF	Cement Compacted Sand using Fly ash from municipal solid Waste and Glass Fiber
SEM	Scanning Electron Microscopy
XRF	X-ray Fluorescence Spectrometer
GHG	Greenhouse Gas
WtE	Waste to Energy
RDF	Refuse Derived Fuel
LFG	Landfill Gas
LHV	Lower Heating Value
LL	Liquid Limit
MC	Moisture Content
AEDP	Alternate Energy Development Plan
ASTM	American Society for Testing and Materials
ACI	American Concrete Institute Standards
U.S.EPA	United States Environmental Protection Agency
USCS	Unified Soil Classification System
UCS	Unconfined Compressive Strength
PEA	Provincial Electricity Authority
FiT	Feed-in Tariff
G_0	Initial Shear Modulus
Gs	Specific Gravity
Cu	Coefficient of Uniformity
Cc	Coefficient of Curvature
Vs	Shear Wave Velocity
LCA	Life Cycle Assessment
ITZ	Interfacial Transition Zone
RSM	Response Surface Methodology
LCA	Life Cycle Assessment

Chapter 1 Introduction

1.1. Background and Rationale

According to Thailand's Pollution Control Department's recommendations, municipal solid waste may be divided into four categories: general waste, hazardous waste, recyclable waste, and compostable waste (Pollution Control Department, 2016). Organic waste, often known as compostable waste, comprises food waste and garden waste (EPA, 1996). Organic waste makes up the greatest portion of MSW created in developing nations, including Thailand, where it accounts for around 49% of total MSW around 25 million tons (Pollution Control Department, 2021a) The ecosystem may be threatened by a variety of contaminants that are generated by biological interactions and leaching brought on by inappropriate handling of organic waste (Chapman et al., 2009). Ineffective waste management adds to dangerous greenhouse gas (GHG) emissions into the atmosphere and endangers human health, posing a major threat to the environment through smoke, particulate matter, and CO_2 (Kothari et al., 2010).

The cement industry is an industry that is important to the Thai economy because it is a basic industry that plays an important role in national development. It also has a tendency to expand in line with the economic conditions of Thailand and the ASEAN region. Thailand is considered a developing country and still has a high demand for cement products, which is consistent with the country's economic growth rate. In terms of energy, the cement industry is considered an industry that uses a relatively high amount of energy and tends to increase its energy consumption level in line with economic expansion (Thailand Greenhouse Gas Management Organization, 2016). Roughly, for every ton of cement produced, around 1 ton of CO_2 is released into the atmosphere. However, with today's more efficient manufacturing processes, the CO_2 emissions are around 800 kg per ton of cement produced. However, the environmental impact of the cement industry is still significant when considering the global cement production rate, which accounts for around 5% of the total global CO_2 emissions from human activities (Energy Cement Industry, 2005).

In order to account for the greenhouse gas emissions from waste management systems and waste technologies, the energy system is crucial. A good way to manage trash is to use energy from non-recyclable garbage, which is crucial for the creation of renewable energy (Ryu, 2010). One of the intriguing options for addressing the issues of municipal solid waste management and global warming is refuse-derived fuel (RDF). Its advantages include lowering local economic losses as well as enhancing the quality of the global environment (Nithikul, 2007). The methods for using waste fuels have been examined by several research teams; nevertheless, the majority of these studies concentrated on thermal deterioration or direct burning (Belgiorno et al., 2003; Di Gregorio & Zaccariello, 2012; Lee et al., 2010; Miskolczi et al., 2011). Waste from agriculture and municipalities are currently important sources for RDF manufacturing. RDF might be made by combining certain agricultural waste with dried, flammable parts of city garbage. Moreover, RDF can burn directly or in combination with other fuels. During the manufacturing and use stages, direct burning of RDF may contribute to global warming even if it may provide heat in a very efficient manner. Therefore, while estimating the greenhouse gas emissions from the manufacturing of RDF, the Life Cycle Assessment (LCA) should be taken into account (Nutongkaew et al., 2014).

Waste to energy (WtE) or energy from waste is an energy recovery process that converts waste chemicals into energy in the form of electricity and heat. It is one of the most appealing solutions for sustainable MSW management in Thailand, with the potential to reduce 75 - 90% of the original waste volume depending on the waste composition (Klinghoffer & Castaldi, 2013) and 50 % of greenhouse gas emissions by 2050 (Kothari et al., 2010). The composition of MSW in Thailand is more combustible than incombustible waste allowing for alternative energy consumption in the forms of electricity and heat (Sutabutr, 2012). WtE technologies such as anaerobic digestion, landfill gas (LFG) to energy, incineration, gasification, pyrolysis, and biodrying can be used to convert MSW into energy sources. RDF, a fuel produced from combustible refuse with a high calorific value, and incineration have been identified as suitable WtE technologies for treating MSW in Thailand. One ton of MSW is assumed

to produce 0.43 tonnes of RDF, and one ton of RDF can generate more than 300 kWh of electricity. Incineration technology is more expensive to invest in than RDF production technology and it produces less power per ton of MSW than RDF technology. MSW incineration will not generate enough thermal energy due to its high moisture content and low calorific value (Intharathirat & Abdul Salam, 2016). Hence, recovering material and energy from MSW through RDF production is more effective for an MSW disposal and fuel recovery solution. It has proven to be an effective alternative fuel for lowering GHG emissions. RDF can replace some coal or oil in a variety of industrial sectors, including the cement industry (Garg et al., 2007; Pohl et al., 2008).

The issue with using MSW as a fuel is an inconsistency in the heating value of the fuel produced due to variations in waste's physical composition and high moisture content (MC) (Kothari et al., 2010). According to the literature, calorific value is highly related to the MC, and it is a significant parameter for assessing the MSW's potential to produce RDF. The low quality of MSW as fuel is due to its high moisture content (40 – 70%) (Velis et al., 2009). The study's finding revealed that waste had good quality fuel for utilization as RDF in the industry (Tambone et al., 2011). However, MSW has the potential to be a viable alternative energy source. The alternate energy development plan (AEDP) program established by the Thai government set a goal encouraging the use of 495 ktoes of MSW for thermal energy by 2037. The goal of 21.51% was not met in 2021 for the use of refuse-derived fuel (RDF) for thermal energy (Ministry of Energy, 2018). Thus, to handle the continually increasing MSW, the Thai government is now constructing new incinerators. In order to treat MSW, municipal solid waste incinerators (MSWI) are invariably used as an efficient solution. It is chosen because MSWI uses up less space at the operating site and has the benefit of effectively lowering MSW volume. Residues often include bottom ash, fly ash, and a variety of minerals and inorganic substances (Lo, 2005). However, MSW incineration is subject to a number of significant environmental regulations. Different solid wastes, including bottom ash, fly ash, and particles, are formed during an incineration process. For every 1,000 kg of municipal solid waste

burned in a standard moving grate incinerator, 250–300 kg of bottom ash and 25–50 kg of fly ash is generated (Banks & Lo, 2003).

The proliferation of innovative materials for numerous purposes has been motivated by increased environmental and economic awareness. Materials made of fibers (i.e., natural or synthetic fibers) offer the distinct benefits of having high strength, high stiffness, and non-corrosive characteristics (Sanjay, et al., 2018; Omrani, et al., 2016; Väisänen, et al., 2016; Vijayan, et al., 2021). This study examined the fly ash (Industrial waste) from the MSW (biological waste) Industrial power plant and polypropylene fiber and glass fiber (synthetic materials) in terms of physical and mechanical properties of compacted cement sand.

1.2. Hypothesis

1. A fly ash from MSW consisting of a fine fraction may be more qualified to apply with cement compacted sand due to its It addresses the issue of using waste in the environment from burning waste, which will reduce management costs in landfills.
2. The fly ash produced by the RDF power plant process may have optimum engineering properties compared to a standard of construction in highway or pipeline in terms of construction and materials engineering.
3. The polypropylene fiber and glass fiber of synthetic materials mix with fly ash from MSW may replace cement ratio for construction infrastructure such as highway or pipeline.

1.3. Objectives

1. Study on the physical and mechanical properties of the cement compacted sand using fly ash from municipal solid waste (MSW) and polypropylene fiber (CCFS-PP) for green construction material
2. Study on the physical and mechanical properties of the cement compacted sand using fly ash from municipal solid waste (MSW) and glass fiber (CCFS-GF) for green construction material

1.4. Scope of study

1. This study uses the sand from typical Bangkok construction sand according to Unconfined compressive strength (ASTM D1633), Flexural Strength (ASTM C1609/C1609M-10) Standard Test Method for Flexural Strength of Concrete (Using Third-point Loading)), Shear Wave Velocity and Initial Shear Modulus in Soil Specimens using Bender Elements (ASTM D8295-19) and Scanning Electron Microscope (SEM).
2. This study uses the Ordinary Portland Cement (OPC) from The Concrete Products and Aggregate Co., Ltd. (CPAC).
3. This study uses the industrial waste in terms of fly ash from municipal solid waste (MSW) of Global Power Synergy Public Company Limited (GPSC) with Rayong Company Limited's solid waste disposal center in Rayong province, Thailand.
4. This study uses the syntactic fibers which are the polypropylene fiber from BEKAERT brand, Synmix macro synthetic fibers for concrete and glass fiber from Owens Coming brand, Advantex CS 979-14 series there is E-glass type.

1.5. The benefits expected

1. Reduction of cement consumption due to cement mining and cement plants are Cement Manufacturing with coal mining and coal power plants There are CO_2 releases.
2. Material of landfill or dump sites is plastic waste that can be used in refuse derived fuel (RDF) power plants for energy and industrial waste from RDF power plants can mixing for green construction material.
3. Study Material in terms of synthetic fiber there are polypropylene fiber and glass fiber of synthetic materials mixed with fly ash from MSW may replace cement ratio, which can be useful in this study.
4. Fly ash of RDF power plants can be mixed for construction infrastructure such as highway or pipeline in terms of green construction material.

Chapter 2 Literature review

2.1. Applications of industrial waste in construction building materials

Municipal solid waste (MSW) is also referring to waste generated on a daily basis by any activity within the community. It also includes organic waste and recyclables (Pilant et al., 2020). Solid waste composition is one of the essential issues in waste management because it influences waste density and suggests appropriate disposal methods as well as assessing waste reduction, reuse, and recycling. MSW composition differs from country to country and region to region. The differences are determined by cultural, socioeconomic structure, income level, consumption, and Municipal Solid Waste Management (MSWM) (Ozcan et al., 2016). Generally, waste composition varies with season, climate, and community character (Kennish, 2002). MSW compositions are highly variable. However, organic materials are assumed to be the main component of MSW. In most countries, organic waste comprises 18.9 - 63.4% of MSW, followed by plastic waste (6 - 35.1%) and paper (5.6 - 28.62%). Organic waste (50 - 55.27%), plastic waste (16.23 - 22.5%), paper (11.3 - 14.04%), and other wastes (14.46 - 17.97%) were the main types of MSW composition in Bangkok, Thailand.

In Thailand, the largest source of solid waste is municipal solid waste (MSW). In 2000-2010, the Thai population increased from 62 to 64 million persons, which was related to an increase of municipal solid waste (MSW) from 38,000 to 41,000 tons/day in 2030 by forecasting grey modeling (Pudcha et al., 2023). A huge amount of solid wastes was left and collected in landfills. Therefore, land for waste disposal is needed. Landfill mining is a new approach applied to expand MSW landfill capacity and reduce the cost for additional land (Rosendal, 2009). In 2016, for waste disposal methods in Thailand, there were several ways to get rid of waste (Figure 1).

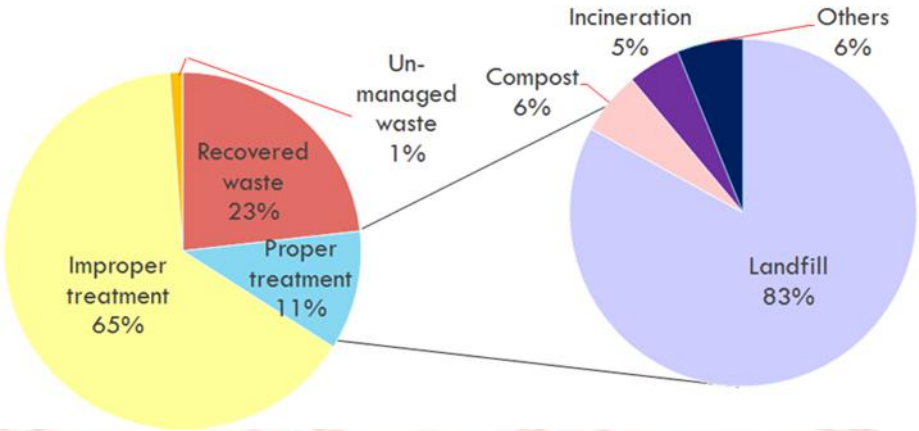

Figure 1 Waste flow in Thailand

(Pollution Control Department Ministry of Natural Resources and Environment Thailand, 2017)

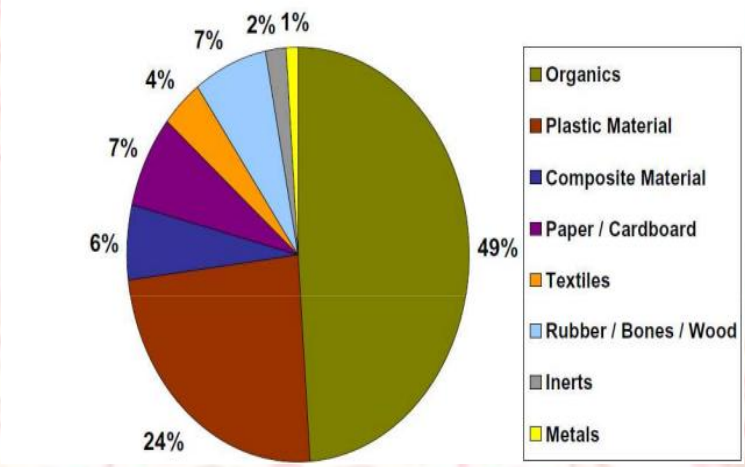

Figure 2 Waste composition of the input material

Rayong Province's Integrated Waste Management Center receives community waste from 21 local administrative organizations in Rayong Province, which produces approximately 1,200 tons of waste per day and high organic waste composition of the input material (Figure 2). The provincial administrative organization originally managed waste by landfilling, which decomposes organic matter in landfills under anaerobic conditions and produces methane gas, since 2012. Then, there is the project to produce fuel from community waste or the RDF project to be used as fuel for electricity generation in power plants and transmitted to the power transmission

system (Figure 3). The RDF project is a collaboration between Rayong Provincial Administrative Organization and Global Power Synergy Public Company Limited (GPSC). The RDF project will receive approximately 500 tons per day of waste from the waste trucks of Rayong Provincial Administrative Organization. It is expected that the RDF production will be approximately 340 days per year and the RDF fuel will be approximately 200 tons per day from the production process. The project implementation will reduce greenhouse gas emissions by 18,033 tCO_2e/y, which can be used to calculate carbon credits for the project over 7 years, totaling approximately 756,237 tCO2e/y (Thailand Greenhouse Gas Management Organization (Public Organization), 2019). Refuse-derived fuel (RDF) is a fuel made from MSW that has a high calorific value and is used to generate energy and heat in power plants (Figure 4).

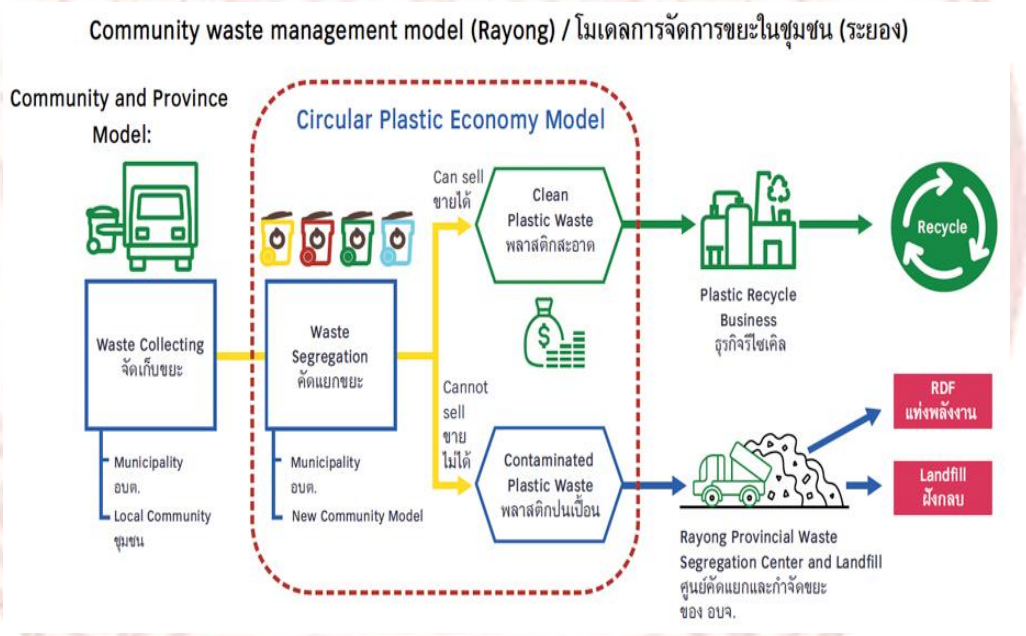

Figure 3 Project to produce RDF from community waste management model (Rayong)

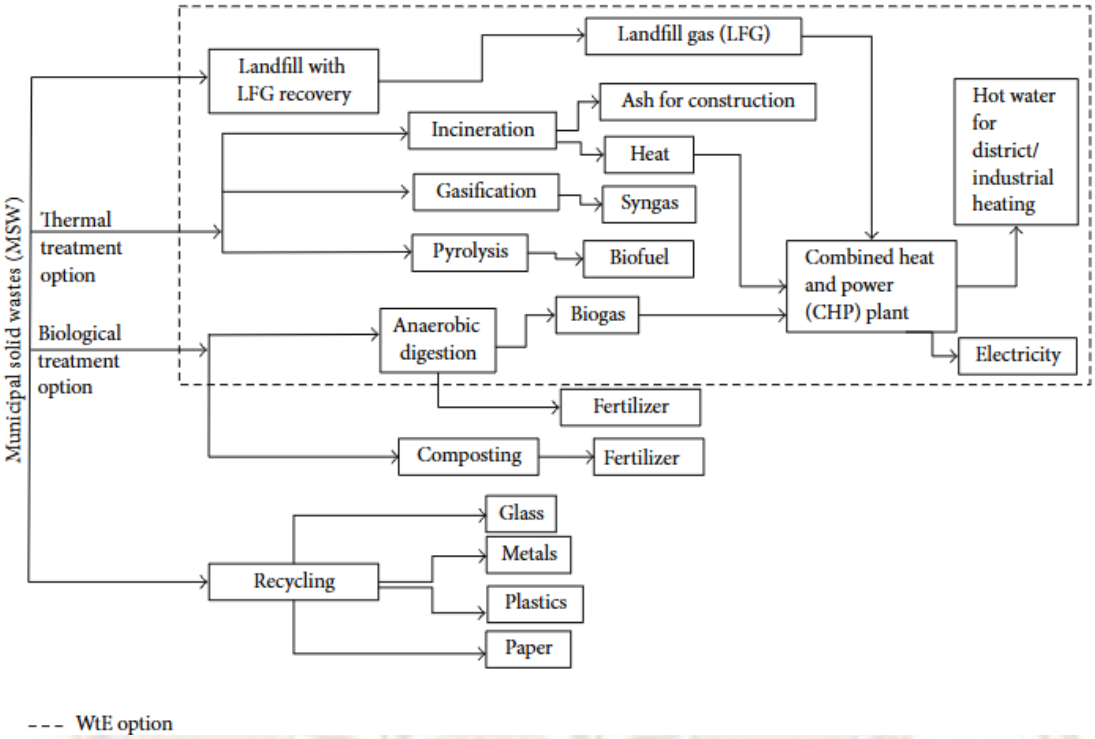

Figure 4 MSW processing for generate energy and heat in power plants (Islam, 2016)

RDF is produced from MSW and industrial waste (combustible materials); non-combustible materials found in MSW and industrial waste, such as glass and metals must be removed. RDF should have a high content of plastics, paper, textiles, wood, and other organic matter (Garg et al., 2007; Pohl et al., 2008). Higher heating value is associated with the content of paper, plastics, wood, and textiles. If these materials contain 40-80% w/w of biogenic compounds, they will become a viable alternative fuel for lowering greenhouse gas emissions. Moreover, it has significant advantages in terms of low production costs and calorific value (Hilber et al., 2007). RDF can be classified into seven categories, according to the American Society for Testing and Materials (ASTM) standards E856-83 (ASTM E856-83, 2006) including RDF-1: Solid waste used as fuel in its discarded form, RDF-2: Solid waste processed to coarse particle size with or without ferrous metal separation such that 95% by weight passes through a 6-inch square mesh screen, namely coarse RDF, RDF-3: Solid wastes processed to separate glass, metal, and inorganic materials, shredded such that 95% by

weight passes a 2-inch square mesh screen, namely Fluff RDF, RDF-4: Combustible solid wastes processed into powder form, 95% weight passes through a 10-mesh screen (0.035-inch square), namely Powder RDF, RDF-5: Combustible solid wastes densified (compressed) into pellets, slugs, cubettes, or briquettes, namely densified RDF, RDF-6: Combustible solid wastes processed into liquid fuels, namely RDF slurry and RDF-7: Combustible solid wastes processed into gaseous fuels, namely RDF syngas. Refuse-derived fuel (RDF) derived from processed municipal solid waste (MSW) with high calorific fractions is used in dedicated energy-to-waste plants and as fuel substitutes in industrial processes. Several processes can be used to produce RDF from domestic and business waste (Násner et al., 2017). Nevertheless, in general, the steps of the RDF production process are 6 processes as follows. 1. Manual separation removes recyclable waste and bulky materials, such as glass bottles, plastic bottles, paper, large pieces of wood, rocks, and so on, by hand before transferring to a mechanical separation. A sorting belt is commonly used in manual separation equipment. 2. Size reduction of the mixed wastes is an important unit operation in the mechanical process of the mixed wastes because the wastes are reduced to a specific uniform size. Depending on the nature of the waste, two types of devices are commonly used for this process: flail or hammer mills and shear shredders, depending on the character of the waste. Hammer mills are made up of rotating sets of swinging steel hammers that pass waste through them. Two horizontal cutting shafts rotate in opposite directions in the shear shredder machine. 3. The objective of screening is size separation. It separates the feedstock into two streams: oversize (left on the screen) and undersize (passes through the screen). Screening and size separation are typically done into two or more stages. There are many different types of screens, i.e., trommel and disc screens. Trommel screens are widely used because they have been shown to be effective and efficient for processing mixed MSW (Diaz et al., 2005). The waste is routed through trommel screens, which are typically rolling drums with varying mesh sizes. Trommels attached to the conveyors at various processing stages are inclined to allow oversized materials to pass through. Some facilities also include spikes inside the trommels that act as bag busters, allowing items trapped inside plastic bags to be freed. 4. Mechanical and electromagnet separators are used in

this step. Magnets can be turned on and off to remove collected metals from mixed MSW, but they remove all the metals. Stainless steel and copper, for example, are only weakly magnetic. Another limitation of this technique is that small magnetic items will not be detected in non-magnetic materials. Unwanted items such as paper, plastic, and food waste can be dragged by larger magnetic items. 5. For air classification, a fan creates an upward moving column of air. As a result, low-density materials are blown upwards, while dense materials are blown downwards. The air carrying light materials, like paper and plastic bags, passes through and falls out of the air stream. The air separation efficiency is determined by the strength of the air currents and how materials are introduced into the column. Moisture content is also critical as water can cause some materials to weigh down or stick together. And 6. Drying is used to improve the quality of RDF, and pelletizing is used to create the final RDF product through briquetting, pelletizing, or cube formation. The finished RDF product can be made into bricks or pellets, or it can be left as fluff. RDF bricks are made up of large pieces that escape the trommel screening stage and lighter materials such as plastic bags that are blown off during air separation. The shredded hammer mill materials and medium size trommels rejected are used for the RDF fluff. Finally, the residual waste is combined with binders such as agricultural husk and fed into pelletizing machine, which converts the waste into pellets. The coarse fraction is either rejected. The medium fraction consists of paper, card, wood, plastic, and textiles, which can be burnt directly as coarse fuel (c-RDF) or dried and pelletized into dense RDF (d-RDF). RDF is used in energy-intensive industries such as cement, power generation, and either co-combustion or mono-combustion in Thailand. the RDF quality standards below the needs of GPSC Power Plant (Figure 5). The essential parameters included in the standards are moisture, ash, Cl, S, content, and LHV. Differences in the quality of RDF used to produce energy and heat are due to each company's critical need (Figure 6).

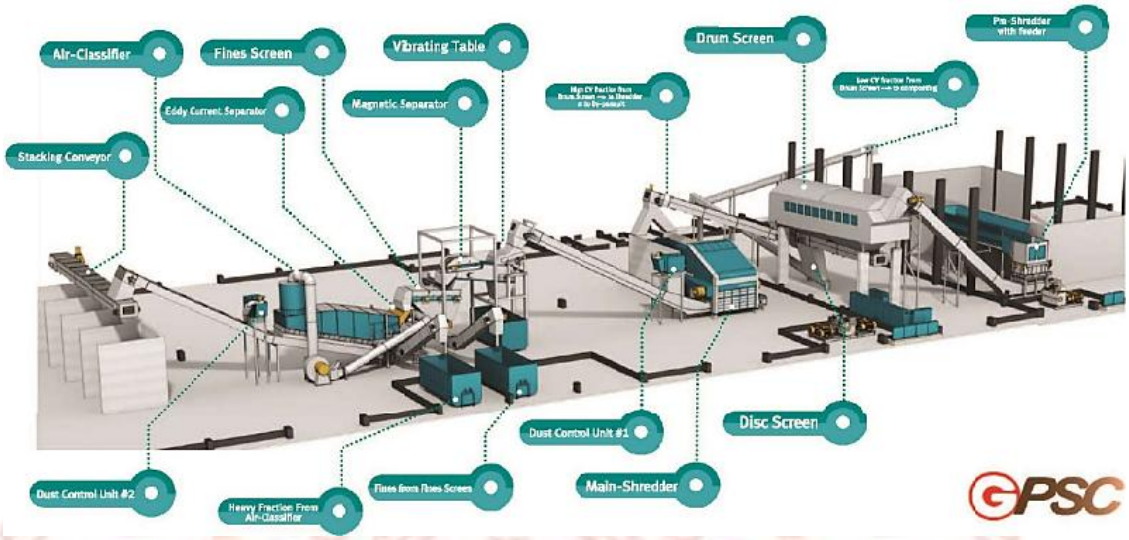

Figure 5 RDF Process from Rayong Province

(Thailand Greenhouse Gas Management Organization (Public Organization), 2019)

B

Waste to energy analysis parameters

MSW incineration	Landfill	Environmental and economic factor
Lower heating value (LHV)	CH_4 emissions	CO2 emission factor for electricity
Ultimate analysis	Methane GWP	Carbon sequestered in forest area
Compositional analysis	CO_2 emission factor	Carbon credit revenue
Heat recovery efficiency	CH_4 volume conversion factor	Electricity sales revenue
Electricity generation	Calorific value of CH_4	
Operating time	Electricity generation factor	

Figure 6 Waste to energy analysis parameters for the quality RDF

(Al-Ghouti et al., 2021)

Furthermore, the cost of traditional building materials continues to rise due to the energy required for manufacturing, scarcity of natural resources, and high transportation costs from manufacturers to construction sites. These environmental and economic concerns have sparked interest in research into alternative building materials (Danso et al., 2015). Earth material requires about 99% less energy during

production than industrial building materials like concrete. Long transportation routes are also superfluous because earth is a locally accessible, affordable, and recyclable building material (Zak et al., 2016). Because of its low cost and minimal impact on the natural environment, the use of earth as a construction or building material to produce rammed earth is gaining popularity (Sharma et al., 2015). However, in terms of durability, tensile strength, and compressive strength, earthen materials are not as strong as more modern building materials like steel and concrete (Ngowi, 1997). Cement is frequently used in these stabilizers to increase the strength characteristics of the soil cement, however, is just one of several factors contributing to the CO_2 emissions indicated (Ayeldeen & Kitazume, 2017; Safiuddin et al., 2010). Consequently, there has been an increased focus on fiber-reinforced cementitious soil for improving the mechanical qualities of the soil (Figure 7) (Ayeldeen & Kitazume, 2017; Consoli et al., 2010; Tang et al., 2007; Tran et al., 2017; Xiao & Liu, 2018).

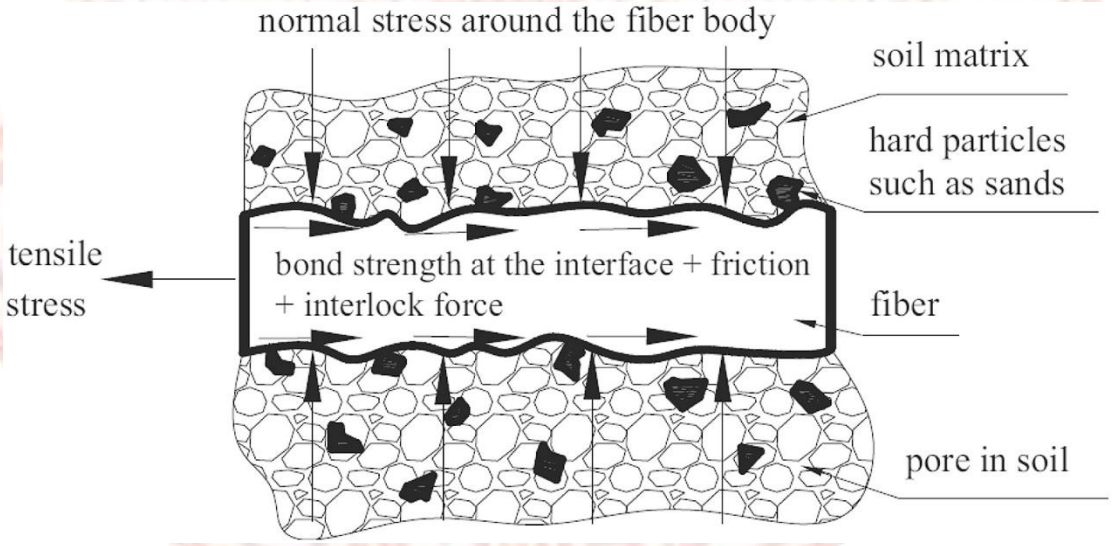

Figure 7 Sketch of fiber-reinforced cementitious soil for improving the mechanical qualities of the soil (Tang et al., 2007)

Because it softens and can undergo plastic deformation when heated gradually, polyethylene (PE) is a lightweight, viscoelastic, and thermoplastic material. It returns to its hard state upon cooling. Their average chain length determines the temperature at which this occurs (Consoli et al., 2010; Elmrabet et al., 2020). As a result, concrete with Fly Ash from Municipal Solid Waste (MSWIFA) blend as a substitute for building material reduces environmental costs, including CO_2 emissions, by eliminating cement, while also providing a location for MSWIFA to develop (currently stored in old mines) (Poranek et al., 2023). These wastes are part of landfill mining. In general, Landfill mining is the excavation and processing of landfilled waste to produce recyclable materials, soil-like material, and refuse-derived fuel (RDF). Effective landfill mining necessitates systematic planning. (Wungsumpow et al., 2018). MSWIFA can be used as sustainable construction material. It is one material of sustainable materials as reviewed by (Al-Ghouti et al., 2021), it is important to know about the introduction and background, the experimentation, the results, and the expected benefits of this study. For introduction and background, (Bellum, 2022) has studied mechanical properties in cement mortars, which used fly ash from industry, and Ground Granulated Blast Furnace Slag (GGBFS) with polypropylene fiber.

2.2. Use of fiber in construction building materials

Fibers are used to improve the tensile behavior of construction building materials. Much research has been used cementitious materials and fibers in their works for many decades for example (Iamchaturapatr et al., 2022b, 2022a; Petcherdchoo et al., 2023; Yingsamphancharoen & Piriyakul, 2022). A group of soil engineers (Pochalard et al., 2024) develop a new eco-friendly functional road material which is made of Bangkok clay, cement, bottom ash from the Refuse Derived Fuel (RDF) power plant and glass fibers (Figure 8).

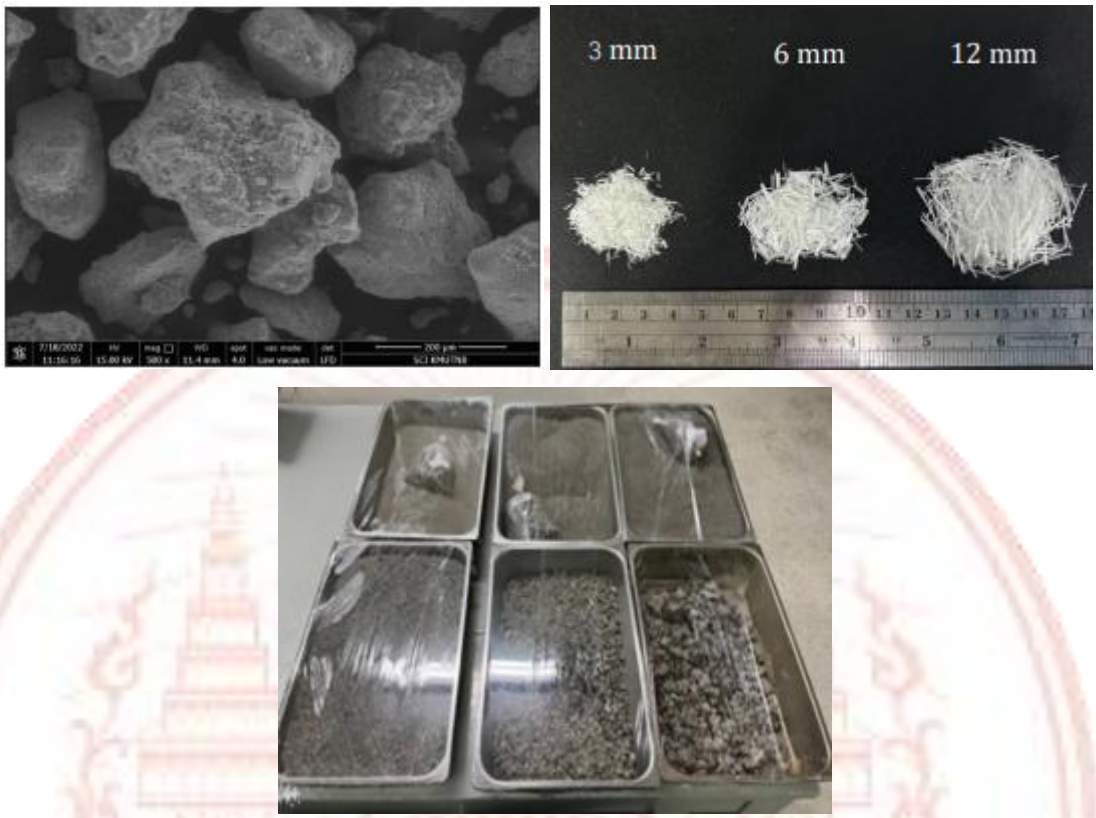

Figure 8 Bottom ash (BA) from Refuse Derived Fuel (RDF) and Glass fiber

(Pochalard et al., 2024)

By using the unconfined compression test (UCS), all samples are mixed at the liquid limit (LL) of 88%, varying glass fiber content between 0.5, 1.0, 1.5, 2.0 and 2.5% by volume respectively and the glass fiber lengths of 3, 6 and 12 mm. The cement content is used between 2, 4, 6, 8 and 10%, respectively by dry weight. The bottom ash (BA) content is used from 5, 10, 15, 20, 25 to 30% by volume respectively. Then, tested samples are cured for 7, 14, 28, 60 and 90 days. From the test results, it was observed that the optimum cement content is 8 to10% according to ACI 230.1R-09 (ACI 230.1R-09, 2009) standard which requires OPC of 10 to16% and the optimum glass fiber content is between 1.0 and 1.5%. The best UCS result for glass fiber length is at 12 mm. Finally, the optimum bottom ash content is 5 to10%, and the curing time should go beyond 28-90 days (Figure 9).

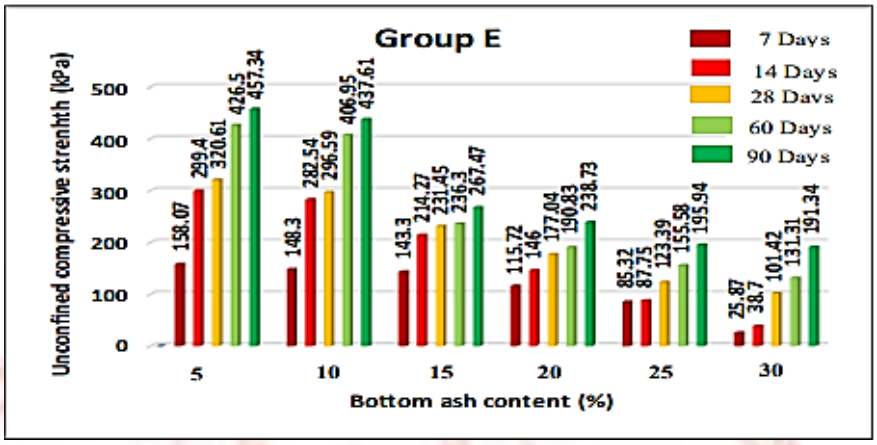

Figure 9 The test results of the optimum bottom ash content and curing time

(Pochalard et al., 2024)

A group of civil engineers (Pochalard et al., 2025) studies the influence of novel high-strength polyethylene fibers on the unconfined compressive strength (UCS) behavior of Bangkok clay cement admixed (Figure 10).

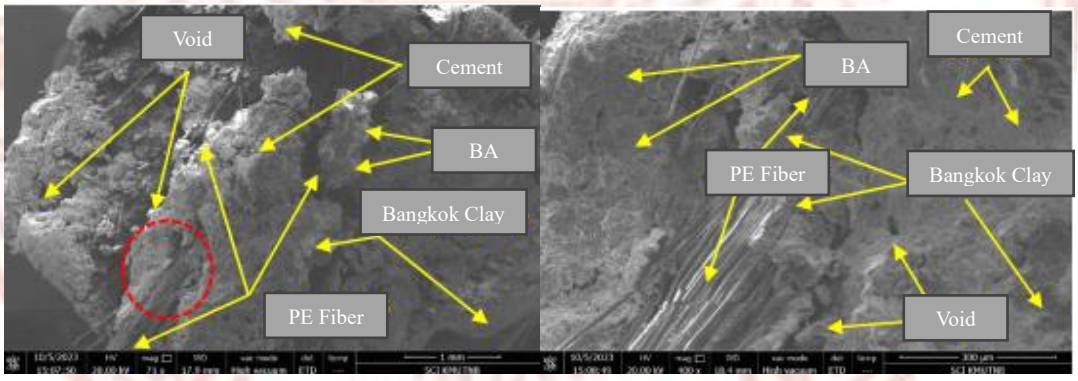

Figure 10 SEM image of the polyethylene fiberand the soil cement matrix

(Pochalard et al., 2025)

Bangkok clay samples are prepared at a liquid limit (LL) of 88% and added to Ordinary Portland Cement (OPC) at 2, 4, 6, 8 and 10% by weight; polyethylene fibers are added at 0.5, 1.0, 1.5, 2.0 and 2.5% by volume. These Bangkok clay samples are cured for 7, 14, and 28 days and tested by the unconfined compressive test. From the

test results, it was found that the cement content of 8% by weight is the optimum, and a novel high-strength polyethylene fiber content of 1% by volume is recommended. Additionally, the novel high-strength polyethylene fiber with 0.2 mm in diameter and 6 mm in length resulted in the maximum UCS value (Figure 11).

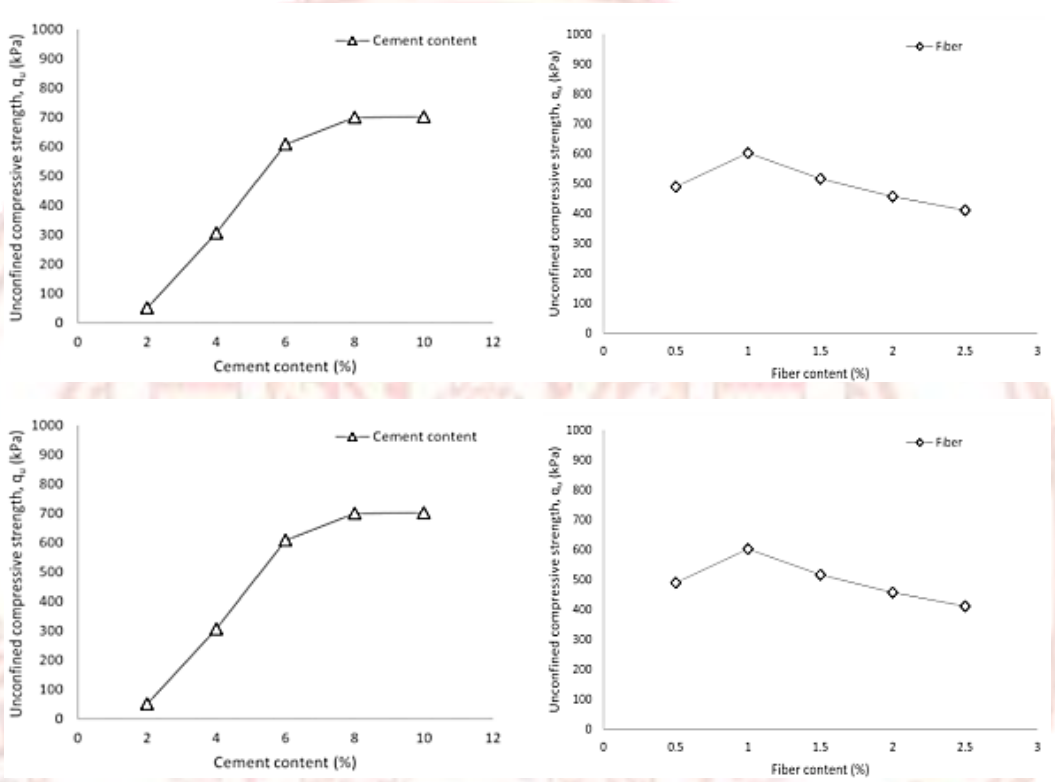

Figure 11 The test results of Bangkok clay cement using novel high strength polyethylene fibers (Pochalard et al., 2025)

A group of geotechnical engineers (Pochalard S. et al., 2023) investigates the strength development of Bangkok clay mixed with cement and Fly Ash (FA) from RDF power plant. The cement is replaced by FA which is an eco-friendly method since FA is an industrial a waste product from Mae Moh power plant in the northern of Thailand. Bangkok clay is added with 20% cement by weight and varied FA from 0 to 30% by weight, after curing time for 7, 14, 28 and 90 days. The initial shear modulus (G_0) is calculated from the shear wave velocity (V_s) measured by a bender element testing

(Figure 12). In practice, the determination of soil dynamics properties can be divided into two methods: laboratory testing and field testing. In Thailand, field testing was previously used by measuring the velocity of stress wave propagation by measuring shear waves (Ashford et al., 1997). The measurement of the velocity of this stress wave will give the modulus value at low stress level and later the study of the modulus value and damping ratio were studied by cyclic trixial test. As it is a laboratory test at high stress levels, this test method cannot determine the dynamic properties at low stress levels. In order to compare the findings of field testing with the modulus at low stress levels and to investigate the modulus behavior in different ways that field tests cannot, a laboratory research is thus required (Teachavorasinskun et al., 2002). For comparison reasons, the strength development of Bangkok clay samples is determined by unconfined compression test (UCS). From the results, it was noted that the optimum of FA content is about 15-20% and established that the strength development of Bangkok clay admixed with cement and FA is increased with increasing the curing time. Furthermore, the relationship is found as G_0=27.57qu (Figure 13).

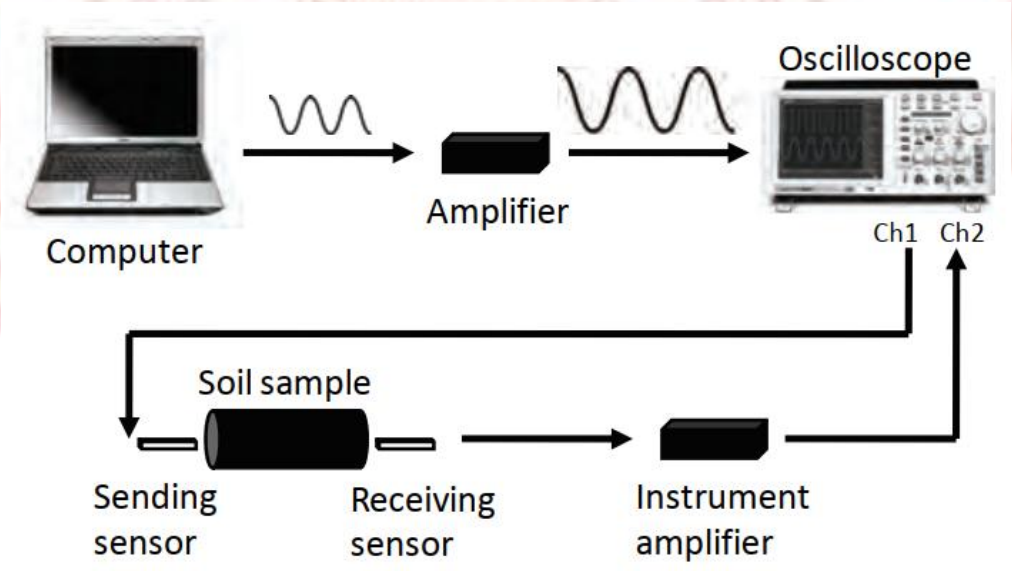

Figure 12 Schematic diagram of bender element test and experimental set-up

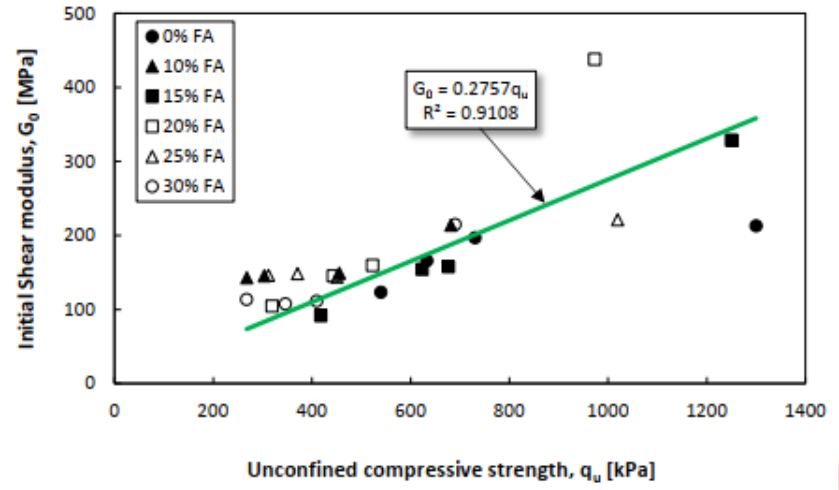

Figure 13 Relationships between G0 and q_u

2.3. Cement and cementitious materials in ground improvement method

The use of fly ash from MSW is an interesting topic in terms of environmental management in Thailand, so the enhancement of flexural strength of cement compacted sand using fly ash from MSW with polypropylene fiber and glass fiber is added in this study to investigate its benefit on the environment. MSW combustor fly ash is the by-product that is created when municipal solid waste is burned in solid waste combustor plants, which is known as MSW combustor fly ash (Figure 14) (Chesner et al., 2002).

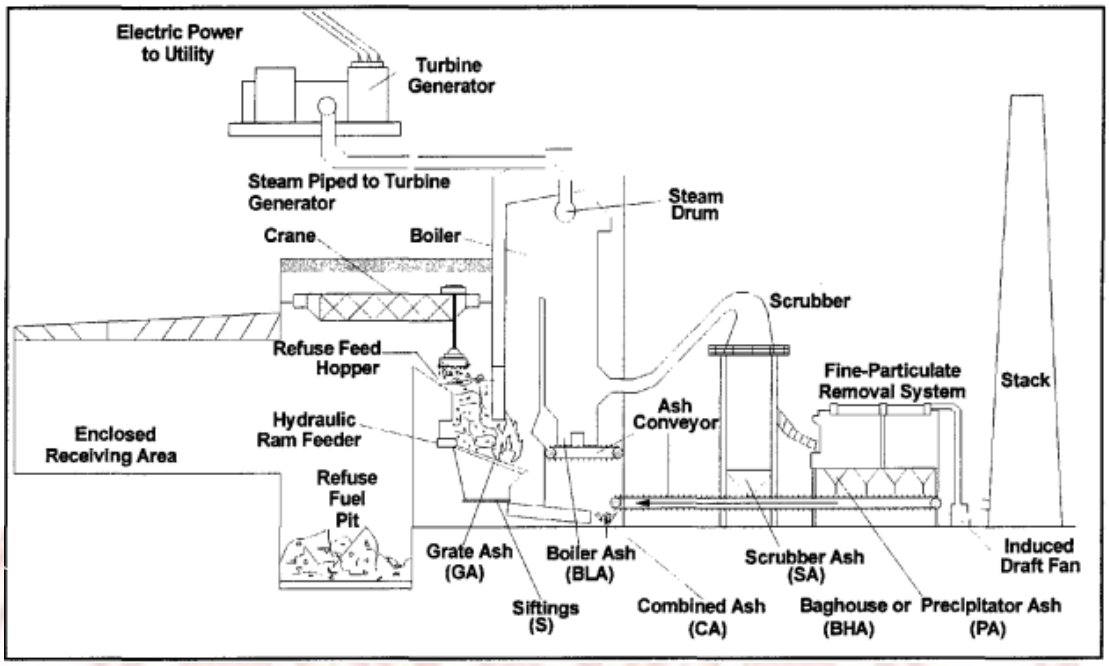

Figure 14 Mass burn WtE facility-typical cross section and ash streams

(Chesner et al., 2002)

Incineration has surpassed landfill mining as the most significant alternative for disposing but release of heavy metals during MSW incineration is affected by MSW composition (Figure 15) (Wang et al., 2019).

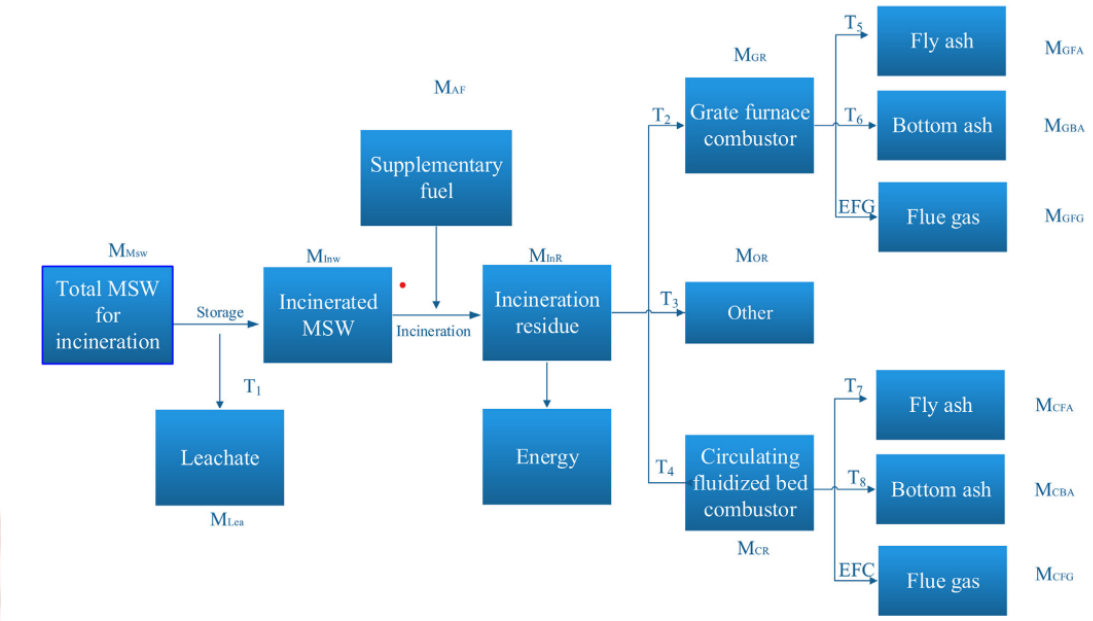

Figure 15 Diagrammatic representation of the mass movement of heavy metals during MSW incineration (Wang et al., 2019)

Simultaneous of Thailand is growing amounts of waste. And, the sand examined came from Thailand's Ayutthaya area (Figure 16) and is often utilized as a building material for embankment fill and pavement applications (Chuenjaidee et al., 2022).

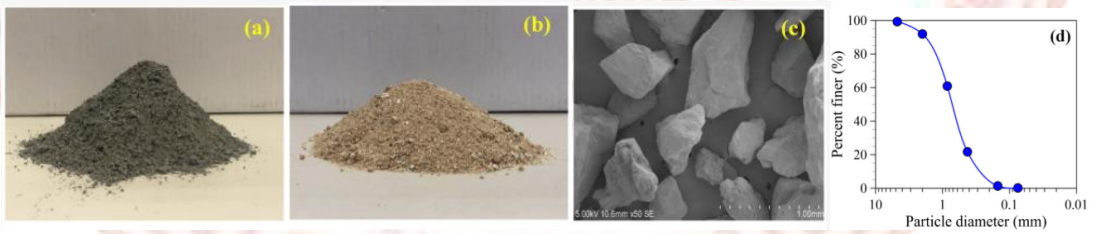

Figure 16 cement (a), sand (b), SEM image (c), and sand particle size distribution curve (d) (Chuenjaidee et al., 2022)

As a cementing agent, type I Portland cement was employed with fly ash from MSW (Aubert et al., 2004), and polypropylene fibers were used as reinforcement material. It works well for controlling cracks of different diameters at different loading stages and cure durations (Figure 17) (Blazy & Blazy, 2021).

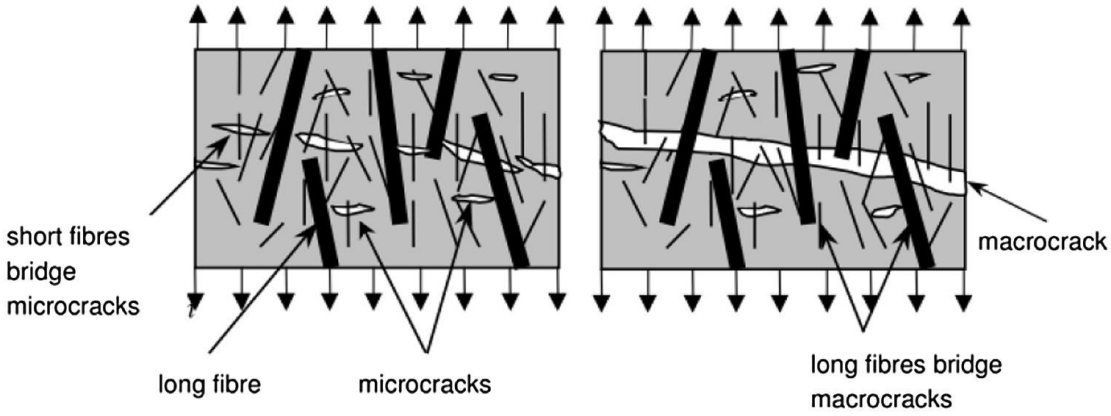

Figure 17 (a) Impact of shorter fibers on bridging microcracks and boosting tensile strength and (b) impact of longer fibers on bridging macrocracks and boosting ductility

Water was added to the sample mixture to achieve the optimal water content as determined by the standard proctor test ASTM D698-12e1 (ASTM D698-12e1, 2012). The experimentation is research on the properties of the sample according to (ASTM C-09, 2013; ASTM C1018, 1997), and the objective of this investigation is study unconfined compressive tests by adding polyethylene on the properties with variations of fiber content, cement content, and curing time. Thus, the sample performance was examined including first peak strength, peak strength, peak strength ratio, toughness, ductility index, equivalent flexural strength, and crack behavior (Figure 18) (Jamsawang et al., 2015).

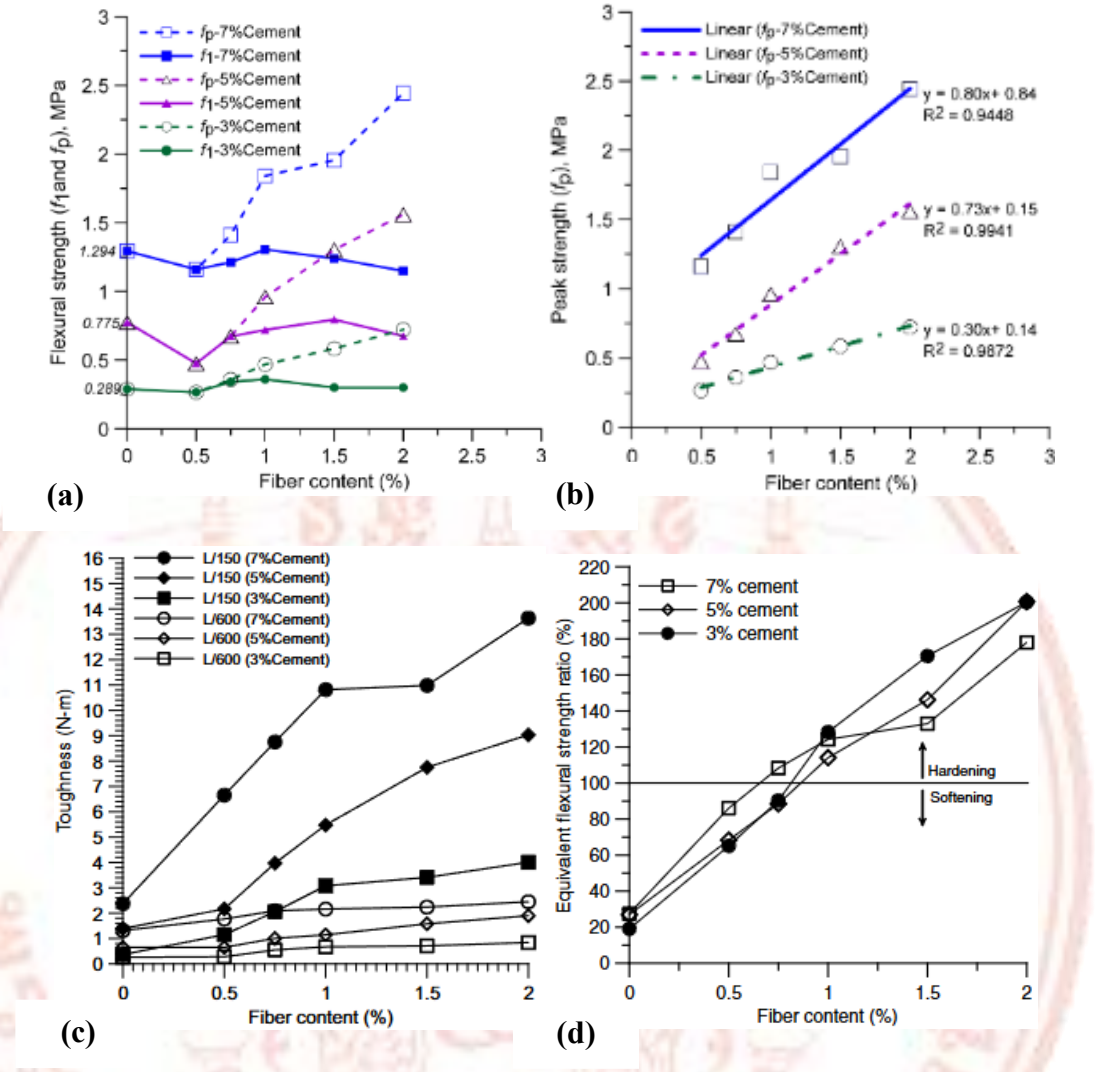

Figure 18 (a) Flexural strength and fiber content relationship (b) linear regression analysis between peak strength and fiber content (c) Toughness versus fiber content relationship and (d) Equivalent flexural strength ratio versus fiber content relationship (Jamsawang et al., 2015)

Large-scale material extraction is required for conventional construction and building materials such as steel bars, cement, concrete, sandcrete blocks, burned bricks, and tiles, which deplete natural resources and harm the environment. The energy-intensive manufacturing process for these materials emits carbon dioxide and other pollutants into the environment, including particulate matter, sulfur oxides, nitrogen oxides, and carbon monoxide. These pollutants pollute water, air, soil, vegetation, wildlife, and

aquatic life while also affecting human health (Safiuddin et al., 2010). In addition, the cost of manufacturing traditional building materials is rising because of the depletion of natural resources, the energy needed for manufacturing, and the high cost of transportation from suppliers to construction sites. Research on substitute building materials is becoming more popular as a result of these financial and environmental issues (Figure 19) (Danso et al., 2015).

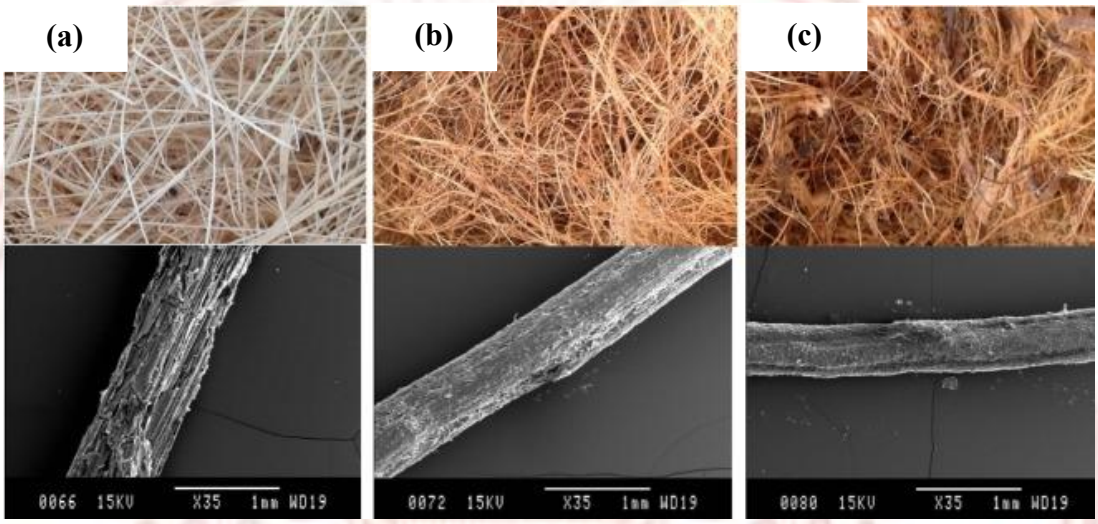

Figure 19 Photographs and SEM micrographs of the types of fiber (a) Bagasse fiber (b) Coconut fiber and (c) Oil palm fiber (Danso et al., 2015)

Compared to industrial building materials like concrete, the production of earth material uses 99 percent less energy. Long transit routes are also unnecessary because earth is an inexpensive, readily available, recyclable building material locally (Zak et al., 2016). Utilizing earth as a building material to create rammed earth is becoming more and more common due to its inexpensive cost and negligible environmental impact (Sharma et al., 2015). Earthen materials are not as strong as more contemporary building materials like steel and concrete, though, in terms of durability, tensile strength, and compressive strength (Ngowi, 1997). To improve the mechanical properties of earthen materials, scientists have proposed a variety of stabilizers, such as lime and cement (Figure 20) (Donkor & Obonyo, 2016; Millogo et al., 2014; Morel et al., 2007; P. Walker, 1997; P. J. Walker, 1995).

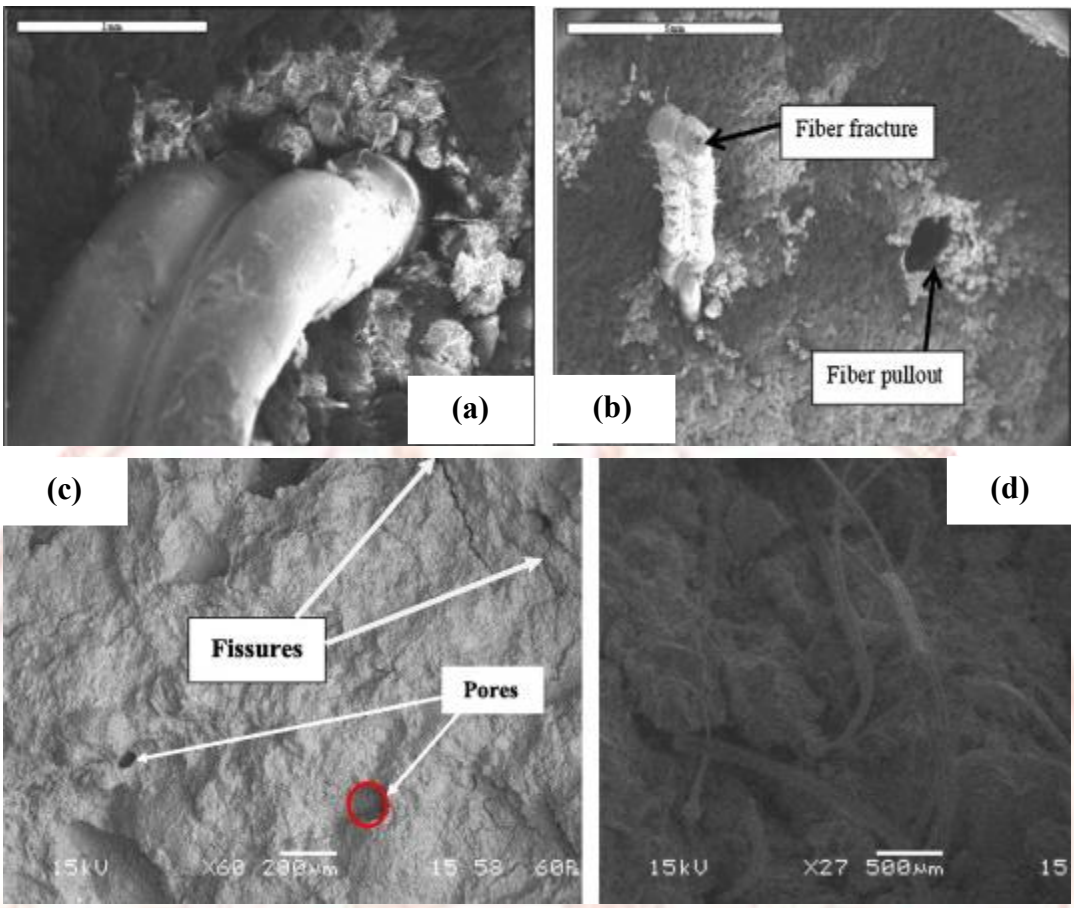

Figure 20 SEM micrograph of fractured beam surfaces (a) Embedded fiber in matrix (b) Fiber fracture and pullout (c) lateritic soil raw and (d) Hibiscus cannabinus fibers (Donkor & Obonyo, 2016; Millogo et al., 2014)

To improve the soil's strength properties, cement is widely used in these stabilizers. But cement is only one of many elements that contribute to the stated CO_2 emissions (Ayeldeen & Kitazume, 2017; Safiuddin et al., 2010). Despite its poor behavior in tension, cement is one of the most common building materials. Use of fiber-reinforced cementitious material is one of the solutions suggested to possess these cracks; this handicap is the primary cause of cracking, which can damage its durability and appearance. The energy-absorbing capacity of hardened concrete is increased when fibers are added to a matrix, making it more appropriate for use in structures subjected to impact loads (Figure 21) (Ayeldeen & Kitazume, 2017; Boulekbache et al., 2010).

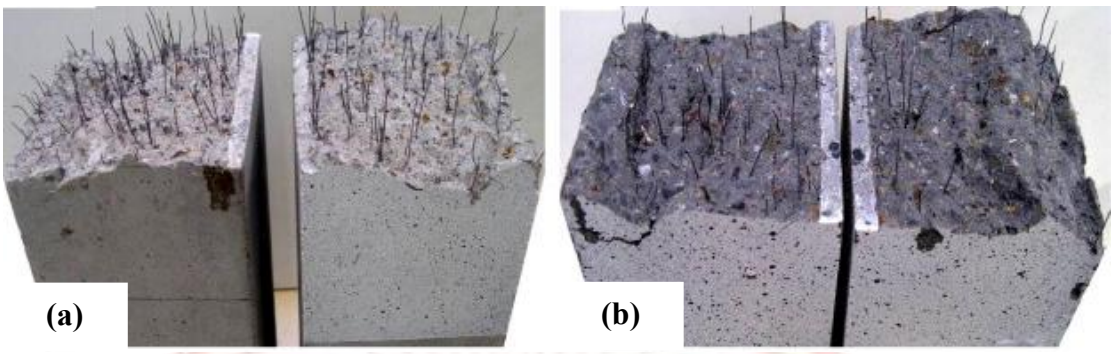

Figure 21 Fiber distribution through a section (a) Fiber-reinforced ordinary concrete and (b) Fiber-reinforced high-strength concrete

Consequently, there has been an increased focus on fiber-reinforced cementitious soil for improving the mechanical qualities of the soil (Ayeldeen & Kitazume, 2017; Consoli et al., 2010; Tran et al., 2017; Xiao & Liu, 2018). Because it softens and can undergo plastic deformation when heated gradually, polyethylene (PE) is a lightweight, viscoelastic, and thermoplastic material. It returns to its hard state upon cooling. Their average chain length, or n, determines the temperature at which this occurs (Figure22) (Elmrabet et al., 2020). The objective of this investigation is to study unconfined compressive tests by adding polyethylene on the properties with variations of fiber content, cement content, and curing time. According to the literature reviews, there are two issues to be further addressed. First, the application of fly ash from the RDF power plant to replace the ordinary Portland cement (OPC) based on the flexural test. Second, the microstructure and bonding between the polypropylene fiber with glass fiber and soil matrix by SEM.

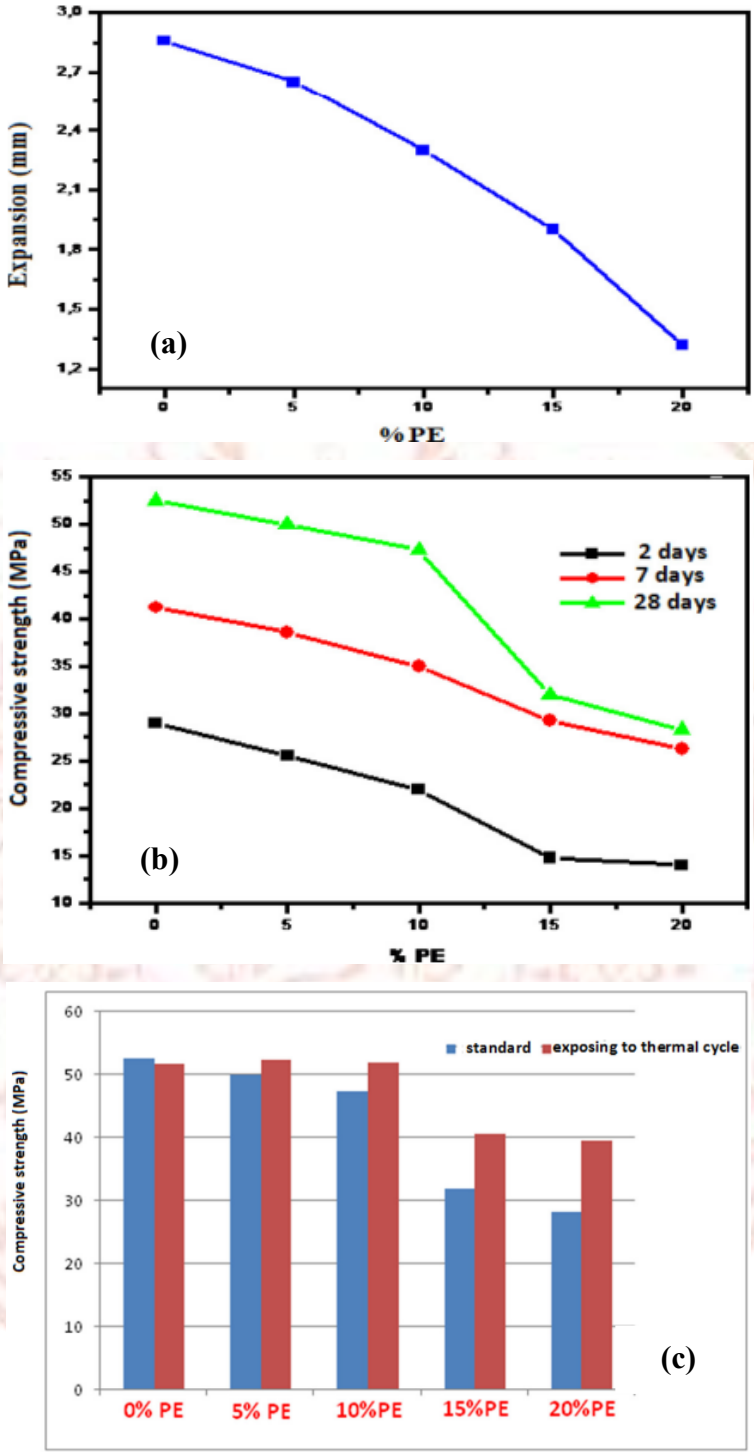

Figure 22 (a) Effect of PE content on expansion (b) Effect of PE content on compressive strength and (c) Effect of thermal cycle on compressive strength of blended cements (Elmrabet et al., 2020)

Chapter 3 Methodology

3.1. Materials

The sand used in these experiments was taken from Bangkok's normal construction sand. The grain size analysis curve with Optimum moisture content curve and physical properties of Bangkok sand are shown in Figure 23 and 25 with Table 1. According to the Unified Soil Classification System (USCS) (American Society for Testing and Materials, 1985), this Bangkok sand is classed as poorly graded sand (SP). Figure 23 also shows an enlargement of the sand particles obtained from the SEM image analysis, which shows angular, sub-angular, round, and sub-round shapes. Ordinary Portland cement (OPC) type I with a specific gravity of 3.15 was the cement used in the test (ASTM Committee D-18 on Soil and Rock, 2009). The chemical composition of the cement used is summarized in Table 2. The fibers used in this experiment were glass fibers and the size are 3, 6 and 12 mm from owens coming band, advantex CS 979-14 series there is E-glass type as shown in Figure 26 and Table 3. And, polypropylene fiber with size is 55 mm from synmix band (macro synthetic fibers for concrete) as shown in Figure 27 and Table 4. FA from RDF power plant waste from lobal Power Synergy Public Company Limited at Numkok Sub-district, Muang District, Rayong Province by using technology to transform sorted solid waste into fuel (refuse derived fuel or RDF) shown in Figure 28. Power generated by this power plant will sell to the provincial electricity authority (PEA) under the municipal waste to energy project in the form of feed-in tariff (FiT) scheme. FA is classified as Type C according to ASTM C618-12 (ASTM C-09, 2013). Its main chemical constituents are listed in Table 5.

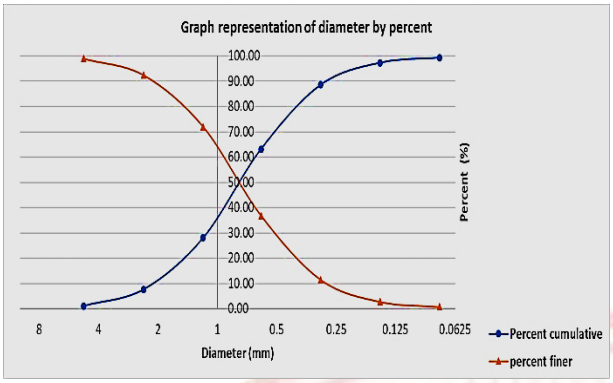

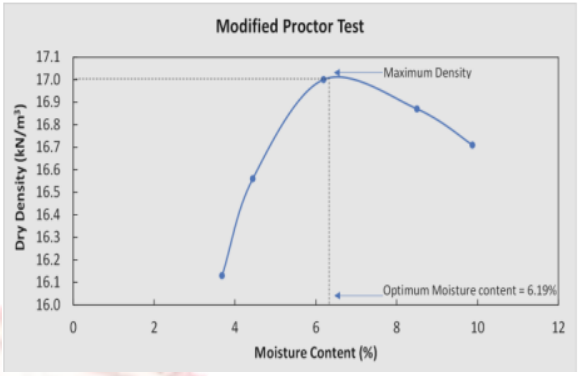

(a) **(b)**

Figure 23 (a) Grain size distribution curve and (b) Optimum moisture content curve

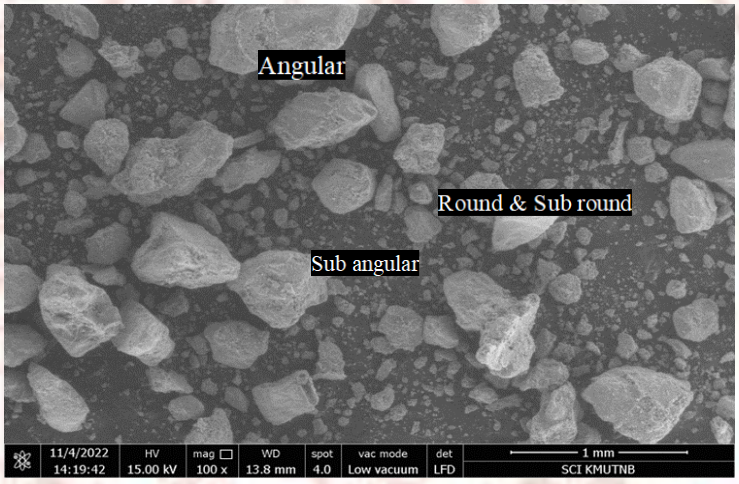

Figure 24 SEM of Bangkok construction sand

Figure 25 Photographs of Bangkok construction sand

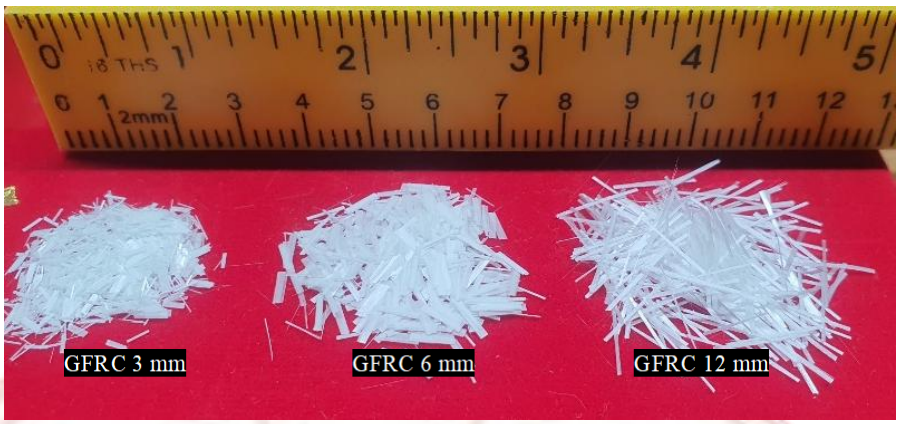

Figure 26 Glass Fiber-Reinforced Concrete lengths of 3,6 and 12 mm

Figure 27 Polypropylene Fiber lengths of 55 mm

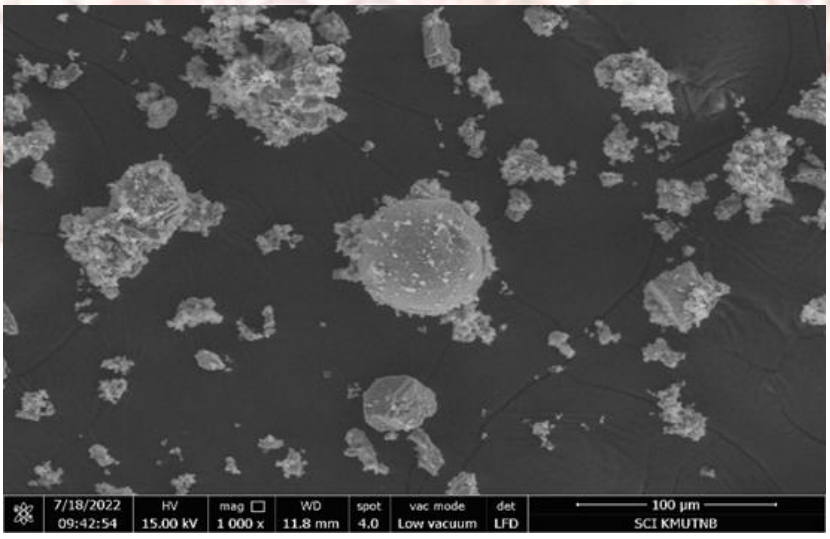

Figure 28 SEM of Fly ash (FA) from Refuse Derived Fuel (RDF) power plant

Table 1 Physical properties of the Bangkok construction sand

Property	Value
Specific gravity (G_s)	2.65
Gravel content (%)	10.52
Sand content (%)	80.58
Fine content (%)	8.90
D_{60} (mm)	0.93
D_{30} (mm)	0.49
D_{10} (mm)	0.29
Coefficient of Uniformity (C_u)	3.21
Coefficient of Curvature (C_c)	0.89
Soil classification (USCS)	SP
Maximum, and minimum void ratios	0.83, 0.28
Maximum dry unit weight (kN/m^3)	15.70
Optimum moisture content (%)	6.19

Table 2 Chemical composition of cement

Oxide	Common name	Mass (%)
SiO_2	Silica	4.45
Al_2O_3	Alumina	1.31
Fe_2O_3	Iron	14.37
SO_3	Sulfuric anhydrite	1.00
CaO	Lime	76.44
MgO	Magnesia	1.79
K_2O	Alkali	0.23
Cr_2O_3	Chromic oxide	0.10
ZnO	Zinc oxide	0.32

Table 3 Properties of glass fiber

Type	Glass Fiber
Length (mm)	3, 6 and 12 mm Section
Diameter (μm)	3.0
Specific weight	2.47
Tensile strength (MPa)	2350
Young's modulus (GPa)	73
Color	White

Table 4 Properties of Polypropylene fiber

Type	Polypropylene Fiber
Length (mm)	55 mm Section
Diameter (mm)	0.85
Specific weight	0.91
Tensile strength (MPa)	250
Young's modulus (GPa)	3.0
Color	White

Table 5 Properties of fly ash (FA)

Oxide	Common name	Mass (%)
SiO_2	Silica	7.94
Al_2O_3	Alumina	1.45
Fe_2O_3	Iron	32.56
SO_3	Sulfuric anhydrite	0.53
CaO	Lime	47.52
MgO	Magnesia	4.56
K_2O	Alkali	0.66
Cr_2O_3	Chromic oxide	0.83
ZnO	Zinc oxide	3.02

3.2. Preparation and experimentation of samples

The experimentation was divided into three sections. First, the geotechnical properties of the examined sand, as well as the physical and engineering features of fiber and fly ash from MSW. There are physical properties testing of the Bangkok construction sand including Specific gravity (G_s), Gravel content, Sand content, Fine content, D60, D30, D10, Coefficient of Uniformity (C_u), Coefficient of Curvature (C_c), Maximum and minimum void ratios, Maximum dry unit weight, Optimum moisture content and Optimum moisture content (Figure 23a and 23b). The chemical composition by using X-ray fluorescence spectrometer (XRF) testing the ordinary portland cement (OPC), those are Silica, Alumina, Iron, Sulfuric anhydrite, Lime, Magnesia, Alkali, Chromic oxide, and Zinc oxide. And the properties of polypropylene fiber include length, shape, section, diameter, specific weight, tensile strength,

Young's modulus, and Colour. And, the chemical composition of RDF fly ash, there are percentage of mass including Silica, Alumina, Iron, Sulfuric anhydrite, Lime, Magnesia, Alkali, Chromic oxide, and Zinc oxide. Second, Dry Bangkok sand with FA from RDF power plant was combined with polypropylene & glass fiber and Portland cement in a concrete mixer to create the CCFS-GF and CCFS-PP specimens. To achieve the optimal amount of water (determined by the modified proctor test) ASTM D698-12e1(ASTM Committee D-18 on Soil and Rock, 2009) water was added to the cement around 6.19 % (optimum moisture content) or 19.81 ml, glass fiber, polypropylene fiber, sand, and FA combination. The CCFS-GF samples were then prepared in the form of a cylinder with a diameter of 50 mm and a height of 100 mm. A wooden hammer was used to compact the uniform mixture until it achieved its maximum dry unit weight. The glass fiber and polypropylene fiber contents varied between 0.5, 1.0, 1.5, 2.0 and 2.5 % or 2.47, 4.93, 7.40, 9.86 and 12.33 g by volume, with glass fiber lengths of 3, 6 and 12 mm and polypropylene fiber lengths 55 mm. Even so, the cement percentage was set at 2, 4, 6, 8 and 10 % or 5.12, 10.24, 15.36, 20.48 and 25.60 g by weight with varied the FA replacement varied between 5, 10, 15, 20 and 25 % or 1.28, 2.56, 3.84, 5.12, 6.40 and 7.68 g by volume. According to Table 6, the optimum amount of water and maximum dry unit weight was virtually the same for all fiber contents. Third, the CCFS-PP specimens were subjected to a series of flexural strength tests as shown in Figure 32 and unconfined compressive strength test as shown in Figure 31 by using a 50 kN load cell used to measure the applied loads. The deflection rate was controlled by an electric motor at 0.05 mm/min, and the test ended with a 3 mm net deflection. The CCFS-PP specimens were made by mixing dry Bangkok sand, fly ash from municipal solid waste (MSW), polypropylene fibers, and Portland cement in a concrete mixer. According to Table 7, CCFS-PP specimens were prepared as a beam measuring 75 mm in width, 75 mm in height, and 300 mm in length. The specimens were cured for 7-, 14-, 28-, 60- and 90-days period before the test date. Fourth, ASTM D8295–19 (ASTM D8295−19, 2019), the bender element test is used to measure the shear wave velocity, V_s, which is used to determine the stiffness of CCFS-PP specimens in terms of initial shear modulus, G_0. This method was used to determine the strength development in consideration of V_s for CCFS-PP specimens (Figure 33).

Lastly, a series of scanning electron microscopes (SEM): FEI QUANTA 450 investigations (Figure 34) were performed on the CCFS-GF and CCFS-PP samples to examine the interaction mechanism of fiber, cement, and fly ash from MSW interface.

Table 6 CCFS-GF specimens for Unconfined Compressive Strength (UCS) test

Serial number	Cement content (%)	FA (%)	Fiber content (%)	Fiber length (mm)	Optimum moisture content (%)	Curing time (days)
A1	2	20	1.0	6	6.19	28
A2	4	20	1.0	6	6.19	28
A3	6	20	1.0	6	6.19	28
A4	8	20	1.0	6	6.19	28
A5	10	20	1.0	6	6.19	28
B1	8	20	0.5	6	6.19	28
B2	8	20	1.0	6	6.19	28
B3	8	20	1.5	6	6.19	28
B4	8	20	2.0	6	6.19	28
B5	8	20	2.5	6	6.19	28
C1	8	20	1.0	3	6.19	28
C2	8	20	1.0	6	6.19	28
C3	8	20	1.0	12	6.19	28
D1	8	5	1.0	6	6.19	7, 14, 28, 60, 90
D2	8	10	1.0	6	6.19	7, 14, 28, 60, 90
D3	8	15	1.0	6	6.19	7, 14, 28, 60, 90
D4	8	20	1.0	6	6.19	7, 14, 28, 60, 90
D5	8	25	1.0	6	6.19	7, 14, 28, 60, 90
D6	8	30	1.0	6	6.19	7, 14, 28, 60, 90
E1	8	20	0.5	6	6.19	7, 14, 28, 60, 90
E2	8	20	1.0	6	6.19	7, 14, 28, 60, 90
E3	8	20	1.5	6	6.19	7, 14, 28, 60, 90
E4	8	20	2.0	6	6.19	7, 14, 28, 60, 90
E5	8	20	2.5	6	6.19	7, 14, 28, 60, 90

Table 7 CCFS-PP specimens for Flexural Strength test

Serial number	Cement content (%)	FA (%)	Fiber content (%)	Fiber length (mm)	Optimum moisture content (%)	Curing time (days)
A1	2	20	1.0	55	6.19	28
A2	4	20	1.0	55	6.19	28
A3	6	20	1.0	55	6.19	28
A4	8	20	1.0	55	6.19	28
A5	10	20	1.0	55	6.19	28
B1	8	20	0.5	55	6.19	28
B2	8	20	1.0	55	6.19	28
B3	8	20	1.5	55	6.19	28
B4	8	20	2.0	55	6.19	28
B5	8	20	2.5	55	6.19	28
C1	8	5	1.0	55	6.19	7, 14, 28, 60, 90
C2	8	10	1.0	55	6.19	7, 14, 28, 60, 90
C3	8	15	1.0	55	6.19	7, 14, 28, 60, 90
C4	8	20	1.0	55	6.19	7, 14, 28, 60, 90
C5	8	25	1.0	55	6.19	7, 14, 28, 60, 90
D1	8	20	0.5	55	6.19	7, 14, 28, 60, 90
D2	8	20	1.0	55	6.19	7, 14, 28, 60, 90
D3	8	20	1.5	55	6.19	7, 14, 28, 60, 90
D4	8	20	2.0	55	6.19	7, 14, 28, 60, 90
D5	8	20	2.5	55	6.19	7, 14, 28, 60, 90

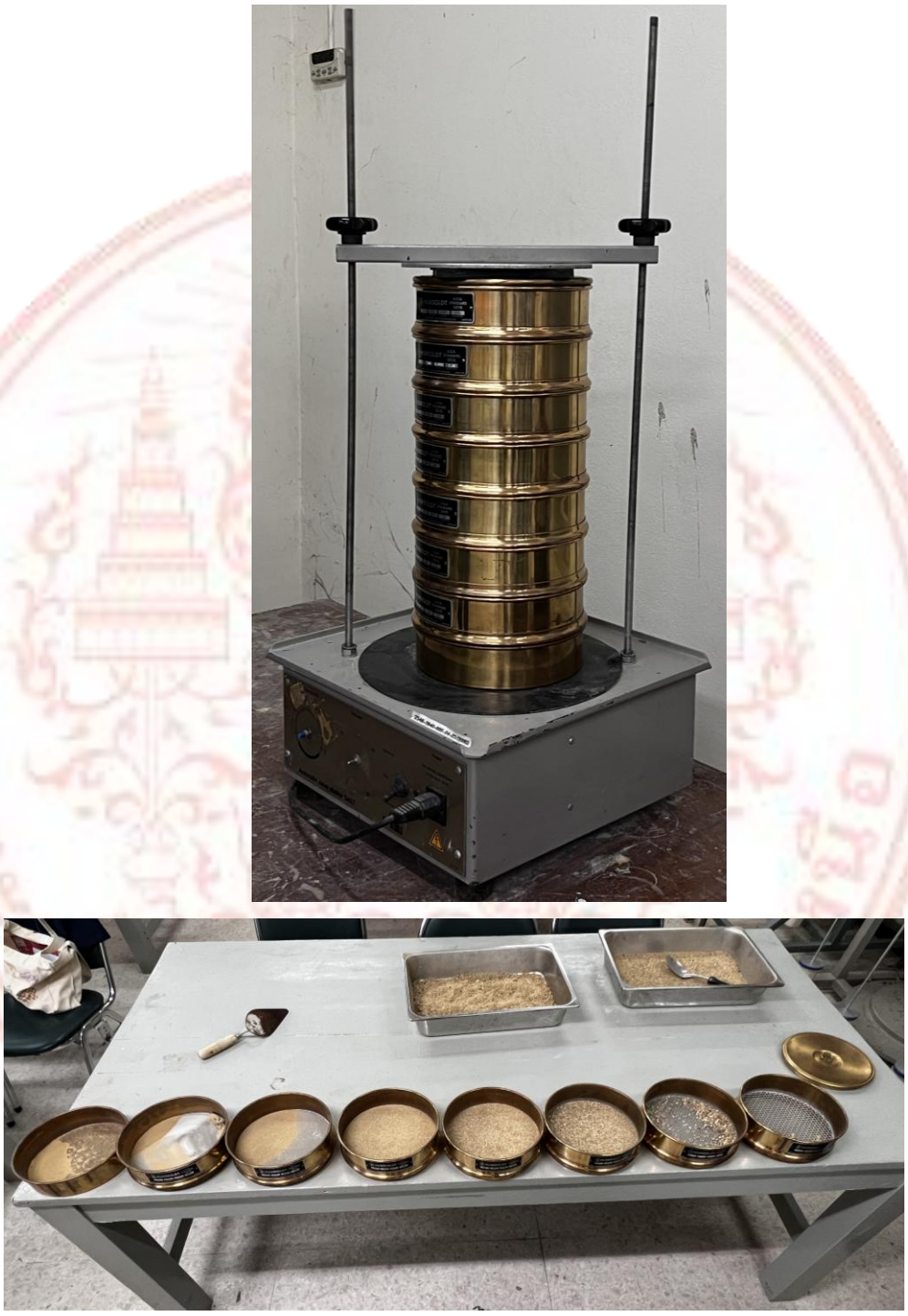

Figure 29 Sand sieve analysis test

Figure 30 Modified proctor compaction test

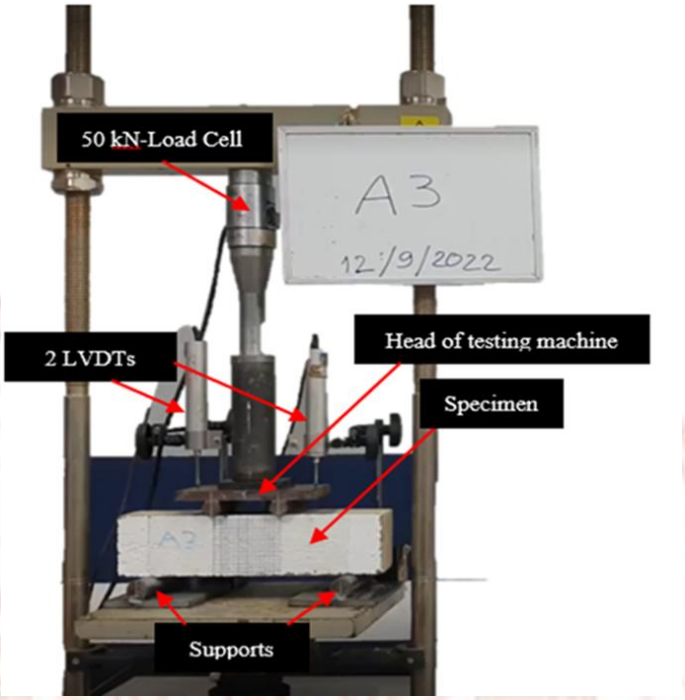

Figure 31 Experimentation set up of Unconfined Compressive Strength (UCS) test

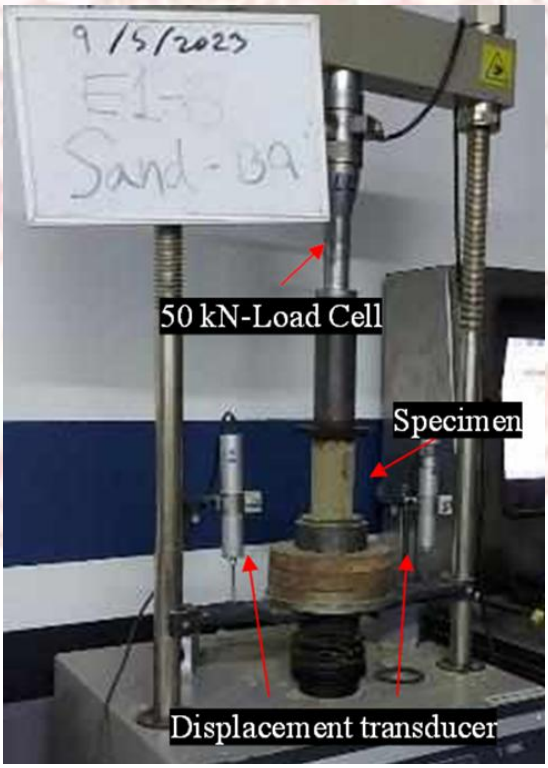

Figure 32 Experimentation set up of Flexural Strength test

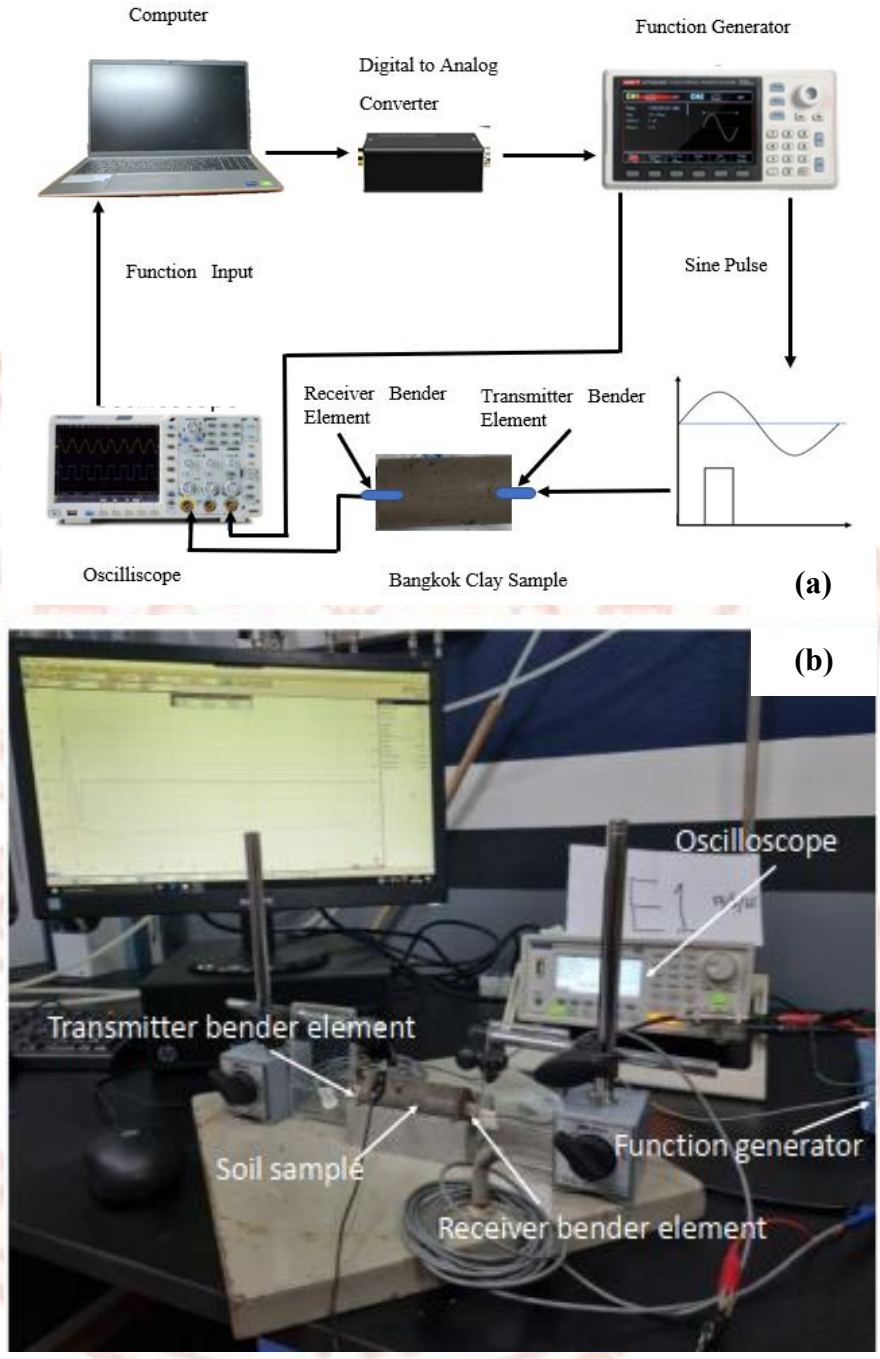

Figure 33 (a) Bender element test and (b) experimental set-up

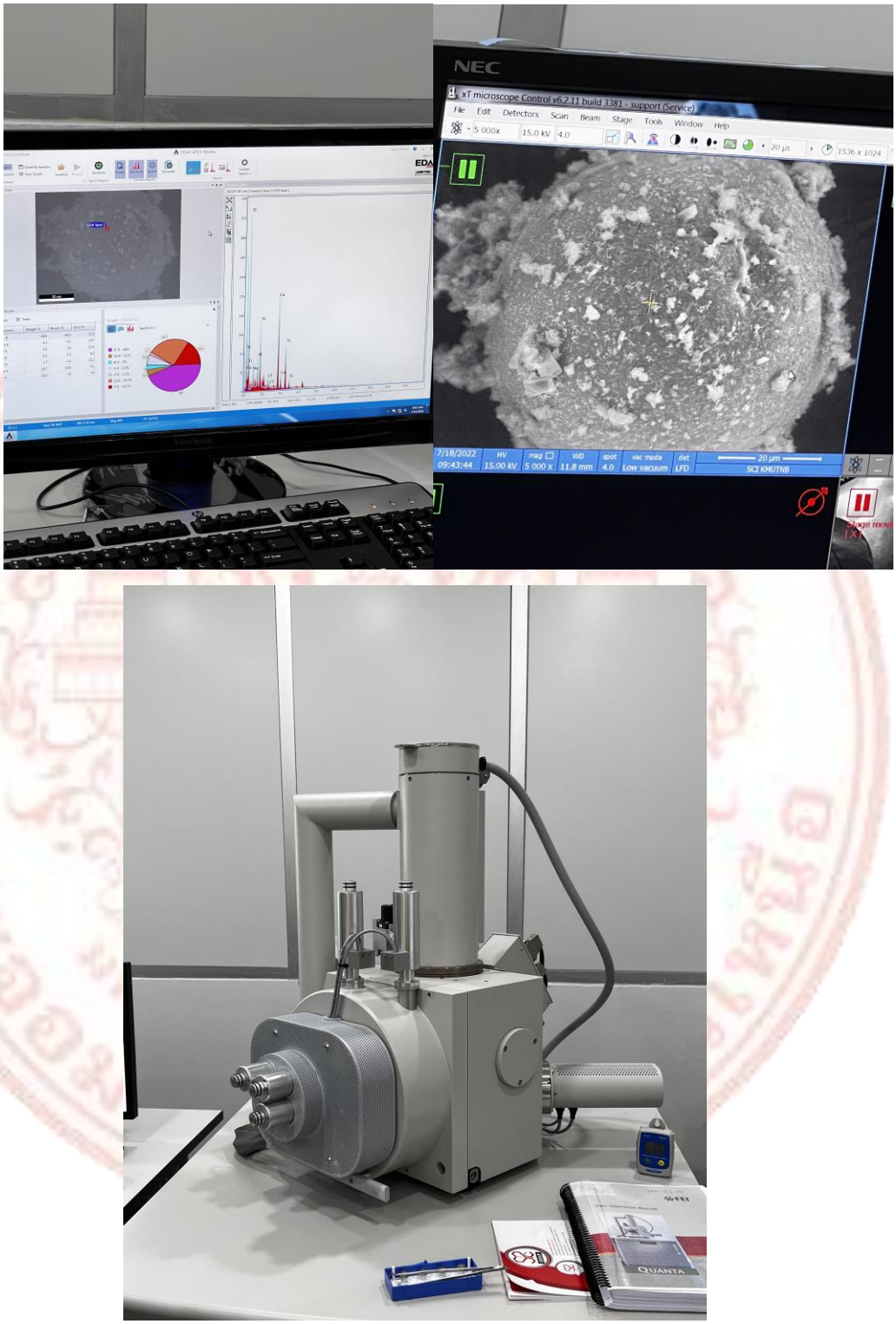

Figure 34 Scanning Electron Microscopes (SEM): FEI QUANTA 450

Chapter 4 Experimental Results

4.1. Experimentation of CCFS-PP specimens

The specimens performed a flexural performance test in accordance with ASTM C 1018 (ASTM C1018, 1997)and ASTM C-09 (ASTM C-09, 2013) after 28 days of curing. The beams turned 90 degrees from their casting location before testing to reduce the impact of the casting direction. The test setup and equipment are displayed in Figures 35. The applied loads were measured using a 50 kN load cell. An electric motor controlled the deflection rate of 0.05 mm/min, and the test ended at a net deflection of 3 mm. Then, the data logger gathered enough data points to create highly sensitive load-deflection curves as seen in Figure 36, which were then utilized to accurately predict each CCFS-PP's dependable flexural performance and interpret the test findings.

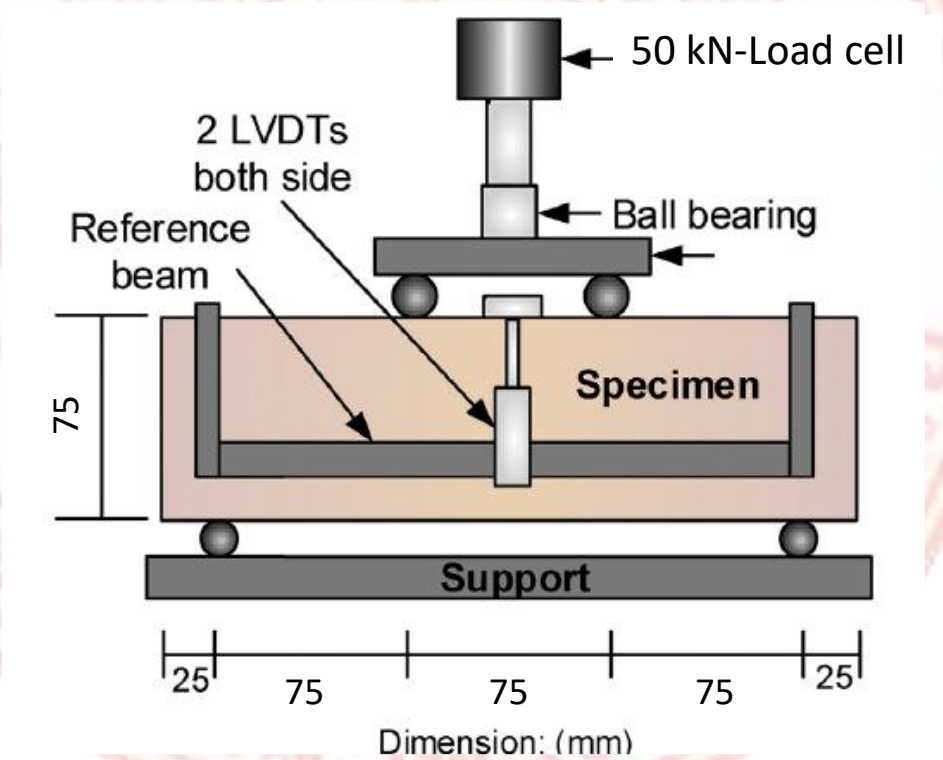

Figure 35 Flexural strength test specimen and set up

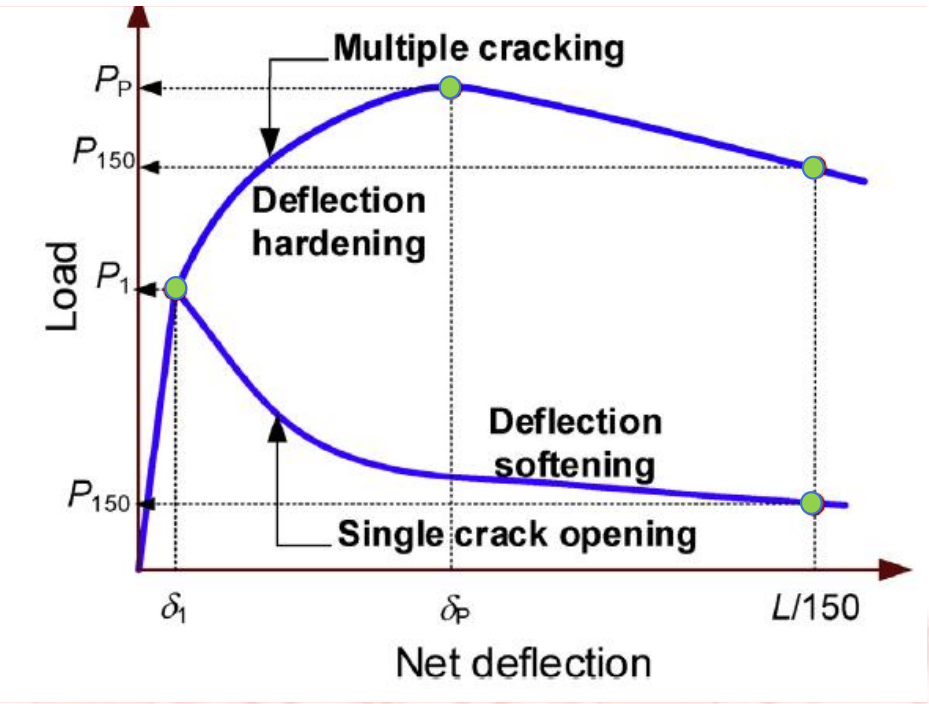

Figure 36 Parameter calculations obtained from load–deflection curves adapted from ASTM C1609/C1609M-10 (ASTM C1609/C1609M-10, 2013)

4.2. The CCFS-PP's flexural behavior parameters

The CCFS-PP flexural responses can be classified as softening or hardening. Figure 37 shows the load-deflection curves for CCFS-PP beams. Beams with no fiber have deflection softening and brittle behaviors while beams containing a lot of fibers shows the deflection hardening and ductile behaviors. Flexural reactions of CCFS-PP can be characterized as either deflection-softening or deflection-hardening as illustrated by curves. In this study, along the load-deflection curve, the point that clearly shows nonlinearity is defined as the first cracking point. After the first crack, a CCFS-PP sample with deflection-hardening behavior has a better load-carrying capacity. According to ASTM standard C 1018 (ASTM C1018, 1997)and ASTM C-09 (ASTM C-09, 2013), this point is suitable for designating the first peak point for CCFFSs displaying either deflection-hardening or softening reactions. P1 is the load value at this point, and δ1 is a corresponding deflection value. The first point of softening following point P1 is known as the peak load (PP). In the case of deflection softening CCFFS, it is noticed that P1 = PP. δP denotes the corresponding deflection value at PP. ASTM C-09 (ASTM C-09, 2013) recommends a deflection point of L/150 equivalent to 1.5 mm for a specimen with a 1.5 mm span in addition to the P1 and PP points. At any deflection, the flexural strength (f) is calculated by Eq. (1) as follows:

$$f = \frac{PL}{bd^2} \qquad (1)$$

P is the load (kN) that corresponds to the needed f (kPa), L is the span length (m), b is the specimen's breadth (m), and d is its depth (m). The P_1 and P_P flexural loads are defined as the first peak strength (f_1) and peak strength (f_P). The residual load P_{150}, which equates to the residual strength at a deflection of L/150 (f_{150}), is the load borne by CCFS-PP after P_1 at the deflection of L/150. Toughness is defined as the energy corresponding to the region beneath the load-deflection curve up to a specific deflection. The toughness value at the deflection of L/150 is indicated as T_{150}. (Nematollahi et al., 2014) state that the ductility of a composite material is defined as the ratio of the first-crack deflection to the deflection at the peak strength (δ_P/δ_1).
In other words, the CCFS-PP is more ductile the larger the ratio of δ_P/δ_1. Thus, the following definition applies to the ductility index (DI) by Eq. (2) as below:

$$DI = \frac{\delta_P}{\delta_1} \quad (2)$$

Which δ_P and δ_1 are the specimen's net deflections at peak strength and first peak strength, in mm. The equivalent flexural strength ratio ($R_{T,150}$), which is derived from the energy absorption capacity up to the deflection of L/150 of the beam span and the initial peak load, is frequently used to assess the flexural performance of CCFS-PP. As a result, using Eq. (3), the value of $R_{T,150}$ could be determined from the load deflection curves obtained from the observations.

$$R_{T,150} = \frac{T_{150}}{P_1 \times \left(\frac{L}{150}\right)} \times 100\% \quad (3)$$

A high toughness material is one with an $R_{T,150}$ value of more than 100%, and is linked to $P_P > P_1$. $R_{T,150}$ values, on the other hand, are less than and larger than 100% for deflection softening ($P_P = P_1$) and deflection hardening ($P_P > P_1$) behaviors, correspondingly.

4.3. Results and discussions of CCFS-PP

4.3.1 Behavior of load-deflection curves

Figure 37 a-e presents the load-deflection curves for CCFS-PP beams with different polypropylene fiber contents varied from 0-2.0%. All figures obviously depict the fly ash affects the load-deflection response at the same polypropylene fiber content, which indicates different flexural performances in term of first peak strength, peak strength, peak strength ratio, residual strength ratio, ductility index and toughness. Figure 37a shows the results of CCFS-PP beams without polypropylene fiber reflecting the brittle behavior and deflection softening manner. By adding 0.5% of polypropylene fiber content, Figure 37b shows the improvement of the ductile behavior and the increment of Residual strength ratio at a deflection of L/150 (RSR150). Figure 37c presents the test data of the CCFS-PP beam mixed at 1% of polypropylene fiber. The test results show that Group B with 25% of fly ash and 75% of Portland cement has the P_{150} data as good as the test results of the controlled Group A with 100% Portland

cement. Figure 37d shows the test results of CCFS-PP beams with 1.5% of polypropylene fiber. Test data of group B is P_{150} higher than the controlled results of group A, showing the ductile behavior and defection hardening style. However, Figure 37e shows the test data of the controlled sample group A has the defection hardening behavior and P_{150} data higher than other test results. Therefore, the research found the optimum polypropylene fiber content of 1.5% for Group B (25% of fly ash and 75% cement).

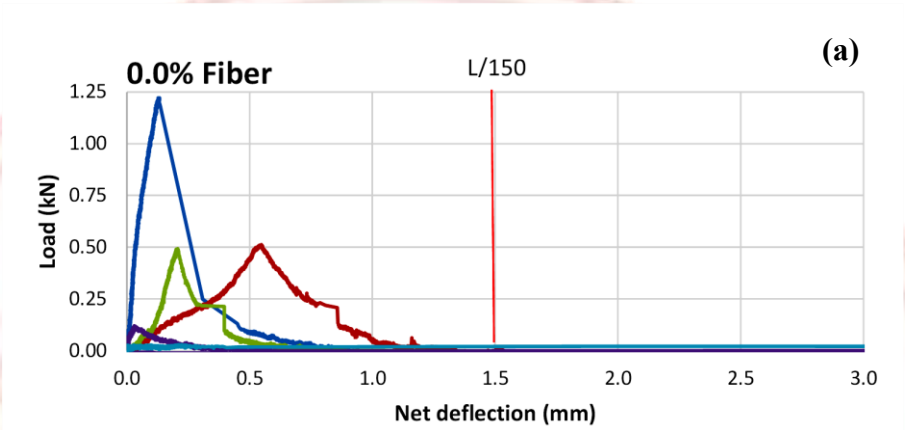

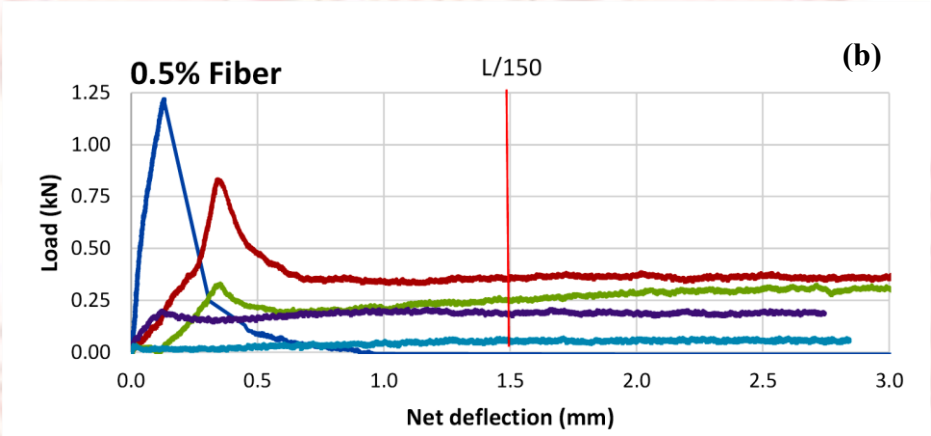

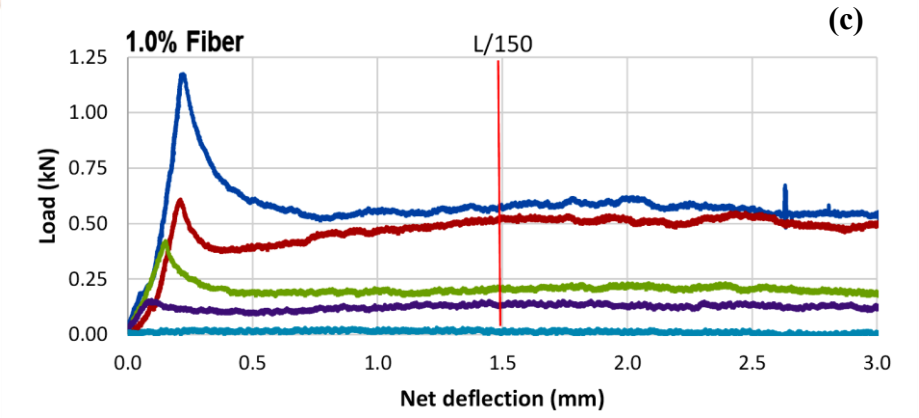

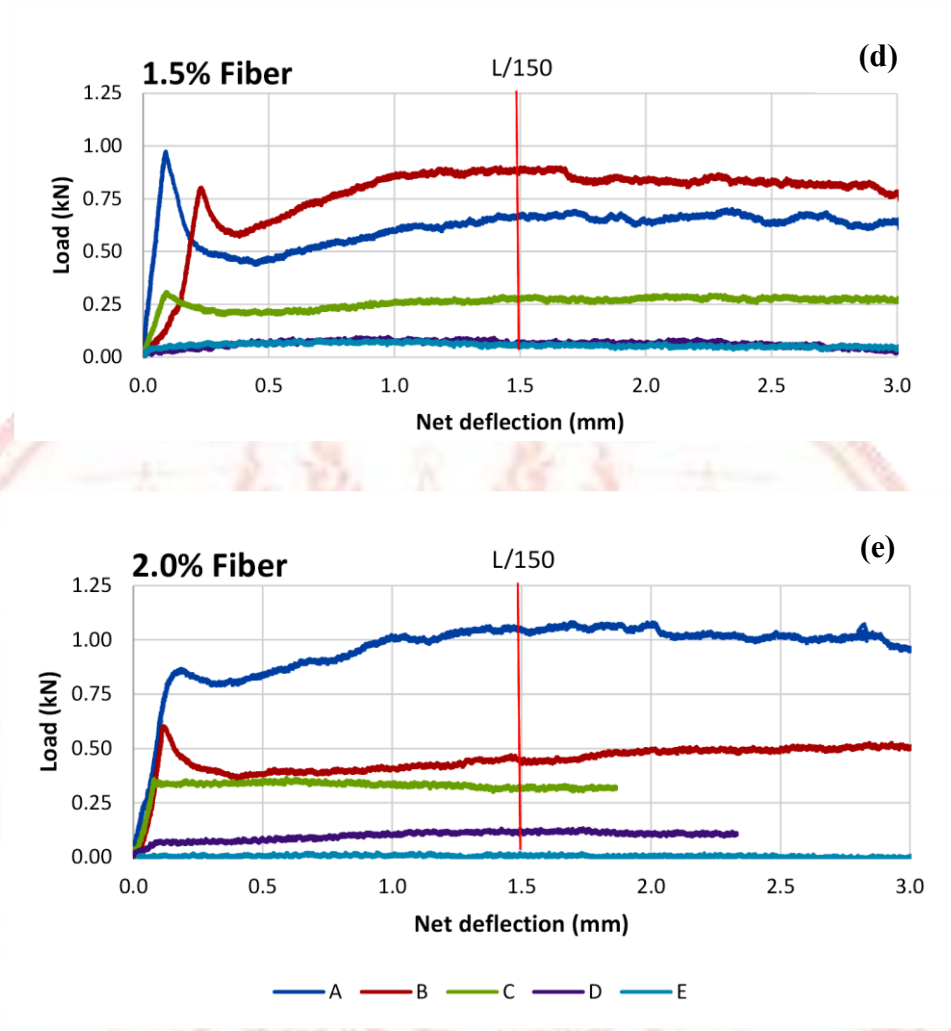

Figure 37 Load-deflection curves for CCFS-PP with different fiber contents

(a) 0% (b) 0.5% (c) 1.0% (d) 1.5% and (e) 2.0%

4.3.2 First peak strength (f_1) and peak strength (f_P)

The first crack's stress, or f_1, was brought on by bending along the bottom face of the beam. The impact of fiber content on the values of f_1 and f_P is depicted in Figures 38 and 39. The CCFS-PP has f_1 values between 0.01 and 0.43 MPa. Because the strength of the cement, sand, and fly ash from MSW matrix, rather than the fiber bridging capacity, determines f_1 for CCFS-PP, an increase in fiber content has a minor effect (Sukontasukkul et al., 2010). so that all CCFS-PP, with the exception of CCFS-PP Group C and CCFS-PP Group E, which have fiber concentrations ranging from 0.5 to 1.5%, have f_1 values that are hardly different from one another. While the fiber content of all CCFFS samples increases, so does the total f_P with the exception of CCFS-PP Group D and CCFS-PP Group E.

4.3.3 Peak strength ratio (PSR)

Peak strength ratio (PSR), which is equal to f_P divided by f_1, is used in this study to compare the hardening levels of each CCFS-PP. This ratio shows how strong the fiber can get following the occurrence of the first crack. More specifically, values of PSR = 1 and PSR > 1 imply responses that are alternately softening and hardening; the greater the PSR, the more hardening has occurred. According to Figure 40, CCFS-PP Group B and CCFS-PP Group D gave PSR increases with increasing fiber content and gave the greatest PSRs of 1.1 and 1.86, respectively, at 1.5 and 2.0% fiber content. In contrast, CCFS-PP Group C and CCFS-PP Group E showed an optimal fiber concentration of 0.97 with maximum PSR of around 2.3. As a result, CCFS-PP Group E has up to 2.45 times the hardness of CCFS-PP. Group C and CCFS-PP Group D (fiber contents 0.5%). With reported values of 1.10 and 1.86, respectively, CCFS-PP Group B (fiber contents 1.5%) and CCFS-PP Group D (fiber contents 2.0%) exhibited PSR better than 1.0 for specified fiber contents. The PSR for completely developed softening in CCFS-PP Group C, however, was unaffected by the fiber content because it was always reported as 1.

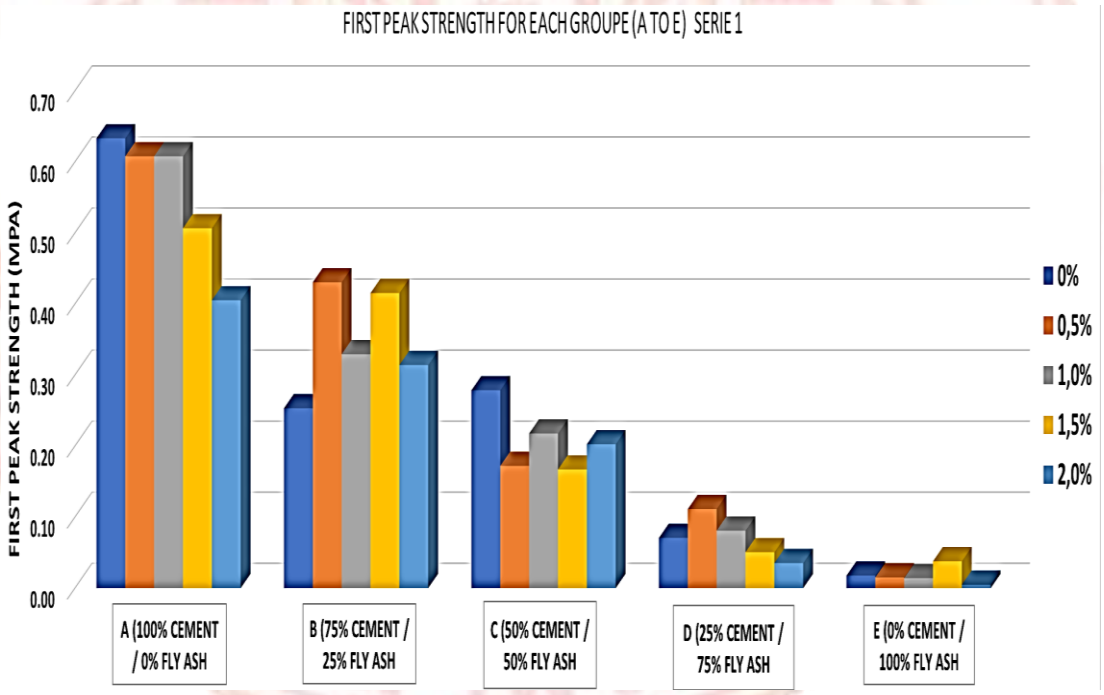

Figure 38 First peak strength (f_1) at different fiber contents and fly ash from WSW replacement to cement ratio

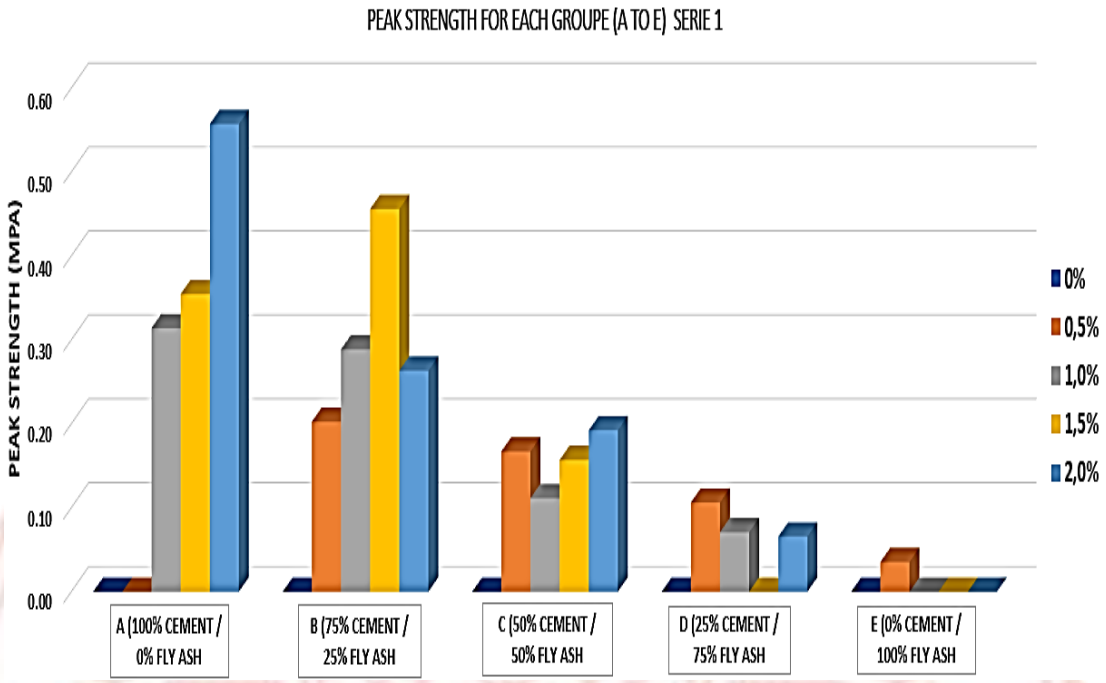

Figure 39 Peak strength (f_P) at different fiber contents and fly ash from WSW replacement to cement ratio

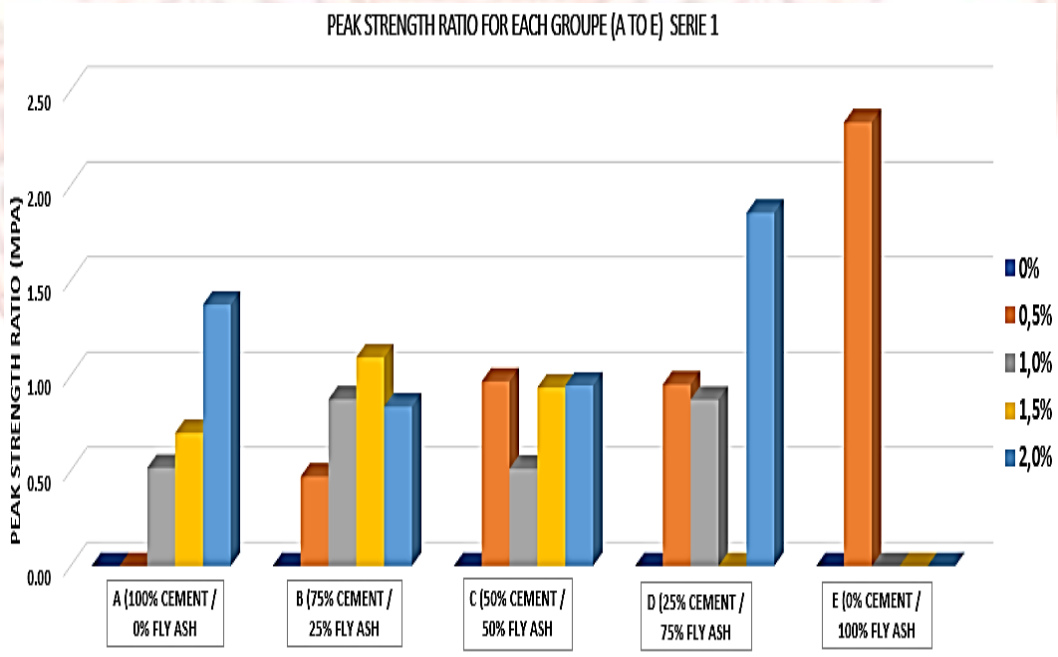

Figure 40 Peak strength ratio (PSR) at different fiber contents and fly ash from WSW replacement to cement ratio

4.3.4 Residual strength ratio deflection L/150 (RSR150)

This research also introduces a residual strength ratio at a deflection of L/150 (RSR150) to test the fiber's capacity to support the residual load from the initial fracture site to the deflection of L/150 in addition to PSR. RSR150 is therefore equal to f150 divided by f1. Additionally, this ratio suggests how well fiber performs in preserving CCFS-PP's hardening at high deflection. According to the findings for CCFS-PP Group B, a fiber concentration of 1.5% is ideal for achieving the highest RSR150 values, which is roughly 1.10. But for CCFS-PP Group A and CCFS-PP Group D RSR150 rose as the fiber content increased, producing the greatest values at 2.0% fiber content for each of 1.38, and 1.71, respectively. Among the various fiber types, it appears that CCFS-PP Group D was the most successful in terms of RSR150 considering the 2.0% fiber content, and CCFS-PP Group E which is 0.5% fiber content as shown in Figure 41.

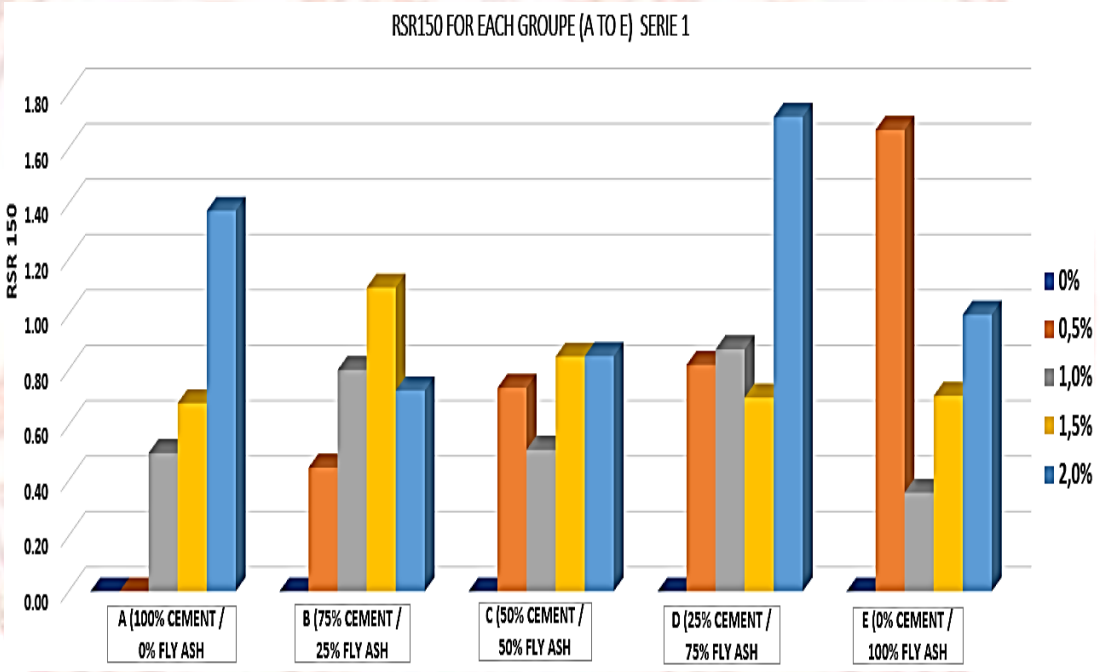

Figure 41 Residual strength ratio at a deflection of L/150 (RSR150) at different fiber contents and fly ash from WSW replacement to cement ratio

4.3.5 Ductility index (DI)

The data indicates that before the polypropylene fibers can support a portion of the load, there needs to be a significant amount of deflection. Unquestionably, ductility is the capability to absorb inelastic energy without reducing load capacity. increased ductility is the result of the same system's increased inelastic energy absorption. It goes without saying that adding fiber greatly increases the system's ductility from this

perspective. For Figure 42, the optimal fiber contents for CCFS-PP Group A, CCFS-PP Group C, and CCFS-PP Group E are 1.5 % and CCFS-PP Group B 2.0 %, respectively, with maximum DI values of around 17, 23, 24 and 24.17, respectively. DI values for CCFS-PP Group C tend to decline and rise with increasing fiber levels, yielding values of 23 to 1 at 0.5-2.0% fiber contents. When creating CCFS-PP with exceptionally high ductility, the CCFS-PP Group A, CCFS-PP Group C and CCFS-PP Group E at 1.5% fiber content and CCFS-PP Group B at 2.0% fiber content are acceptable.

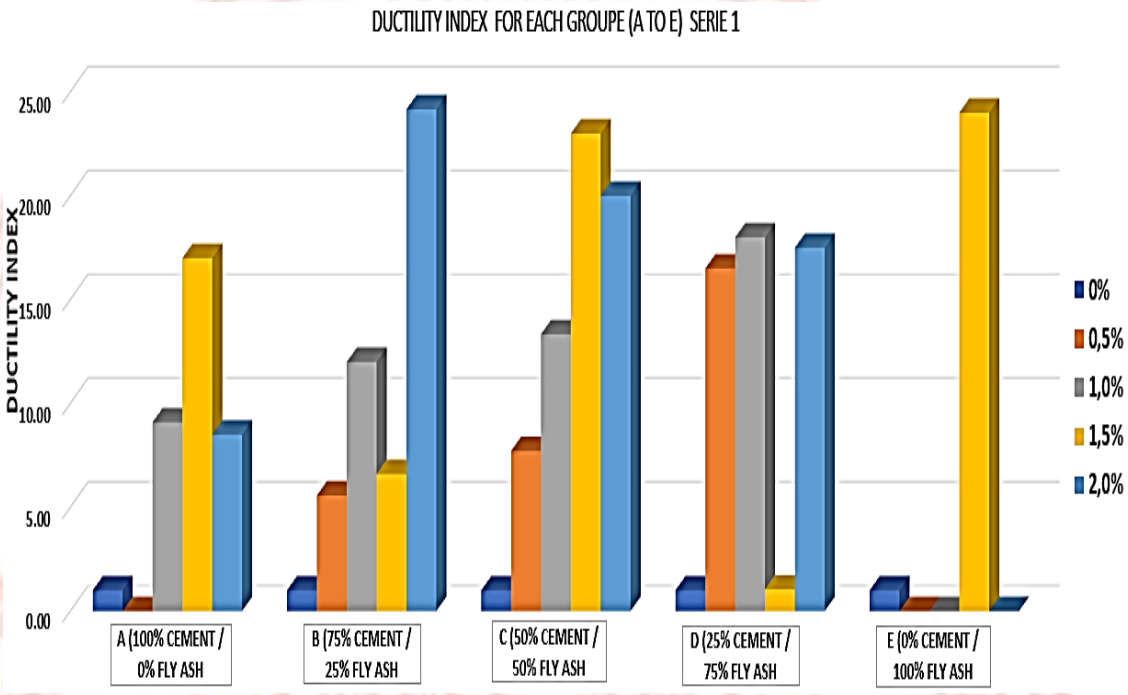

Figure 42 Ductility index (DI) different fiber contents and fly ash from WSW replacement to cement ratio

4.3.6 Toughness deflection L/150 (T_{150})

This research has taken consideration of the toughness at a 1.5 mm deflection point equivalent to L/150 (T_{150}). The findings demonstrate that, as shown in Figure 43, the fiber content has an impact on the T_{150} of CCFS-PP. Because the fiber bridging capacity at the fracture surfaces has improved, higher fiber contents have a higher T_{150}. In terms of toughness, CCFS-PP beams with deflection-hardening behavior outperformed those with deflection-softening behavior because they absorbed more energy following cracking (Hannawi et al., 2016).

As a result, when compared to CCFS-PP with fiber content, CCFS-PP Group A and CCFS-PP Group B can absorb the most $T_{150,}$ whilst CCFS-PP Group E produced the least T_{150}. T_{150} values from CCFS-PP Group A and CCFS-PP Group B ranged from 1.18 to 1.84 N-m and 0.74 to 1.25 N-m, correspondingly And, T_{150} values from CCFS-PP Group C, CCFS-PP Group D, and CCFS-PP Group E were comparable

(between 0.01-0.81 N-m). Values between 0.74 to 1.25 N-m were given by CCFS-PP Group B. T_{150} for CCFS-PP Group B has a value of 1.25 N-m. Therefore, the CCFS-PP Group B increased the T_{150} of CCFS-PP by up to 2.5 and 1.63 times, for the 0.5% and 1.5% fiber content.

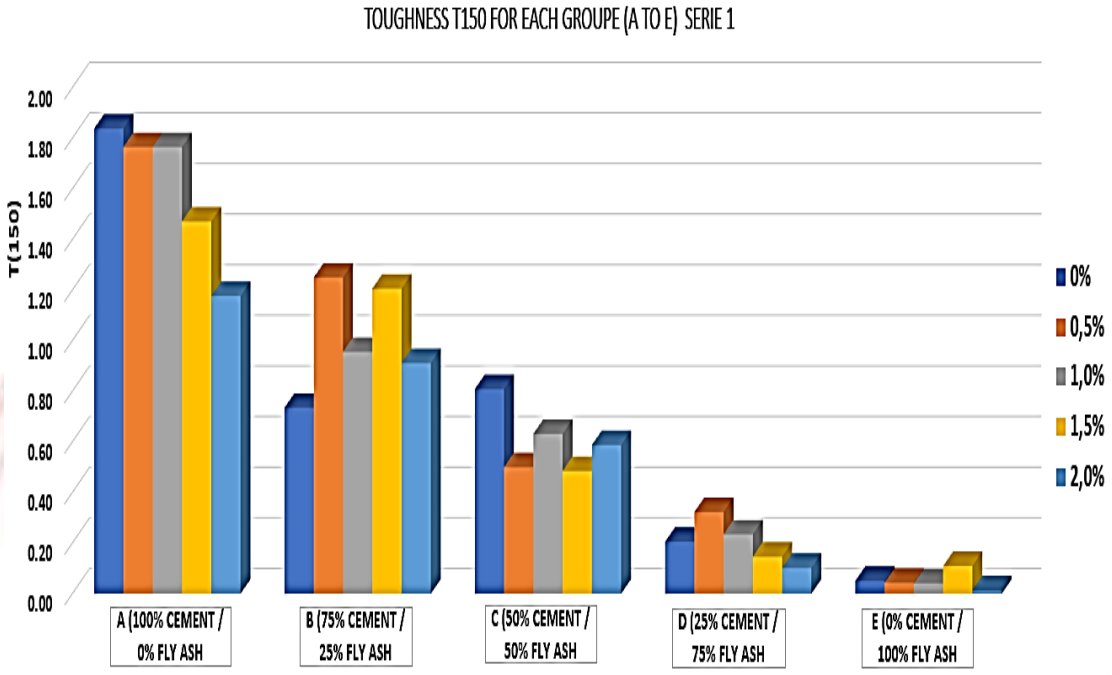

Figure 43 Toughness at a deflection of L/150 (T_{150}) at different fiber contents and fly ash from WSW replacement to cement ratio

4.3.7 Bender Element Test

The stiffness of CCFS-PP specimen is determined in terms of initial shear modules, G_0, using the bender element test, which measures the shear wave velocity, Vs, in accordance with ASTM D8295-19 (ASTM D8295−19, 2019). Using a combination of regular Portland cement and fly ash that experienced a pozzolanic reaction through shear modulus, this technique was utilized to calculate strength development while taking Vs into account for all CCFS-PP specimens. The shear wave test technique is illustrated by setting up the apparatus to produce a shear wave signal. One signal cable equipped with CCFS-PP specimens sends the sine pulse signal to the transmitter bender element after the function generator transforms the analog input into a sine pulse signal. CCFS-PP specimens will allow the signal to pass through them. The signal passes via the receiver bender element, into the oscilloscope, and then into the computer via a second line that is directly linked to the oscilloscope. This creates a pattern of the signal passing through the CCFS-PP specimens. The shear wave measuring example is shown in Figure 44. A sine pulse shear wave frequency produced by sine waves passing through CCFS-PP specimens is broadcast back to the signal originating computer via an oscilloscope transmitter via a sine pulse signal

pattern. As advised by the manufacturer, a digital to analog converter is used to provide a 10 V amplitude signal at a frequency of 10 kHz in order to create sine pulse waves. The shear wave signal passing through the CCFS-PP specimen is received by the receiver bender element after the wave has passed through its height.

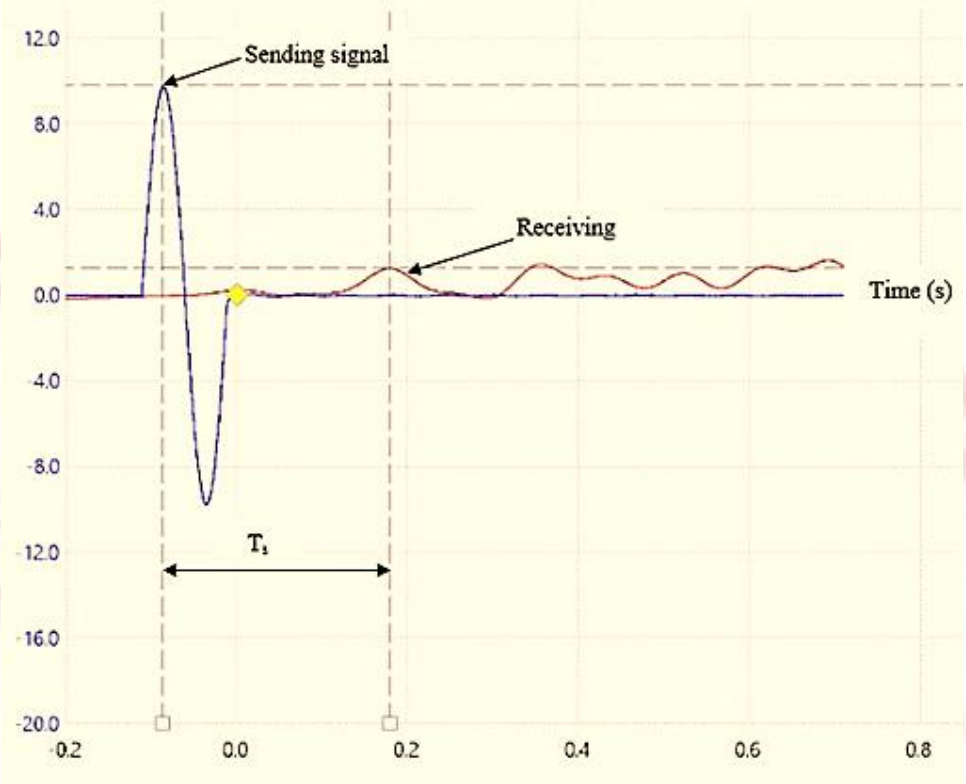

Figure 44 Samples of measurements for shear waves

The duration of a wave passage from the transmitter to the receiver is known as the shear voyage. Examining the shear wave's travel length the wave entering wave 1's highest point in Figure 44 serves as the beginning of the journey time count from transmitting to wave 2's peak, which marks the conclusion of the receiving wave's voyage. The following Equation (4) may thus be used to find V_s (represented as V_s-V_h) combined (ASTM D1633-17, 2017; ASTM D8295−19, 2019). In this case, Vs is the shear wave velocity expressed in meters per second.

$$V_s = (L_i - L_b)/(T_s - T_c) \quad (4)$$

The effect of FA content with the change in V_s on the CCFS-PP mixed FA content of 5, 10, 15, 20, and 25% are shown in Figure 45. The maximum V_s result at 28 days was found to be 500.67 m/s at 5% FA. This indicates the tendency that an

increase in FA content will result in a decrease in V_s, so it is advised that 5% FA be used for the CCFS-PP mixing.

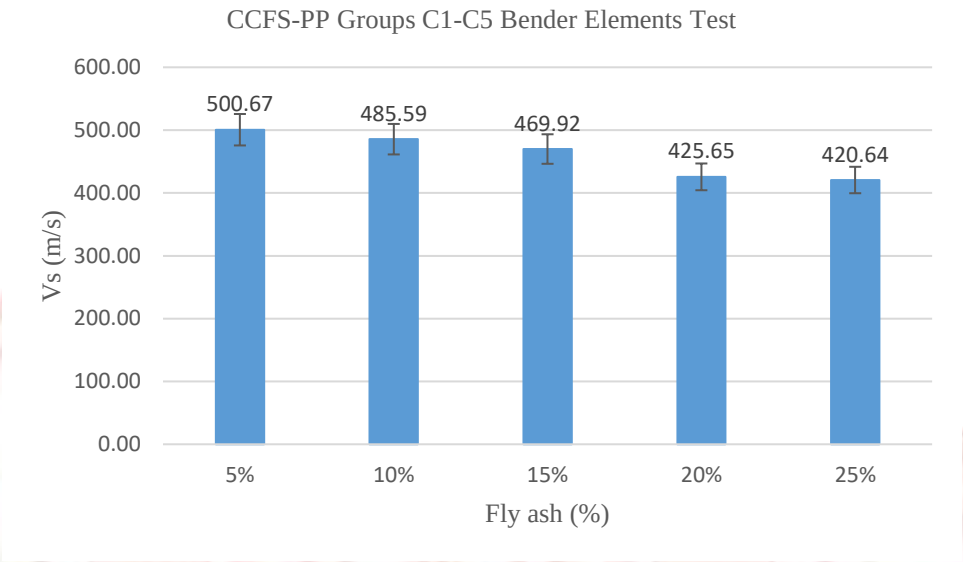

Figure 45 Relationship V_s and FA content of CCFFS-PP Groups C1-C5

The effect of fiber content on the CCFFS-PP mixed in terms of fiber content of 0.5, 1.0, 1.5, 2.0, and 2.5% is shown in Figure 46 as a function of V_s. The highest Vs result of 448.83 m/s was recorded at 0.5% PP after 28 days. Therefore, it is advised to utilize 0.5% PP for the CCFFS-PP mixture. It demonstrates how increasing the amount of PP fiber lowers the Vs.

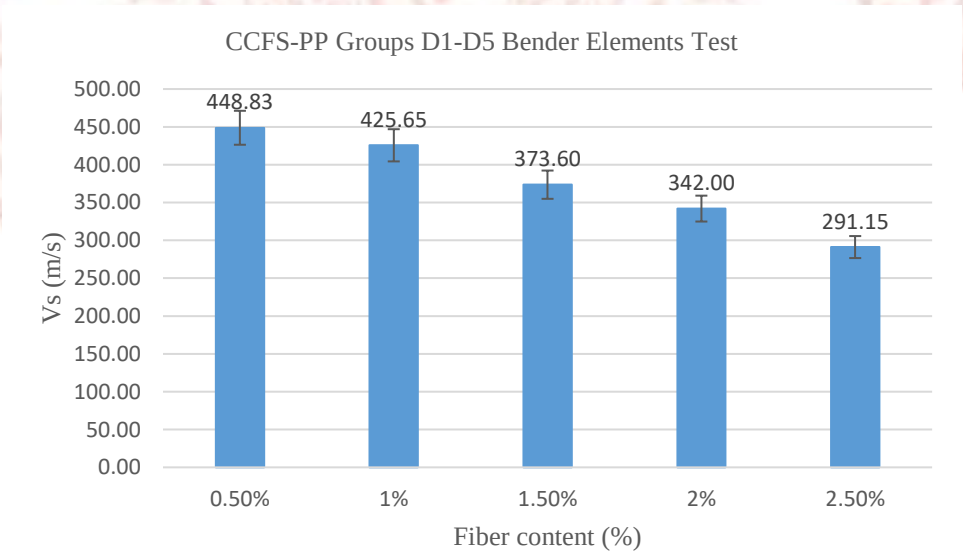

Figure 46 Relationship V_s and Fiber content of CCFFS-PP Groups D1-D5

4.3.8 SEM image analysis of CCFS-PP

The effect of fiber type on the crack patterns and crack widths of CCFS-PP beams. Macroscale crack behavior, which is visible to the unaided eye, is an indication of this study. To study the micro-scale interaction mechanisms between the fiber surface micro-scale behavior and the cement-sand matrix interface, however, microstructural observation is necessary. This intricate process is impacted by various factors such as the shape, surface roughness, and length of the embedded fiber. In order to support the macro-scale test data, it is interesting and reasonable to interpret comparative flexural performances based on a micromechanical approach as presented in the preceding sections. The comparative interfacial bond nature for fiber was characterized in this study using SEM observation. The matrix and fiber are first bonded to one another along the whole fiber length by chemical or physical adhesion before the flexural test. According to (Hannawi et al., 2016), the SEM images displayed the hydrophobic and synthetic polyolefin and polypropylene fibers. Moreover, SEM analyses verify the presence of $CaCO_3$ binding sand particles together and the enhancement of the physical strengths of the sand soil samples (Iamchaturapatr et al., 2021). Furthermore, the use of SEM and X-ray diffractometer (XRD) to identify the $CaCO_3$ precipitation found in biocemented sand were discussed. There are identified potential benefits and anticipated uses for biocemented soil improvement (Piriyakul & Iamchaturapatr, 2013). As a result, partially separated interfacial zones were seen because the hydrophobic synthetic fiber was able to, more or less, prevent water required for cement hydration from penetrating the cement sand specimens' structure during the curing period and increase the number of air bubbles present in the interfacial transition zone. The reduced hardening-deflection response and lower peak strength were caused by this study. So, the interaction mechanism of fiber-matrix interface is presented by SEM image as shown in Figures 47-51. Figure 47 shows the SEM image of CCFS-PP in Group A which consists of 100% OPC and no fly ash. The result shows the bonding between cemented sand matrix and PP fiber due to the hydration reaction. Similarly, Figure 48 expresses the SEM image of sample in Group B which are 75% OPC and 25% fly ash. The hydrophobic zone occurred on the fiber surface, resulting in less bonding and UCS. Moreover, the hydrophobic zone is more happen in Group C to Group E since the mixing ratios with fly ash is increased as shown in Figures 49 – 51. The SEM image of sample in Group E which is 100% fly ash and no OPC shows the severe problem of hydrophobic zone showing no bonding on the PP fiber surface and poor UCS results. It was noted that the microstructure of the polypropylene fiber surface, fly ash – cement – sand matrix, hydration products and several interfaces. By adding a small amount of fiber content, the bond strength between fly ash from MSW – cement – sand matrix and the polypropylene fiber is created at the polypropylene fiber surface due to the hydration products and its crimped-shaped fiber, showing the bonding manner.

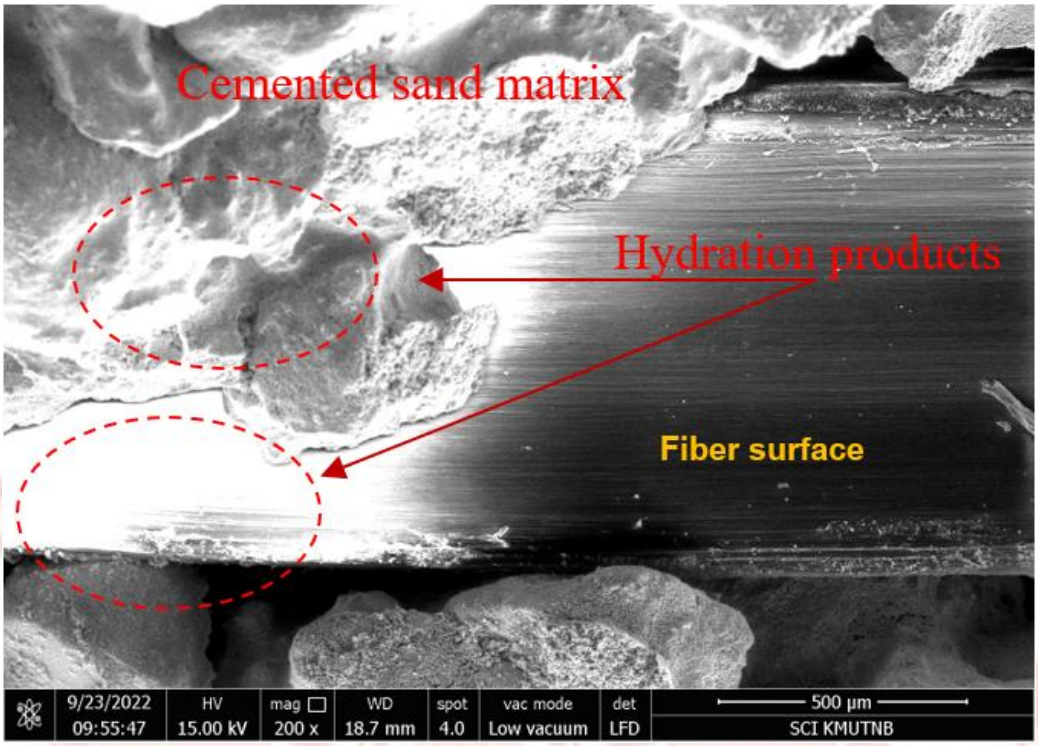

Figure 47 SEM image of the sample A

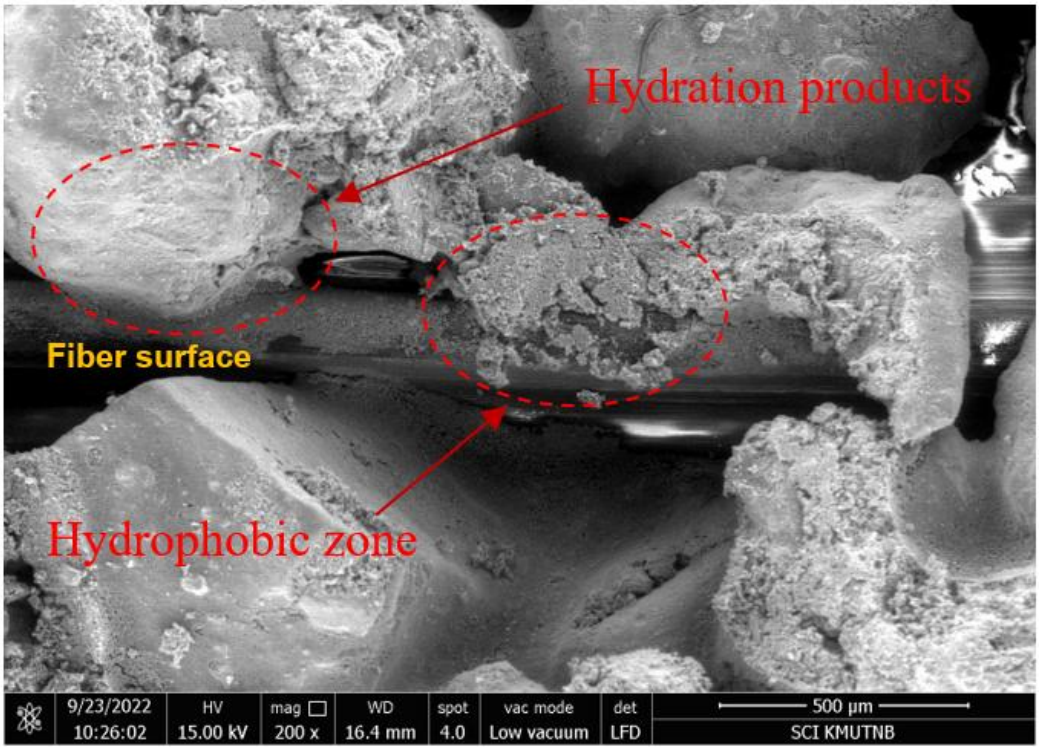

Figure 48 SEM image of the sample B

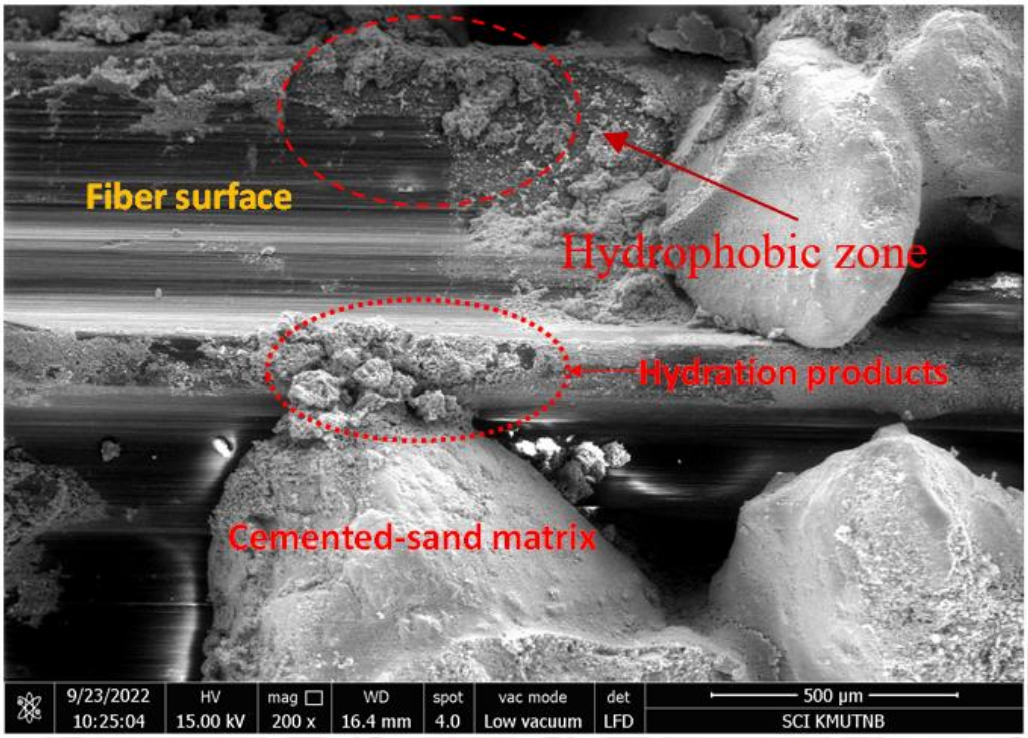

Figure 49 SEM image of the sample C

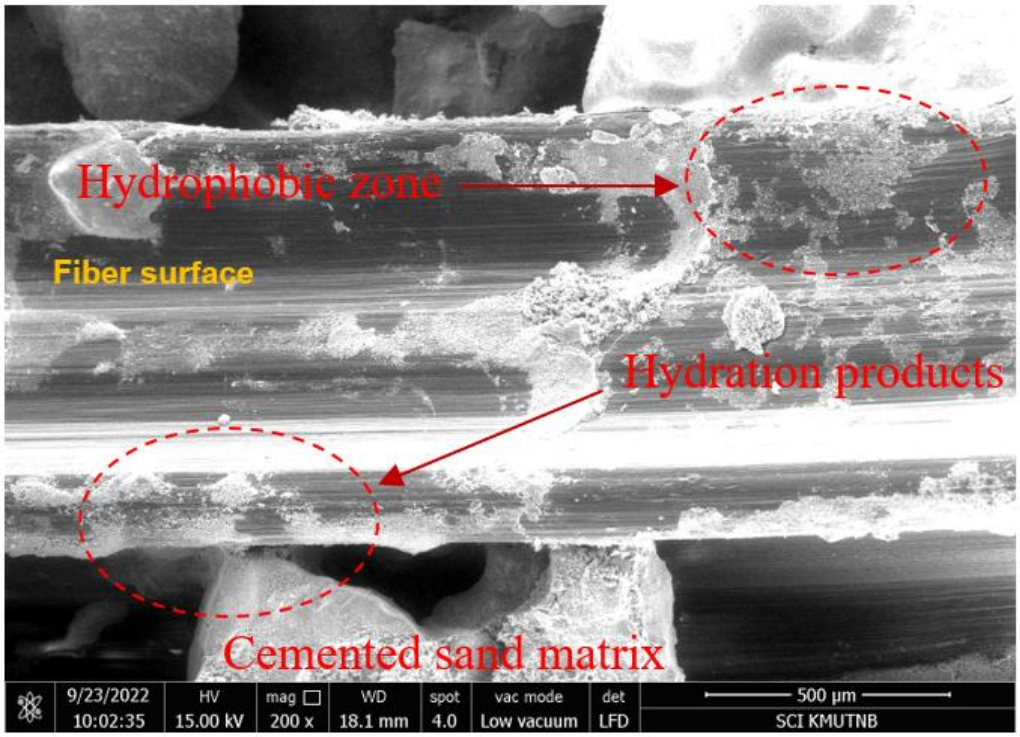

Figure 50 SEM image of the sample D

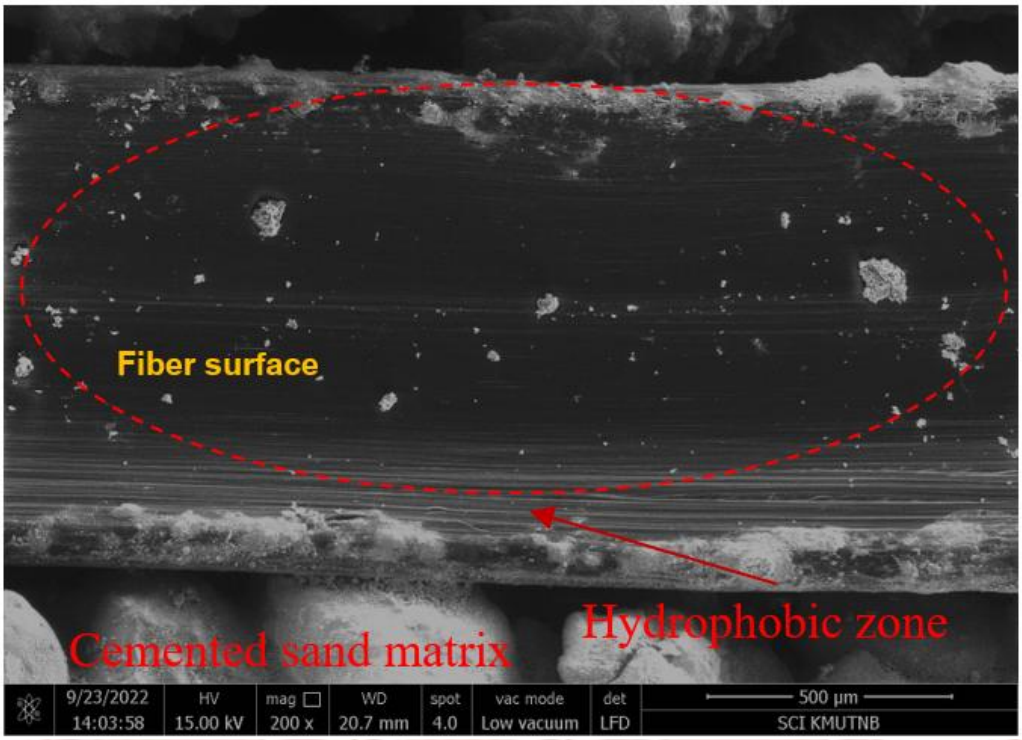

Figure 51 SEM image of the sample E

4.4. Experimentation of CCFS-GF specimens

The specimens performed an unconfined compressive strength (UCS) test in accordance with ASTM D1633–17(ASTM D1633-17, 2017) after 7-, 14-, 28-, 60- and 90-days. The applied loads were measured using a 50 kN load ell. An electric motor controlled the compression rate of 0.05 mm/min, and the test ended at a net displacement of 3 mm or failure. Then, the data logger then gathered enough data points to create curves, which were then utilized to accurately predict each CCFS-GF's dependable UCS and interpret the test findings.

4.5. The CCFS-GF's unconfined compression behavior parameters

According to ASTM D1633–17 (ASTM D1633-17, 2017), the UCS test is performed here for comparison purposes. Even though this type of testing is destructive, it has many benefits, like time savings. In experimenting with FA samples. Thus, the CCFS-GF focused on each parameter including effect of FA content, effect of glass fibers content, effect of glass fibers length, effect of aging, relationships of unconfined compressive strength and curing time.

4.6. Results and discussions of CCFS-GF

4.6.1 Effect of fly ash (FA) and cement content

Effect of cement content on compressive strength development with the same ratio of FA and glass fiber. Figure 52 respectively present shows a comparison of the development of uniaxial compression strength with cement ratios of 2, 4, 6, 8, and 10%. And, using FA at a ratio of 20% of cement and using glass fibers length 6 mm. at a ratio of glass fibers of 1% using a curing period of 28 days. From the experiment, it was found that the development of compressive strength with a greater cement ratio directly resulted in a large increase in compressive strength corresponding to the cement volume ratio. From the ACI 230.1R-09 standard (ACI 230.1R-09, 2009) (in category A-1-b, SP group, cement content is between 5% -8%). The compressive strength value of subgrades and subbases for concrete pavements is set at around 345-690 kPa (ACPA Subgrades, 2007). The results of the experiment from the sample showed that the cement ratio that passed the standard was in the range of 6 % and 8 %. Therefore, the cement ratio was chosen at 8 % because it can provide the best compressive strength according to the above standards.

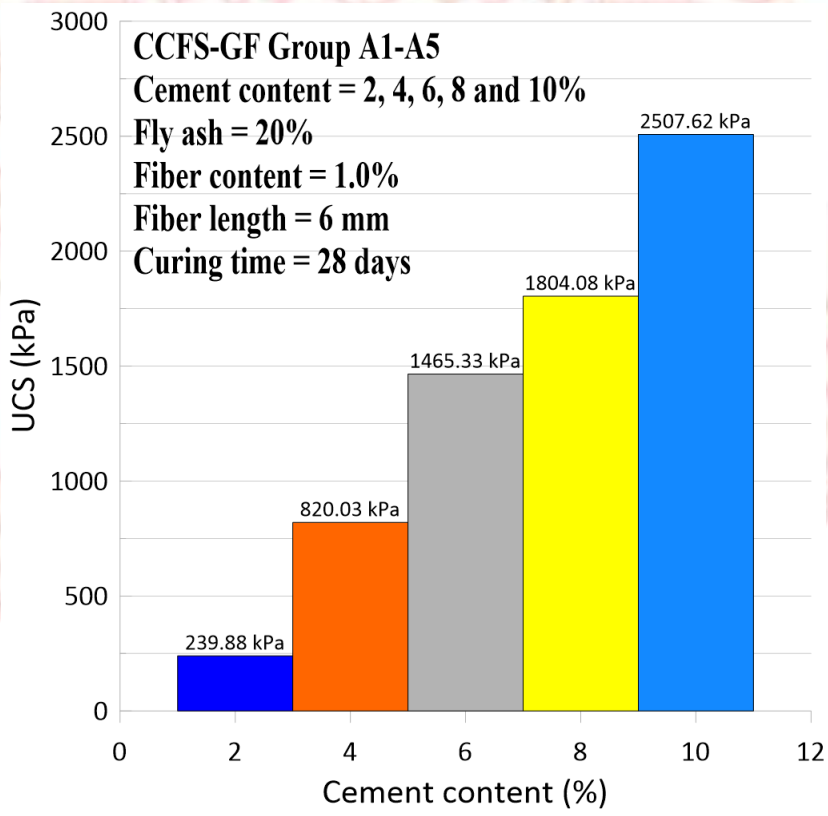

Figure 52 Bar chart Group A showing the relationship between UCS VS cement content

4.6.2 Effect of glass fiber content

Effect of glass fiber content on compressive strength development with the same ratio of cement and FA. Figure 53 respectively present shows a comparison of the development of uniaxial compression strength with glass fibers ratios of 0.5, 1.0, 1.5, 2.0, and 2.5 %. And, using cement at ratio of 8 % with FA at a ratio of 20 % of cement and using glass fibers length 6 mm by using a curing period of 28 days. From the experiment, it was found that the development of compressive strength with an increasing ratio of glass fibers resulted in a higher value of compressive strength. From the experiment, it was found that the compressive strength was improved with an increase in the glass fiber ratio. Resulting in higher compressive strength values. The optimum glass fiber ratio is 1 %, although increasing the glass fiber ratio does not result in an increase in compressive strength. But it makes the compressive strength decrease. Therefore, mixing glass fibers in a higher ratio does not increase the compressive strength as well.

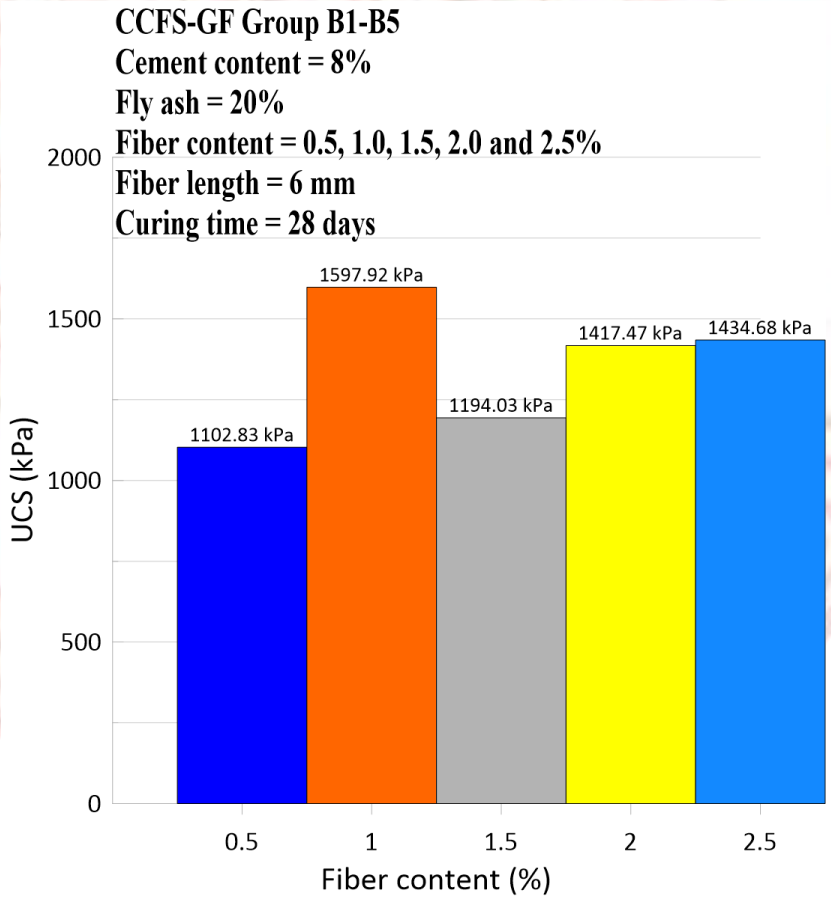

Figure 53 Bar chart Group B showing the relationship between UCS VS fiber content

4.6.3 Effect of glass fibers length

Effect of glass fiber length on compressive strength development with the same ratio of cement and FA. Figure 54 respectively present shows a comparison of the development of uniaxial compression strength with glass fibers length of 3, 6 and 12 mm. And, using cement at ratio of 8 % with FA at a ratio of 20 % of cement and using glass fibers content 1% by using a curing period of 28 days. From the ACI 230.1R-09 standard (ACI 230.1R-09, 2009)(in category A-1-b, SP group, cement content is between 5 %-8 %). The compressive strength value of subgrades and subbases for concrete pavements is set at around 345- 690 kPa (ACPA Subgrades, 2007). Therefore, a glass fiber length of both 3 and 6 mm can be chosen because it meets the above standards, but the result of 6 mm is better.

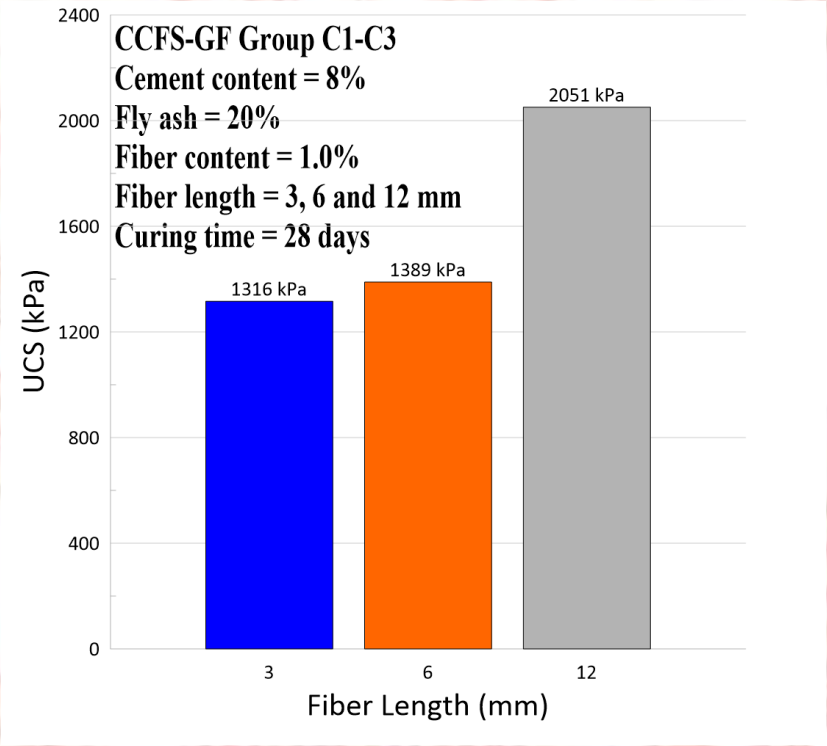

Figure 54 Bar chart Group C showing the relationship between UCS VS fiber length

4.6.4 Effect of curing time

Effect From the experiment on the development of compressive strength, it was found that increasing the volume ratio of FA to the curing period by using the same volume ratio of cement and glass fibers. Figures 55 to 59 respectively present shows a comparison of the development of uniaxial compression strength with FA at a ratio of 5, 10, 15, 20, 25 and 30 % of cement. And, using cement at ratio of 8 % with glass fibers content 1 % by using a curing period of 7, 14, 28, 60 and 90 days. From the ACI 230.1R-09 standard (ACI 230.1R-09, 2009) (in category A-1-b, SP group, cement content is between 5 %-8 %). The compressive strength value of subgrades and subbases for concrete pavements is set at around 345- 690 kPa (ACPA Subgrades, 2007). Therefore, a glass fiber length of 6 mm can be chosen because it meets the above standards. It was noted that the ash content of 20 % and 25 % in the curing period of 28 days or more was most suitable. At the same time, it is still able to pass the above standards with a compressive strength value not lower than the standard value.

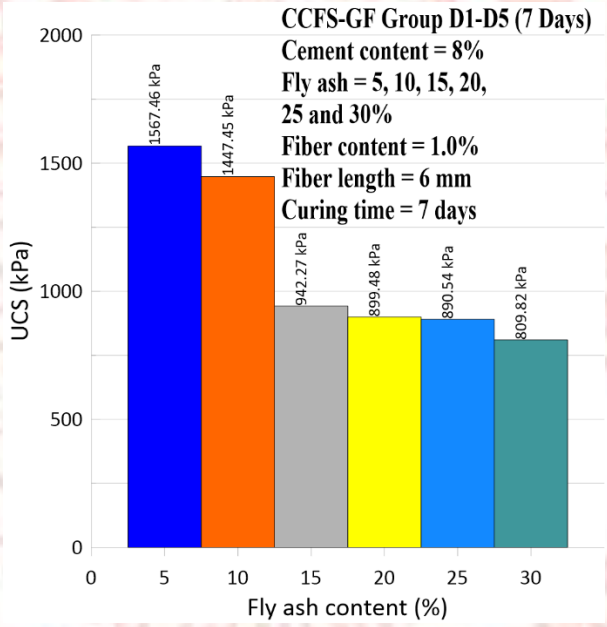

Figure 55 Bar chart Group D (7days) showing the relationship between UCS VS fly ash content

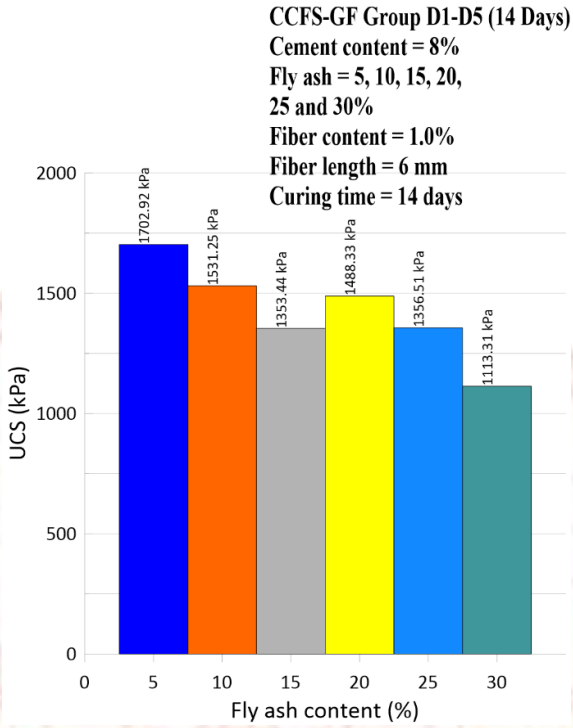

Figure 56 Bar chart Group D (14days) showing the relationship between UCS VS fly ash content

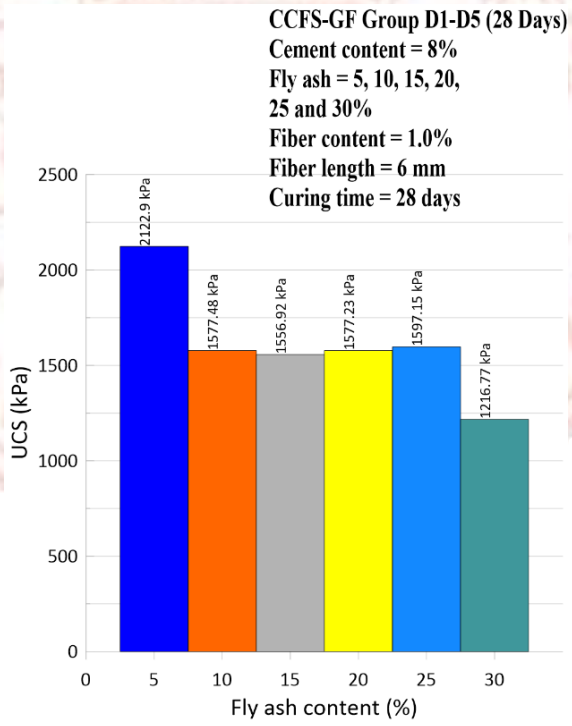

Figure 57 Bar chart Group D (28days) showing the relationship between UCS VS fly ash content

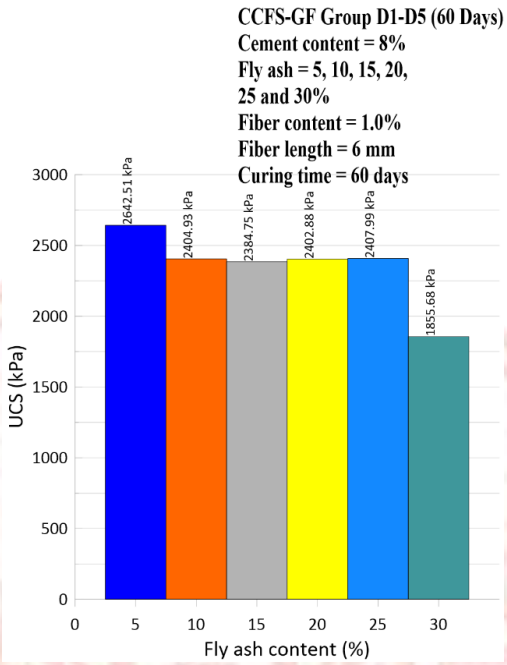

Figure 58 Bar chart Group D (60days) showing the relationship between UCS VS fly ash content

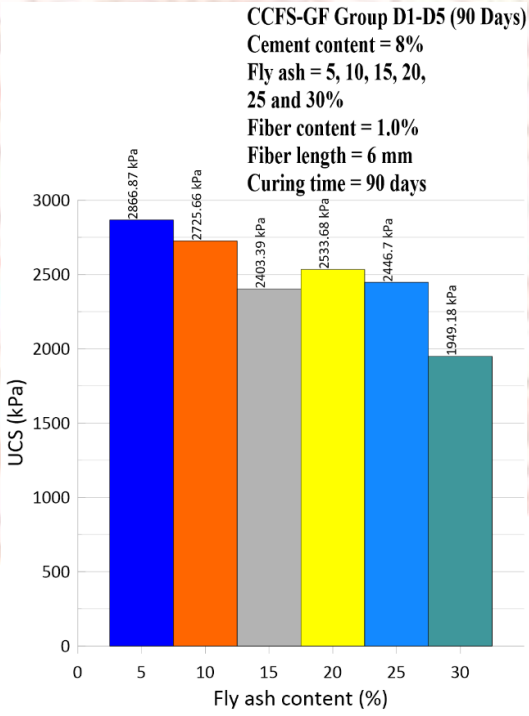

Figure 59 Bar chart Group D (90days) showing the relationship between UCS VS fly ash content

4.6.5 Relationships of unconfined compressive strength and curing time

From the experiment to develop compressive strength, it was found that by increasing the ratio of the amount of glass fibers to the curing time with the same ratio of the amount of cement and FA. Figures 60 to 64 respectively present shows a comparison of the development of uniaxial compression strength with glass fibers ratios of 0.5, 1.0, 1.5, 2.0, and 2.5 %. And, using cement at a ratio of 8% with FA at a ratio of 20% of cement and using glass fibers length 6 mm by using a curing period of 7, 14, 28, 60 and 90 days. So, it was confirmed that the sample had the highest compressive strength at a glass fiber ratio of 1% during the curing period of 7, 14, 28, 60 and 90 days. The curing period of 90 days gives the highest compressive strength. Therefore, the optimum ratio of glass fiber volume and curing time is a curing time of 90 days with a glass fiber ratio of 1%.

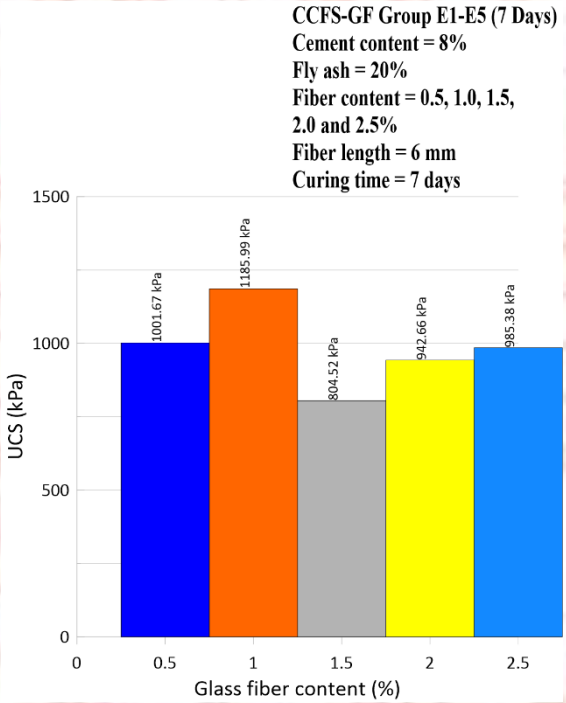

Figure 60 Bar chart Group E (7days) showing the relationship between UCS VS Glass fiber content

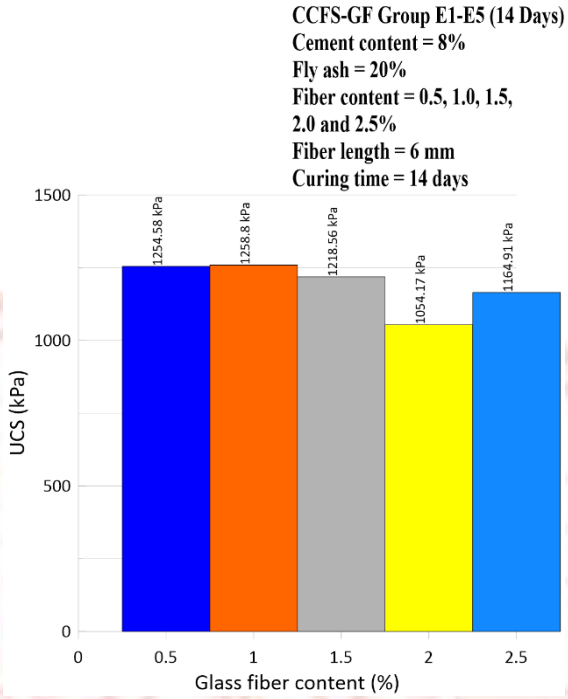

Figure 61 Bar chart Group E (14days) showing the relationship between UCS VS Glass fiber content

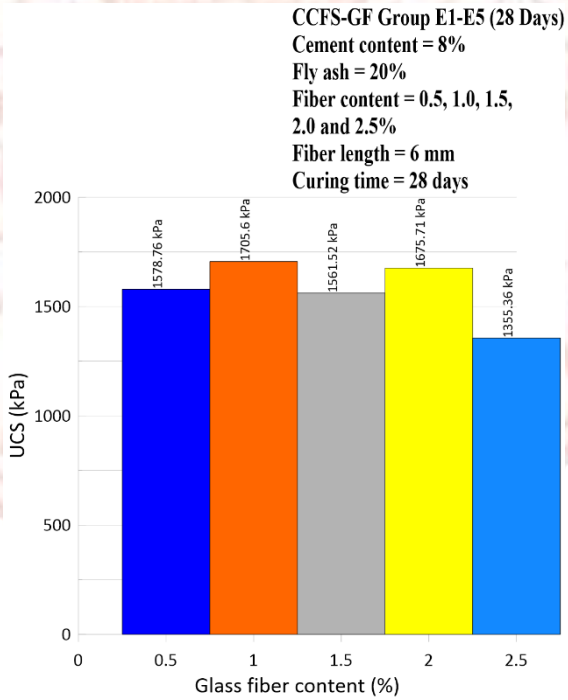

Figure 62 Bar chart Group E (28days) showing the relationship between UCS VS Glass fiber content

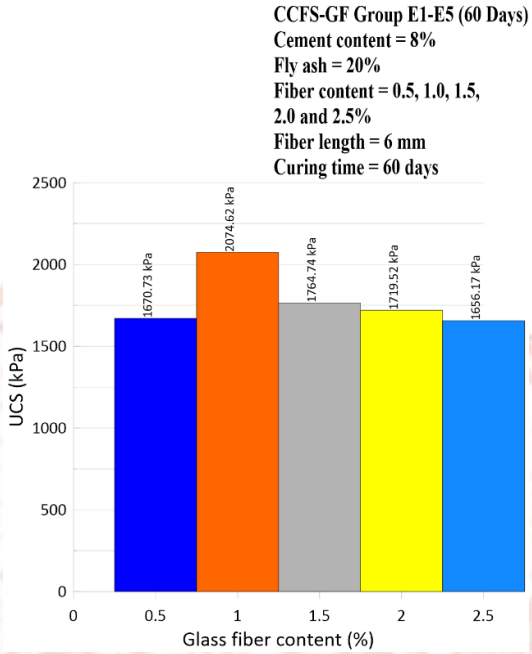

Figure 63 Bar chart Group E (60days) showing the relationship between UCS VS Glass fiber content

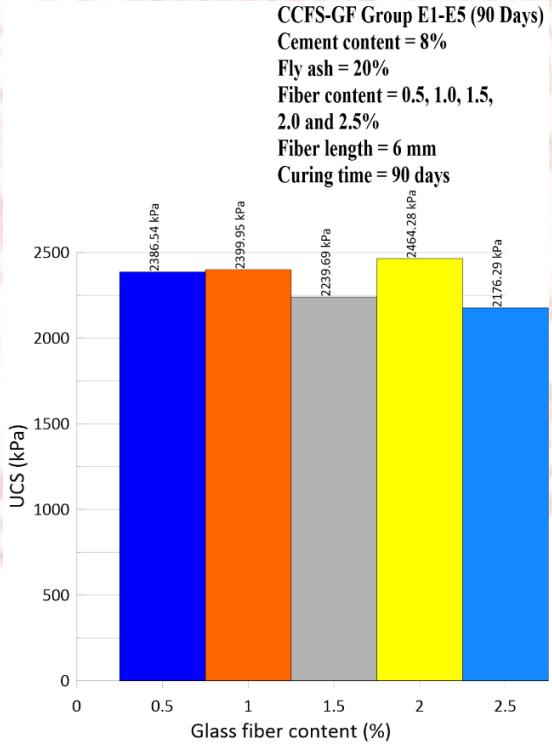

Figure 64 Bar chart Group E (90days) showing the relationship between UCS VS Glass fiber content

4.6.6 SEM image analysis of CCFS-GF

The interaction mechanism of glass fiber-matrix interface is presented by SEM image as shown in Figures 65 and 66. The microstructure of the glass fiber surface, FA with cement sand matrix, hydration products and several interfaces. By adding a small amount of glass fiber content, the bond strength between FA with cement sand matrix and the glass fiber is created at the glass fiber surface due to the hydration products and its crimped shaped glass fiber, showing the compressive strength behavior.

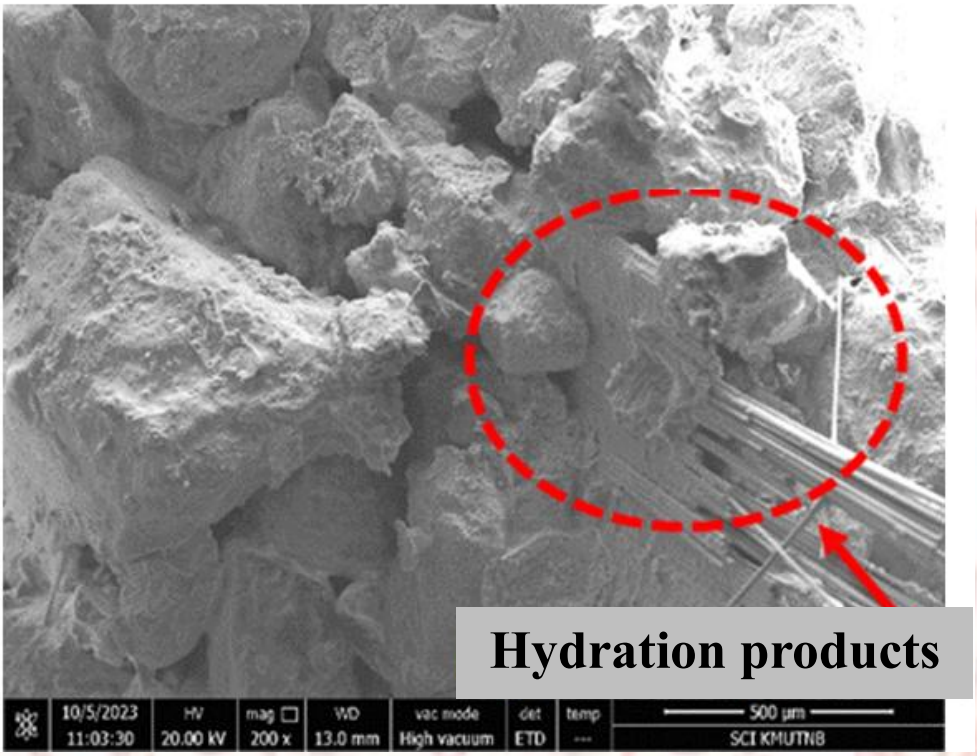

Figure 65 SEM image of the interaction mechanism of cemented-sand and fiber matrix interface

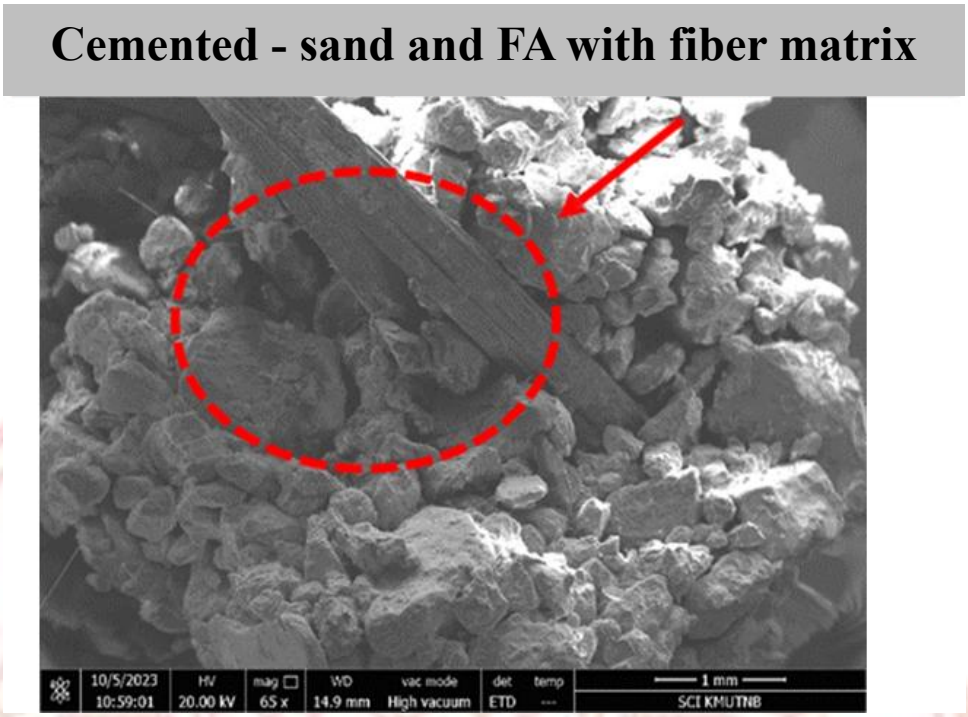

Figure 66 SEM image of the microstructure of the CCFS-GF with hydration products and several interfaces

Chapter 5 Conclusions

5.1. Conclusions of CCFS-PP specimens

The research was conducted as a comparative analysis of the impact of compacted sand using fly ash from MSW and polypropylene fiber (CCFS-PP) on flexural strength tests, according to ASTM standard C 1018 (ASTM C1018, 1997)and ASTM C-09 (ASTM C-09, 2013). The cement percentage was set at 5% by dry weight, while the 55 mm polypropylene fiber amounts ranged from 0.5% to 2.0% by volume. And, varying the fly ash replacement to cement ratio of 0:100, 25:75, 50:50, 75:25 and 100:0 by weight. The interaction mechanism of the fiber matrix interface was observed by SEM. Thus, the following conclusions are reached considering the research findings:

5.1.1 Fiber composition has an impact on how CCFS-PP responds to loading. Depending on the amount of fiber present, the CCFS-PP exhibits either a softening or a hardening reaction. Polypropylene fiber is recommended in terms of achieving a hardening reaction at the fiber content of 1.5%.

5.1.2 Fly ash from MSW can be used as a substitute for cement and should not be used more than the ratio of 25 to cement 75 for maximum efficiency in the selection of ash materials from MSW.

5.1.3 With a non-compact interfacial zone that produces only a partial-contact interfacial surface, the synthetic fibers (polypropylene fiber) under study are hydrophobic materials. For a hardening-deflection response to be obtained, these need a higher fiber content to establish a strong enough bond.

5.1.4 More fiber length improves performance for the polypropylene fiber material because it increases the interfacial surface area; however, in the case of differential lengths, the fiber surface type takes precedence over length because the interfacial bond is different.

5.1.5 Polypropylene fiber contributes to the strength of the strengthened sand. The polypropylene fiber worked well to stabilize and reinforce the structure. This is a result of the sand's uniformly distributed fibers.

5.2. Conclusions of CCFS-GF specimens

The research was conducted as a comparative analysis of the impact of the compacted cement sand mixed with industrial waste from refuse derived fuel power plant and glass fiber (CCSIWGF). The cement was set at 2 %, 4 %, 6 %, 8 % and 10 % by weight of the dry weight, and varying the RDF bottom ash used were 5 %, 10 %, 15 %, 20 %, 25% and 30 % by volume. Subsequently, the samples were cured for 7, 14, 28, 60 and 90 days. Thus, the following conclusions are reached in light of the research findings:

5.2.1 A cement ratio of 10% is the ratio that gives the highest compressive strength. Giving an approximate unconfined compressive strength value of 2500 kPa. The ratios with compressive strength values are arranged in order from highest to lowest as 10 %, 8 %, 6 %, 4 % and 2 % with compressive strength values around 2500, 1800, 1400, 820 and 240 kPa.

5.2.2 Glass fiber content composition has an impact on how CCFS-GF respond to loading. Depending on the amount of glass fiber of 1.0 % and giving an approximate unconfined compressive strength value of 1600 kPa. The CCFS-GF exhibits either a softening or a hardening reaction. Glass fiber is recommended in terms of achieving a hardening reaction at the fiber content of 1.0 %. Moreover, the glass fibers length at 12 mm gives the highest compressive strength approximate unconfined compressive strength value of 2050 kPa. They are arranged in order from highest to lowest as 12 mm, 6 mm and 3 mm with compressive strength values around 2050, 1390 and 1315 kPa.

5.2.3 RDF fly ash ratio at 5 % give the highest compressive strength approximate unconfined compressive strength value of 2870 kPa. The ratios with compressive strength values are arranged in order from highest to lowest as 5 %, 10 %, 15 %, 2 0%, 25 % and 30 % with compressive strength values around 2870, 2725, 2535, 2446, 2400 and 1950 kPa.

5.2.4 From the CCFS-GF of changing the mixing ratio of RDF fly ash, it was found that changing the ratio of fly ash contributes to the development of compressive strength a period of 7 - 14 days, increasing by an average of 280 kPa. During 14-28 days, an average increase of 330 kPa. During 28-60 days, an average increase of 740 kPa and during 60-90 days, an average increase of 138 kPa. Thus, RDF fly ash greatly contributes to the development of compressive strength over a period of 28-60 days. And, the mixing ratio of glass fibers, it was found that changing the ratio of glass fiber contributes to the development of compressive strength a period of 7 - 14 days, increasing by an average of 205 kPa. During 14-28 days, an average increase of 385 kPa. During 28-60 days, an average increase of 200 kPa and during 60-90 days, an average increase of 495 kPa. Thus, glass fibers greatly contribute to the development of compressive strength over a period of 60-90 days.

5.3. Practical recommendations of CCFS-PP and CCFS-GF

Based on the findings regarding the physical and mechanical properties of cement-compacted sand incorporating fly ash from refuse-derived fuel (RDF) power plants, combined with synthetic fibers, it is evident that such materials show promise as green construction materials for infrastructure projects such as roads and pipelines. The following practical recommendations are proposed for real-world application:

5.3.1 Utilization of RDF fly ash as partial cement replacement

It is recommended to use fly ash derived from RDF incineration as a partial replacement for ordinary Portland cement in cement-compacted sand mixtures (CCFS). Initial trial replacement ratios of 10%, 20%, and 30% are suggested to determine the optimal balance between mechanical strength and sustainability. This substitution can significantly reduce CO_2 emissions associated with cement production and lower overall material costs.

5.3.2 Incorporation of synthetic fibers for enhanced mechanical performance
Synthetic fibers such as polypropylene (PP) and glass fiber (GF) should be added to enhance mechanical performance, including flexural strength, tensile resistance, and crack control. The recommended fiber content ranges from 0.5% to 1.5% by volume. PP fibers are particularly suitable for applications requiring ductility and toughness (e.g., road bases), while GF is more appropriate for enhancing stiffness and strength in structural components such as pipelines.

5.3.3 Promotion of circular economy in waste management
A collaboration between RDF power plants, local municipalities, and the construction sector is encouraged to establish a circular economy framework that facilitates the collection and reuse of RDF fly ash as a construction material. This approach not only reduces landfill volume but also adds value to industrial waste.

5.3.4 Implementation of standardized testing and quality control
To ensure the reliability and consistency of the developed materials, standardized testing should be conducted regularly, including:

- Unconfined Compressive Strength (ASTM D1633)
- Flexural Strength of Concrete (ASTM C1609/C1609M)
- Shear Wave Velocity and Initial Shear Modulus (ASTM D8295-19)
- Microstructural analysis via Scanning Electron Microscope (SEM)

These tests are essential for verifying performance and enabling the safe substitution of conventional construction materials.

5.3.5 Development of pilot projects
Pilot-scale implementations of CCFS-PP and CCFS-GF materials are recommended in real construction settings, such as road sub-bases or pipe bedding systems. These pilot projects will provide valuable insights into the long-term performance of the materials and serve as a foundation for future large-scale adoption.

5.3.6 Policy integration and government incentives
Pilot-scale implementations of CCFS-PP and CCFS-GF materials are recommended in real construction settings, such as road sub-bases or pipe bedding systems. These pilot projects will provide valuable insights into the long-term performance of the materials and serve as a foundation for future large-scale adoption.

5.3.7 Knowledge dissemination and industry collaboration
Workshops, seminars, and training sessions should be organized for contractors, civil engineers, material manufacturers, and municipal agencies to promote awareness and practical understanding of RDF-based construction materials. Highlighting the benefits such as cost reduction, environmental impact mitigation, and performance durability can accelerate adoption and create cross-sector collaboration.

5.4. Discussion of Contribution of CCFS-PP and CCFS-GF

This study offers significant contributions to the academic field, environmental sustainability, and practical engineering applications by exploring the use of fly ash derived from refuse-derived fuel (RDF) power plants and synthetic fibers—namely polypropylene (PP) and glass fiber (GF) as alternative additives in the development of cement compacted sand using fly ash from municipal solid waste (CCFS) for infrastructure construction. The integration of these materials not only enhances

mechanical performance but also aligns with global objectives for sustainable construction and waste management.

5.4.1 Academic contributions

The research provides a novel contribution to the body of knowledge in construction materials engineering by investigating the mechanical and microstructural behavior of CCFS incorporating RDF-derived fly ash and synthetic fibers. Although numerous studies have evaluated the use of coal fly ash, research focused on fly ash from RDF incineration is limited. This study addresses that gap by presenting empirical data on unconfined compressive strength (UCS), flexural strength, shear wave velocity (Vs), and microstructural characteristics observed through Scanning Electron Microscopy (SEM). Furthermore, the study reinforces interdisciplinary collaboration across civil engineering, environmental science, and materials technology, offering a framework for further research on resource-efficient materials. It establishes foundational insights that may inform future studies on the use of alternative binders and reinforcement strategies in sustainable construction.

5.4.2 Environmental contributions

From an environmental perspective, the research promotes the reuse of industrial by-products and municipal solid waste, thereby contributing to reduced environmental burdens associated with landfill disposal and greenhouse gas emissions. Cement production is known to be energy-intensive and carbon-emitting; thus, partial replacement with RDF-derived fly ash offers a viable pathway toward carbon footprint reduction in the construction sector. Moreover, the integration of plastic waste into RDF production and the subsequent utilization of its fly ash in construction aligns with circular economy principles, promoting resource recovery and long-term waste valorization strategies. This approach supports national and international efforts to address climate change, urban waste challenges, and sustainable urban development.

5.4.3 Practical and industrial contributions

Practically, the study demonstrates that incorporating RDF fly ash and synthetic fibers enhances the engineering properties of CCFS, making it suitable for applications in highways, pipeline bedding, and other infrastructure projects. The improved mechanical properties observed in fiber-reinforced specimens indicate potential for performance optimization in real-world scenarios. Additionally, this research offers valuable insights into industrial adaptation by proposing the use of locally available waste materials to reduce dependence on conventional cement and natural resources. The findings may guide construction practices in regions with similar waste compositions and infrastructure needs, particularly in Southeast Asia and other developing contexts. The outcomes may also serve as a preliminary basis for developing technical standards and specifications for green construction materials, thereby facilitating wider adoption by industry stakeholders and public agencies.

5.5. Comparative discussion of CCFS-PP and CCFS-GF

This section presents a comparative evaluation of the physical and mechanical properties of cement compacted sand using fly ash from municipal solid waste (CCFS) modified with refuse-derived fuel (RDF) fly ash and synthetic fiber specifically polypropylene fiber (PP) and glass fiber (GF) (BEKAERT, 2024; Owens Corning,

2024). The results are discussed in relation to the control sample (CCFS without fiber), focusing on unconfined compressive strength (UCS), flexural strength, shear wave velocity (Vs), ductility, and microstructural characteristics observed through Scanning Electron Microscopy (SEM).

5.5.1 Mechanical performance

The inclusion of RDF fly ash combined with synthetic fibers significantly enhances the mechanical performance of CCFS. However, the degree and type of improvement depend on the nature of the fiber used.

- Unconfined Compressive Strength (UCS):
  The CCFS-GF mixture exhibited the highest UCS among all samples, indicating that glass fibers contribute effectively to compressive load resistance. This can be attributed to their high tensile modulus and strong interfacial bonding with the cement matrix.
- Flexural Strength:
  The CCFS-PP mixture demonstrated superior flexural strength and post-crack resistance, attributed to the bridging effect of polypropylene fibers. These fibers provide energy absorption capacity and control crack propagation, thus improving toughness.
- Shear Wave Velocity (Vs):
  CCFS-GF also showed higher shear wave velocity, indicating increased material stiffness. This is consistent with the strong interfacial transition zone (ITZ) between glass fibers and the cementitious matrix, as confirmed by SEM analysis.
- Ductility:
  Polypropylene fibers enhanced the ductility of the composite significantly more than glass fibers. This behavior suggests that CCFS-PP is better suited for applications requiring flexibility, such as in seismic zones or subsidence-prone areas.

5.5.2 Microstructural observations

SEM analysis revealed notable differences in the fiber-matrix interface:

- Polypropylene Fiber: Exhibits a relatively rough surface, promoting mechanical interlocking. However, its hydrophobic nature leads to limited chemical bonding with the matrix.
- Glass Fiber: Demonstrates excellent adhesion to the matrix, with denser and more uniform ITZ. This supports its higher UCS and Vs values.

5.5.3 Engineering implications

Each fiber type imparts distinct mechanical characteristics, thus offering targeted benefits depending on infrastructure requirements:

Table 8 CCFS, CCFS-PP and CCFS-GF specimens for engineering implications

Property	CCFS (Control)	CCFS-PP	CCFS-GF
UCS	Moderate	High	Very High
Flexural Strength	Low	Very High	Moderate
Shear Wave Velocity	Moderate	Moderate	High
Ductility	Low	Very High	Moderate

As summarized in Table 8, CCFS-GF mixtures are more appropriate for high-load applications such as pavements and structural foundations due to their superior compressive strength and stiffness. In contrast, CCFS-PP mixtures are more suitable for applications where ductility and crack resistance are prioritized, such as underground piping or road subgrades in soft soil areas.

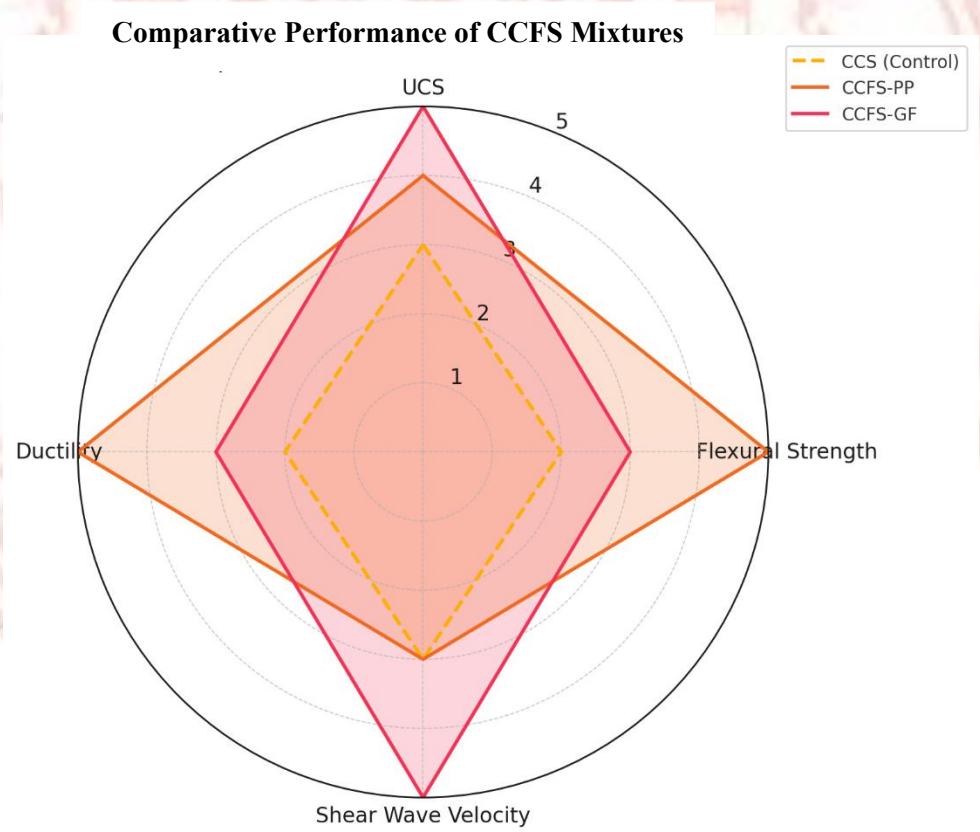

Figure 67 Radar chart comparing the performance of the CCFS mixtures

Here is the radar chart comparing the performance of the CCFS mixtures:

- CCFS (Control): Moderate performance across all parameters.
- CCFS-PP: Strong in flexural strength and ductility, ideal for flexible infrastructure.
- CCFS-GF: High compressive strength and stiffness, suitable for heavy-load applications.

The results suggest that both fiber-reinforced mixtures offer substantial improvements over control CCFS. CCFS-GF is better suited for structural applications requiring strength and rigidity, such as pavements and foundations. Conversely, CCFS-PP is more appropriate for applications requiring high ductility and crack resistance, such as backfills for pipelines or flexible pavement layers. By integrating RDF fly ash and synthetic fibers, the proposed materials offer sustainable alternatives to conventional cement-based materials, aligning with green construction goals and contributing to the circular economy.

5.5.4 Material cost comparison

One of the key comparative advantages of using fly ash from RDF incinerators lies in the cost-effectiveness. While Ordinary Portland Cement (OPC) is priced at approximately 2,000–3,000 THB/ton, RDF-derived fly ash is typically available at a much lower cost, ranging between 0–1,000 THB/ton depending on processing level (Global Power Synergy Public Company Limited, 2024). This represents a substantial economic benefit, especially for large-scale infrastructure projects.

Table 9 Material approximate cost comparison

Material	Approximate Cost (THB/ton)	Notes
OPC Cement	2,000–3,000	Primary binder, high CO_2 emission
Fly Ash (MSW RDF)	0–1,000	By-product, often free from incineration plants
Polypropylene Fiber	45,000–65,000	Moderate tensile strength, lightweight
Glass Fiber	80,000–120,000	Higher stiffness, better crack resistance

5.5.5 Comparative total cost per mix design

A comparative cost analysis was conducted to evaluate the economic feasibility of integrating fly ash derived from municipal solid waste (MSW) and synthetic fibers into cement-compacted sand mixtures. Four mix designs were considered: the conventional mix using 100% Ordinary Portland Cement (OPC), a reduced-cement mix using MSW fly ash (CCFS), a fly ash mix reinforced with polypropylene fiber (CCFS-PP), and a fly ash mix reinforced with glass fiber (CCFS-GF). The estimated

material cost per cubic meter (THB/m³) for each mix was calculated based on market prices in Thailand as of 2024 (Siam Market Research, 2024).

Table 10 Comparative total cost per mix design

Mix Design	Key Components	Estimated Cost (THB/m³)	Cost Reduction vs. OPC (%)
OPC (100%)	300 kg Portland cement	900	–
CCFS	150 kg cement + 150 kg sand + MSW fly ash	550	−38.9%
CCFS-PP	100 kg cement + 50 kg MSW fly ash + PP fiber	555	−38.3%
CCFS-GF	100 kg cement + 50 kg MSW fly ash + glass fiber	600	−33.3%

Note: The fly ash was assumed to be supplied at no cost from the RDF power plant. Fiber dosage was maintained at 1 kg/m³ for both polypropylene and glass fiber.

The 100% OPC mix resulted in the highest cost due to the exclusive use of Portland cement. In contrast, the inclusion of MSW-derived fly ash as a partial cement replacement significantly reduced material costs in all alternative mixes. The CCFS mix, which uses no fibers, demonstrated the lowest overall cost, making it a cost-effective solution for large-scale applications.

The CCFS-PP mix, despite the addition of polypropylene fiber, maintained a low cost comparable to the CCFS mix. This is attributed to the relatively low market price of synthetic polypropylene fibers. The CCFS-GF mix showed a slightly higher cost, primarily due to the higher unit price of glass fibers. However, this cost is justified by the improved mechanical performance observed in the experimental phase.

These results suggest that incorporating MSW fly ash and synthetic fibers not only enhances environmental sustainability but also contributes to cost optimization in infrastructure construction. The selection of a specific mix design may depend on the project's performance requirements, with CCFS being optimal for cost-sensitive applications, and CCFS-GF offering superior mechanical performance for structurally demanding uses.

5.5.6 Cost-performance analysis

To comprehensively assess the viability of alternative cement-compacted sand (CCS) mixtures incorporating fly ash from municipal solid waste (MSW) and synthetic fibers, a cost-performance analysis was conducted. This analysis considers both the total material cost per cubic meter and the engineering performance, particularly unconfined compressive strength (UCS) and flexural strength (FS). The results offer a

balanced evaluation of economic and structural efficiency for infrastructure applications.

Table 11 Cost and performance comparison of mixed designs

Mix Design	Estimated Cost (THB/m³)	UCS (MPa)	Flexural Strength (MPa)	Cost per MPa UCS (THB/MPa)	Cost per MPa FS (THB/MPa)
OPC (100%)	900	5.2	0.75	173.08	1200.00
CCFS	550	4.8	0.60	114.58	916.67
CCFS-PP	555	5.6	0.90	99.11	616.67
CCFS-GF	600	6.0	1.10	100.00	545.45

Note: Performance values are illustrative and based on typical laboratory outcomes observed in previous studies. Actual results may vary depending on specific material sources and curing conditions.

- UCS Efficiency: The CCFS-PP and CCFS-GF mixtures show superior performance in terms of unconfined compressive strength (5.6–6.0 MPa), compared to OPC (5.2 MPa) and CCFS (4.8 MPa), while maintaining a significantly lower cost per unit strength. This indicates that the inclusion of fly ash and synthetic fibers can increase mechanical strength while reducing or maintaining cost levels.
- Flexural Strength Efficiency: CCFS-GF displays the highest flexural strength (1.10 MPa) and the lowest cost per unit of flexural strength (545.45 THB/MPa), making it particularly effective for structural elements subjected to bending or tensile stress.
- Cost Efficiency: The CCFS mix is the most economical in terms of material cost alone. However, its slightly lower mechanical performance suggests it is better suited for non-critical structural applications where cost savings are prioritized over strength.
- Optimal Mix Recommendation: CCFS-PP provides the best overall balance between cost and performance. It delivers high UCS and FS values at the lowest relative cost, making it ideal for sustainable infrastructure applications such as road bases, pipe bedding, or subgrade stabilization.

5.5.7 Environmental and practical implications

Utilizing RDF-derived fly ash not only contributes to reducing cement usage thus lowering CO_2 emissions but also provides a practical solution for MSW disposal (Pollution Control Department, 2021b). Moreover, by integrating synthetic fibers, the material can achieve performance levels suitable for infrastructure applications like highway bases or pipeline bedding, making it a sustainable alternative to traditional cement-based materials.

5.6. Answer to the hypotheses of CCFS, CCFS-PP and CCFS-GF

This study sets out three key hypotheses regarding the use of fly ash from municipal solid waste incineration and synthetic fibers in cement compacted sand using fly ash from municipal solid waste (CCFS) for sustainable construction materials. The following are the findings and how they correspond to each hypothesis (Table 12):

Hypothesis 1: A fly ash from MSW consisting of a fine fraction may be more qualified to apply with cement compacted sand due to it addressing the issue of using waste in the environment from burning waste, which will reduce management costs in landfills.

- This hypothesis is supported by the findings. The fly ash obtained from the refuse-derived fuel (RDF) incineration process was found to be fine-grained and exhibited suitable pozzolanic characteristics. Its incorporation into the CCS matrix improved the compaction and contributed to strength development. Additionally, reusing fly ash as a construction material helps divert waste from landfills and aligns with circular economy and waste valorization strategies, thus reducing environmental burden and long-term landfill costs.

Hypothesis 2: The fly ash produced by the RDF power plant process may have optimum engineering properties compared to a standard of construction in highway or pipeline in terms of construction and materials engineering.

- This hypothesis is also validated by experimental data. The mechanical properties of the CCFS mixtures containing MSW fly ash (especially UCS and flexural strength) met or exceeded standard benchmarks for highway subbase and utility trench backfill materials. The material demonstrated good workability, adequate strength, and satisfactory stiffness characteristics, making it a viable substitute in infrastructure construction.

Hypothesis 3: The polypropylene fiber and glass fiber of synthetic materials mix with fly ash from MSW may replace cement ratio for construction infrastructure such as highway or pipeline.

- The results support this hypothesis. The partial replacement of cement with fly ash, in combination with polypropylene (PP) or glass fiber (GF), led to improved mechanical behavior of the CCFS specimens. The fibers contributed to increased ductility and flexural strength, while the fly ash helped reduce cement demand without compromising compressive strength. This synergy shows strong potential for reducing cement usage hence CO_2 emissions while maintaining performance, particularly in flexible pavements and underground infrastructure.

Table 12 Summary of hypotheses and research findings

Hypothesis	Statement	Findings	Conclusion
H 1	Fly ash from MSW with fine particles is suitable for cement compacted sand and reduces landfill costs.	MSW fly ash showed good pozzolanic properties, enhanced compaction, and reduced waste to landfill.	Supported ✅
H 2	RDF-derived fly ash exhibits engineering properties comparable to highway/pipeline standards.	UCS and flexural strength met infrastructure material standards. Good workability and stiffness were observed.	Validated ✅
H 3	PP and GF fibers mixed with MSW fly ash can partially replace cement in infrastructure.	PP and GF fibers improved ductility and flexural performance. Fly ash reduced cement consumption without reducing strength.	Supported ✅

5.7. Bill of Quantities (BOQ)

Here is a structured Bill of Quantities (BOQ) tailored for this research comparing different cement-compacted sand mixes (Table 13) (Department of Alternative Energy Development and Effciency, 2023):

- OPC (Ordinary Portland Cement)
- CCFS (Cement compacted sand with MSW fly ash),
- CCFS-PP (Cement compacted sand with MSW fly ash + polypropylene fiber),
- CCFS-GF (Cement compacted sand with MSW fly ash + glass fiber).

Table 13 Bill of Quantities (BOQ) comparative mix designs (per 1 m^3)

Material	Unit	OPC Mix	CCFS	CCFS-PP	CCFS-GF
Ordinary Portland Cement (OPC)	kg	400	300	280	280
Sand (Bangkok Construction Sand)	kg	1,000	1,000	1,000	1,000
MSW Fly Ash (GPSC, Rayong)	kg	–	100	100	100
Polypropylene Fiber (BEKAERT)	kg	–	–	2.0	–
Glass Fiber (Owens Corning E-glass)	kg	–	–	–	2.0
Water	liter	200	200	200	200
Estimated Unit Cost (THB/kg)	–	–	–	–	–
– OPC	THB/kg	4.50	4.50	4.50	4.50
– Sand	THB/kg	0.60	0.60	0.60	0.60
– MSW Fly Ash	THB/kg	–	1.20	1.20	1.20
– Polypropylene Fiber	THB/kg	–	–	180.00	–
– Glass Fiber	THB/kg	–	–	–	250.00
– Water	THB/liter	0.10	0.10	0.10	0.10
Total Cost per Mix (THB)	THB	2,010.00	1,770.00	2,130.00	2,270.00

Notes:

- Prices are approximate market rates in Thailand (2024–2025) and may vary slightly by location or bulk purchase.
- MSW fly ash cost includes logistics and processing from the RDF plant.
- Polypropylene and glass fibers are high-performance additives with relatively high costs but improve mechanical properties.
- The water cost is minimal but included for completeness.

5.8. Future Work

Based on the findings of this study, several avenues for future research are recommended to enhance the development and application of green construction materials using fly ash from municipal solid waste (MSW) and synthetic fibers as shown in Figure 68:

- Field Application and Life Cycle Assessment are top priorities, reflecting the urgent need for practical implementation and environmental evaluation.
- Durability Testing and Policy & Standard Support are also highly recommended for ensuring long-term feasibility and institutional adoption.
- Mix Optimization and Alternative Waste Integration hold medium priority but are essential for enhancing the material's versatility and sustainability.

5.8.1 Long-term durability testing: Utilizing RDF-derived fly ash not only contributes to reducing cement usage thus lowering CO_2 emissions but also provides a practical solution for MSW disposal. Moreover, by integrating synthetic fibers, the material can achieve performance levels suitable for infrastructure applications like highway bases or pipeline bedding, making it a sustainable alternative to traditional cement-based materials.

5.8.2 Field-scale implementation and performance monitoring: Pilot-scale or field-scale trials should be conducted to evaluate the in-situ performance of the developed materials in highway subbases, utility trenches, or pipeline bedding. Performance indicators such as settlement behavior, cracking resistance, and moisture sensitivity should be monitored over time.

5.8.3 Optimization of mix proportions: Further research should focus on optimizing the proportions of MSW fly ash, polypropylene fiber, and glass fiber in the mix design. Advanced statistical methods such as Response Surface Methodology (RSM) or machine learning approaches may be employed to achieve optimal cost-performance balance.

5.8.4 Life Cycle Assessment (LCA) and Environmental Impact:

Comprehensive LCA should be conducted to quantify the environmental benefits of using RDF-derived fly ash and synthetic fibers in construction, including reductions in greenhouse gas emissions, landfill usage, and embodied energy compared to traditional cement-based materials.

5.8.5 Integration of other waste materials: Additional industrial by-products such as bottom ash, rice husk ash, or construction and demolition waste could be explored in combination with MSW fly ash to further enhance sustainability and circular economic benefits.

5.8.6 Standardization and regulatory guidelines: Future research should contribute to the development of technical standards and regulatory frameworks that support the use of RDF fly ash and synthetic fiber-modified cementitious materials in infrastructure projects.

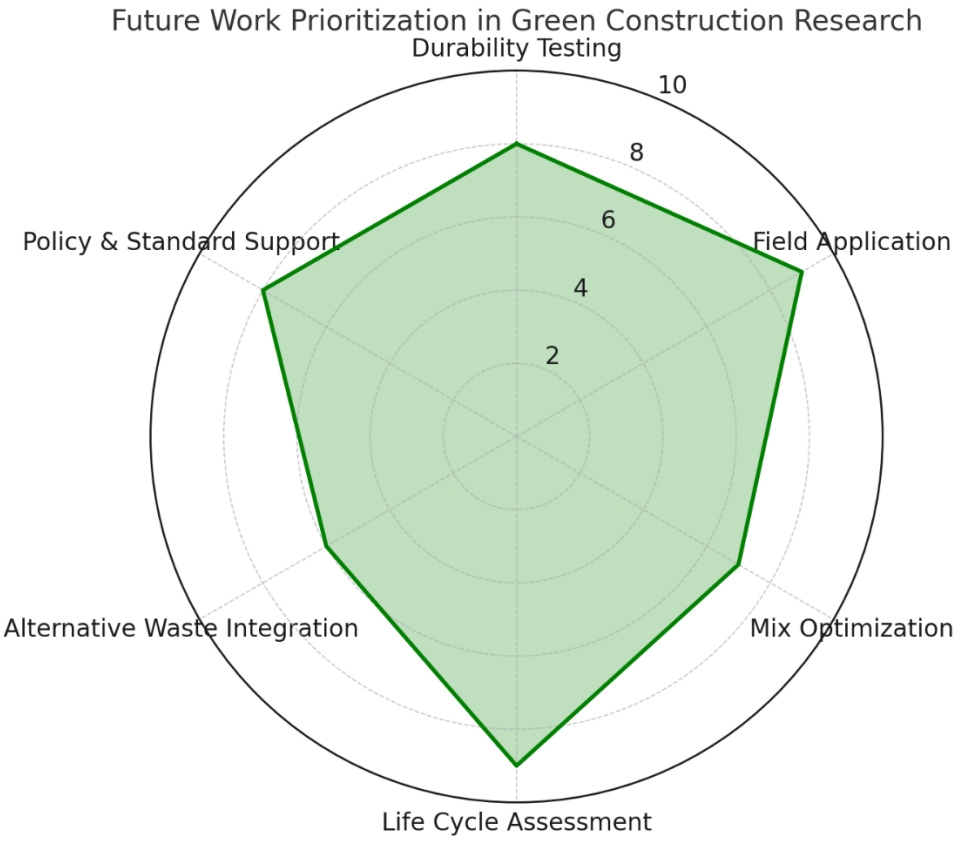

Figure 68 Future research prioritization

REFERENCES

ACI 230.1R-09. (2009). *Report on soil cement (ACI 230.1R-09)*. American Concrete Institute.

ACPA Subgrades. (2007). Subbases for Concrete Pavements. *EB204P, American Concrete Pavement Association*.

Al-Ghouti, M. A., Khan, M., Nasser, M. S., Al-Saad, K., & Heng, O. E. (2021). Recent advances and applications of municipal solid wastes bottom and fly ashes: Insights into sustainable management and conservation of resources. *Environmental Technology & Innovation*, *21*, 101267.

American Society for Testing and Materials. (1985). *Classification of Soils for Engineering Purposes: Annual Book of ASTM Standards*. ASTM International West Conshohocken, PA, USA.

Ashford, S. A., Jakrapyanun, W., & Lukkanaprasit, P. (1997). Amplification of earthquake ground motions in Bangkok. Final report on research sponsored by the Royal Thai Government. *Public Works Department, Ministry of Interior, Thailand*.

ASTM C-09. (2013). Committee C-09 on Concrete and Concrete Aggregates. Standard specification for coal fly ash and raw or calcined natural pozzolan for use in concrete. *ASTM International*.

ASTM C1018. (1997). *Standard test method for flexural toughness and first-crack strength of fiber-reinforced concrete (using beam with third-point loading)*.

ASTM C1609/C1609M-10. (2013). *Standard Test Method for Flexural Performance of Fiber-Reinforced Concrete (Using Beam With Third-Point Loading)*.

ASTM Committee D-18 on Soil and Rock. (2009). *Standard Test Methods for Laboratory Compaction Characteristics of Soil Using Modified Effort (56,000 Ft-Lbf/Ft3 (2,700 KN-M/M3))* .

ASTM D698-12e1. (2012). *Test Methods for Laboratory Compaction Characteristics of Soil Using Standard Effort (12 400 ft-lbf/ft3 (600 kN-m/m3))*. ASTM International. https://doi.org/10.1520/D0698-12E01

ASTM D1633-17. (2017). Standard Test Methods for Compressive Strength of Molded Soil-Cement Cylinders. *ASTM International, West Conshohocken, PA*.

ASTM D8295−19. (2019). *Standard Test Method for Determination of Shear Wave Velocity and Initial Shear Modulus in Soil Specimens using Bender Elements*. ASTM International. https://doi.org/10.1520/D8295-19

ASTM E856-83. (2006). *Standard Definitions of Terms and Abbreviations Relating to Physical and Chemical Characteristics of Refuse Derived Fuel*.

Aubert, J.-E., Husson, B., & Vaquier, A. (2004). Use of municipal solid waste incineration fly ash in concrete. *Cement and Concrete Research*, *34*(6), 957–963.

Ayeldeen, M., & Kitazume, M. (2017). Using fiber and liquid polymer to improve the behaviour of cement-stabilized soft clay. *Geotextiles and Geomembranes*, *45*(6), 592–602.

Banks, C. J., & Lo, H.-M. (2003). Assessing the effects of municipal solid waste incinerator bottom ash on the decomposition of biodegradable waste using a completely mixed anaerobic reactor. *Waste Management & Research*, *21*(3), 225–234.

BEKAERT. (2024). *Product manual: Synmix polypropylene fiber for concrete*. https://www.bekaert.com/en/product-catalog/construction/polypropylene-fibers

Belgiorno, V., De Feo, G., Della Rocca, C., & Napoli, R. M. A. (2003). Energy from gasification of solid wastes. *Waste Management*, *23*(1), 1–15.

Bellum, R. R. (2022). Influence of steel and PP fibers on mechanical and microstructural properties of fly ash-GGBFS based geopolymer composites. *Ceramics International*, *48*(5), 6808–6818.

Blazy, J., & Blazy, R. (2021). Polypropylene fiber reinforced concrete and its application in creating architectural forms of public spaces. *Case Studies in Construction Materials*, *14*, e00549.

Boulekbache, B., Hamrat, M., Chemrouk, M., & Amziane, S. (2010). Flowability of fibre-reinforced concrete and its effect on the mechanical properties of the material. *Construction and Building Materials*, *24*(9), 1664–1671.

Chapman, S., Clardy, N., & Webb, N. (2009). The Ecological Footprint of Composting and Incineration of Garden Waste in Denmark. *An Evaluation of the Ecological Benefits of Incinerating Garden Waste in Waste-to-Energy Facilities versus Composting. Bachelor Thesis, Worchester Polytechnic Institute, USA. Accessed Last June*.

Chesner, W. H., Collins, R. J., MacKay, M. H., & Emery, J. (2002). *User guidelines for waste and by-product materials in pavement construction*. Recycled Materials Resource Center.

Chuenjaidee, S., Jamsawang, P., Jongpradist, P., & Chen, X. (2022). Flexural Performance of Cement-Treated Sand Reinforced with Geogrids for Use as Sub-Bases of Pavement and Railway Structures. *Materials*, *15*(8), 2877.

Consoli, N. C., Bassani, M. A. A., & Festugato, L. (2010). Effect of fiber-reinforcement on the strength of cemented soils. *Geotextiles and Geomembranes*, *28*(4), 344–351.

Danso, H., Martinson, D. B., Ali, M., & Williams, J. (2015). *Effect of Fibre Aspect Ratio on Mechanical Properties of Soil Building Blocks*.

Department of Alternative Energy Development and Effciency. (2023). Energy price and market summary report. In *Ministry of Energy, Thailand*. http://www.dede.go.th

Di Gregorio, F., & Zaccariello, L. (2012). Fluidized bed gasification of a packaging derived fuel: energetic, environmental and economic performances comparison for waste-to-energy plants. *Energy*, *42*(1), 331–341.

Diaz, L. F. ., Savage, G. M. ., Eggerth, L. L. ., & Rosenberg, Larry. (2005). *Solid waste management*. United Nations Environment Programme.

Donkor, P., & Obonyo, E. (2016). Compressed soil blocks: Influence of fibers on flexural properties and failure mechanism. *Construction and Building Materials*, *121*, 25–33.

Elmrabet, R., Elharfi, A., & Elyoubi, M. S. (2020). Study of properties of polyethylene and cement mixtures. *Materials Today: Proceedings*, *27*, 3017–3020.

Energy Cement Industry. (2005). *The Cement Sustainability Initiative*.

EPA, I. (1996). Municipal Waste Characterisation. *Environmental Protection Agency, Ireland*.

Garg, A., Smith, R., Hill, D., Simms, N., & Pollard, S. (2007). *Wastes as co-fuels: the policy framework for solid recovered fuel (SRF) in Europe, with UK implications*. ACS Publications.

Global Power Synergy Public Company Limited. (2024). *Fly ash technical specifications and cost from RDF processing facility [Internal report]*.

Hannawi, K., Bian, H., Prince-Agbodjan, W., & Raghavan, B. (2016). Effect of different types of fibers on the microstructure and the mechanical behavior of ultra-high performance fiber-reinforced concretes. *Composites Part B: Engineering*, *86*, 214–220.

Hilber, T., Maier, J., Scheffknecht, G., Agraniotis, M., Grammelis, P., Kakaras, E., Glorius, T., Becker, U., Derichs, W., & Schiffer, H.-P. (2007). Advantages and possibilities of solid recovered fuel cocombustion in the European energy sector. *Journal of the Air & Waste Management Association*, *57*(10), 1178–1189.

Iamchaturapatr, J., Piriyakul, K., & Petcherdchoo, A. (2022a). Characteristics of sandy soil treated using EICP-based urease enzymatic acceleration method and natural hemp fibers. *Case Studies in Construction Materials*, *16*, e00871.

Iamchaturapatr, J., Piriyakul, K., & Petcherdchoo, A. (2022b). Use of a piezoelectric bender element for the determination of initial and final setting times of metakaolin geopolymer pastes, with applications to laterite soils. *Sensors*, *22*(3), 1267.

Intharathirat, R., & Abdul Salam, P. (2016). Valorization of MSW-to-energy in Thailand: status, challenges and prospects. *Waste and Biomass Valorization*, *7*, 31–57.

Islam, K. M. N. (2016). Municipal solid waste to energy generation in Bangladesh: possible scenarios to generate renewable electricity in Dhaka and Chittagong city. *Journal of Renewable Energy*, *2016*(1), 1712370.

Jamsawang, P., Voottipruex, P., & Horpibulsuk, S. (2015). Flexural strength characteristics of compacted cement-polypropylene fiber sand. *Journal of Materials in Civil Engineering*, *27*(9), 04014243.

Kennish, M. J. (2002). Environmental threats and environmental future of estuaries. *Environmental Conservation*, *29*(1), 78–107. https://doi.org/10.1017/S0376892902000061

Klinghoffer, N. B., & Castaldi, M. J. (2013). *Waste to energy conversion technology*. Elsevier.

Kothari, R., Tyagi, V. V., & Pathak, A. (2010). Waste-to-energy: A way from renewable energy sources to sustainable development. *Renewable and Sustainable Energy Reviews*, *14*(9), 3164–3170.

Lee, J.-M., Kim, D.-W., Kim, J.-S., Na, J.-G., & Lee, S.-H. (2010). Co-combustion of refuse derived fuel with Korean anthracite in a commercial circulating fluidized bed boiler. *Energy*, *35*(7), 2814–2818.

Lo, H.-M. (2005). Metals behaviors of MSWI bottom ash co-digested anaerobically with MSW. *Resources, Conservation and Recycling*, *43*(3), 263–280.

Millogo, Y., Morel, J. C., Aubert, J. E., & Ghavami, K. (2014). Experimental analysis of Pressed Adobe Blocks reinforced with Hibiscus cannabinus fibers. *Construction and Building Materials*, *52*, 71–78. https://doi.org/10.1016/j.conbuildmat.2013.10.094

Ministry of Energy. (2018). *Ministry of Energy Power Development Plan (PDP2018)*.

Miskolczi, N., Borsodi, N., Buyong, F., Angyal, A., & Williams, P. T. (2011). Production of pyrolytic oils by catalytic pyrolysis of Malaysian refuse-derived fuels in continuously stirred batch reactor. *Fuel Processing Technology*, *92*(5), 925–932.

Morel, J.-C., Pkla, A., & Walker, P. (2007). Compressive strength testing of compressed earth blocks. *Construction and Building Materials*, *21*(2), 303–309.

Násner, A. M. L., Lora, E. E. S., Palacio, J. C. E., Rocha, M. H., Restrepo, J. C., Venturini, O. J., & Ratner, A. (2017). Refuse Derived Fuel (RDF) production and gasification in a pilot plant integrated with an Otto cycle ICE through Aspen plus^{TM} modelling: Thermodynamic and economic viability. *Waste Management*, *69*, 187–201.

Nematollahi, B., Sanjayan, J., & Shaikh, F. U. A. (2014). Comparative deflection hardening behavior of short fiber reinforced geopolymer composites. *Construction and Building Materials*, *70*, 54–64.

Ngowi, A. B. (1997). Improving the traditional earth construction: a case study of Botswana. *Construction and Building Materials*, *11*(1), 1–7.

Nithikul, J. (2007). Potential of refuse derived fuel production from Bangkok municipal solid waste. *Thailand, Asian Institute of Technology School of Environment, Resources and Development*.

Nutongkaew, P., Waewsak, J., Chaichana, T., & Gagnon, Y. (2014). Greenhouse gases emission of refuse derived fuel-5 production from municipal waste and palm kernel. *Energy Procedia*, *52*, 362–370.

Owens Corning. (2024). *Advantex® E-glass fiber specification sheet*. https://www.owenscorning.com/en-us/composites/products/advantex

Ozcan, H., Guvenc, S., Guvenc, L., & Demir, G. (2016). Municipal Solid Waste Characterization According to Different Income Levels: A Case Study. *Sustainability*, *8*(10), 1044. https://doi.org/10.3390/su8101044

Petcherdchoo, A., Pochalard, S., & Piriyakul, K. (2023). Use of bender element tests for determining shear modulus of fly-ash and cement admixed Bangkok clay with considering unconfined compressive strength. *Case Studies in Construction Materials*, *18*, e02040.

Pilant, A., Endres, K., Rosenbaum, D., & Gundersen, G. (2020). US EPA EnviroAtlas meter-scale urban land cover (MULC): 1-m pixel land cover class definitions and guidance. *Remote Sensing*, *12*(12), 1909.

Piriyakul, K., & Iamchaturapatr, J. (2013). Biocementation through microbial calcium carbonate precipitation. *The Journal of Industrial Technology*, *9*(3), 195–218.

Pochalard S., Wungsumpow C., & Piriyakul K. (2023). Strength development in cement and fly ash admixed Bangkok clay with considering shear wave velocity. *The 21st Southeast Asian Geotechnical Conference and 4th AGSSEA Conference (SEAGC-AGSSEA2023)*. .

Pochalard, S., Wungsumpow, C., & Piriyakul, K. (2024). Enhancement on compressive strength of Bangkok clay cement using novel high-strength polyethylene fibers. *IOP Conference Series: Earth and Environmental Science*, *1335*(1), 012008.

Pochalard, S., Wungsumpow, C., & Piriyakul, K. (2025). Enhancement of Compressive Strength in Cement Admixed Bangkok Clay with Glass Fiber and Bottom Ash for Eco-Friendly Functional Road Materials. *Mechanics of Advanced Composite Structures*, *12*(2), 279–292.

Pohl, M., Gebauer, K., & Beckmann, M. (2008). Characterisation of refuse derived fuels in view of the fuel technical properties. *The 8th European Conference on Industrial Furnaces and Boilers (INFUB-8)*, *25*(28.03).

Pollution Control Department. (2021a). *A Study of the Composition of Solid Waste*.

Pollution Control Department. (2021b). Municipal solid waste management in Thailand annual report. In *Ministry of Natural Resources and Environment*. http://www.pcd.go.th

Pollution Control Department Ministry of Natural Resources and Environment Thailand. (2017). *Thailand State of Pollution Report 2016*. www.pcd.go.th

Poranek, N., Pizoń, J., Łaźniewska-Piekarczyk, B., Czajkowski, A., & Lagashkin, R. (2023). Recycle option for municipal solid waste incineration fly ash (MSWIFA) as a partial replacement for cement in mortars containing calcium sulfoaluminate cement (CSA) and portland cement to save the environment and natural resources. *Materials*, *17*(1), 39.

Pudcha, T., Phongphiphat, A., Wangyao, K., & Towprayoon, S. (2023). Forecasting Municipal Solid Waste Generation in Thailand with Grey Modelling: 10.32526/ennrj/21/202200104. *Environment and Natural Resources Journal*, *21*(1), 35–46.

Rosendal, R. M. (2009). Landfill mining—process, feasibility, economy, benefits and limitations. *Reno Sam, København*.

Ryu, C. (2010). Potential of municipal solid waste for renewable energy production and reduction of greenhouse gas emissions in South Korea. *Journal of the Air & Waste Management Association*, *60*(2), 176–183.

Safiuddin, M., Jumaat, M. Z., Salam, M. A., Islam, M. S., & Hashim, R. (2010). Utilization of solid wastes in construction materials. *International Journal of the Physical Sciences*, *5*(13), 1952–1963.

Sharma, V., Vinayak, H. K., & Marwaha, B. M. (2015). Enhancing compressive strength of soil using natural fibers. *Construction and Building Materials*, *93*, 943–949.

Siam Market Research. (2024). Construction material price index Q1–Q2/2024. In *Thai Construction Materials Market Watch*. http://www.thaimarketwatch.com

Sukontasukkul, P., Pomchiengpin, W., & Songpiriyakij, S. (2010). Post-crack (or post-peak) flexural response and toughness of fiber reinforced concrete after exposure to high temperature. *Construction and Building Materials*, *24*(10), 1967–1974.

Sutabutr, T. (2012). Alternative energy development plan: AEDP 2012-2021. *Journal of Renewable Energy and Smart Grid Technology*, *7*(1), 1–10.

Tambone, F., Scaglia, B., Scotti, S., & Adani, F. (2011). Effects of biodrying process on municipal solid waste properties. *Bioresource Technology*, *102*(16), 7443–7450.

Tang, C., Shi, B., Gao, W., Chen, F., & Cai, Y. (2007). Strength and mechanical behavior of short polypropylene fiber reinforced and cement stabilized clayey soil. *Geotextiles and Geomembranes*, *25*(3), 194–202.

Teachavorasinskun, S., Thongchim, P., & Lukkunaprasit, P. (2002). Shear modulus and damping of soft Bangkok clays. *Canadian Geotechnical Journal*, *39*(5), 1201–1208.

Thailand Greenhouse Gas Management Organization. (2016). *Greenhouse Gas Mitigation Potential of Cement Industry in Thailand*.

Thailand Greenhouse Gas Management Organization (Public Organization). (2019). *Thailand Voluntary Emission Reduction Program*.

Tran, K. Q., Satomi, T., & Takahashi, H. (2017). Study on strength behavior of cement stabilized sludge reinforced with waste cornsilk fiber. *GEOMATE Journal*, *13*(39), 140–147.

Velis, C. A., Longhurst, P. J., Drew, G. H., Smith, R., & Pollard, S. J. T. (2009). Biodrying for mechanical–biological treatment of wastes: A review of process science and engineering. *Bioresource Technology*, *100*(11), 2747–2761.

Walker, P. (1997). Characteristics of pressed earth block in compression. *Proceedings of the 11th International Brick and Block Masonry Conference*.

Walker, P. J. (1995). Strength, durability and shrinkage characteristics of cement stabilised soil blocks. *Cement and Concrete Composites*, *17*(4), 301–310.

Wang, P., Hu, Y., & Cheng, H. (2019). Municipal solid waste (MSW) incineration fly ash as an important source of heavy metal pollution in China. *Environmental Pollution, 252*, 461–475.

Wungsumpow, C., Towprayoon, S., Chiemchaisri, C., Suanburi, D., & Wangyao, K. (2018). *Applying electrical resistivity tomography measurement in landfill mining: A study on configuration and spacing setting*.

Xiao, H., & Liu, Y. (2018). A prediction model for the tensile strength of cement-admixed clay with randomly orientated fibres. *European Journal of Environmental and Civil Engineering*, *22*(9), 1131–1145.

Yingsamphancharoen, T., & Piriyakul, K. (2022). Feasibility study of steel reinforcement of polyethylene corrugated horizontal pipe for on-site underground water storage tanks and their applications. *Case Studies in Construction Materials*, *17*, e01578.

Zak, P., Ashour, T., Korjenic, A., Korjenic, S., & Wu, W. (2016). The influence of natural reinforcement fibers, gypsum and cement on compressive strength of earth bricks materials. *Construction and Building Materials*, *106*, 179–188.

APPENDIX

Research publication in The Journal of Material Cycles and Waste Management, 2025, DOI: https://doi.org/10.1007/s10163-024-02129-9, Enhancing landfill mining assessments: a dual-method approach using electrical resistivity and UAV photogrammetry at Buriram landfill

Journal of Material Cycles and Waste Management (2025) 27:699–711
https://doi.org/10.1007/s10163-024-02129-9

SPECIAL FEATURE: ORIGINAL ARTICLE

10th 3R International Scientific Conference (10th 3RINCs 2024)

Enhancing landfill mining assessments: a dual-method approach using electrical resistivity and UAV photogrammetry at Buriram landfill

Pornchanok Boonsakul[1,2] · Bongkoch Chungam[1,2] · Parichat Suknark[1,2] · Chalermpon Wungsumpow[3] · Panida Payomthip[4] · Komsilp Wangyao[1,2]

Received: 2 June 2024 / Accepted: 25 November 2024 / Published online: 10 December 2024

Abstract
This study explores the potential of conducting landfill mining at Thailand's Buriram landfill based on a combination of resistivity investigation and surveys conducted with unmanned aerial vehicles (UAVs). Landfill mining is a solution for managing waste buildup and recovering valuable resources; however, it is essential to conduct initial technical feasibility assessments to ensure the viability of such projects. In this study, electrical resistivity imaging is combined with UAV photogrammetry to qualitatively and quantitatively evaluate municipal solid waste in old and new landfill areas. The qualitative findings indicate a relationship between electrical resistivity values and waste composition, with higher resistivity values recorded in areas containing significant plastic content ($r = 0.52$). The total volumes of solid waste in the old and new landfill sites were calculated as ~ 271,500 m^3 and ~ 336,900 m^3, respectively, with an estimated refuse-derived fuel production potential of around 43,053 tons and 55,244 tons across both areas. A financial analysis confirmed the feasibility of the project. This integrated approach facilitated reliable data collection, which is crucial for evaluating the viability of landfill mining projects. By adopting a similar methodology, the decision-making accuracy for landfill mining projects can be improved to support effective waste management practices.

Keywords Geophysical survey · Site characterization · Cost–benefit analysis · Municipal solid waste · Resource recovery

Introduction

Even though reducing waste generation is a major priority in the waste management hierarchy, vast amounts of accumulated municipal solid waste (MSW) have nonetheless accumulated in landfills due to decades of improper waste disposal [1]. Landfill mining (LFM) has emerged as a common practice in waste management to address the need for landfill space reclamation and environmental concerns [2]. LFM was first reported in 1953 in Israel [3, 4], and this technique has since gained more widespread attention with a notable increase in LFM research between 1990 and 2022 [5]. The LFM process involves extracting valuable substances, soil-like materials, and refuse-derived fuel (RDF) from stabilized MSW in landfills [6–9]. RDF obtained from MSW typically consists of cellulose, hemicellulose, lignin, and various plastics [10]. The recovery of materials such as plastics for RDF production is essential for the circular

✉ Komsilp Wangyao
komsilp.wan@kmutt.ac.th

[1] The Joint Graduate School of Energy and Environment (JGSEE), King's Mongkut University of Technology Thonburi (KMUTT), Bangkok, Thailand

[2] Center of Excellence on Energy Technology and Environment (CEE), PERDO, Ministry of Higher Education, Science, Research and Innovation (MHESI), Bangkok, Thailand

[3] KMUTNB Techno Park, King Mongkut's University of Technology North Bangkok, Bangkok, Thailand

[4] Center for Material Cycles and Waste Management Research, National Institute for Environmental Studies, Tsukuba, Japan

economy in the waste-to-energy concept, promoting efficient resource use and environmental sustainability [11]. However, not all landfills can support effective RDF recovery; therefore, LFM planning is crucial. The planning stage for this method encompasses several procedures, including site characterization, economic potential assessment, regulatory considerations, health and safety planning, and cost estimation [12]. A key challenge in LFM is selecting an assessment method to quantitatively and qualitatively assess the amount of usable material from the total recovered fraction [3]. Current practices in LFM often rely on traditional invasive sampling methods for site assessment [13, 14], which are time-consuming and provide limited spatial data. Therefore, non-invasive investigation methods that provide spatial insights and rapid results are required for disposal site assessment before conducting LFM.

To tackle this challenge, one promising technique is the use of electrical resistivity imaging (ERI). ERI surveys have become a crucial tool for characterizing waste composition within landfills by measuring the subsurface electrical resistivity values of waste disposal sites. This surveying technique is a non-intrusive method that is cost-effective, allows rapid data acquisition, and provides spatial model data. The ERI technique is widely used in a range of subsurface applications, including groundwater exploration, landfill characterization, and slope stability assessments [15–17]. In addition, ERI can be used as an efficient preliminary method to identify suitable LFM candidate areas within landfill sites for RDF production. Chungam et al. [17] revealed that the electrical resistivity value of the waste layer was about 42.0 Ω m in areas with low plastic material content (20–30%). In contrast, electrical resistivity values exceeding 100.0 Ω m indicated areas with very high plastic material content (> 40%) because plastics are resistive materials that contribute to high resistivity in waste. Furthermore, their study revealed a strong correlation ($r^2 = 0.81$) between electrical resistivity and waste compositions suitable for RDF production (i.e., waste containing abundant plastic). Therefore, resistivity measurement techniques offer a reliable method for analyzing waste composition and identifying areas with RDF production potential. In addition, resistivity results provide valuable insights into the quality of the buried substrate in the disposal site, which is essential for site evaluation. The moisture content of legacy waste within a disposal site is crucial as it significantly impacts energy recovery. ERI results can identify saturated zones, which must be avoided in the RDF reclamation process. While ERI offers an indirect method for assessing overall site moisture content, it is important to note that high moisture levels typically correlate with low-resistivity values due to increased ion concentration in leachate [18, 19].

From the perspective of determining the amount of MSW present, aerial photogrammetry has been applied to landfill surveys for volumetric assessment. Bhatsada et al. [20] and Kaamin et al. [21] used an unmanned aerial vehicle (UAV) to evaluate the waste capacity and waste volume in landfill sites. These studies were successful in using this approach to systematically manage and enhance waste management. Accordingly, UAV photogrammetry is a method that can be used to rapidly and accurately estimate the quantity of waste above ground level in a landfill.

As detailed above, UAV photogrammetry and ERI measurements can be utilized to assess quality and quantity of RDF production potential. While UAV imaging techniques can estimate the volume of a landfill above ground level, ERI can be used to estimate the proportion of RDF in underground waste piles based on the relationship between the electrical resistivity and the amount of plastic material; thus, integrating ERI and UAV photogrammetry techniques can be used to achieve reliable and prompt results in LFM site assessment. However, the combination of ERI and UAV photogrammetry for LFM applications has not been extensively studied to date. Given this limitation, the present study focuses on comprehensively characterizing waste material in the Buriram landfill in Thailand to assess RDF production potential using a combination of ERI, UAV photogrammetry, and a comprehensive economic cost–benefit analysis. By combining ERI and UAV photogrammetry, this study proposes a robust disposal site assessment methodology that can potentially improve MSW management practices. This study's key findings support LFM feasibility studies by demonstrating an integrated method to help minimize the risks associated with LFM. Overall, this approach contributes to a circular economy by closing the loop on MSW management and promoting sustainable waste management practices.

Materials and methods

Study site description

The study area is located within the Buriram landfill in Phrakru Subdistrict, Mueang Buriram District, Buriram Province, in the northeastern region of Thailand (15.11709° N, 103.04392° E). This landfill was opened in 2000 and covers an area of approximately 160,000 m^2. This sanitary landfill site receives 107 tons of waste per day [22]. The landfill is divided into three phases, each designed to accommodate three cells of waste with a height of 2 m per cell. Phases 1 and 2 consist of closed areas that are approximately 5–13 years old (Fig. 1a, b). Both phases have been capped with soil, and gas collection and venting pipes have been installed. Phase 3 is currently an active waste disposal site that has been operational for approximately eight months to 1 year, with over 70% of the second cell currently filled (Fig. 1c). Due to the prolonged use of this landfill, its

economy in the waste-to-energy concept, promoting efficient resource use and environmental sustainability [11]. However, not all landfills can support effective RDF recovery; therefore, LFM planning is crucial. The planning stage for this method encompasses several procedures, including site characterization, economic potential assessment, regulatory considerations, health and safety planning, and cost estimation [12]. A key challenge in LFM is selecting an assessment method to quantitatively and qualitatively assess the amount of usable material from the total recovered fraction [3]. Current practices in LFM often rely on traditional invasive sampling methods for site assessment [13, 14], which are time-consuming and provide limited spatial data. Therefore, non-invasive investigation methods that provide spatial insights and rapid results are required for disposal site assessment before conducting LFM.

To tackle this challenge, one promising technique is the use of electrical resistivity imaging (ERI). ERI surveys have become a crucial tool for characterizing waste composition within landfills by measuring the subsurface electrical resistivity values of waste disposal sites. This surveying technique is a non-intrusive method that is cost-effective, allows rapid data acquisition, and provides spatial model data. The ERI technique is widely used in a range of subsurface applications, including groundwater exploration, landfill characterization, and slope stability assessments [15–17]. In addition, ERI can be used as an efficient preliminary method to identify suitable LFM candidate areas within landfill sites for RDF production. Chungam et al. [17] revealed that the electrical resistivity value of the waste layer was about 42.0 Ω m in areas with low plastic material content (20–30%). In contrast, electrical resistivity values exceeding 100.0 Ω m indicated areas with very high plastic material content (>40%) because plastics are resistive materials that contribute to high resistivity in waste. Furthermore, their study revealed a strong correlation (r^2 =0.81) between electrical resistivity and waste compositions suitable for RDF production (i.e., waste containing abundant plastic). Therefore, resistivity measurement techniques offer a reliable method for analyzing waste composition and identifying areas with RDF production potential. In addition, resistivity results provide valuable insights into the quality of the buried substrate in the disposal site, which is essential for site evaluation. The moisture content of legacy waste within a disposal site is crucial as it significantly impacts energy recovery. ERI results can identify saturated zones, which must be avoided in the RDF reclamation process. While ERI offers an indirect method for assessing overall site moisture content, it is important to note that high moisture levels typically correlate with low-resistivity values due to increased ion concentration in leachate [18, 19].

From the perspective of determining the amount of MSW present, aerial photogrammetry has been applied to landfill surveys for volumetric assessment. Bhatsada et al. [20] and Kaamin et al. [21] used an unmanned aerial vehicle (UAV) to evaluate the waste capacity and waste volume in landfill sites. These studies were successful in using this approach to systematically manage and enhance waste management. Accordingly, UAV photogrammetry is a method that can be used to rapidly and accurately estimate the quantity of waste above ground level in a landfill.

As detailed above, UAV photogrammetry and ERI measurements can be utilized to assess quality and quantity of RDF production potential. While UAV imaging techniques can estimate the volume of a landfill above ground level, ERI can be used to estimate the proportion of RDF in underground waste piles based on the relationship between the electrical resistivity and the amount of plastic material; thus, integrating ERI and UAV photogrammetry techniques can be used to achieve reliable and prompt results in LFM site assessment. However, the combination of ERI and UAV photogrammetry for LFM applications has not been extensively studied to date. Given this limitation, the present study focuses on comprehensively characterizing waste material in the Buriram landfill in Thailand to assess RDF production potential using a combination of ERI, UAV photogrammetry, and a comprehensive economic cost–benefit analysis. By combining ERI and UAV photogrammetry, this study proposes a robust disposal site assessment methodology that can potentially improve MSW management practices. This study's key findings support LFM feasibility studies by demonstrating an integrated method to help minimize the risks associated with LFM. Overall, this approach contributes to a circular economy by closing the loop on MSW management and promoting sustainable waste management practices.

Materials and methods

Study site description

The study area is located within the Buriram landfill in Phrakru Subdistrict, Mueang Buriram District, Buriram Province, in the northeastern region of Thailand (15.11709° N, 103.04392° E). This landfill was opened in 2000 and covers an area of approximately 160,000 m^2. This sanitary landfill site receives 107 tons of waste per day [22]. The landfill is divided into three phases, each designed to accommodate three cells of waste with a height of 2 m per cell. Phases 1 and 2 consist of closed areas that are approximately 5–13 years old (Fig. 1a, b). Both phases have been capped with soil, and gas collection and venting pipes have been installed. Phase 3 is currently an active waste disposal site that has been operational for approximately eight months to 1 year, with over 70% of the second cell currently filled (Fig. 1c). Due to the prolonged use of this landfill, its

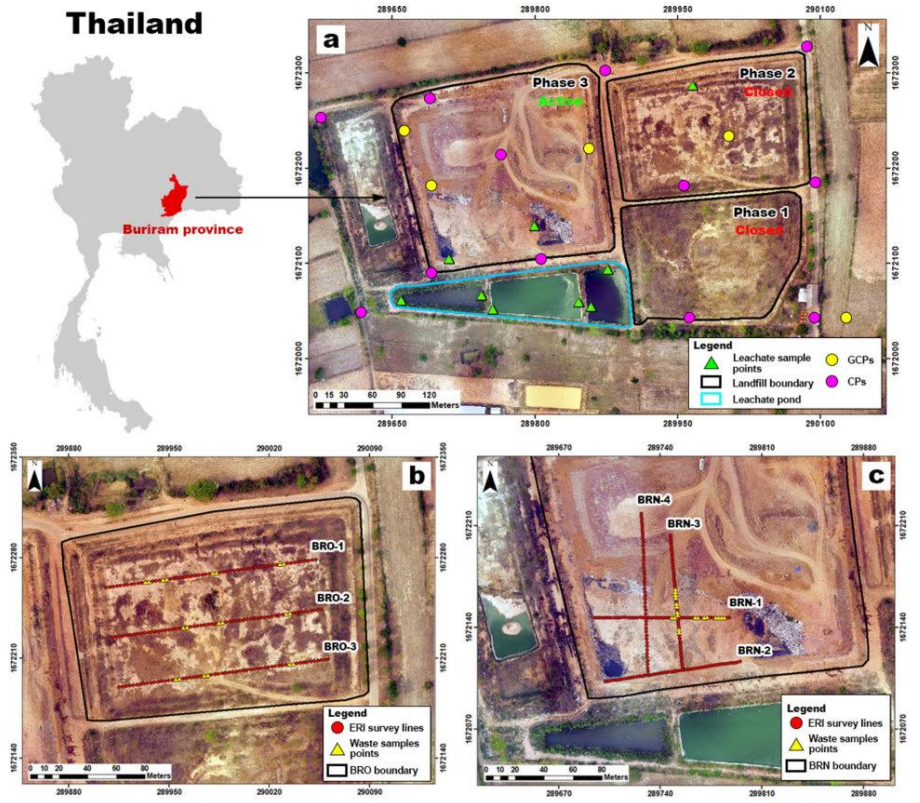

Fig. 1 Site description: **a** location and aerial photographic map of the Buriram landfill, including leachate sampling locations, **b** aerial image showing ERI survey lines and waste sampling points in phase 2 (inactive area, BRO), and **c** aerial image showing the active area (BRN) in phase 3

capacity is nearing its designed limit. Therefore, the Buriram municipality must find ways to reclaim landfill space, with LFM being one of the options under consideration.

The general topography of the study area is characterized by a combination of plateaus and mountains, forming part of the Phanom Dong Rak Mountain Range. The elevation of the landfill site ranges from 150.0 to 200.0 m above mean sea level. The study area is underlain by sedimentary deposits of the Khorat Group, which primarily consists of claystone and siltstone (Department of Mineral Resources, 2010). According to data from the Meteorological Department of Thailand, the climate of the study area is tropical and humid, with an average annual temperature of approximately 27.0 °C (22.2–33.0 °C temperature range) and an average annual rainfall of 1000.0–1200.0 mm. This area's climate can be divided into two distinct seasons: a rainy season (May–October) and a dry season (November–April). Groundwater in this area was found at 35–45 m from ground level within the fracture of bedrock. The pH value of groundwater was 7.3–7.7, and electrical conductivity varies from 0.30 to 0.34 mS/m.

Waste quantity evaluation

In this study, a DJI Phantom 3 Professional (DJI, China) was used for aerial photography. The UAV's flight configuration

used for image acquisition was controlled using the Pix4D-capture application (Pix4D, Switzerland). The quality of UAV photogrammetry was controlled by placing an appropriate number of ground control points (GCPs) and checkpoints (CPs) around the study site, with five GCPs and 12 CPs positioned as shown in Fig. 1a. The accuracy of the GCPs and CPs was determined as a root mean square error (RMSE) value, ensuring high-quality results. This study followed the guidelines from Bhatsada et al. [23], which indicate that a ground sampling distance (GSD) of 5 cm, a frontal overlap of 80%, and a side overlap of 75% are suitable for accurate landfill mapping purposes in open dumpsites. Agisoft Photoscan V.1.4.4 software (Agisoft, Russia) was used to align and merge the aerial images. A dense point cloud and orthophoto were then calculated from the merged images. The orthophoto was used to locate the ERI survey lines. In addition, a digital surface model (DSM) was generated from the orthophoto, and the overground waste volume was then calculated using the generated DSM.

ERI survey

In previous studies, the ERI method has been applied to an MSW disposal site to analyze and characterize the spatial distribution of the disposed MSW [16, 17]. ERI measurements are conducted by applying an electrical current (I), which passes through a pair of metal electrodes to the ground. The resulting electricity potential difference (ΔV) is then measured using another pair of electrodes [24]. The apparent electrical resistivity (ρ_a) can subsequently be calculated using Ohm's law, as shown in Eq. (1):

$$\rho_a = K\frac{\Delta V}{I} \tag{1}$$

where ρ_a (Ω·m), ΔV (mV), I (amp), and K represent apparent resistivity, potential difference, applied current, and geometric factor, respectively. The value of K was determined by the chosen measurement array. In this study, an automatic multi-electrode GD-10 Supreme electrical resistivity meter (Geomative Co., Ltd., China) was used for the resistivity measurements. The electrical resistivity measurements were acquired in both inactive areas with old disposed MSW (Buriram old landfill; BRO) and active areas with newly disposed MSW (Buriram new landfill; BRN). Three ERI resistivity survey lines were acquired in BRO (BRO-1, BRO-2, and BRO-3), which were aligned in the NE–SW direction, as shown in Fig. 1b. In addition, four ERI survey lines were acquired in BRN. Lines BRN-1 and BRN-2 were oriented E–W, whereas BRN-3 and BRN-4 crossed the previous two lines in a N–S direction, as shown in Fig. 1c. The ERI profile length varied between 96 and 150 m. The spacing between electrical probes was 2–2.5 m, which is suitable for ERI surveys in disposal sites [25]. A Wenner–Schlumberger array was applied in this work as it allows data with moderate horizontal and vertical resolution to be acquired, which is suitable for waste disposal sites [26, 27]. The ERI measurements were collected in April–May 2020 during Thailand's dry season. The measured ρ_a values were processed using RES2DINV X64 ver. 4.03 software (Geotomo, Malaysia). The disposal site's true 2D electrical resistivity (ρ; Ω·m) was calculated using an iterative Jacobian matrix–constrained least-squares inversion approach. The number of iterations in this process was set to five. The RMSE values are shown in the resistivity section, which reflect the percentage differences between the true and apparent resistivity. The RMSE represents the accuracy and reliability of ERI models, where lower RMSE values indicate greater consistency and smaller differences between the calculated and measured values [17, 28]. The RDF production potential in %w/w can be calculated based on the approach of Suknark et al. [16], as shown in Eq. (2):

$$\begin{aligned}\text{RDF} &= 79.499 - 0.665(\text{Conductive materials}) \\ &\quad + 0.021(\text{Resistivity value}) - 0.191(\text{Moisture content})\end{aligned} \tag{2}$$

where the conductive material content is expressed in %w/w, the ER value is measured in Ω·m, and the moisture content is in %w/w. The RDF fraction models were calculated using the Surfer ver. 27 program (Goldensoftware, USA). Kriging interpolation was used to estimate the RDF fraction. Kriging is a sophisticated technique that can be used to estimate values in unsampled locations by considering the spatial trends and relationships within the existing data [29]. Cross-validation was used to check the validity of the Kriging interpolation results. The RMSE and mean error (ME) of the interpolation results were controlled to not exceed 10% of the data range and ± 1%, respectively.

Waste sampling and characterization

Waste sampling points were selected to correspond to locations with variations in electrical resistivity values. The locations of the sampling points along the ERI survey lines were determined using a real-time kinematics global navigation satellite system (RTK-GNSS). Both rover-GNSS and base-GNSS receivers were Hi-Target V100 systems (Hi-Target Surveying Instrument Co., Ltd., China). The sampling points include locations with high and low electrical resistivity. Areas of high electrical resistivity typically indicate the presence of resistive materials, such as plastic, rubber, and leather, whereas low-resistivity areas usually contain conductive materials, such as food waste and organic yard waste [15, 16]. High moisture content of food waste leads to low electrical resistivity [18]. The sampling depth was 1–3 m below ground level. In total, 20 samples were collected in

each active and inactive area. The systematic random sampling method was used to collect landfill waste samples. The resistivity values of the waste in both the BRN and BRO areas were divided into 20 strata, ranging from the lowest to the highest values in each area. Sampling points were then selected to represent each stratum based on their resistivity values. At each location, an excavator collected a 200 kg sample. The excavated sample was then divided using the cone and quartering method until 50 kg of MSW remained. The selected sample was then sorted according to the IPCC waste model [30]. Approximately 1 kg of MSW was collected for moisture content (MC) analysis in the laboratory. The gravimetric method was used for MC analysis. The Pearson correlation between ER values and MSW composition was analyzed to elucidate how the composition of MSW influences the ER values. Additionally, this study employed a random sampling method for leachate collection ($n=9$). Samples were taken from surface runoff and leachate collection ponds (Fig. 1a). These leachate samples were then analyzed using a portable meter (HM Digital, USA) to measure their pH, electrical conductivity (EC), and total dissolved solids (TDS). The meter's measurement ranges are 0–14 for pH, 0–999 mS/m for EC, and 0–8,560 mg/L for TDS. These leachate characteristics represent leachate from the dry season, which may differ from characteristics observed during other times due to temporal and seasonal variations.

Economic cost–benefit analysis

The cost–benefit analysis (CBA) performed in this study includes both financial costs and benefits, which are categorized into direct and indirect benefits. The financial costs are divided into investment costs, including construction and equipment expenses, and operational costs, which include maintenance and RDF transportation costs, as detailed in Supplementary Table S1. The financial cost for construction and equipment was approximately 1,419,221 USD, while the costs for maintenance, RDF operation, and transportation were 1.70 USD, 3.41 USD, and 14.05 USD per ton of waste, respectively [31]. The financial costs were converted to economic costs using conversion factors for equipment, construction, transportation, labor, electricity fees, and other costs, with values of 0.84, 0.88, 0.87, 0.92, 0.90, and 0.92, respectively [32]. The benefits include direct and indirect benefits from selling RDF and soil-like materials and recovering waste capacity within the dump site. The CBA conducted in this study was based on the hypothesis of RDF production potential estimated from the ERI and UAV photogrammetry surveys, with an assumed productivity rate of 40 tons per hour, working 310 days per year and 8 h per day with the efficiency of the sorting machine was approximately 50% [33]. The RDF price was based on its heating value, with a 0.01 USD per megacalorie rate. Approximately 30% of the recovered material by volume, with a density of 300 kg/m^3 and a value of 7.95 USD/m^3, can be used to reduce the cost of soil cover [17, 34, 35]. Additionally, the recovery of waste dump capacity could provide financial benefits via the disposal fee of 7.10 USD/ton. The CBA used the net present value (NPV) to assess profitability, with a discount rate of 10% to reserve the decreased return rate in future [36]. However, this study did not investigate the density of MSW at the site, which is a limitation of this research. Future studies should address this aspect to enhance the accuracy of CBA calculations. To indicate the project's economic feasibility, the NPV should exceed zero, as shown in Eq. (3):

$$NPV = \sum_{t=0}^{n} \left(\frac{B_t - C_t}{(1+r)^t} \right) \tag{3}$$

where B_t is the benefit at year t, C_t is the cost value at year t, r is the discount rate, and t is project time measured in years from 0 to n.

In addition, the benefit–cost ratio (B/C ratio) was used to identify the project's cost management efficiency, as shown in Eq. (4):

$$B/C = \frac{PVB}{PVC} \tag{4}$$

where PVB is the present value benefit, and PVC is the present value cost.

The economic internal rate of return (EIRR) metric was used to represent the actual rate of return, as shown in Eq. (5). The project is economically optimal when the EIRR is greater than the opportunity cost, which refers to the return rate value from a missed opportunity in utilizing domestic resources.

$$NPV = \frac{\sum_{t=0}^{n} \left(B_t - C_t \right)}{(1+EIRR)^t} = 0 \tag{5}$$

Results and discussion

Waste volume evaluation

The RMSE values for the CPs used in the UAV photogrammetry of the study site were calculated, yielding a horizontal X error (RMSE$_x$) of 0.732 pixels, a horizontal Y error (RMSE$_y$) of 1.135 pixels, and a vertical Z error (RMSE$_z$) of 0.125 pixels, indicating high accuracy. According to the ASPRS 2014 standard, an aerial map with a GSD of 5 cm suggests precise imaging [37]. In the case of the present study, the RMSE$_x$ and RMSE$_z$ values are less than 1 pixel

and thus meet this requirement, signifying high accuracy; however, the $RMSE_y$ value of 1.135 pixels exceeds this threshold, placing it in the standard accuracy range for mapping and GIS applications. This higher $RMSE_y$ value may relate to wind-induced UAV drift, which can disrupt the camera's position and decrease image sharpness.

The UAV photogrammetry-generated DSM has vertical and horizontal errors of less than 5 cm, as shown in Fig. 2. Based on the DSM, the top of the BRO area is 6.3 m above ground level, while the bottom is 7.4 m below ground level; thus, the thickness of the MSW layer in the BRO area is 13.7 m. At BRN, the thickness of the MSW layer is 10 m, with the top of the site located 4.7 m above ground level and the base 5.3 m below ground level, as listed in Table 1. The volume of disposed waste in BRO is 271,497.9 m^3, consisting of 168,395.5 m^3 above ground and 103,102.4 m^3 below ground. The volume of disposed waste in BRN is 336,860.9 m^3, with 137,478.1 m^3 below ground and 199,382.9 m^3 above ground. However, there is also a soil cover of 15–30 cm added daily at both BRO and BRN. The daily soil cover volume can be estimated as 15–30% of the total waste volume [38, 39]. Therefore, the true volumes of MSW in BRO and BRN are estimated as 190,048.6 m^3 and 269,488.8 m^3, respectively, while the volumes of daily soil cover in BRO and BRN are 81,449.4 m^3 (30% of total volume) and 67,372.2 m^3 (30% of total volume), respectively. Thicker soil cover at BRO results in a higher percentage of daily soil cover than that at BRN. Based on the above values, the masses of MSW in BRO and BRN are 211,768.4 tons and 262,751.6 tons of waste, respectively, assuming a density of 0.78 tons/ m^3 based on the findings of a previous study [34].

Table 1 Information of sub-survey areas

Physical properties	BRO	BRN
Site operation	Closed	Active
Age of disposal waste (yrs.)	5–13	0.6–1
Height from ground (m)	6.3	4.7
Bottom level from the ground (m)	7.4	5.3
Chemical properties		
pH	8.0	5.0–7.0
EC (mS/m)	49.3	93.2–120.5
TDS (mg/l)	33,100.0	63,350–83,500

ERI investigation

Figure 3 presents the ERI models of survey lines BRO–1 and BRN–3, representing inactive and active areas, respectively. Both models effectively illustrate the distinct electrical resistivity characteristics of landfill phases 2 and 3, covering the entire Buriram landfill site. The remaining ERI models are shown in the supplementary section in Figures S1 and S2. The average electrical resistivity is similar in both areas (Fig. 3a). The average electrical

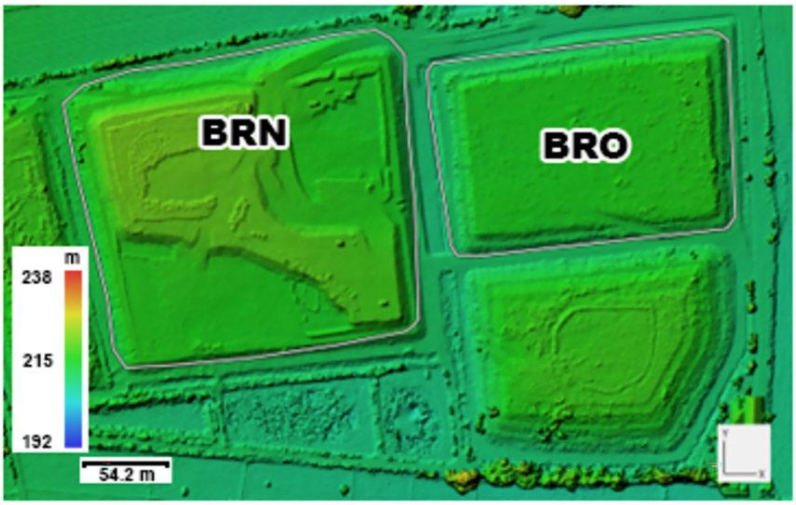

Fig. 2 DSM map of BRN and BRO landfills

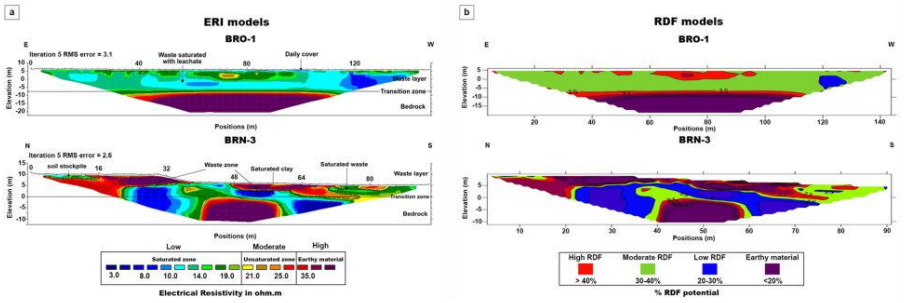

Fig. 3 **a** Inverted ERI model showing the observed electrical resistivity of the BRO–1 profile in the closed region and the BRN–3 profile in the active area. **b** RDF models showing the predicted percentage of RDF recovery potential in the BRO and BRN areas

resistivity value of the closed area (BRO; average 20.0 Ω m, S.D. = 9.01, min/max = 5.9/72.6 Ω m) is higher than that of the active area (BRN; average 18.6 Ω m, S.D. = 8.03, min/max = 3.2/192.8 Ω m). A t-test assuming unequal variances confirmed that the resistivity in BRO was significantly higher than in BRN ($t = -5.712$, $p < 0.05$). A t-test assuming unequal variances confirmed that the resistivity in BRO was significantly higher than in BRN ($t = -5.712$, $p < 0.05$). The results of this study correspond to the findings of a previous investigation by Suknark et al. [16], which found that soil cover affects the characteristics of waste more than the disposal period. Furthermore, the electrical resistivity of the old MSW (BRO area) is more uniform than that of the new MSW (BRN area). The uniformity of the BRO's resistivity may stem from the stability of degradable waste in the BRO area. The stabilized degradation activity in BRO led to a homogeneity of moisture in the waste substrate, which is reflected in the uniformity of resistivity. The RMSE values obtained from the ERI models for profiles in the Buriram landfill ranged from 1.8 to 5.0.

From the ERI models (Fig. 3a), the electrical resistivity values can be divided into three ranges: 4–20, 20–30, and > 30 Ω m. These electrical resistivity ranges represent the saturated zone, unsaturated zone, and earthy material, respectively [40, 41]. The saturated zone was influenced solely by leachate, with no intrusion of groundwater due to the disposal area's bottom being located above the groundwater level. Leachate plumes were captured within low-resistivity zones. Leachate typically exhibits low resistivity due to its high ion content. This classification scheme is applied to analyze the ERI models from this study as described below:

BRO area: the top layer of the BRO area shows low-to-moderate ER values (10–20 Ω·m), with some areas exhibiting pockets of higher resistivity. These are interpreted as old waste layers with lower MC content. The migration of leachate from old waste occurs from the top of the site to the bottom due to gravity, resulting in higher resistivity and lower MC at the top of the waste [42]. The layer below is more conductive than the top layer with lower resistivity values (4–15 Ω·m), which is interpreted as waste saturated with leachate. The presence of soil cover promoted anaerobic biodegradation, thus inhibiting leachate migration and allowing leachate to accumulate in pores, which in turn influenced the fluid saturation in the waste body [16]. Finally, the bottom layer of the BRO area has high ER values (30 Ω·m), corresponding to the sedimentary base underlying the landfill, as shown in Fig. 3a.

BRN area: the top layer exhibits moderate-to-high electrical resistance, indicating the presence of a new waste layer with low density and compaction [43, 44]. Low compaction generates free air spaces in the waste substrate, which act as barriers to electrical current flow, leading to high resistivity. Conversely, higher compaction results in fewer free air spaces, which can increase volumetric moisture content through in situ moisture. Consequently, newly disposed waste with lower compaction typically exhibits higher resistivity values compared to older waste. The layer below has low-to-moderate resistivity values, indicating the presence of waste with high MC or leachate saturation. The bottom layer has low to high resistivity values and represents the geological base of the site. The observed low-resistivity zones represent weathered bedrock underlying the landfill, which allows it to become saturated with groundwater or leachate (Fig. 3a).

Waste characteristics

This study revealed that the Buriram landfill area is dominated by saturated zones. Due to an inefficient leachate collection system and the flat-lying elevation of the landfill area, there is a high MC in the waste composition, which can decrease the quality of RDF [17, 45]. The average MC values for the waste sampled in BRO and BRN were 44.8 and 47.49%, respectively. In addition, the conditions and leachate properties of both sub-survey areas are shown in Table 1. The chemical properties of the leachate measured in this study indicate that the pH in BRN was lower than in BRO, while the EC and TDS values in BRN were higher than those in BRO. In the anaerobic biodegradation pathway, bacteria use volatile fatty acids to produce methane, thus decreasing the acidity of the leachate, indicating that the BRO area was more stabilized than BRN [46, 47]. In addition, the TDS concentration reflects the mineralization degree from dissolved organic matter and increases the salinity of the leachate, thus resulting in improved leachate conductivity [47, 48]. This implies that the leachate in BRN has higher ion exchangeability, resulting in lower ER values.

Figure 4 shows the MSW composition measured in the BRO and BRN sites. The BRN sample contains more biodegradable material (food waste and yard waste) than BRO, around 10% of the total sample (*w*/*w*), because the organic matter in the old waste has fully decomposed and the waste has stabilized [49, 50]. However, the BRO area contains a similar amount of plastic material (i.e., polyethylene bags, packaging, and foam) to the BRN area, with a plastic fraction of 35–42% recorded in the disposed MSW. The relative proportion of plastic recorded in BRO was higher than that in BRN due to the reduced proportion of biodegradable materials. Despite the significant plastic content in BRO and BRN samples, which could potentially be used for RDF production, the high moisture content and the removal of certain burnable fractions during processing reduced the overall RDF recovery. This disparity suggests that the actual RDF yield may be lower than indicated by the compositional analysis. Furthermore, the results indicate that the content of soils and fine fractions was higher in BRO than in BRN due to the transformation of biodegradable materials, which reduced the size of the material to fine particles [29, 51].

In addition to the age of the waste, seasonal variations can also influence waste characteristics, especially the chemical properties of leachate and MC. Buriram landfill operates with daily soil cover, thus reducing the likelihood of rain infiltration and gas emissions [52, 53]; however, some rainfall will still infiltrate the waste body. This implies that moisture from rainfall could change the leachate's characteristics by increasing or reducing the concentrations of certain chemicals within the leachate [48]. In contrast, the concentration of heavy metals may increase during the summer and winter, resulting in high levels of RDF pollutants [54]. In addition, variations in waste generation and composition are also driven by anthropogenic factors, such as human behavior or socio-economic levels [55]. Based on historical seasonal data in Thailand, variations in waste generation and composition should be investigated in detail in future research.

In addition, the correlations between waste composition and resistivity were analyzed as shown in Table 2, which illustrates the effect of MSW composition on resistivity values. According to Pearson's correlation coefficient analysis, the data were normally distributed, and the *p*-value was less than 0.05, indicating the reliability and significance of the correlations. The results indicate that the correlation coefficients in BRO were stronger than those in BRN, which may be due to the heterogeneity of the waste in BRN, resulting in difficulties in investigating waste composition. As observed

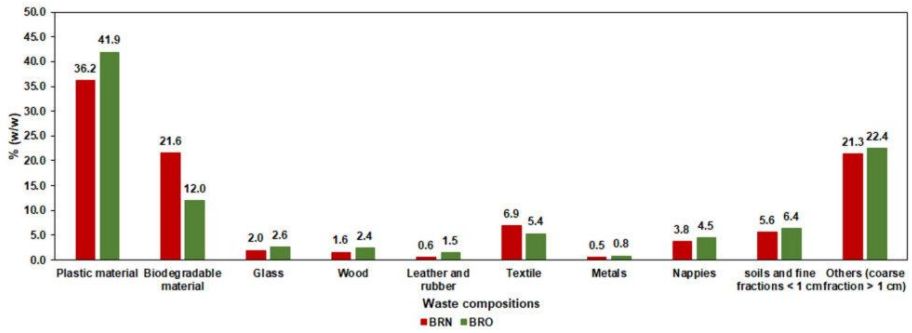

Fig. 4 Waste composition (percentage of wet weight) from both sites

Table 2 Correlation coefficients of waste composition and ER values

Waste composition	Correlation coefficient (r)	
	BRO*[1]	BRN
Food waste	0.63	0.00
Yard waste	0.17	0.36
Paper and cardboard	−0.41	0.36
Wood	−0.42	0.35
Textiles	−0.24	−0.47
Nappies	−0.62	0.30
Rubber and leather	−0.36	−0.41
Plastics	−0.37	0.52
Metal	−0.61	−0.17
Glass	−0.57	0.61
Other	0.46	−0.50

*1 = the sample size is 20 samples per area

in Table 2, the absolute values of correlation coefficients for BRO are generally higher than those for BRN, indicating stronger correlations. The positive or negative sign simply denotes the direction of the relationship: a negative sign signifies an inverse relationship, while a positive sign indicates a direct relationship.

However, the correlations in BRO were negative, whereas those in BRN were positive. Since the MC of BRO was lower than that in BRN, the obtained results may be influenced primarily by MC rather than waste composition, as noted by Clement et al. [56]. The increased MC, which led to lower electrical resistivity values, followed Archie's law. This implies that the electrical resistivity values in BRO are more sensitive to MC than those in BRN. In addition to MC, waste density may also affect the electrical resistivity as the density of old waste may be higher than that of new waste due to the pore spaces in the old waste being progressively filled by degraded particles, resulting in increased density [57–59]. This may explain the uniform direction of correlation and stronger correlation coefficients recorded in BRO. However, the results of this study overall imply that directly assessing RDF production potential from electrical resistivity values may not produce accurate results due to variations in waste characteristics and the limitations of ERI. Accordingly, the multiple linear regression equation from Suknark et al. [16] was used in this study to assess RDF production potential.

RDF production potential

Pearson's correlation coefficient was used to determine the correlations between plastic waste content and electrical resistivity. These correlations were then utilized to estimate the RDF fraction. In comparing the two areas, BRN exhibited a stronger positive correlation (r = 0.52) between plastic waste content and resistivity than BRO (r = − 0.37). This indicates a moderate positive correlation for BRN (r = − 0.40 to − 0.69) and a weaker negative correlation for BRO (r = 0.10 to − 0.39) [60]. However, the relationships between plastic waste content and electrical resistivity show some unusual characteristics: BRN is positively correlated with resistivity, while BRO is negatively correlated. Due to the high saturation of old waste with leachate, the properties of the layer exhibit spatial variability, resulting in lower electrical resistivity [28, 44]. Corresponding to the classification of Chungam et al. [17], open dump waste with 0.1–80 Ω m electrical resistivity is a low potential waste to recovery RDF. In contrast, the moderate and high RDF recovery potential classes are characterized by resistivity ranges of 80–250 Ω m and over 250 Ω m, respectively, corresponding to plastic contents of 30–45% for the moderate potential class and over 40% for the high potential class.

Although the resistivity range (high, moderate, and low) in this study was lower than in previous studies, the estimated RDF values were not significantly lower. This suggests that the estimation of RDF values using the Kriging interpolation method based on resistivity may vary between open dump and landfill sites. However, the results of this study indicate that almost all of the disposed waste consists of moderate to low RDF potential, as depicted in Fig. 3b. The cross-validation statistics showed that the RMSE of the Kriging interpolation ranged from 0.09 to 1.46, which is below the 1.66 threshold (10% of the range). Moreover, the ME value from cross-validation varied from − 0.25% to 0.13%, which is less than 1%. Therefore, the Kriging interpolation results were acceptable.

In addition, the potential of RDF production could be converted using the equation described in Suknark et al. [16]. The results show that the RDF production potential of the BRO area was approximately 40.66% (40.36–41.77%), while that of BRN was approximately 42.05% (41.64–47.35%), which corresponds to moderate potential according to the classification of Chungam et al. [17]. The results show that the difference between actual and predicted RDF potential from Suknark et al. [16] has a correlation coefficient (r) of 0.29, while the RMSE is approximately 10.54%. This indicates that the prediction model's accuracy for RDF production potential was relatively good.

When comparing this study with those by Suknark et al. [16] and Chungam et al. [17], it was found that MSW management practices significantly influence electrical resistivity, which indicates the location and quantity of the RDF fraction. Specifically, landfill management exhibits lower electrical resistivity for the RDF fraction compared to open dump and thin-layer management methods. This is due to differences in management systems (e.g., covering systems, leachate collection systems) and seasonal external factors in the waste management areas, which affect the electrical

resistivity of the waste. These studies demonstrate that ERI surveys improve the assessment of landfill mining potential across all waste management scenarios, including both proper management, such as landfilling, and improper management, such as open dumping.

This study's investigation was conducted during the summer, which resulted in a relatively high RDF production potential, consistent with the findings of Saravanan and Ramesh [54]. RDF produced during the summer has lower MC, resulting in a higher calorific heating value. In contrast, the presence of heavy metals or volatile material in RDF during the summer could lead to pollution in incinerators. To address this problem, performing LFM during the post-monsoon and pre-winter periods could reduce the concentration of heavy metals and volatile materials. Previous studies have reported that MSW landfills are influenced by rainfall infiltration during the monsoon, resulting in reduced concentrations of heavy metals and volatile material [54].

As noted above, the MC present in this study area was relatively high even in the summer due to the difficulty of leachate migration produced from anaerobic biodegradation and the presence of daily soil cover. Thus, a leachate collection system should be installed to reduce the MC of the waste body, or RDF pre-treatment should be performed using mechanical drying. This study indicates that the quantity of MSW that could be used as RDF from LFM, including the recovery benefits from the daily soil cover, represented over 50% of the total material in the studied waste dump. In terms of quantity, the buried MSW in BRO and BRN were ~ 271,500 m^3 and ~ 336,900 m^3, respectively. This study provides a basic overview of the feasibility of recovering energy and materials via LFM. However, developing a more comprehensive waste operation process could enhance the RDF production potential, including land and material recovery, ultimately contributing to improved environmental sustainability.

Economic cost–benefit analysis

The results obtained from the ERI and DSM revealed that the RDF production potential values of the BRO and BRN areas were 43,053 and 55,244 tons, respectively. These values indicate that the BRO and BRN projects would take approximately 3 years to completely mine MSW mass from landfills. The total financial cost of the BRO was calculated as 3,080,734 USD, equivalent to an economic cost of 2,882,989 USD. In contrast, the total financial cost of BRN was calculated as 3,506,434 USD, equivalent to an economic cost of 3,302,083 USD. The PVC values for BRO and BRN were 2,516,680 USD and 2,828,623 USD, respectively. The benefit analysis showed an estimated total benefit from BRO of 3,882,341 USD, resulting in a PVB of 3,340,432 USD. This comprised 599,325 USD from RDF sales, 1,448,132 USD from soil-like material recovery, and 1,292,975 USD from disposal fees.

In comparison, the total benefit value of BRN was 4,770,037 USD, leading to a PVB of 4,003,241 USD, which comprised 685,892 USD from RDF sales, 1,752,562 USD from soil-like material recovery, and 1,564,787 USD from disposal fees. The CBA indicated that the NPVs of RDF production from BRO and BRN were 823,752 USD and 1,174,619 USD, respectively. However, it was found that the projects would not be economically viable if their indirect benefits were neglected. Considering only construction costs, the BRO and BRN projects could become economically viable within approximately four and a half years. When operational costs are included, the results of the CBA suggest it would take approximately 9 years for BRO and 11 years for BRN to become economically viable without government financial support. Additionally, the results indicate that the BRO project could provide greater benefits and a shorter payback time than BRN. This is due to the higher heating value and greater quantity of RDF at the BRO site, which was determined by moisture content. Therefore, improving RDF quality through optimal drying technology in BRN could enhance its benefits and reduce the payback period, making this area economically comparable to BRO. However, RDF production costs in Thailand are relatively high compared to other countries based on the result from Kara [61] and Hamidat et al. [62]. Based on the fact, acceptable RDF production cost was 24.24 USD per ton [61] while the RDF production cost in this study was approximately 60–70 USD per ton. The high transportation costs, especially for landfill projects located far from cement plants, along with the need to enhance heating value, necessitate RDF pre-treatment, which increases production costs.

In summary, this study provides a basic overview of integrating photogrammetry and geophysical techniques to evaluate RDF production potential. This evaluation technique offers a more accurate estimation of waste volume by combining the upper surface measurements from UAV data with subsurface data obtained from geophysical methods, surpassing the accuracy of prior estimations based solely on disposal history records [63–65]. This improvement in accuracy is essential, as the volume of waste can change over time due to organic degradation and chemical reactions. Additionally, the direct sampling method used in this study provided a sampling density of one sample per 15,210 m^3 of disposed waste, which falls within the range reported in previous studies, where sampling densities varied from 1,416 to 297,768 m^3 of waste per sample. The sample size appeared relatively low compared to the total volume of disposed waste, potentially limiting the accuracy of the assessment results. However, increasing the number of sampling points would raise analysis costs and extend the time required for sample processing. In this study, spatial distribution data was

efficiently provided through ER geophysical survey results, allowing for rapid processing and interpretation. However, the key limitations of this study are the ERI results and the nature of the waste operation process in the studied disposal site. The ERI technique has notable limitations due to its sensitivity to MC and density. Thus, the gaps in the ERI technique could be addressed using other geophysical survey techniques, such as induced polarization, electromagnetic, or seismic surveys. Moreover, key chemical characteristics of MSW examined in previous studies include volatile content, carbon, ash, and Kjeldahl nitrogen [64, 65]. These characteristics can significantly impact both energy and material recovery processes. Additionally, they influence the cost of residual fraction treatment, highlighting the need for further study to optimize recovery and treatment efficiency. Furthermore, the Buriram landfill operates with soil cover—the benefits from the recovery of material with soil cover could be more significant than material recovered from other landfill operations, such as thin-layer landfills without soil cover, resulting in fewer benefits [66]. In addition to variations in the benefits of different sites, there is also a cost consideration since the transportation costs are related to the distance between the landfill and the power plant or cement kiln that uses RDF as its fuel. Policies for promoting RDF use in power plants or cement kilns should be developed to reduce transportation costs and encourage investors to invest in LFM businesses. In addition, waste management hierarchies should be implemented to recover energy and raw materials from LFM. In summary, this study provides guidance to assess landfill recovery potential quantitatively, qualitatively, and from an economic analysis perspective. Future studies should also include energy recovery based on landfill gas recovery to achieve a more comprehensive analysis.

Conclusion

This study demonstrated the effectiveness of combining ERI with UAV surveying to assess the feasibility of LFM at the Buriram landfill. The estimated RDF using multiple techniques in this study at BRO and BRN was 43,053 tons and 55,244 tons, respectively. Furthermore, the estimated total revenue from selling RDF was 823,752 USD and 1,174,619 USD at BRO and BRN, respectively. This analysis enhances the predictive model proposed by Suknark et al. [16] by offering a detailed examination of the relationship between electrical resistivity values and waste composition in our dataset. The identified moderate correlation between these variables supports the model's accuracy in predicting RDF potential. This integrated methodology provided reliable data essential for evaluating LFM viability and confirmed the proposed project's financial feasibility. By enhancing decision-making accuracy and supporting sustainable waste management practices, this method helps to facilitate efficient resource recovery and contributes to the circular economy. Despite the promising results from this investigation, further research is still required to refine the relationship between electrical resistivity and waste composition to improve this method's accuracy, explore the long-term stability of landfill mining sites to ensure environmental safety. Additionally, comparing the methods and results of this study with similar studies worldwide on RDF potential and landfill mining feasibility paves the way for improved resource recovery efforts and contributes to a more sustainable circular economy.

Supplementary Information The online version contains supplementary material available at https://doi.org/10.1007/s10163-024-02129-9.

Acknowledgements The authors thank the National Research Council of Thailand (NRCT) for funding this study and the Buriram town municipality for providing the study site.

References

1. Pitak I, Denafas G, Baltušnikas A et al (2023) Proposal for implementation of extraction mechanism of raw materials during landfill mining and its application in alternative fuel production. Sustainability. https://doi.org/10.3390/su15054538
2. Pecorini I, Iannelli R (2020) Characterization of excavated waste of different ages in view of multiple resource recovery in landfill mining. Sustainability. https://doi.org/10.3390/su12051780
3. Krook J, Svensson N, Eklund M (2012) Landfill mining: a critical review of two decades of research. Waste Manag 32:513–520. https://doi.org/10.1016/j.wasman.2011.10.015
4. Muttaraid A, Towprayoon S, Chiemchaisri C et al (2023) Economic assessment of medium and large-scale landfill mining business: case study Thailand. E3S Web Conf 428:2002. https://doi.org/10.1051/e3sconf/202342802002
5. da Duarte CLA, Jesus TB, Valentim ACS (2024) Bibliometric analysis of landfill mining: worldwide research evolution. Detritus. https://doi.org/10.31025/2611-4135/2024.18351
6. P D, Rathod D, Muthukkumaran K (2023) Characterisation of soil-like material restored from landfill mining activities in Indian cities. Aust J Civ Eng. https://doi.org/10.1080/14488353.2023.2192022
7. Devahi P, Rathod D, Muthukkumaran K (2024) Correction: sustainable reuse potential of landfill mining waste retrieved from urban mining sites in South India. J Mater Cycles Waste Manag 26:2599. https://doi.org/10.1007/s10163-024-01979-7
8. Payomthip P, Wangyao K (2024) Evaluating the key success factors for low-carbon waste management of local administrative organizations: RDF production and semi-aerobic landfill in Thailand. J Mater Cycles Waste Manag. https://doi.org/10.1007/s10163-024-01941-7
9. Faitli J, Nagy S, Romenda R et al (2019) Assessment of a residual municipal solid waste landfill for prospective 'landfill mining.' Waste Manag Res 37:1229–1239. https://doi.org/10.1177/0734242X19881197
10. Gerassimidou S, Velis CA, Williams PT, Komilis D (2020) Characterisation and composition identification of waste-derived fuels obtained from municipal solid waste using thermogravimetry: a

review. Waste Manag Res 38:942–965. https://doi.org/10.1177/0734242X20941085
11. Mateus MM, Cecílio D, Fernandes MC, Neiva Correia MJ (2023) Refuse derived fuels as an immediate strategy for the energy transition, circular economy, and sustainability. Bus Strateg Environ 32:3915–3926. https://doi.org/10.1002/bse.3345
12. Joseph K, Visvanathan C, Nagendran R, et al (2008) Dumpsite Rehabilitation
13. Balia R (2017) Old municipal and industrial waste landfills: some examples of possible contribution of geophysical survey techniques for their assessment before reclamation. In: 16th International waste management and landfill symposium. Cagliari, Italy
14. Ghosh A, Kartha SA (2020) Assessment of feasibility and viability of landfill mining of open dumpsites in INDIA. In: Fifth Symposium on Urban Mining and Circular Economy. CISA Publisher, Assam
15. Boonsakul P, Buddhawong S, Wangyao K (2022) Optimization of multi-frequency electromagnetic surveying for investigating waste characteristics in an open dumpsite. J Air Waste Manag Assoc 72:1290–1306. https://doi.org/10.1080/10962247.2022.2113181
16. Suknark P, Buddhawong S, Wangyao K (2023) Investigating the effect of waste age and soil covering on waste characteristics prior to landfill mining using an electrical resistivity tomography technique. J Environ Manage 339:117898. https://doi.org/10.1016/j.jenvman.2023.117898
17. Chungam B, Vinitnantharat S, Towprayoon S et al (2021) Evaluation of the potential of refuse-derived fuel recovery in the open dump by resistivity survey prior to mining. J Mater Cycles Waste Manag 23:1320–1330. https://doi.org/10.1007/s10163-021-01207-6
18 Aranda CN, Elis V, Prado R et al (2021) Electrical resistivity methods to characterize the moisture content in Brazilian sanitary landfill. Environ Monit Assess. https://doi.org/10.1007/s10661-021-09050-w
19. Molua C (2022) Assessing leachate migration and gas emissions in landfill sites using seismic and electrical resistivity tomography (ERT) methods. J Environ Impact Manag Policy 2:41–52. https://doi.org/10.5552/jeimp.26.41.52
20. Bhatsada A, Towprayoon S, Garivait S, et al (2020) Evaluation of UAV Photogrammetric Accuracy for Mapping of Open Dump Based on Variation of Image Overlaps. pp 131–140
21. Kaamin M, Asrul N, Daud ME et al (2019) Volumetric change calculation for a landfill stockpile using UAV photogrammetry. Int J Integr Eng 11:53–62. https://doi.org/10.3088/jie.00.00
22. Pollution Control Department (PCD) (2020) 2019 Thailand State of Pollution Report. PCD. No. 06–072
23. Bhatsada A, Towprayoon S, Wangyao K (2019) Assessment of UAV photogrammetric accuracy based on the variation of flight configuration for landfill mapping
24. Dumont G, Pilawski T, Dzaomuho-Lenieregue P et al (2016) Gravimetric water distribution assessment from geoelectrical methods (ERT and EMI) in municipal solid waste landfill. Waste Manag 55:129–140. https://doi.org/10.1016/j.wasman.2016.02.013
25. Chungam B, Vinitnantharat S, Wangyao K (2023) Evaluation of the proper electrode spacing for ERI surveys in open dumpsites using forward modeling. Polish J Environ Stud 32:535–545. https://doi.org/10.1524/pjoes/155969
26. Bichet V, Grisey E, Aleya L (2016) Spatial characterization of leachate plume using electrical resistivity tomography in a landfill composed of old and new cells (Belfort, France). Eng Geol 211:61–73. https://doi.org/10.1016/j.enggeo.2016.06.026
27. Kondracka M, Stan-Kleczek I, Sitek S, Ignatiuk D (2021) Evaluation of geophysical methods for characterizing industrial and municipal waste dumps. Waste Manag 125:27–39. https://doi.org/10.1016/j.wasman.2021.02.015
28. Boonsakul P, Buddhawong S, Wangyao K (2023) Maximizing RDF recovery potential through the integration of electrical resistivity tomography and frequency-domain electromagnetic surveys for waste characterization in open dump mining. Sci Total Environ 904:166807. https://doi.org/10.1016/j.scitotenv.2023.166807
29. Wangyao K, Sutthasil N, Chiemchaisri C (2021) Methane and nitrous oxide emissions from shallow windrow piles for biostabilisation of municipal solid waste. J Air Waste Manag Assoc 71:650–660. https://doi.org/10.1080/10962247.2021.1880498
30. Wangyao K, Towprayoon S, Chiemchaisri C et al (2010) Application of the IPCC waste model to solid waste disposal sites in tropical countries: case study of Thailand. Environ Monit Assess 164:249–261. https://doi.org/10.1007/s10661-009-0889-6
31. Technologymedia (2019) Green Network Issue 91 January–February 2019. Rung Ruang Karn Phim
32. Ahmed S (1984) Shadow prices for economic appraisal of projects: an application to Thailand.
33. Muttarid A, Chiamchaisri C, Silalertsuksa T, et al (2023) Material flow analysis of a large-scale landfill mining: Case study Thailand. In: The 9th3R International Scientific Conference on Material Cycle and Waste Management
34. Prechthai T, Visvanathan C, Cheimchaisri C (2006) RDF production potential of municipal solid waste. In: The 2 nd Joint International Conference on "Sustainable Energy and Environment (SEE 2006). pp 21–23
35. Prechthai T, Padmasri M, Visvanathan C (2008) Quality assessment of mined MSW from an open dumpsite for recycling potential. Resour Conserv Recycl 53:70–78. https://doi.org/10.1016/j.resconrec.2008.09.002
36. Limmeechokchai B, Winyuchakrit P, Pita P (2022) The Role of Discount Rate and Social Cost of Carbon in Long Term Climate Policy on Renewable Electricity in Thailand. In: 2022 International Conference and Utility Exhibition on Energy, Environment and Climate Change (ICUE). pp 1–7
37. ASPRS (2015) ASPRS positional accuracy standards for digital geospatial data. Photogramm Eng Remote Sens 81:A1–A26
38. Hossain MDS, Haque MA (2009) The effects of daily cover soils on shear strength of municipal solid waste in bioreactor landfills. Waste Manag 29:1568–1576
39. Choudhury D, Savoikar P (2009) Simplified method to characterize municipal solid waste properties under seismic conditions. Waste Manag 29:924–933
40. Abdulrahman A, Nawawi MNM, Saad R (2015) Landfill characterization using geoelectrical tools. 256–259. https://doi.org/10.1190/iceg2015-071
41. Georgaki I, Soupios P, Sakkas N et al (2008) Evaluating the use of electrical resistivity imaging technique for improving CH4 and CO2 emission rate estimations in landfills. Sci Total Environ 389:522–531
42. Feng S-J, Zhao Y, Zhang X-L, Bai Z-B (2020) Leachate leakage investigation, assessment and engineering countermeasures for tunneling underneath a MSW landfill. Eng Geol 265:105447. https://doi.org/10.1016/j.enggeo.2019.105447
43. Ling C, Zhang Q (2017) Evaluation of surface water and groundwater contamination in a MSW landfill area using hydrochemical analysis and electrical resistivity tomography: a case study in Sichuan province, Southwest China. Environ Monit Assess 189:1–18
44. Feng S-J, Bai Z-B, Cao B-Y et al (2017) The use of electrical resistivity tomography and borehole to characterize leachate distribution in Laogang landfill, China. Environ Sci Pollut Res 24:20811–20817. https://doi.org/10.1007/s11356-017-9853-0
45. Boonsakul P, Buddhawong S, Towprayoon S et al (2021) Applying electromagnetic surveys as pre-screening tools prior to open dump mining. J Mater Cycles Waste Manag 23:1518–1530. https://doi.org/10.1007/s10163-021-01232-5

46. Gurusamy S, Thangam RSP (2023) Potential health risk assessment of contaminants in soil-like material recovered from landfill mining. Environ Monit Assess 195:330. https://doi.org/10.1007/s10661-022-10850-x
47. Lindamulla L, Nanayakkara N, Othman M et al (2022) Municipal solid waste landfill leachate characteristics and their treatment options in tropical countries. Curr Pollut Rep 8:273–287. https://doi.org/10.1007/s40726-022-00222-x
48 Gautam P, Kumar S (2021) Characterisation of Hazardous waste landfill leachate and its reliance on landfill age and seasonal variation: a statistical approach. J Environ Chem Eng 9:105496. https://doi.org/10.1016/j.jece.2021.105496
49. Qiu Z, Li M, Zhang L et al (2020) Effect of waste compaction density on stabilization of aerobic bioreactor landfills. Environ Sci Pollut Res 27:4528–4535. https://doi.org/10.1007/s11356-019-06902-4
50. Sutthasil N, Chiemchaisri C, Chiemchaisri W et al (2014) Comparison of solid waste stabilization and methane emission from anaerobic and semi-aerobic landfills operated in tropical condition. Environ Eng Res 19:261–268. https://doi.org/10.4491/eer.2014.S1.003
51. Huang M, Zhang Z, Zhu B et al (2023) Effects of moisture content and landfill age on the shear strength properties of municipal solid waste in Xi'an, China. Environ Sci Pollut Res 30:65011–65025. https://doi.org/10.1007/s11356-023-26905-6
52 Udomsri S, Petrov MP, Martin AR, Fransson TH (2011) Clean energy conversion from municipal solid waste and climate change mitigation in Thailand: waste management and thermodynamic evaluation. Energy Sustain Dev 15:355–364. https://doi.org/10.1016/j.esd.2011.07.007
53. Kaosol T (2009) Sustainable solutions for municipal solid waste management in Thailand. World Acad Sci Eng Technol 60:665–670
54. Saravanan G, Ramesh ST (2024) Statistical analysis of seasonal variation in the characteristics of soil like material and refuse derived fuel recovered from landfill mining. Stoch Environ Res Risk Assess 38:127–146. https://doi.org/10.1007/s00477-023-02569-z
55. Cheela VRS, Goel S, John M, Dubey B (2021) Characterization of municipal solid waste based on seasonal variations, source and socio-economic aspects. Waste Dispos Sustain Energy 3:275–288. https://doi.org/10.1007/s42768-021-00084-x
56. Clement R, Moreaux S, Günther T (2011) Estimating the effect of temperature, density and water content on waste electrical resistivity. In: Near Surface 2011 - 17th European Meeting of Environmental and Engineering Geophysics. pp 10–15
57. Reddy KR, Hettiarachchi H, Gangathulasi J, Bogner JE (2011) Geotechnical properties of municipal solid waste at different phases of biodegradation. Waste Manag 31:2275–2286. https://doi.org/10.1016/j.wasman.2011.06.002
58. Shihada H, Hossain MS, Kemler V, Dugger D (2013) Estimating moisture content of landfilled municipal solid waste without drilling: innovative approach. J Hazard, Toxic, Radioact Waste 17:317–330
59. Cirone A, Park C (2020) MASW survey to estimate the unit weight of municipal solid waste at a landfill in Brazil. In: Proceedings of the Institution of Civil Engineers-Waste and Resource Management. Thomas Telford Ltd, pp 1–5
60. Schober P, Schwarte LA (2018) Correlation coefficients: appropriate use and interpretation. Anesth Analg 126:1763–1768. https://doi.org/10.1213/ANE.0000000000002864
61 Kara M (2012) Environmental and economic advantages associated with the use of RDF in cement kilns. Resour Conserv Recycl 68:21–28. https://doi.org/10.1016/j.resconrec.2012.06.011
62 Hemidat S, Saidan M, Al-Zu'bi S et al (2019) Potential utilization of RDF as an alternative fuel to be used in cement industry in Jordan. Sustainability. https://doi.org/10.3390/su11205819
63. Hapsari O, Syafrudin S, Budihardjo M (2023) The potential of landfill waste in Rembang city as raw material for refuse derived fuel (RDF). J Presipitasi Media Komun dan Pengemb Tek Lingkung 20:219–228. https://doi.org/10.14710/presipitasi.v20i1.219-228
64. Kristanto G, Jansen A, Koven W (2020) The potential of landfill mining in two inactive zones of the Bantar Gebang Landfill in Jakarta, Indonesia. Int J Technol 11:1430. https://doi.org/10.14716/ijtech.v11i7.4571
65. Resmianty T, Fauzi A, Hartulistiyoso E, Pertiwi S (2022) Potential utilization of municipal solid waste in landfill mining TPST Bantargebang Bekasi to become refuse derived fuel (RDF) feed stock. J Nat Resour Environ Manag 12:281–289. https://doi.org/10.29244/jpsl.12.2.281-289
66. Suknark P, Buddhawong S, Towprayoon S et al (2022) Assessment of refuse-derived fuel production from a thin-layer landfill. J Sustain Energy Environ 13:19–23

Research publication in Proceedings of the Annual Conference of Japan Society of Material Cycles and Waste Management, DOI: https://doi.org/10.14912/jsmcwm.t3rincs2024.0_121, A Geophysical Approach to Assessing Landfill Mining Feasibility: The Buriram Landfill Experience

A Geophysical Approach to Assessing Landfill Mining Feasibility: The Buriram Landfill Experience

Komsilp Wangyao [1*], Parichat Suknark [1], Pornchanok Boonsakul [1], Chalermpon Wungsumpow [2], Panida Payomthip [3], Bongkoch Chungam [1]

1: Joint Graduate School of Energy and Environment (JGSEE), King's Mongkut University of Technology Thonburi (KMUTT), Bangkok, Thailand

2: KMUTNB Techno Park, King Mongkut's University of Technology North Bangkok, Bangkok, Thailand

3: National Institute for Environmental Studies, Japan

*corresponding author: komsilp.wan@kmutt.ac.th

Keywords: waste characterization, material recovery, subsurface imaging, RDF optimization

INTRODUCTION

The pressing need to reclaim landfill space has turned landfill mining into a standard practice in waste management. This process not only addresses space constraints but also focuses on recovering valuable materials, particularly plastics for Refuse Derived Fuel (RDF). However, not all landfills possess the potential for effective RDF recovery. To tackle this challenge, one promising technique is the use of Electrical Resistivity Investigation (ERI). ERI serves as a preliminary method to characterize the waste composition within a landfill. This study applied ERI to the Buriram landfill in Thailand. This study aims to thoroughly characterize the waste materials present, and assess the feasibility of mining and separating waste specifically for RDF.

MATERIALS AND METHODS

Electrical resistivity imaging (ERI) was conducted at the Buriram sanitary landfill. ERI data was collected during the dry season in May 2020. Buriram sanitary landfill was operated from the year 2000. This landfill receives approximately 107 tons of MSW per day. The received MSW was dumped in the disposal area and covered with clayey - soil. The disposal area settles on weathering clay and mud base rock. There were 2 sub - survey areas in this study consisting of active and closed areas. Area conditions are shown in Table 1.

Table 1 Information of sub–survey areas.

Areas	Age of disposal waste (yrs.)	Height from ground (m)	Bottom level from ground (m)
Active	0.6 - 1	4.7	5.3
Closed	5 - 13	6.3	7.4

In this study, 2D ERI survey was applied to collect the electrical resistivity data. The resistivity meter from GEOMETIVE studio with multi-channel was used in this observation. The length of ERI lines was between 96 – 150 meters. The spacing of electrodes was 2 – 2.5 meters, which is suitable for disposal site surveys (Chungam et al., 2023). Leachate and disposed of MSW characteristics were analyzed in this study.

RESULTS AND DISCUSSION

From the study, the average electrical resistivity of both areas shows the same value. However, the average electrical resistivity value of the closed area (20.0 Ω·m) is higher than the active area (18.6 Ω·m). The results of this study correspond to the previous study by Suknark et al., (2023) that the cover of soil affects to

characteristics of waste more than the disposal period. Moreover, the electrical resistivity characteristic of the old MSW (closed area) shows homogeneity than the new MSW (active area). The electrical resistivity characteristics of the Buriram landfill are shown in Figure 1.

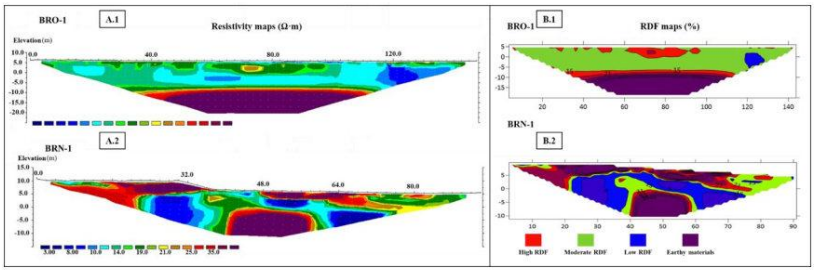

Figure 1 presents the findings in two parts: A.1 and A.2 display the observed electrical resistivity values, while B.1 and B.2 illustrate the estimated percentage of RDF recovery potential.

From ERI maps, electrical resistivity value can be divided into 3 ranges, consisting of 4 – 20 Ω·m, 20 – 30 Ω·m and more than 30 Ω·m. Those ranges of electrical resistivity of the site represent to saturated zone, unsaturated zone, and earthy material, respectively. Waste sampling shows 23% – 34% of plastic fraction in disposed MSW. Then, the correlation of waste composition and resistivity was applied to predict the RDF fraction. This study found that almost the disposal fraction consists of low RDF. Corresponding to the study by Chungam et al., (2021), disposed waste with 0.1 – 80 Ω·m electrical resistivity is a low potential waste to recovery RDF. In contrast, medium and high potential categories for RDF recovery, characterized by the resistivity of 80 – 250 Ω·m and over 250 Ω·m respectively, would correspond to higher plastic contents of 30–45% for medium potential and over 40% for high potential, which are not observed at this site.

CONCLUSION

This study demonstrates the effective use of Electrical Resistivity Imaging (ERI) at the Buriram landfill to assess the potential for mining and RDF recovery. Findings reveal similar electrical resistivity in both active and closed areas, indicating homogeneity in old MSW and potential low RDF yield. This method offers a promising approach to evaluate waste composition for optimizing resource recovery in landfills.

ACKNOWLEDGEMENT

The authors thank the National Research Council of Thailand (NRCT) for funding this study and the Buriram town municipality for the provision of the study site.

REFERENCES

Chungam, B., Vinitnantharat, S., et al., Evaluation of the Proper Electrode Spacing for ERI Surveys in Open Dumpsites Using Forward Modeling. Polish Journal of Environmental Studies, 32, 535 - 545, 2023

Suknark, P., Buddhawong, S., et al., Investigating the effect of waste age and soil covering on waste characteristics prior to landfill mining using an electrical resistivity tomography technique. Journal of Environmental Management, 339, 117898, 2023

Chungam, B., Vinitnantharat, S., et al., Evaluation of the potential of refuse-derived fuel recovery in the open dump by resistivity survey prior to mining. Journal of Material Cycles and Waste Management, 23, 1320 – 1330, 2021

Research publication in The Journal of Industrial Technology, ISSN (online): 2697-5548, DOI: 10.14416/j.ind.tech.2024.12.014, Effect of Glass Fiber and Municipal Solid Waste Incineration on Bending Stress of Compacted Cement Sand

วารสารวิชาการเทคโนโลยีอุตสาหกรรม (The Journal of Industrial Technology)
ISSN (online): 2697-5548
DOI: 10.14416/j.ind.tech.2024.12.014

บทความวิจัย

อิทธิพลของเส้นใยแก้วและของเสียจากโรงไฟฟ้าเชื้อเพลิงขยะมูลฝอยชุมชนที่มีต่อกำลังดัดของทรายซีเมนต์บดอัด

เฉลิมพล วังสำเภา[1,3] สกล โพฉลาด[2,3] พิมพ์นภัส คำมาวงศ์[3] สุนันทา สีมาจารย์[3] อารยา บุญมี[3] และ กีรติกานต์ พิริยะกุล[3*]

[1] อุทยานเทคโนโลยี มหาวิทยาลัยเทคโนโลยีพระจอมเกล้าพระนครเหนือ, มหาวิทยาลัยเทคโนโลยีพระจอมเกล้าพระนครเหนือ
[2] กองอาคารและสถานที่, มหาวิทยาลัยสวนดุสิต
[3] ภาควิชาเทคโนโลยีวิศวกรรมโยธาและสิ่งแวดล้อม, วิทยาลัยเทคโนโลยีอุตสาหกรรม, มหาวิทยาลัยเทคโนโลยีพระจอมเกล้าพระนครเหนือ
[*] ผู้ประสานงานเผยแพร่ (Corresponding Author), E-mail: keeratikan.p@cit.kmutnb.ac.th

วันที่รับบทความ: 3 กันยายน 2567; วันที่ทบทวนบทความ: 17 พฤศจิกายน 2567; วันที่ตอบรับบทความ: 3 ธันวาคม 2567
วันที่เผยแพร่ออนไลน์: 23 ธันวาคม 2567

บทคัดย่อ: บทความนี้ศึกษาอิทธิพลของเส้นใยแก้วและของเสียจากโรงไฟฟ้าเชื้อเพลิงขยะมูลฝอยชุมชนต่อกำลังดัดของทรายซีเมนต์บดอัด เพื่อลดปริมาณซีเมนต์และนำของเสียจากจากโรงไฟฟ้าเชื้อเพลิงขยะมูลฝอยชุมชนมาใช้สำหรับพัฒนาวัสดุก่อสร้างที่เป็นมิตรต่อสิ่งแวดล้อม โดยใช้เถ้าลอยและเถ้าจมเป็นส่วนผสมทำการทดสอบกำลังดัดตามมาตรฐาน ASTM C1609-10 ทรายซีเมนต์บดอัดผสมปูนซีเมนต์ร้อยละ 3, 5 และ 7 โดยน้ำหนักทรายแห้ง ผสมเส้นใยแก้วร้อยละ 0, 0.5, 1, 1.5 และ 2 โดยปริมาตร ใช้ความยาวของเส้นใยแก้วที่ 3, 6 และ 12 มิลลิเมตร สัดส่วนเถ้าลอย:เถ้าจมที่ 100:0, 75:25, 50:50, 25:75 และ 0:100 ทำการบ่มที่ 7, 14, 28, 60 และ 90 วัน ผลการทดสอบพบว่ากำลังดัดเพิ่มขึ้นตามปริมาณปูนซีเมนต์ที่เพิ่มขึ้น แสดงปริมาณปูนซีเมนต์มีผลต่อกำลังดัดของเมทริกซ์ โดยปริมาตรปูนซีเมนต์ที่เหมาะสมที่ร้อยละ 5 ความเหนียวที่ระยะแอ่นตัวของทรายซีเมนต์แปรผันโดยตรงกับปริมาณปูนซีเมนต์ที่เพิ่มขึ้น ปริมาณเส้นใยแก้วที่ร้อยละ 1.0 ถึง 1.5 เป็นสัดส่วนที่เหมาะสม ซึ่ง DI และ PSR เป็น 1 แสดงพฤติกรรมการแอ่นแบบวัสดุอ่อน ความยาวของเส้นใยแก้วแปรผันโดยตรงต่อระยะการแอ่นตัวซึ่งความยาวของเส้นใยแก้วที่เหมาะสมคือ 12 มิลลิเมตร ปริมาณเถ้าลอยทดแทนปูนซีเมนต์อยู่ระหว่างร้อยละ 10 ถึง 15 ปริมาณสัดส่วนเถ้าลอย:เถ้าจมที่เหมาะสมคือ 25:75 และพบว่าที่บ่ม 90 วันมีค่าความเหนียวสูงที่สุด

คำสำคัญ: กำลังดัด; ทรายซีเมนต์บดอัด; เส้นใยแก้ว; ของเสียจากโรงไฟฟ้าเชื้อเพลิงขยะมูลฝอยชุมชน

บทความวิจัย

วารสารวิชาการเทคโนโลยีอุตสาหกรรม (The Journal of Industrial Technology)
ISSN (online): 2697-5548
DOI: 10.14416/j.ind.tech.2024.12.014

Effect of Glass Fiber and Municipal Solid Waste Incineration on Bending Stress of Compacted Cement Sand

Chalermpon Wungsumpow[1,3], Sakol Pochalard[2,3], Pimnapat Kammawong[3], Sunantha Simachan[3], Araya Boonmee[3] and Keeratikan Piriyakul[3*]

[1] KMUTNB Techno Park, King Mongkut's University of Technology North Bangkok, Bangkok

[2] Building and Landscape Division, Suan Dusit University, Bangkok

[3] Department of Civil and Environmental Engineering Technology, College of Industrial Technology, King Mongkut's University of Technology North Bangkok

[*] Corresponding author, E-mail: keeratikan.p@cit.kmutnb.ac.th

Received: 3 September 2024; Revised: 17 November 2024; Accepted: 3 December 2024
Online Published: 23 December 2024

Abstract: This research article studies on the effect of glass fiber and municipal solid waste from the RDF power plant to bending stress of compacted cement sand to reduce cement and municipal solid waste for development of the green construction materials. Fly ash (FA) and Bottom ash (BA) are mixed into the compacted cement sand and tested according to ASTM C1609-10 standard. Samples are prepared by adding the cement content between 3%, 5% and 7% by weight. The glass fiber is mixed at 0%, 0.5%, 1%, 1.5% and 2% by volume. The glass fiber lengths are 3, 6 and 12 mm. The FA:BA ratios are 100:0, 75:25, 50:50, 25:75 and 0:100. The curing times are 7, 14, 28, 60 and 90 days. It was found that bending stress is increased with increasing the cement content, that is direct proportion to the bending stress of the matrix. The optimum cement content is 5%. The toughness is in direct proportion to the cement content. The glass fiber content is optimum at 1% to 1.5%. The DI and PSR are 1, showing that the softening behavior. The glass fiber length is recommended at 12 mm. The FA content is optimum of about 10% to 15%. The FA:BA ratio is recommended at 25:75. The curing time is recommended at 90 days

Keywords: Bending Stress; Compacted Cement Sand; Glass Fiber; Municipal Solid Waste Incineration.

วารสารวิชาการเทคโนโลยีอุตสาหกรรม (The Journal of Industrial Technology)
ISSN (online): 2697-5548
DOI: 10.14416/j.ind.tech.2024.12.014

บทความวิจัย

1. บทนำ

ในสถานการณ์ปัจจุบัน การเติบโตอย่างต่อเนื่องของพื้นที่เมืองเพิ่มขึ้นเนื่องจากมีการเติบโตด้านอุตสาหกรรมอย่างรวดเร็ว มีการก่อสร้างจำนวนมาก และมีการขยายตัวของเมืองเกิดขึ้นอย่างรวดเร็ว เช่น อาคารที่อยู่อาศัยและอุตสาหกรรม ระบบขนส่งมวลชนเพื่อการเคลื่อนย้ายผู้คน และสิ่งอำนวยความสะดวกในการจัดการน้ำดื่มและสิ่งปฏิกูลสำหรับประชาชน [1] อัตราการเติบโตของประชากรสูง และมีการเปลี่ยนแปลงทางเศรษฐกิจ สังคม สิ่งแวดล้อม ตลอดจนเทคโนโลยี [2] และความจำเป็นในการจัดการกับการเปลี่ยนแปลงสภาพภูมิอากาศทำให้จำเป็นต้องลดลงการใช้ถ่านหินในการผลิตพลังงานและกระบวนการทางอุตสาหกรรม เป็นสาเหตุของการปล่อยก๊าซเรือนกระจกในภาคอุตสาหกรรมการก่อสร้างก็มีการพัฒนาผลิตภัณฑ์ปูนซีเมนต์คาร์บอนต่ำ เพื่อมุ่งมั่นในการลดการปล่อยก๊าซคาร์บอนไดออกไซด์ [3] การใช้ตะกรันและเถ้าลอยในคอนกรีตเป็นบ่งชี้ถึงความต้องการที่จะลดปริมาณการใช้ซีเมนต์อย่างมีนัยสำคัญ [4] การนำเถ้าลอยซึ่งเป็นผลพลอยได้ของเสียจากโรงไฟฟ้าแม่เมาะในประเทศไทย โดยการนำมาแทนที่ปูนซีเมนต์ปอร์ต-แลนด์ ในการผสมในดินเหนียวกรุงเทพ ซึ่งเถ้าลอยสามารถใช้ทดแทนปูนซีเมนต์ปอร์ตแลนด์บางส่วนได้ [5] นอกจากการนำผลพลอยได้จากถ่านหินมาช่วยลดปัญหาสิ่งแวดล้อมแล้ว ยังพบว่ามีการใช้เถ้าจมที่มาจากการเผาขยะชุมชนอีกด้วย โดยพบว่าปริมาณขยะมูลฝอยชุมชนในประเทศไทยในปี พ.ศ. 2565 มีรายงานประมาณ 26.59 ล้านตัน ตามรายงานของ กรมควบคุมมลพิษ กระทรวงทรัพยากรธรรมชาติและสิ่งแวดล้อม [6]โดยทั่วไปงานก่อสร้างจะนำทรายแม่น้ำเป็นซึ่งเป็นแหล่งทรายสำหรับการนำมาใช้ในการผลิตคอนกรีต ซึ่งมีการใช้กันอย่างแพร่หลายและรวมถึงใช้เป็นวัสดุในงานก่อสร้าง มีการประมาณการการใช้ทรายของอุตสาหกรรมที่นำทรายจากแม่น้ำมาใช้มีปริมาณมากกว่า 60% ของจำนวนทรายทั้งหมดที่ใช้ในอุตสาหกรรมการผลิตคอนกรีตทั่วโลก [7] ถึงแม้ว่าการนำทรายมาใช้ยังคงมีส่วนที่ต้องคำนึงถึงด้านคุณสมบัติของทรายแม่น้ำที่นำมาใช้ทางด้านคุณภาพและลักษณะที่แตกต่างกันไปซึ่งขึ้นอยู่กับแหล่งกำเนิด ความแปรผันที่กล่าวมานี้อาจส่งผลกระทบอย่างมีนัยสำคัญต่อคุณสมบัติของส่วนผสมที่มีการนำทรายเข้ามาเป็นส่วนผสม [8] และการกำหนดความเหมาะสมของทรายก่อนนำไปใช้ในการออกแบบส่วนผสมซึ่งจะทำให้คุณสมบัติของส่วนผสมที่มีทรายผสมผสมอยู่มีคุณภาพดีและทนทาน แต่ยังคงพบปัญหาโดยเฉพาะรอยแตกร้าวของวัสดุที่ผสมด้วยทราย [9]

การใช้เส้นใยเพื่อปรับปรุงประสิทธิภาพของดินซีเมนต์และชะลอการเกิดรอยแตกร้าวได้ ด้วยเติมปริมาณเส้นใยที่เพิ่มขึ้น จำนวนและความกว้างของรอยแตกร้าวจะลดลง [10] สำหรับดินซีเมนต์เสริมเส้นใย พบว่าการเติมเส้นใยสามารถปรับปรุงความต้านทานแรงเฉือนของวัตถุที่แข็งตัวด้วยซีเมนต์ได้ [11] คุณสมบัติแรงดึงตามธรรมชาติ คุณสมบัติการเสียดสีที่พื้นผิว และการกระจายตัวที่ดีของวัสดุเหล่านี้ ทำให้วัสดุเหล่านี้เชื่อมต่อกับสารประสานที่เกิดจากปฏิกิริยาไฮเดรชั่นของซีเมนต์ในโครงสร้างเครือข่าย ซึ่งช่วยเพิ่มแรงยึดเกาะของส่วนต่อประสานหน้าสัมผัส และปรับปรุงความสามารถของดินในการ ด้านทานการเสียรูป ผลของการเสริมเส้นใยต่อความต้านทานแรงดัดงอของทรายเสริมซีเมนต์ สามารถเพิ่มประสิทธิภาพต่อ

วารสารวิชาการเทคโนโลยีอุตสาหกรรม (The Journal of Industrial Technology)
ISSN (online): 2697-5548
DOI: 10.14416/j.ind.tech.2024.12.014

การดัดงอของทรายเสริมซีเมนต์ได้ [12] งานวิจัยนี้ศึกษาคุณสมบัติเบื้องต้นของสัดส่วนผสมทรายซีเมนต์บดอัดเสริมเส้นใยแก้ว โดยนำเถ้าลอย และเถ้าจมจากเตาเผาขยะชุมชน (municipal solid waste incineration) มาผสมในอัตราส่วนผสมต่างๆ โดยเถ้าลอย และเถ้าจมนำมาใช้ในการศึกษาเพื่อลดปริมาณปูนซีเมนต์ และเส้นใยแก้วนำมาเสริมกำลังดัด เพื่อเป็นแนวทางในการต่อยอดใช้ประโยชน์จากของเสียจากโรงไฟฟ้าเชื้อเพลิงขยะมูลฝอยชุมชนให้เกิดนวัตกรรมวัสดุที่เป็นมิตรกับสิ่งแวดล้อม โดยเรียกวัสดุที่นำมาศึกษานี้ว่า ทรายซีเมนต์บดอัดสีเขียว (Green Compacted Cement Sand)

2. ขั้นตอนการวิจัย

2.1 ทราย

ทรายซิลิกามีอยู่มากมายในหลายภูมิภาคของประเทศไทย โดยมีลักษณะทางกายภาพที่โดดเด่นเช่น ความแข็ง ทนต่อสารเคมี และทนความร้อน ตลอดจนราคาที่ต่ำ หินและแร่ธาตุที่มีในซิลิกา เช่น ควอทซ์ ควอทซ์ไซต์ ทรายซิลิกา ร่วมกับซิลิกาชนิดอื่นๆ เช่น อาเกต อเมทิสต์ แจสเปอร์ หินเหล็กไฟ ฯลฯ ถูกนำมาใช้ในอุตสาหกรรมต่างๆ โดยทรายที่ใช้ในงานวิจัยนี้เป็นทรายแม่น้ำจากร้านขายวัสดุก่อสร้างในพื้นที่กรุงเทพมหานครที่มีการกระจายขนาดเม็ดทรายดังรูปที่ 1 และ มีคุณสมบัติทางกายภาพดังตารางที่ 1

ตารางที่ 1 คุณสมบัติทางกายภาพของทรายแม่น้ำ

Property	Value
Specific gravity (G_s)	2.65
Gravel content (%)	10.52
Sand content (%)	80.58
Fine content (%)	8.90
D_{60} (mm)	0.93
D_{30} (mm)	0.49
D_{10} (mm)	0.29
Coefficient of Uniformity (C_u)	3.21
Coefficient of Curvature (C_c)	0.89
Soil classification (USCS)	SP
Maximum void ratio	0.83
Minimum void ratio	0.28
Maximum dry unit weight (kN/m^3)	15.70
Optimum moisture content (%)	6.19

2.2 เส้นใยแก้ว

ใยแก้วเป็นวัสดุที่ประกอบด้วยเส้นใยแก้วที่ละเอียดมากจำนวนมาก ใยแก้วมีคุณสมบัติเชิงกลที่เทียบเคียงได้กับเส้นใยอื่นๆ เช่น โพลีเมอร์และคาร์บอนไฟเบอร์ ใยแก้วจึงถูกนำมาใช้เป็นสารเสริมแรงสำหรับผลิตภัณฑ์โพลีเมอร์หลายชนิด เพื่อสร้างวัสดุคอมโพสิตโพลีเมอร์เสริมแรงด้วยเส้นใย (FRP) ที่แข็งแรงมากและค่อนข้างมีน้ำหนักเบา เรียกว่าพลาสติกเสริมด้วยแก้ว (GRP) เส้นใยแก้ว แบ่งตาม ASTM แบ่งเป็น 2 ประเภท คือ เส้นใยสำหรับงานทั่วไป และเส้นใยชนิดพิเศษสูง ซึ่งเกือบประมาณ 90% เป็นเส้นใยสำหรับใช้งานทั่วไป สำหรับการจำแนกเส้นใยแก้วตาม ASTM บริษัท Owens Corning, Ventrotex, Ahlstrom และ Pilkinston เป็นบริษัทผลิตเส้นใยแก้ว และองค์ประกอบดังแสดงในตารางที่ 2 โดยในการวิจัยนี้ได้ใช้เส้นแก้วยี่ห้อ Owens Corning รุ่น Advantex CS 979-14 ชนิด E-glass ที่ความยาว 3, 6 และ 12 มิลลิเมตร

วารสารวิชาการเทคโนโลยีอุตสาหกรรม (The Journal of Industrial Technology)
ISSN (online): 2697-5548
DOI: 10.14416/j.ind.tech.2024.12.014

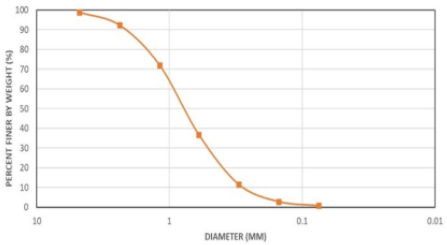

รูปที่ 1 กราฟแสดงการกระจายตัวของตัวอย่างทราย

ตารางที่ 2 ส่วนประกอบของเส้นใยแก้ว (เปอร์เซ็นต์น้ำหนัก)

Components	AR-glass	C-glass	E-glass	S-glass
SiO_2	62.2	65	55.2	65
ZrO_2	16.7	-	-	-
TiO_2	0.1	-	-	-
Al_2O_3	0.74	4	14.8	25
Fe_2O_3	0.09	0.3	0.3	-
B_2O_3	-	5	7.3	-
CaO	5.2	14	18.7	-
MgO	0.16	3	3.3	-
Na_2O	14.3	8.5	0.3	-
K_2O	0.4	-	0.2	-
LiO_2	-	-	-	-
F_2	-	-	0.3	-

2.3 ปูนซีเมนต์ปอร์ตแลนด์

ปูนซีเมนต์ปอร์ตแลนด์เป็นส่วนประกอบหลักของซีเมนต์เพสต์ ปูนซีเมนต์ปอร์ตแลนด์ประเภท 1 (ORDINARY PORTLAND CEMENT TYPE 1) ผลิตขึ้นโดยให้คุณภาพของปูนซีเมนต์มีคุณสมบัติถูกต้องเป็นไปตามเกณฑ์ที่กำหนด ในมาตรฐานอุตสาหกรรม ปูนซีเมนต์ปอร์ตแลนด์ มอก. 15-2562 ประเภท 1 และมาตรฐานอเมริกัน ASTM C-150 TYPE 1 การผสมปูนซีเมนต์จะทำให้ดินเพิ่มความสามารถในการรับกำลังอัด กำลังเฉือน และลดการซึมผ่านของน้ำ

2.4 เถ้าลอย (Fly Ash) และ เถ้าจม (Bottom Ash)

เถ้าที่เกิดจากการเผาไหม้ขยะมูลฝอยชุมชนจากบริษัท โกลบอล เพาเวอร์ ซินเนอร์ยี่ จำกัด (มหาชน) หรือ GPSC จังหวัดระยอง ซึ่งใช้วิธีการเก็บตัวอย่างตามมาตรฐาน ASTM C311/C311M-22 ซึ่งเม็ดที่ตกลงมาด้านล่างเรียกว่าเถ้าจม Bottom Ash (BA) โดยมีขนาดเส้นผ่านศูนย์กลางตั้งแต่ 0.2 ถึง 0.5 มิลลิเมตร ดังแสดงในรูปที่ 2 และเม็ดที่ลอยขึ้นด้านบนปล่องไฟเรียกว่า เถ้าลอย Fly Ash (FA) โดยมีขนาดเส้นผ่านศูนย์กลางตั้งแต่ 10 ถึง 50 ไมโครเมตร ตามมาตรฐาน ASTM C618 ประกอบด้วยซิลิคอนไดออกไซด์ (SiO_2), อะลูมิเนียมออกไซด์ (Al_2O_3) และเฟอร์ริกออกไซด์ (Fe_2O_3) ประกอบขึ้นเป็นองค์ประกอบทางเคมีของ BA วัสดุเหล่านี้จัดอยู่ในประเภทวัสดุปอซโซลานิก ASTM C 618 และ FA ถูกใช้เป็นตัวเพิ่มความคงตัวในการรักษาเสถียรภาพของดินบ่อยกว่า BA เนื่องจากมีปริมาณ SiO_2 สูงมากกว่า BA ซึ่งเป็นประโยชน์สำหรับกระบวนการเกิดปฏิกิริยาไฮเดรชั่นของปูนซีเมนต์ FA ยังมีอนุภาคที่ละเอียดมากโดยมีจำนวนอนุภาคบนพื้นผิวที่สูงกว่า ซึ่งช่วยเร่งปฏิกิริยาไฮเดรชั่นอีกด้วย [13]

3. การเตรียมตัวอย่างทดสอบ

ขั้นตอนการเตรียมตัวอย่างสำหรับทดสอบ ทำการผสมทรายให้ได้ความชื้นที่ร้อยละ 6.19 โดยใช้น้ำต่อปูนซีเมนต์ในอัตราส่วนคงที่ (W/C) ร้อยละ 0.5 ในทุกสัดส่วน ผสมปูนซีเมนต์ เถ้าลอย เถ้าจม และเส้นใยแก้วในสัดส่วน ดังตารางที่ 3

วารสารวิชาการเทคโนโลยีอุตสาหกรรม (The Journal of Industrial Technology)
ISSN (online): 2697-5548
DOI: 10.14416/j.ind.tech.2024.12.014

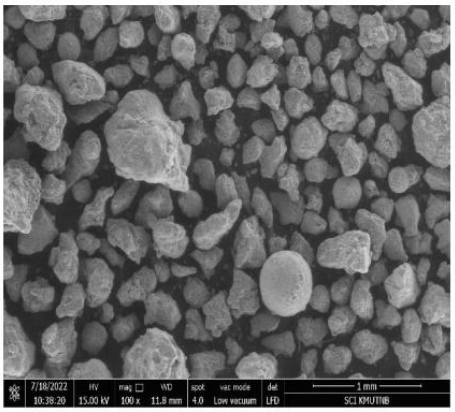

รูปที่ 2 ภาพถ่าย SEM ของเถ้าจมจากโรงไฟฟ้าเชื้อเพลิงขยะมูลฝอยชุมชน

ทดสอบกำลังรับแรงดัด สอดคล้องตามมาตรฐาน ASTM C 1609-10 ด้วยเครื่องทดสอบ Universal Testing Machine (UTM) ยี่ห้อ United Test รุ่น WDW-100Y มาตรวัดน้ำหนักแบบ Load Cell ขนาด 100 kN โดยมีวิธีการติดตั้งเครื่องมือทดสอบและขั้นตอนการทดสอบนำคานตัวอย่างวางบนแท่นเครื่องทดสอบโดยวางด้านที่เรียบเข้าหาแท่นกดน้ำหนัก การวางให้หัวกดอยู่ที่ระยะ *L*/2 ของคานทดสอบ และมีระยะพาดตัวอย่างเท่ากับ 225 มิลลิเมตร ดังรูปที่ 3 (ก) และ 3 (ข)

ตั้งค่าโปรแกรมของเครื่องทดสอบ โดยโปรแกรมทดสอบเป็นการทดสอบในห้องปฏิบัติการเพื่อคุณสมบัติเบื้องต้น

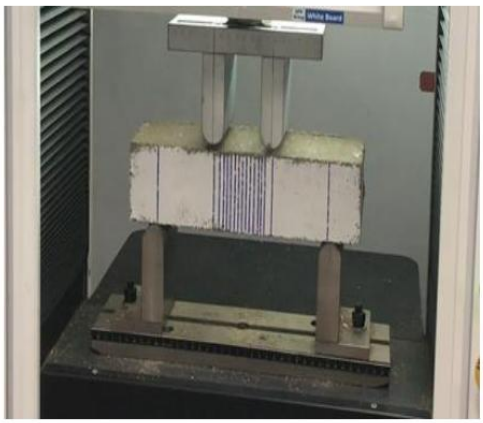

(ก) รูปแสดงการวางตัวอย่างทดสอบ

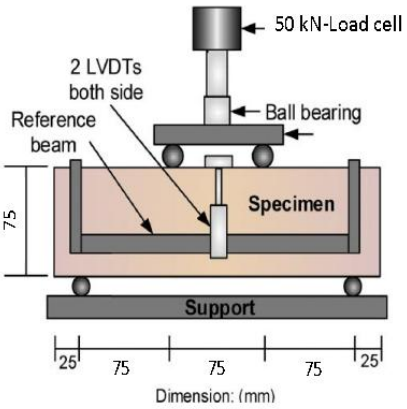

(ข) รูปแสดงการติดตั้งอุปกรณ์

รูปที่ 3 แสดงการติดตั้งอุปกรณ์ และตัวอย่างทดสอบ

วารสารวิชาการเทคโนโลยีอุตสาหกรรม (The Journal of Industrial Technology)
ISSN (online): 2697-5548
DOI: 10.14416/j.ind.tech.2024.12.014

ตารางที่ 3 แสดงสัดส่วนการผสมตัวอย่างของทรายซีเมนต์

Group	Cement Content (g)	Fiber Content (g)	Cement (g)	Fiber Length (mm)	Fly Ash (g)	Bottom Ash (g)	Day
A1	94.12	44.82	70.59	6	23.53	0	28
A2	156.87	44.82	117.65	6	39.22	0	28
A3	219.61	44.82	164.71	6	54.90	0	28
B1	156.87	0.00	117.65	6	39.22	0	28
B2	156.87	22.41	117.65	6	39.22	0	28
B3	156.87	44.82	117.65	6	39.22	0	28
B4	156.87	67.23	117.65	6	39.22	0	28
B5	156.87	89.64	117.65	6	39.22	0	28
C1	156.87	44.82	117.65	3	39.22	0	28
C2	156.87	44.82	117.65	6	39.22	0	28
C3	156.87	44.82	117.65	12	39.22	0	28
D1	156.87	44.82	141.18	6	15.69	0	28
D2	156.87	44.82	133.34	6	23.53	0	28
D3	156.87	44.82	125.49	6	31.37	0	28
D4	156.87	44.82	117.65	6	39.22	0	28
D5	156.87	44.82	109.81	6	47.06	0	28
D6	156.87	44.82	101.96	6	54.90	0	28
D7	156.87	44.82	94.12	6	62.75	0	28
E1	156.87	44.82	117.65	6	39.22	0	7
E2	156.87	44.82	117.65	6	39.22	0	14
E3	156.87	44.82	117.65	6	39.22	0	28
E4	156.87	44.82	117.65	6	39.22	0	60
E5	156.87	44.82	117.65	6	39.22	0	90
F1	156.87	44.82	117.65	6	39.22	0	28
F2	156.87	44.82	117.65	6	29.41	9.80	28
F3	156.87	44.82	117.65	6	19.61	19.61	28
F4	156.87	44.82	117.65	6	9.80	29.41	28
F5	156.87	44.82	117.65	6	0	39.22	28
CM	156.87	0	0	0	0	0	28
CM+FB	156.87	44.82	0	6	0	0	28

วารสารวิชาการเทคโนโลยีอุตสาหกรรม (The Journal of Industrial Technology)
ISSN (online): 2697-5548
DOI: 10.14416/j.ind.tech.2024.12.014

โดยกำหนดอัตราการแอ่นตัวเพิ่มขึ้นเท่ากับ 0.0.5 มม./นาที และระยะเวลาการแอ่นตัวสุทธิเท่ากับ 3มิลลิเมตร หรือจนกว่าการทดสอบดำเนินจนถึงการเกิดวิบัติ จึงหยุดการทดสอบแล้วเก็บข้อมูลที่บันทึกนำข้อมูลที่บันทึกได้มาแปลงเป็นพารามิเตอร์ระหว่างน้ำหนักและระยะการแอ่นตัวสุทธิ แสดงในรูปที่ 3 ตามมาตรฐานการทดสอบ ASTM C78/C78M

ตารางที่ 3 แสดงสัดส่วนการผสมตัวอย่างของทรายซีเมนต์ โดยแบ่งเป็น 6 กลุ่ม ประกอบด้วย กลุ่ม A ศึกษาผลกระทบของปริมาณปูนซีเมนต์ กลุ่ม B ศึกษาผลกระทบของปริมาณเส้นใยแก้ว กลุ่ม C ศึกษาผลกระทบของความยาวเส้นใยแก้ว กลุ่ม D ศึกษาผลกระทบของปริมาณเถ้าลอย กลุ่ม E ศึกษาผลกระทบของระยะเวลาการบ่ม กลุ่ม F ศึกษาผลกระทบของปริมาณเถ้าจม และ กลุ่ม CM กับกลุ่มCM+FB เป็นกลุ่มตัวอย่างควบคุม

4. การคำนวณ

หลังการทดสอบจะได้ค่าข้อมูลเพื่อมาแปลงเป็นพารามิเตอร์เส้นโค้งความสัมพันธ์ระหว่างน้ำหนักกับระยะแอ่นตัวสุทธิดังรูปที่ 4 (ก) และ 4 (ข) ตามมาตรฐาน ASTM C1609-10 เพื่อหาพฤติกรรมของทรายซีเมนต์บดอัด โดยมีตัวแปรดังนี้

L = ช่วงความยาวพาดคาน
P_p = น้ำหนักสูงสุด
P_1 = น้ำหนักสูงสุดครั้งแรก
δ_p = ระยะการแอ่นตัวสุทธิที่น้ำหนักสูงสุด
δ_1 = ระยะการแอ่นตัวสุทธิที่น้ำหนักสูงสุดครั้งแรก
f_p = กำลังดัดสูงสุด

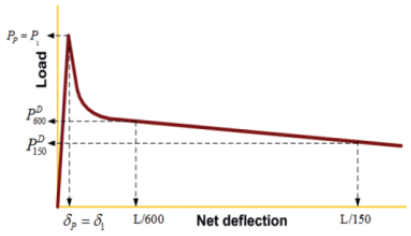

(ก) ตัวแปรที่ใช้ในการคำนวณสำหรับน้ำหนักสูงสุดครั้งแรกเท่ากับน้ำหนักสูงสุด

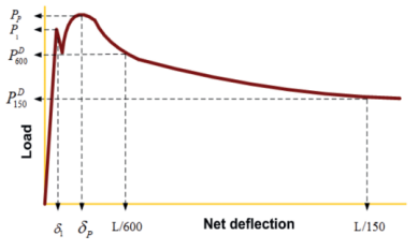

(ข) ตัวแปรที่ใช้ในการคำนวณเมื่อน้ำหนักสูงสุดมากกว่าน้ำหนักสูงสุดในตอนแรก

รูปที่ 4 เส้นโค้งความสัมพันธ์ระหว่างน้ำหนักกับระยะแอ่นตัว

f_1 = กำลังดัดสูงสุดครั้งแรก
P^D_{600} = น้ำหนักคงเหลือที่ระยะแอ่นตัวสุทธิ $L/600$
f^D_{600} = กำลังดัดคงเหลือที่ระยะแอ่นตัวสุทธิ $L/600$
P^D_{150} = น้ำหนักคงเหลือที่ระยะแอ่นตัว สุทธิ $L/150$
f^D_{150} = กำลังดัดคงเหลือที่ระยะแอ่นตัวสุทธิ $L/150$

วารสารวิชาการเทคโนโลยีอุตสาหกรรม (The Journal of Industrial Technology)
ISSN (online): 2697-5548
DOI: 10.14416/j.ind.tech.2024.12.014

T_{150}^{D} = พื้นที่ใต้โค้งความสัมพันธ์ระหว่างน้ำหนักกับระยะแอ่นตัว ตั้งแต่ 0 ถึง $L/150$

DI = ดัชนีความยืด

PSR = อัตราส่วนกำลังดัดสูงสุด

กำลังดัด (f) สามารถคำนวณดังสมการ (1)

$$f = \frac{PL}{bd^2} \quad (1)$$

โดย P คือน้ำหนักใดๆ ที่ต้องการทราบค่ากำลังดัด สำหรับอัตราส่วนกำลังเทียบเท่า

L = ความยาวช่วง

b = ความกว้างของตัวอย่างทดสอบ

d = ความลึกของตัวอย่างทดสอบ

ดังนั้น เส้นโค้งของน้ำหนักกับระยะการแอ่นตัวสามารถคำนวณค่า $R_{T,150}^{D}$ ได้ [14] ดังสมการที่ (2)

$$R_{T,150}^{D} = \frac{150T_{150}^{D}}{f_1 bd^2} \times 100\% = \frac{150T_{150}^{D}}{\frac{PL}{bd^2}bd^2} = \frac{T_{150}^{D}}{P_1 \frac{L}{150}} \quad (2)$$

โดยค่า $R_{T,150}^{D}$ ที่สูงกว่า 100% บ่งบอกว่าตัวอย่างจะมีความเหนียวสูงในทางกลับกันหากค่า $R_{T,150}^{D}$ ที่น้อยกว่า 100 % หมายถึงตัวอย่างจะมีความเหนียวต่ำ

$$DI = \frac{\delta_p}{\delta_1} \quad (3)$$

โดยค่า DI บ่งบอกคุณสมบัติความเป็นวัสดุเหนียว (Ductile) ของตัวอย่าง [14] ดังสมการที่ (3)

$$PSR = \frac{f_p}{f_1} \quad (4)$$

โดยค่า PSR ที่มีค่าเท่ากับ 1 บ่งบอกว่าตัวอย่างแสดงพฤติกรรมการแอ่นแบบวัสดุอ่อน (Softening) แต่ถ้ามีค่ามากกว่า 1 จะบ่งบอกว่าตัวอย่างแสดงพฤติกรรมการแอ่นแบบวัสดุเหนียว (Hardening) [14] ดังสมการที่ (4)

5. ผลการทดสอบและการวิเคราะห์

5.1 ผลการทดสอบเพื่อหาปริมาณปูนซีเมนต์และเถ้าลอยที่เหมาะสม

รูปที่ 5 แสดงผลการทดสอบกำลังดัดในห้องปฏิบัติการของทรายซีเมนต์บดอัดของกลุ่ม A ที่ผสมเถ้าลอยร้อยละ 25 เส้นใยแก้วยาว 6 มิลลิเมตร ในสัดส่วนร้อยละ 1 โดยปริมาตร และปริมาณซีเมนต์ที่แตกต่างกัน โดย A1 เป็นตัวอย่างคานที่ผสมด้วยซีเมนต์ร้อยละ 3 โดยน้ำหนัก A2 ตัวอย่างคานที่ผสมด้วยซีเมนต์ร้อยละ 5 โดยน้ำหนัก และ A3 เป็นตัวอย่างคานที่ผสมด้วยซีเมนต์ร้อยละ 7 โดยน้ำหนัก จากผลการทดสอบกำลังดัดพบว่ากำลังดัดเพิ่มขึ้นตามปริมาณปูนซีเมนต์ที่เพิ่มขึ้น แสดงให้เห็นว่าปริมาณปูนซีเมนต์มีผลโดยตรงต่อกำลังของเมทริกซ์ เมื่อเปรียบเทียบผลการทดสอบของตัวอย่าง A2 กับตัวอย่างควบคุม CM ที่ผสมปูนซีเมนต์เพียงอย่างเดียวที่ร้อยละ 5 พบว่ากำลังดัดลดลง แสดงให้เป็นว่าการเพิ่มเถ้าลอย FA ในสัดส่วนที่ร้อยละ 25 ทดแทนปูนซีเมนต์จะทำให้กำลังดัดลดลงแต่ระยะการแอ่นตัวเพิ่มขึ้น สอดคล้องกับผลการทดสอบของตัวอย่างควบคุม CM+FB ที่ผสมปูนซีเมนต์ร้อยละ 5 โดยน้ำหนักและเส้นใยแก้วร้อยละ 1 โดยปริมาตร พบว่ามีกำลังดัดและระยะการแอ่นตัวสูงที่สุดเมื่อเทียบกับทุกตัวอย่าง โดยมี DI และ PSR เป็น 1 แสดงว่าคานมีพฤติกรรมการแอ่นแบบวัสดุอ่อน (Softening) รูปที่ 6 แสดงความเหนียวที่ระยะแอ่นตัวที่ L/150 ของคาน A1 ถึง A3 พบว่าความเหนียวที่ระยะแอ่นตัว (Toughness at L/150) แปรผันโดยตรงกับปริมาณปริมาณปูนซีเมนต์ที่เพิ่มขึ้น

วารสารวิชาการเทคโนโลยีอุตสาหกรรม (The Journal of Industrial Technology)
ISSN (online): 2697-5548
DOI: 10.14416/j.ind.tech.2024.12.014

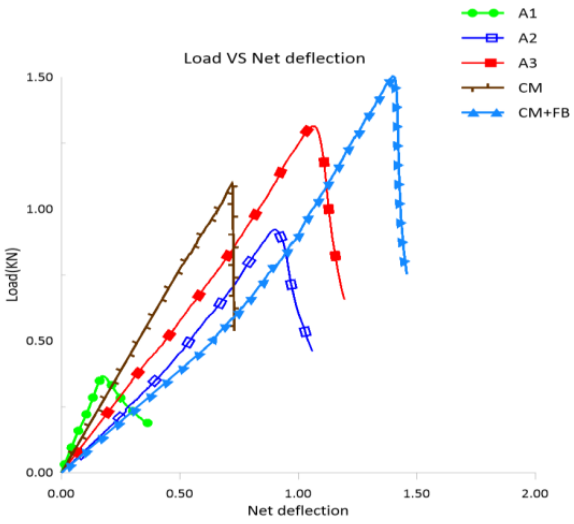

รูปที่ 5 กำลังดัดของทรายซีเมนต์บดอัดกลุ่ม A

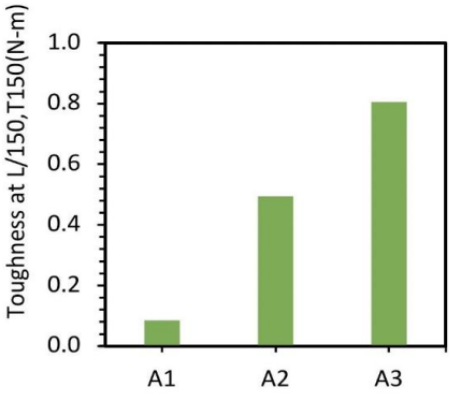

รูปที่ 6 ความเหนียวที่ระยะแอ่นตัวของกลุ่ม A (Toughness at L/150,T150 (N-m))

วารสารวิชาการเทคโนโลยีอุตสาหกรรม (The Journal of Industrial Technology)
ISSN (online): 2697-5548
DOI: 10.14416/j.ind.tech.2024.12.014

5.2 ผลการทดสอบเพื่อหาปริมาณเส้นใยที่เหมาะสม

รูปที่ 7 แสดงผลการทดสอบกำลังดัดของทรายซีเมนต์บดอัดที่เสริมแรงด้วยเส้นใยแก้วของกลุ่ม B โดยคาน B3 และคาน B4 แสดงให้เห็นว่าเมื่อมีปริมาณเส้นใยแก้วที่ร้อยละ 1.0 ถึง 1.5 โดยปริมาตร จะมีระยะการแอ่นตัวเพิ่มขึ้น ซึ่งกำลังดัดของคานในกลุ่ม B ใกล้เคียงกันอยู่ที่ประมาณ 1 kN รูปที่ 8 แสดงความเหนียวที่ระยะแอ่นตัวของกลุ่ม B และยืนยันว่าปริมาณเส้นใยแก้วที่ร้อยละ 1.0 ถึง 1.5 โดยปริมาตร ให้ระยะการแอ่นตัวที่สูง โดย DI และ PSR เป็น 1 แสดงว่าคานมีพฤติกรรมการแอ่นแบบวัสดุอ่อน (Softening) โดยปริมาณดังกล่าวยังสอดคล้องกับปริมาณการเติมเส้นใยโพลีเอทีลีนในการปรับปรุงคุณภาพดิน [15]

5.3 ผลการทดลองเพื่อหาความยาวเส้นใยที่เหมาะสม

รูปที่ 9 แสดงผลการทดสอบกำลังดัดของทรายซีเมนต์บดอัดที่เสริมแรงด้วยเส้นใย ที่ใช้ความยาวของเส้นใยแก้วที่แตกต่างกันของกลุ่ม C โดย C1 ใช้เส้นใยแก้วยาว 3 มิลลิเมตร C2 ใช้เส้นใยแก้วยาว 6 มิลลิเมตร และ C3 ใช้เส้นใยแก้วยาว 12 มิลลิเมตร จากผลการทดสอบกำลังดัดพบว่า C3 มีระยะการแอ่นตัวสูงสุด รูปที่ 10 แสดงความเหนียวที่ระยะแอ่นตัวของกลุ่ม C และยืนยันว่าปริมาณเส้นใยแก้วที่ความยาว 12 มิลลิเมตร มีความเหนียวสูงที่สุด ค่า DI และ PSR เป็น 1 แสดงว่าคานมีพฤติกรรมการแอ่นแบบวัสดุอ่อน (Softening)

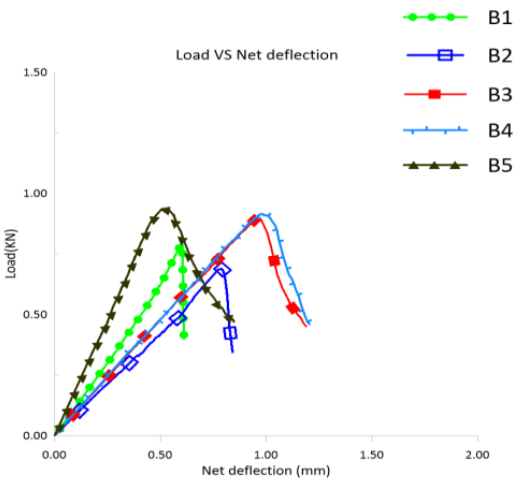

รูปที่ 7 กำลังดัดของทรายซีเมนต์บดอัดกลุ่ม B

วารสารวิชาการเทคโนโลยีอุตสาหกรรม (The Journal of Industrial Technology)
ISSN (online): 2697-5548
DOI: 10.14416/j.ind.tech.2024.12.014

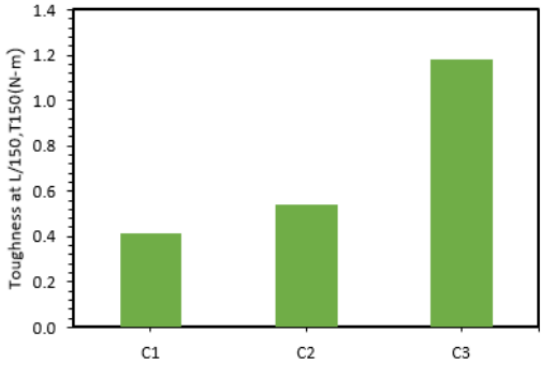

รูปที่ 10 ความเหนียวที่ระยะแอ่นตัวของกลุ่ม C (Toughness at L/150,T150 (N-m))

5.4 ผลการทดลองเพื่อหาปริมาณเถ้าลอยที่เหมาะสม

รูปที่ 11 แสดงผลการทดสอบกำลังดัดของทรายซีเมนต์บดอัดที่เสริมแรงด้วยเส้นใยแก้วและเถ้าลอยทดแทนปูนซีเมนต์ในอัตราส่วนที่แตกต่างกันของกลุ่ม D โดย D1 ใช้เถ้าลอยทดแทนซีเมนต์ที่ร้อยละ 10 โดย D2, D3, D4, D5, D6 และD7 ใช้เถ้าลอยทดแทนซีเมนต์ที่ร้อยละ 15, 20, 25, 30, 35 และ 40 จากการทดสอบพบว่าคาน D1 และ D2 มีค่ากำลังดัดสูงที่สุดและมีระยะแอ่นตัวสูง รูปที่ 12 แสดงความเหนียวที่ ระยะแอ่นตัวของกลุ่ม D อย่างไรก็ตาม DI และ PSR เป็น 1 แสดงว่าคานมีพฤติกรรมการแอ่นแบบวัสดุอ่อน (Softening)

5.5 ผลการทดสอบเพื่อหาระยะเวลาบ่มที่เหมาะสม

รูปที่ 13 ผลการทดสอบกำลังดัดของทรายซีเมนต์บดอัดที่เสริมแรงด้วยเส้นใยแก้วที่บ่มในระยะเวลาที่แตกต่างกัน โดย E1, E2, E3, E4 และ E5 ใช้เวลาบ่มที่ 7, 14, 28, 60 และ 90 วันตามลำดับ จากการทดสอบพบว่ากำลังดัดจะมีค่าเพียงพอเมื่อบ่มตั้งแต่ 28 วันขึ้นไป โดยคาน E3, E4 และ E5 มีกำลังดัดสูง จากรูปที่ 14 ความเหนียวที่ระยะแอ่นตัวของกลุ่ม E พบว่า E5 ที่ บ่ม 90 วันมีค่าความเหนียวสูงที่สุด

5.6 ผลการทดสอบเพื่อหาปริมาณเถ้าจมที่เหมาะสม

รูปที่ 15 แสดงผลการทดสอบกำลังดัดของทรายซีเมนต์บดอัดที่เสริมแรงด้วยเส้นใยแก้ว เถ้าลอยและเถ้าจมทดแทนปูนซีเมนต์ในอัตราส่วนที่แตกต่างกันของกลุ่ม F โดย F1 ใช้เถ้าลอยร้อยละ 100 ต่อเถ้าจมร้อยละ 0 ส่วน F2, F3, F4, และ F5 ใช้สัดส่วยเถ้าลอยต่อเถ้าจม (FA:BA) ทดแทนซีเมนต์ที่ร้อยละ 75:25, 50:50, 25:75 และ 0:100 ตามลำดับ ระยะเวลาบ่ม 28 วัน จากการทดสอบพบว่าคาน F4 มีค่ากำลังดัดสูงที่สุด และใกล้เคียงกับตัวอย่างควบคุมของคาน F1 รูปที่ 16 ยืนยันว่าคาน F4 มีค่าความเหนียว (Toughness at L/150,T150 (N-m)) สูงที่สุด

วารสารวิชาการเทคโนโลยีอุตสาหกรรม (The Journal of Industrial Technology)
ISSN (online): 2697-5548
DOI: 10.14416/j.ind.tech.2024.12.014

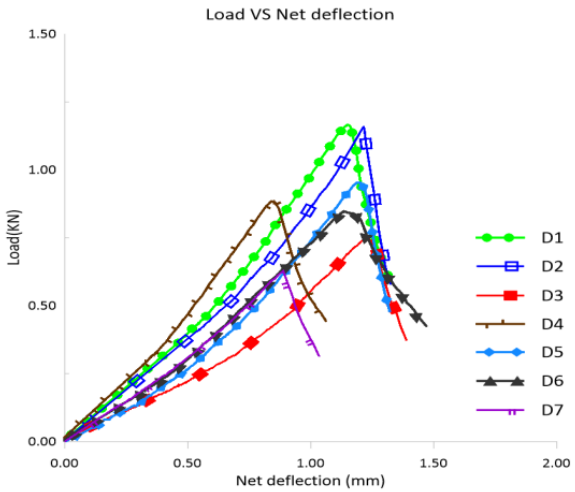

รูปที่ 11 กำลังดัดของทรายซีเมนต์บดอัดกลุ่ม D

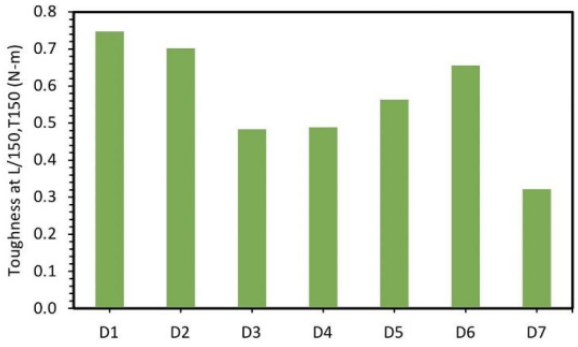

รูปที่ 12 ความเหนียวที่ระยะแอ่นตัวของกลุ่ม D (Toughness at L/150,T150 (N-m))

วารสารวิชาการเทคโนโลยีอุตสาหกรรม (The Journal of Industrial Technology)
ISSN (online): 2697-5548
DOI: 10.14416/j.ind.tech.2024.12.014

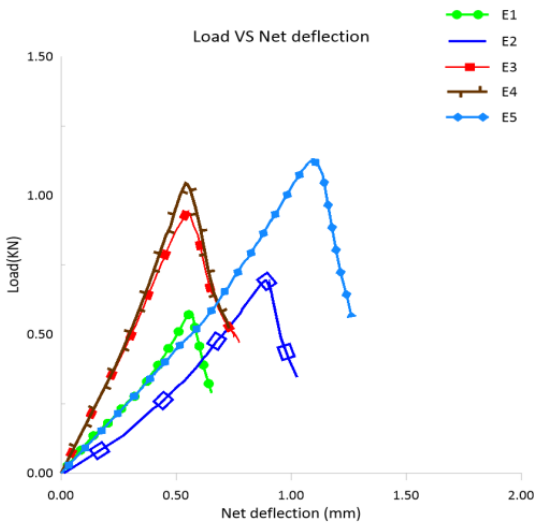

รูปที่ 13 กำลังดัดของทรายซีเมนต์บดอัดกลุ่ม E

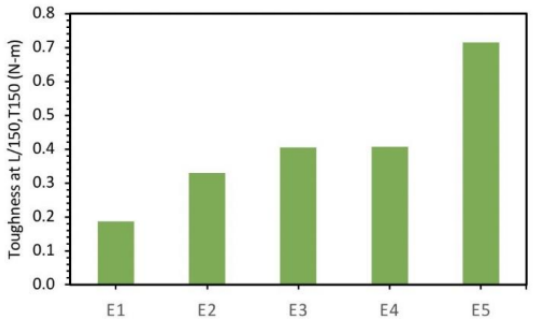

รูปที่ 14 ความเหนียวที่ระยะแอ่นตัวของกลุ่ม E (Toughness at L/150,T150 (N-m))

วารสารวิชาการเทคโนโลยีอุตสาหกรรม (The Journal of Industrial Technology)
ISSN (online): 2697-5548
DOI: 10.14416/j.ind.tech.2024.12.014

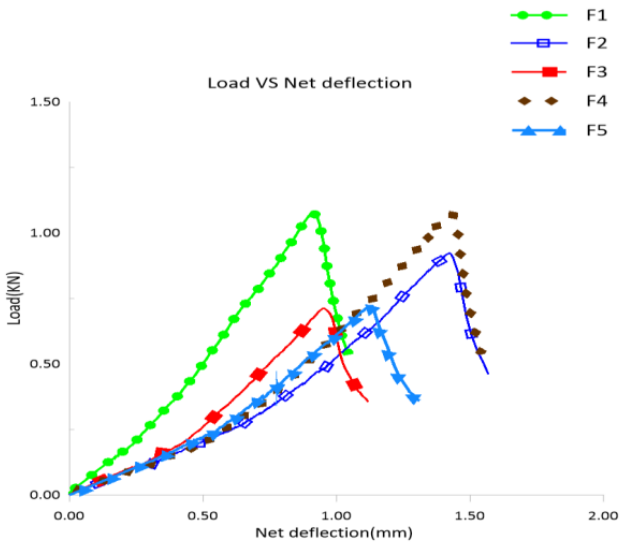

รูปที่ 15 กำลังดัดของทรายซีเมนต์บดอัดกลุ่ม F

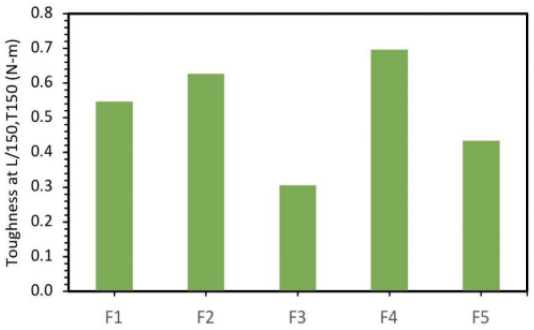

รูปที่ 16 ความเหนียวที่ระยะแอ่นตัวของกลุ่ม F (Toughness at L/150,T150 (N-m))

วารสารวิชาการเทคโนโลยีอุตสาหกรรม (The Journal of Industrial Technology)
ISSN (online): 2697-5548
DOI: 10.14416/j.ind.tech.2024.12.014

[11] C. Tang, B. Shi, W. Gao, F. Chen and Y. Cai, Strength and mechanical behavior of short polypropylene fiber reinforced and cement stabilized clayey soil, Geotextiles and Geomembranes, 2007, 25, 194-202.

[12] P. Jamsawang, P. Voottipruex and S. Horpibulsuk, Flexural strength characteristics of compacted cement-polypropylene fiber sand, Journal of Materials in Civil Engineering, 2014, 27(9), C4014243.

[13] J. Hu, Z. Ge and K. Wang, Influence of cement fineness and water-to-cement ratio on mortar early-age heat of hydration and set times", Construction and building materials, 2014, 50, 657-663.

[14] P. Jamsawang, P. Voottipruex, and S. Inthapichai, Improvement of the bending stress of polypropylene fiber-reinforced compacted cement sand", The Journal of King Mongkut's University of Technology North Bangkok, 2014, 24, 43-55.

[15] S. Pochalard, C. Wungsumpow and K. Piriyakul, Enhancement on compressive strength of Bangkok clay cement using novel high-strength polyethylene fibers, IOP Conference Series: Earth and Environmental Science, 2024, 1-8.

วารสารวิชาการเทคโนโลยีอุตสาหกรรม (The Journal of Industrial Technology)
ISSN (online): 2697-5548
DOI: 10.14416/j.ind.tech.2024.12.014

5.7การวิเคราะห์ภาพ SEM

รูปที่ 17 แสดงภาพจากกล้องจุลทรรศน์อิเล็กตรอนแบบส่องกราด (Scanning Electron Microscope: SEM) ของทรายแม่น้ำที่ใช้ในอุตสาหกรรมการก่อสร้าง ซีเมนต์ เถ้าจม และเส้นใยแก้ว การขยายภาพ SEM 70x แสดงให้เห็นว่าเถ้าจมถูกผสมเข้าเป็นเนื้อเดียวกันกับใยแก้วและเมทริกซ์ทราย-ซีเมนต์ โดยสัมพันธ์กับแรงเสียดทานในสัดส่วนกับความยาวของเส้นใยแก้วที่ใช้ในการแสดงให้เห็นว่าวัสดุคอมโพสิตสามารถปรับปรุงให้ดีขึ้นได้อย่างไร และยังส่งผลต่อการปรับปรุงคุณภาพความแข็งแรงของซีเมนต์ในทรายอีกด้วย ตัวอย่างนี้แสดงให้เห็นถึงการยึดเกาะของวัสดุคอมโพสิตและการกระจายตัวของเส้นใยแก้ว ความแข็งแรงจะเพิ่มมากขึ้นตามความยาวของเส้นใยแก้ว และสามารถเกาะติดกันได้

6. สรุปผลการทดสอบ

จากผลการศึกษาของงานวิจัยนี้ สามารถสรุปได้ดังนี้

- กำลังอัดของทรายซีเมนต์บดอัดเพิ่มขึ้นตามปริมาณปูนซีเมนต์ที่เพิ่มขึ้น แสดงให้เห็นว่าปริมาณปูนซีเมนต์มีผลโดยตรงต่อกำลังของเมทริกซ์ โดยปริมาตรปูนซีเมนต์ที่เหมาะสมแนะนำอยู่ที่ร้อยละ 5 ความเหนียวที่ระยะแอ่นตัว (Toughness at L/150) ของทรายซีเมนต์บดอัดแปรผันโดยตรงกับปริมาณปริมาณปูนซีเมนต์ที่เพิ่มขึ้น
- ปริมาณเส้นใยแก้วที่ร้อยละ 1.0 ถึง 1.5 เป็นสัดส่วนที่เหมาะสมในการผสมทรายซีเมนต์บดอัด ซึ่ง DI และ PSR เป็น 1 แสดงพฤติกรรมการแอ่นแบบวัสดุอ่อน (Softening)

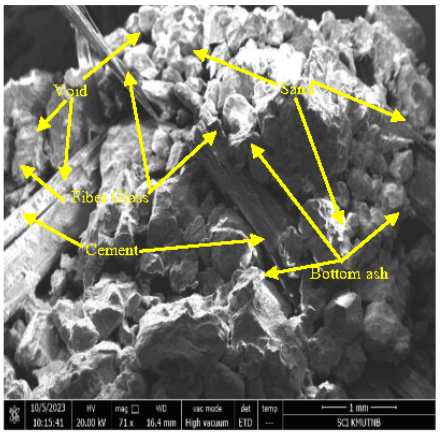

รูปที่ 17 ภาพถ่าย SEM 70 X ของทราย ซีเมนต์ เถ้าจม และเส้นใยแก้ว

- ความยาวของเส้นใยแก้วแปรผันโดยตรงต่อระยะการแอ่นตัวของทรายซีเมนต์บดอัด โดยความยาวของเส้นใยแก้วที่เหมาะสมสำหรับผสมในทรายซีเมนต์บดอัดควรจะเป็น 12 มิลลิเมตร
- ปริมาณเถ้าลอยทดแทนปูนซีเมนต์ของทรายซีเมนต์บดอัดควรอยู่ระหว่างร้อยละ 10 ถึง 15 ซึ่งให้กำลังอัดและการแอ่นตัวสูงที่สุด
- ปริมาณเถ้าจมที่เหมาะสมในส่วนผสมของทรายซีเมนต์บดอัด สัดส่วนเถ้าลอยต่อเถ้าจม (FA:BA) ที่เหมาะสมควรใช้ 25:75 ให้ค่าความเหนียว (Toughness at L/150) สูงที่สุด
- ระยะเวลาในการบ่มทรายซีเมนต์บดผสมเถ้าลอยควร อยู่ระหว่าง 28 ถึง 90 วัน โดยกำลังอัดจะมีค่าเพียงพอเมื่อบ่มตั้งแต่ 28 วันขึ้นไป และพบว่าที่บ่ม 90 วันมีค่าความเหนียวสูงที่สุด

วารสารวิชาการเทคโนโลยีอุตสาหกรรม (The Journal of Industrial Technology)
ISSN (online): 2697-5548
DOI: 10.14416/j.ind.tech.2024.12.014

5. กิตติกรรมประกาศ

งานวิจัยนี้ได้รับทุนสนับสนุนการศึกษาจากวิทยาลัยเทคโนโลยีอุตสาหกรรม มหาวิทยาลัยเทคโนโลยีพระจอมเกล้าพระนครเหนือ สัญญารับทุน CIT-2022-Grad-23

6. เอกสารอ้างอิง

[1] A. Dubey, S. Gangopadhyay and W. Wadhwa, Occupational structure and incidence of poverty in Indian towns of different sizes, Review of Development Economics, 2001, 5, 49-59.

[2] T. Sadashivam and S. Tabassu, Trends of urbanization in India: Issues and challenges in the 21st century", International Journal of Information Research and Review, 2016, 3, 2375-2384.

[3] H. Lu, C. Wang, Q. Li, R. Wiser and K. Porter, Reducing wind power curtailment in China: Comparing the roles of coal power flexibility and improved dispatch, Climate Policy, 2019, 19, 623-635.

[4] C.Y. Lin and T.A. Chen, Effects of composition type and activator on fly ash-based alkali activated materials, Polymers, 2021, 14, 63.

[5] A. Petcherdchoo, S. Pochalard and K. Piriyakul, Use of bender element tests for determining shear modulus of fly-ash and cement admixed Bangkok clay with considering unconfined compressive strength, Case Studies in Construction Materials, 2023, 18, 1-13.

[6] https://thaimsw.pcd.go.th/report1.php?year=2565. (Accessed on 30 August 2024)

[7] H.L. Dinh, J. Liu, D.E. Ong and J.H. Doh, A Sustainable solution to excessive river sand mining by utilizing by-products in concrete manufacturing: A state-of-the-art review, Cleaner Materials, 2022, 6, 1-85.

[8] https://civiltoday.com/civil-engineering-materials/concrete/270-concrete-definition-components-types. (Accessed on 30 August 2024)

[9] M.W.M. Abdias, M.M. Blanche, U.J.P. Nana, H.F. Abanda, N. François, and P. Chrispin, River sand characterization for its use in concrete: A revue, Open Journal of Civil Engineering, 2023, 13, 353-366.

[10] X. Yang, S. Liang, Z. Hou, D. Feng, Y. Xiao and S. Zhou, Experimental study on strength of polypropylene fiber reinforced cemented silt soil, Applied Sciences, 2022, 12, 8318.

Research publication in Proceedings of the International Conference on Eco-friendly Fibers and Polymeric Materials, ISBN (online): 978-981-97-7071-7, DOI: https://doi.org/10.1007/978-981-97-7071-7_5, Improving Mechanical Behavior of Compacted Cement Sand Mixed with Glass Powder from Glass Industry and Glass Fiber for Green Construction Materials

Improving Mechanical Behavior of Compacted Cement Sand mixed with Glass Powder from Glass Industry and Glass Fiber for Green Construction Materials

Prapatsorn Prathungthai[1], Chalermpon Wungsumpow[2], Sakol Pochalard[3] and Keeratikan Piriyakul[4,*[0000-0002-8670-0379]]

[1] Ceramics Innovation Product Design, Faculty of Architecture and Design, King Mongkut's University of Technology North Bangkok, Bangkok, Thailand
[2] Doctor of Engineering Program in Construction Engineering Technology, Graduate College, and KMUTNB Techno Park, King Mongkut's University of Technology North Bangkok
[3] Building and Landscape Division, Suan Dusit University, and Doctor of Engineering Program in Construction Engineering Technology, Graduate College, King Mongkut's University of Technology North Bangkok, Bangkok, Thailand
[4] Center of Excellence in Structural Dynamics and Urban Management, Science and Technology Research Institute, and Department of Civil and Environmental Engineering Technology, College of Industrial Technology, King Mongkut's University of Technology North Bangkok, Bangkok, Thailand
keeratikan.p@cit.kmutnb.ac.th

Abstract. The purpose of this research is to examine the mechanical behavior of compacted cement sand with the addition of glass fibers, glass powder from the glass industry, and Ordinary Portland Cement (OPC). Finding the optimal proportions of OPC, glass powder, and glass fibers in the soil-cement mixture to create a novel green building material is the aim of this study. Every sample of compacted cement sand was created with a glass fiber content of 0.5%, 1.0%, 1.5%, 2.0%, and 2.5% by volume, and a variation in glass fiber lengths of 3, 6, and 12 mm. The optimal moisture content for the samples was 6.19%. OPC content was applied at weights of 2%, 4%, 6%, 8%, and 10%. At 10%, 20%, 30%, 40%, and 50% of the cement, glass powder was added. After that, the samples of compacted cement were left for 7, 14, and 28 days in order to examine how the green building materials aged. The unconfined compression test was conducted on these samples of compacted cement sand in accordance with ASTM D1633–17. Based on the testing findings, it was determined that 8% cement is the right amount to combine with clayey soil, 1.0% glass fibers with a length of 6–12 mm, and 20% glass powder with a curing period up to 28 days are the right amounts. As a result, it has been demonstrated that glass fiber and powder are green building materials. By lowering the required amount of cement, our findings help Thailand's future cement demand.

Keywords: Unconfined Compressive Strength, Glass Powder, Glass Fiber, Compacted Cement Sand.

1 Introduction

Cement is the most widely used material for ground improvement in construction projects because of its affordability, high strength, and long lifespan. Over 10 billion tons of concrete are used annually in these construction projects worldwide, and by 2050, that number will rise to 16 billion tons [1]. However, eco-friendly building and ground improvement materials reduce their negative effects on the environment, protect natural resources, and encourage sustainability. A team of material engineers [2] examined cutting-edge materials and technologies for use in engineering. They discovered that the primary drivers of industry demand for those materials are, firstly, lower costs and higher profitability through a decrease in the frequency of component replacement. Second, because of their superior attributes that suit client wants and have fewer flaws, which boost competitiveness, they have enhanced consumer happiness and loyalty. Finally, utilizing state-of-the-art materials to satisfy regulatory requirements without sacrificing performance will ensure sustainability and regulatory compliance. The most recent developments in bio composites innovation were evaluated by researchers looking at natural composites [3]. Natural fibers such as flax, hemp, jute, sisal wood, cotton, bamboo, wool, feather silk, and so forth must be used to develop eco-friendly building and construction materials. Research is being conducted to enhance the properties of bio composites for common engineering applications. Innovative bio-composite materials made from agro-waste were developed by a team of material engineers [4]. This study aims to provide a comprehensive analysis of the many techniques for extracting and modifying natural fibers. It offers a comprehensive examination of several extraction techniques from the initial harvesting process through the decortication stage. A multitude of elements, such as local customs, climate, water availability, and the desired degree of fiber quality, determine the choice of extraction processes. This study also looks at chemical and physical treatments, demonstrating how each modality changes the properties and content of natural fibers. Their study offers helpful details on how to improve the final product's quality and performance while converting biomass from agricultural waste into the desired natural fiber and then bio-composite material.

Ordinary Portland Cement (OPC) was utilized as a binder for soil-cement stabilization of Bangkok soft clay by a geotechnical engineering group [5]. To examine the mechanical characteristics of this Bangkok soil-cement, they conducted tests for unconfined compressive strength and the bender element. The Bangkok soft clay, together with industrial waste such fly ash from the Mae Moh power plant in Thailand, was combined with OPC (20% by weight) and varying FA replacement (0-30% by weight) before being cured for 7, 14, 28, and 90 days. The early-age normalized unconfined compressive strength is determined to be 0.09, and the connection between the normalized unconfined compressive strength and the curing time is found to be naturally logarithmic with an increase rate of 0.3433. A team of soil experts [6] tracked the strength development of Bangkok soft clay combined with fly ash (FA) and OPC using the shear wave velocity. The ideal replacement fly ash percentage was discovered to be between 15% and 20%. It was also observed that the strength development of this Bangkok clay that had been blended with OPC and FA rose as the curing period increased.

G_0=27.57q_u is the established relationship between shear modulus, G_0 (MPa), and ultimate bearing capacity, q_u (MPa).

A number of nations, including Thailand, have focused heavily on municipal solid waste (MSW) management throughout the last ten years. Due to the complex and heterogeneous content of wastes, as well as their various origins and connections to consumption patterns, MSW management faces significant challenges [7]. Numerous academics conducted study on the use of environmentally friendly materials in green construction. In order to enhance the mechanical qualities of sandy soil, Iamchaturapatr et al. [8] investigated green cement, which is produced through the biocementation process. They created their own soybean urease enzymes to speed up the biocementation process and finish it in seven days. The ideal Ca^{2+} concentration was found to be 250 mM, and the ideal urease enzyme concentration was 20% by volume (v/v). The occurrence of $CaCO_3$ binding sand particles together is confirmed by the SEM picture and X-ray diffraction (XRD). The mechanical characteristics of sandy soil treated with natural hemp fibers and the urease enzymatic acceleration method based on Enzyme Induced Carbonate Precipitation (EICP) were evaluated by a team of environmental engineers [9]. The bending element test was employed to track the biocemented sand's strength growth. Based on the test results, 2.5% by volume of natural hemp fibers was determined to be the ideal amount to mix with biocemented sand. A few days are needed for the biocementation process before the reaction begins. Furthermore, the reaction completes at day six, while it starts at day four. The control dry sand sample had an internal friction angle of 32.9° and a cohesiveness of 0 T/m^2, according to the results of the direct shear test. Following treatment by the biocementation method using 2.5% optimal natural hemp fiber, the internal friction angle rises to 35° and the cohesiveness of the sand to 0.9 T/m^2. This result validated the use of hemp fibers and biocementation to improve the characteristics of sandy soil. The bender element test was employed by a team of civil engineering researchers [10] to ascertain the metakaolin geopolymer pastes' start and final setting timeframes. A novel, environmentally friendly building material with a high compressive strength and quick strength development is metakaolin geopolymer. Bender element and Vicat needle tests were used to examine the first and last setting times. Kaolin was treated at 0, 200, 800, 1000, and 1200 °C to create metakaolin powder. Subsequently, the geopolymer solution was combined with each metakaolin powder sample at varying ratios: 0.8:1.0, 1.0:1.0, 1.2:1.0, and 1.5:1.0. Ten standard concentrations of sodium hydroxide (10 N NaOH) were added to sodium silicate (Na_2SiO_3) at different solution ratios of 1.0:1.0, 1.0:1.2, 1.0:1.5, 1.0:2.0, 1.2:1.0, 1.5:1.0, and 2.0:1.0 to create the geopolymer solution. It was discovered that the ideal temperature for treating metakaolin is 1000 °C, and that the ideal solution ratio between NaOH and Na_2SiO_3 is 2.0:1.0. Additionally, the ideal mixing ratio between the metakaolin powder and the geopolymer solution is 1.0:1.0. One helpful way to detect geopolymerization by shear wave velocity in real-time is to utilize piezoelectric bender elements to measure the initial and ultimate setting times of metakaolin geopolymer pastes. Lastly, CBR tests were used to determine which metakaolin geopolymer pastes were best for improving laterite soils.

A specialist in natural fiber composites [11] examined the applicability of natural fiber in several military technology variations. Their importance has expanded due to

the main benefits of the environment, safety, cost, and competition in a variety of engineering issues. Utilizing the distinct qualities and capabilities of many materials in lightweight structures while simultaneously optimizing the efficiency of each material is one useful strategy hybrid systems attempt to implement. Fiber reinforced polymer (FRP) composites have been the focus of much interest recently, along with other lightweight materials. A group of researchers in material engineering [12] examined the novel properties of both hardened concrete and concrete to find out how to use glass fibers with structural components like beams and cubic cylinders. to determine the M20 grade of concrete's strength and durability using glass fiber-reinforced concrete (GFRC). To find the fresh properties and hardening strength of the concrete, three different GFRC variations are mixed with the concrete. Its properties, such as toughness, modulus of elasticity, flexure strength, and compressive strength, have all been studied. The amount of GFRC in concrete can vary from 0 to 1. A team of geotechnical engineering researchers [13] used fly ash from municipal solid waste (MSW) and polypropylene fiber to increase the flexural strength of cement-compacted sand. This municipal solid waste fly ash was produced as a byproduct of burning the waste in solid waste combustor facilities. They investigated fracture behavior, toughness, ductility index, equivalent flexural strength, peak strength, peak strength ratio, and first peak strength. Using different ratios of fly ash replacement to cement (0:100, 25:75, 50:50, 75:25, and 100:0 by weight) and polypropylene fiber (0, 0.5, 1, 1.5, and 2% by volume), all samples were made with 5% of cement by weight. Every sample was then cured for a total of 28 days. The maximum flexural strength was found to be achieved with a polypropylene fiber content of 1.5% by volume and a fly ash replacement to cement ratio of 25:75. It has been demonstrated that cement-compacted sand is a green building material that can fulfil Thailand's future cement needs while reducing greenhouse gas emissions from the cement industry.

The aim of this study is to determine the effect of glass powder and glass fiber on the enhancement for the physical properties and mechanical behavior for a sandy soil as a new green construction material.

2 Experimentation

The experimentation section was separated into three parts. Firstly, the geotechnical properties of the Bangkok construction sand, as well as the physical and engineering features of fiber and glass powder from industrial waste. Secondly, the sample preparation of this compacted cement sand mixed with glass powder from industrial waste and glass fiber. Then, all samples were performed to a series of unconfined compression tests. Lastly, the test methodology was described. All samples were prepared into a cylinder mold with a diameter of 50 mm and a height of 100 mm. Then, they were wrapped with a plastic film to prevent moisture. Based on ASTM D1633–17 [14], the UCS test was cured and performed at 7, 14 and 28 days.

2.1 Materials

The tested sand in this research was generally supplied from Bangkok's usual construction sand. The sieve analysis depicts the grain size curve in Fig. 1. It presents the grain size distribution in semi-log scale. At percent finer of 60%, the diameter (D_{60}) of Bangkok sand is 0.93 mm and at percent finer of 10%, the diameter (D_{10}) of Bangkok sand is 0.29 mm. The ratio between D_{60} and D_{10} is 3.21 which is less than 6, indicating that it is a poorly grade sand (SP). The engineering properties of this Bangkok sand are shown in Table 1. According to the Unified Soil Classification System (USCS), this Bangkok construction sand is classified as the poorly graded sand (SP). The SEM image of this Bangkok sand is also depicted in Fig. 2, displaying its round, sub-round, angular, and sub-angular shapes. The Ordinary Portland cement (OPC) type I was used in this research has the specific gravity of 3.15. Its chemical composition of this OPC cement is summarized in Table 2. It is shown that the three major chemical compositions of this OPC are lime, iron and silica. As shown in Figure 3, the Glass Fiber-Reinforced Concrete (GFRC) used in this experiment was produced by Owens Corning under the number Advantex CS 979-14, available in three distinct lengths of 3, 6, and 12 mm. The properties of GFRC are shown in Table 3 which the diameter of 3 μm, the tensile strength of 2,350 MPa, the Young's modulus of 73 GPa and the specific gravity of 2.47. Glass powder, especially soda lime glass powder, is a typical byproduct of industrial processes. Soda lime glasses are a common type of glass made of lime, soda ash, and silica. Broken or recycled glass can be processed into glass powder, which has numerous applications. Despite being considered an industrial waste product, glass powder's regular recycling and use in other production processes reduce its environmental impact. The size of this glass powder is 75 μm. The glass powder is typically white or light gray color. It has the specific gravity of around 2.5 g/m^3. The melting point is around 1,300-1,400 ºC. It is mostly used in construction materials, ceramics, glass manufacturing, and other industrial processes as a filler or additive.

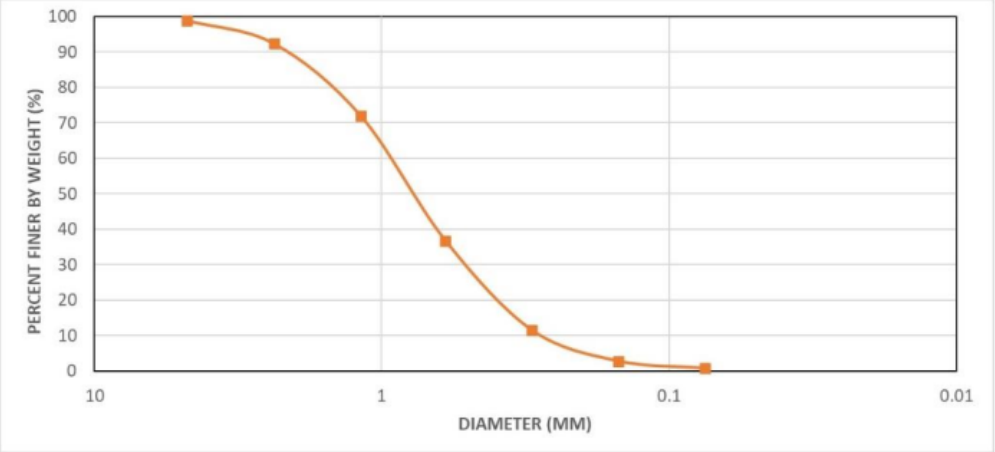

Fig. 1. Grain size distribution curve of typical Bangkok construction sand.

Fig. 2. SEM of Bangkok construction sand.

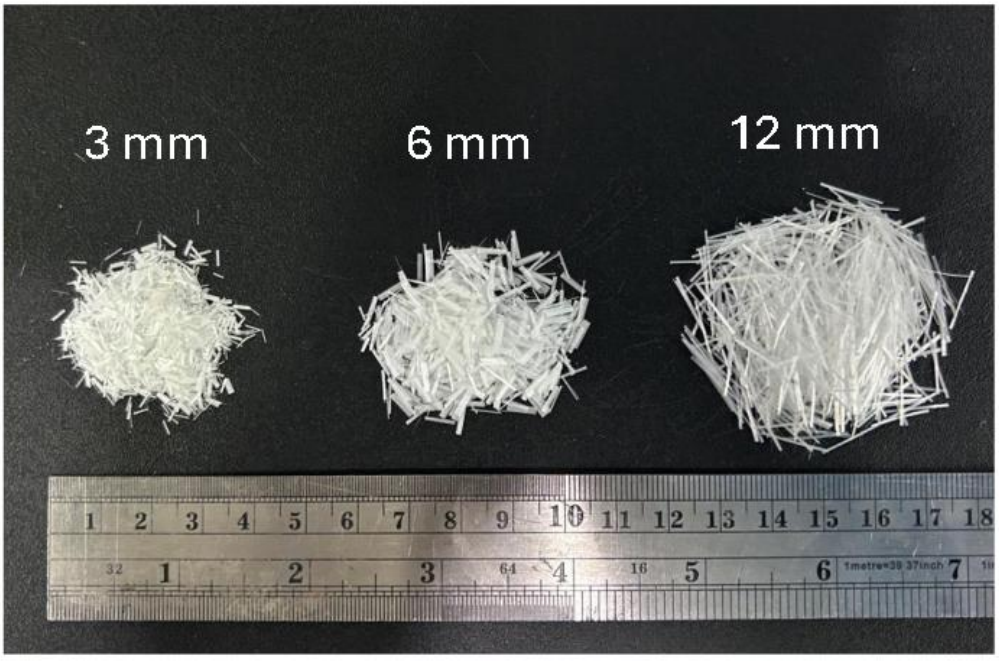

Fig. 3. Glass Fiber-Reinforced Concrete (GFRC) lengths of 3, 6 and 12 mm.

Table 1. Physical properties of the Bangkok construction sand.

Property	Value
Specific gravity (G_s)	2.65
Gravel content (%)	10.52
Sand content (%)	80.58
Fine content (%)	8.90
D_{60} (mm)	0.93
D_{30} (mm)	0.49
D_{10} (mm)	0.29
Coefficient of Uniformity (C_u)	3.21
Coefficient of Curvature (C_c)	0.89
Soil classification (USCS)	SP
Maximum, and minimum void ratios	0.83, 0.28
Maximum dry unit weight (kN/m^3)	15.70
Optimum moisture content (%)	6.19

Table 2. Chemical composition of cement (OPC).

Oxide	Common name	Mass (%)
CaO	Lime	76.44
Fe_2O_3	Iron	14.37
SiO_2	Silica	4.45
MgO	Magnesia	1.79
Al_2O_3	Alumina	1.31
SO_3	Sulfuric anhydrite	1.00
ZnO	Zinc oxide	0.32
K_2O	Alkali	0.23
Cr_2O_3	Chromic oxide	0.10

Table 3. Properties of glass fiber-reinforced concrete (GFRC).

Type	Glass Fiber
Length (mm)	3, 6, 12
Diameter (μm)	3.0
Specific weight	2.47
Tensile strength (MPa)	2350
Young's modulus (GPa)	73
Color	White

2.2 Preparation of Specimens

For at least the entire day, Bangkok construction sand was heated to 105 °C until it lost all of its moisture. It was combined with glass fibers (GFRC), glass powder, fly ash from municipal solid waste (MSW), and OPC. In accordance with ASTM D698-12E1, all specimens were prepared at the ideal water content of 6.19%, as established by the modified proctor test [15]. Subsequently, as shown in Fig. 4, each sample was placed inside a cylinder mold of 50 mm in diameter and 100 mm in height. A plastic covering was then used to keep the samples from becoming dry. The average diameter and average length of each specimen were measured, and the results are displayed in Figs. 5 and 6, respectively. Glass fiber lengths of 3, 6 and 12 mm and glass fiber contents of 0.5%, 1.0%, 1.5%, 2.0%, and 2.5% by volume were used to prepare all specimens of compacted cement sand. OPC content was applied at weight percentages of 2%, 4%, 6%, 8%, and 10%. At 10%, 20%, 30%, 40%, and 50% of the glass powder was added. The unconfined compression test was then carried out on the compacted cement samples after they had been cured for 7, 14, and 28 days. Table 4 presents the UCS testing program. Specimens were divided into 5 groups. First, Group A presents the effect of OPC content. The OPC is added into the compacted sand specimens by varied its content from 2-10% and fixed the glass powder content at 20%, the glass fiber content at 1%, the fiber length of 6 mm and the curing time at 28 days. Second, Group B presents the effect of fiber content. The glass fiber content is added into the compacted sand specimens by varied its content from 0.5-2.5% by volume and fixed the OPC content at 8%, the glass powder content at 20%, the fiber length of 6 mm and the curing time at 28 days. Third, Group C presents the effect of fiber length. The glass fiber length is added into the compacted sand specimens by varied its length from 3, 6, and 12 mm fixed the OPC content at 8%, the glass fiber content at 1%, the glass powder content at 20% and the curing time at 28 days. Fourth, Group D presents the effect of the glass powder content and aging. The glass powder is added into the compacted sand specimens by varied its content from 5-30% and fixed the OPC content at 8%, the glass fiber content at 1%, the fiber length of 6 mm and the curing time at 7, 14 and 28 days. Last, Group E presents the effect of fiber content and aging. The glass fiber content is added into the compacted sand specimens by varied its content from 0.5-2.5% by volume and fixed the OPC content at 8%, the glass powder content at 20%, the fiber length of 6 mm and the curing time at 7, 14 and 28 days.

Fig. 4. Molding of specimen.

Fig. 5. Measurement of specimen diameter.

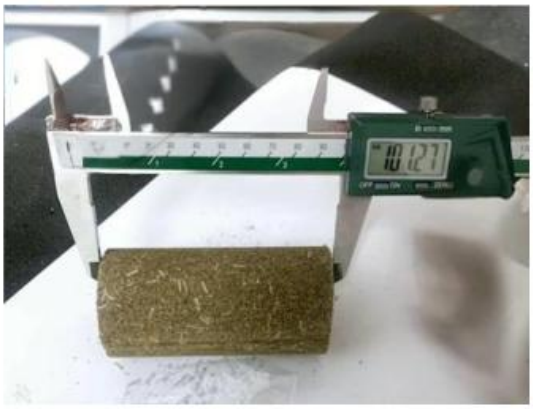

Fig. 6. Measurement of specimen length.

Table 4. Physical properties of the Bangkok construction sand.

Serial number	Cement content (%)	Glass powder content (%)	Fiber content (%)	Fiber length (mm)	Optimum moisture content (%)	Curing time (days)
A1	2	20	1.0	6	6.19	28
A2	4	20	1.0	6	6.19	28
A3	6	20	1.0	6	6.19	28
A4	8	20	1.0	6	6.19	28
A5	10	20	1.0	6	6.19	28
B1	8	20	0.5	6	6.19	28
B2	8	20	1.0	6	6.19	28
B3	8	20	1.5	6	6.19	28
B4	8	20	2.0	6	6.19	28
B5	8	20	2.5	6	6.19	28
C1	8	20	1.0	3	6.19	28
C2	8	20	1.0	6	6.19	28
C3	8	20	1.0	12	6.19	28
D1	8	5	1.0	6	6.19	7,14,28
D2	8	10	1.0	6	6.19	7,14,28
D3	8	15	1.0	6	6.19	7,14,28
D4	8	20	1.0	6	6.19	7,14,28
D5	8	25	1.0	6	6.19	7,14,28
D6	8	30	1.0	6	6.19	7,14,28
E1	8	20	0.5	6	6.19	7,14,28
E2	8	20	1.0	6	6.19	7,14,28
E3	8	20	1.5	6	6.19	7,14,28
E4	8	20	2.0	6	6.19	7,14,28
E5	8	20	2.5	6	6.19	7,14,28

2.3 Unconfined Compression Test

According to ASTM D1633–17 [14], the unconfined compression test is a geotechnical testing technique used to determine the soil-cement specimens' Unconfined Compressive Strength (UCS). Table 4 shows the testing program. As illustrated in Fig. 7, a cylindrical soil-cement sample is put within a testing device for the unconfined compression test. After that, the sample is loaded axially along its vertical axis without being constrained laterally. A 50kN capacity load cell is used to measure the axial load. Until the soil-cement sample fails or has considerable deformation, this loading process is continued. Linear Variable Differential Transformer (LVDT) devices measure deformation. Up to 15% strain, all specimens were exposed to a uniaxial force at a shearing rate of 0.5-2.0 mm/min. This unconfined compression test has its advantage due to the fact that it is a simple, fast, and cheap method.

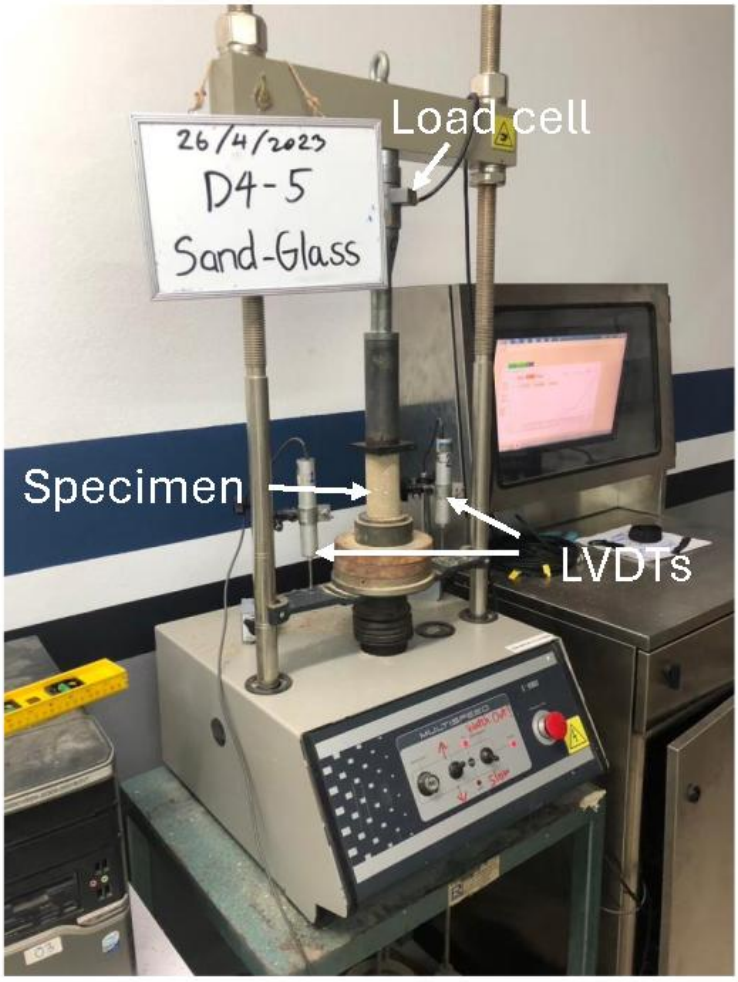

Fig. 7. Unconfined compression test set-up.

3 Results and Discussions

3.1 Effect of Cement Content

The impact of cement content on UCS growth for compacted cement Bangkok sand is depicted in Fig. 8. The cement percentage was varied between 2 and 10% by fixing the glass fiber content at 1.0%, fiber length of 6 mm, glass content at 20%, and curing duration at 28 days. It was discovered that the UCS results rise as the cement content does. ACI 230.1R-09 [16] states that ground stabilization requires a soil-cement strength of roughly 1,200 kPa. It was advised to employ 8% cement content as a result.

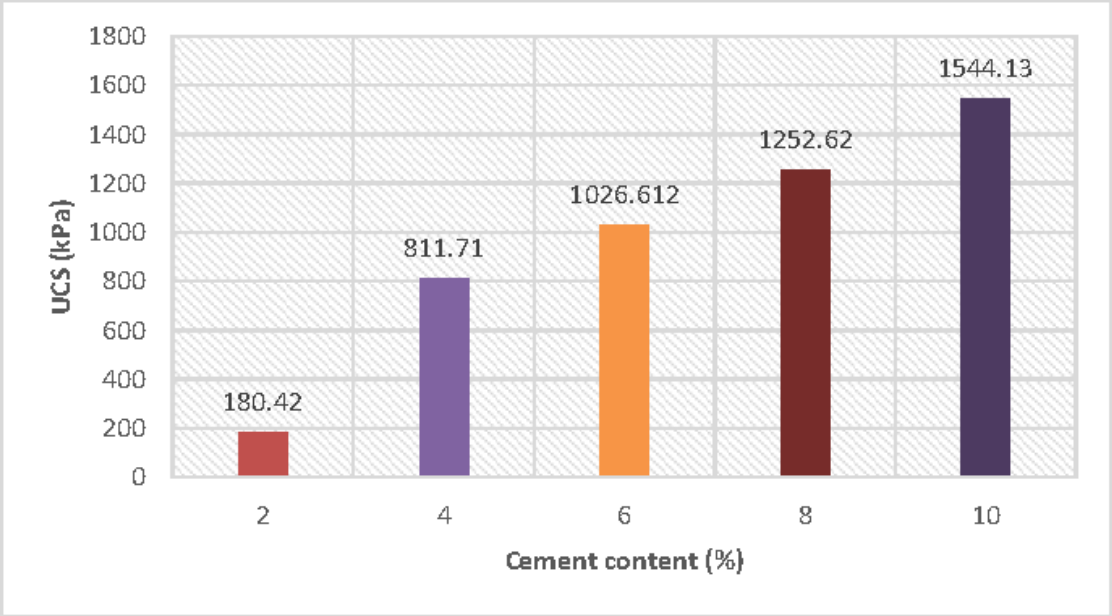

Fig. 8. UCS results of Group A vs cement content.

3.2 Effect of Glass Fiber Content

Fig. 9 shows, as in the previous section, how the amount of glass fiber affects the development of the UCS for compacted cement Bangkok sand. Glass fiber content was altered between 0.5-2.5% by fixing the cement content at 8%, fiber length at 6 mm, glass powder content at 20%, and curing duration at 28 days. The UCS was found to be at its peak at 1.0%, which is in good accordance with ACI 230.1R-09 [16]. Stabilization may be achieved with a soil-cement strength of roughly 1,200 kPa. Therefore, using 1.0% glass fiber content was advised.

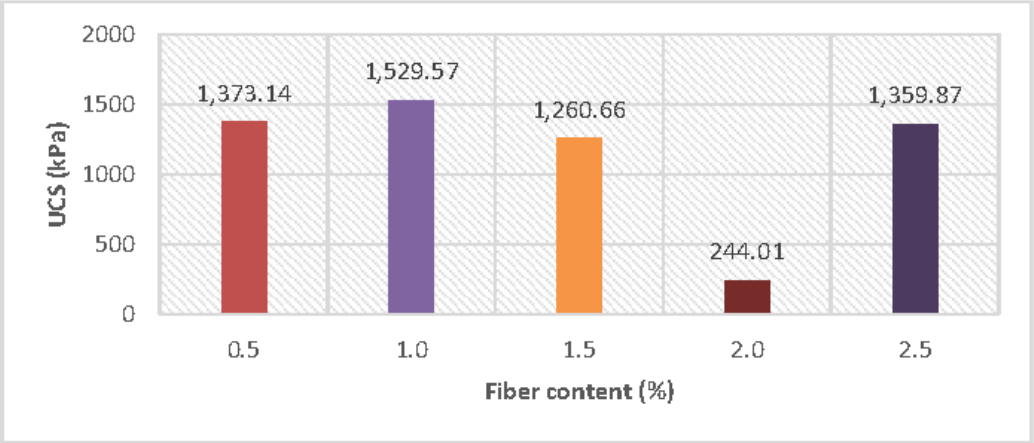

Fig. 9. UCS results of Group B vs glass fiber content.

3.3 Effect of Glass Fiber Length

The influence of glass fiber length on the development of UCS for compacted cement Bangkok sand is shown in Fig. 10. Glass fiber length was changed between 3, 6 and 12 mm by fixing the cement amount at 8%, glass fiber content at 1.0%, glass powder content at 20%, and curing period at 28 days. The highest UCS was reported to occur at a glass fiber length of 12 mm. ACI 230.1R-09 [16] states that stabilization requires a soil-cement strength of roughly 1,200 kPa. As a result, it was advised to employ glass fiber lengths of 6 to 12 mm.

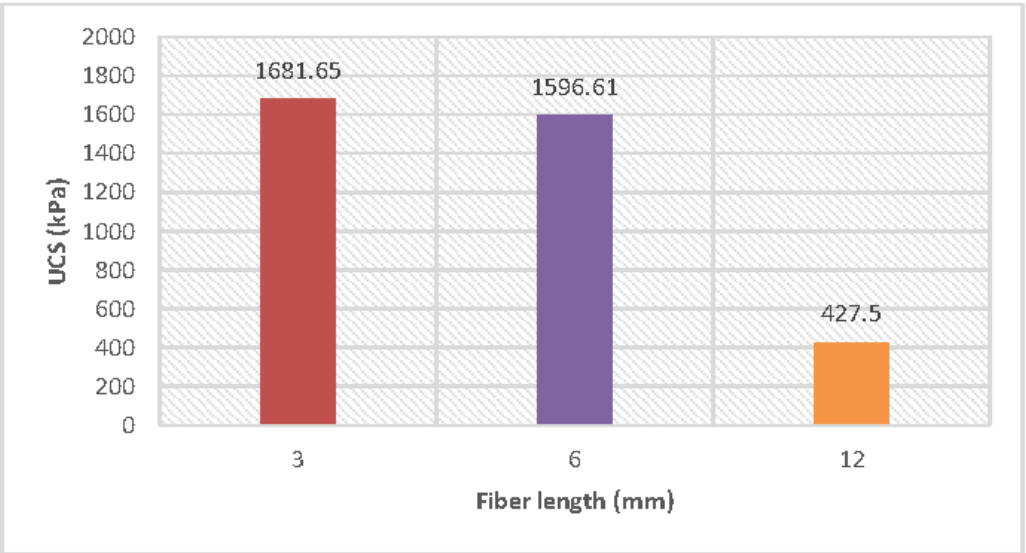

Fig. 10. UCS results of Group C vs glass fiber length.

3.4 Effect of Glass Powder Content

The effect of glass powder content with ageing effect is shown in Fig. 11. By fixing the cement content at 8%, glass fiber content of 1.0%, glass fiber length of 6 mm and curing time at 7, 14 and 28 days, the glass powder content was changed between 10, 20, 30, 40 and 50%. The maximum UCS data were found at 10% replacement of glass powder which was logic due to highest amount of cement in the mixture. According to the ACI 230.1R-09 [16], the soil-cement strength of about 1200 kPa is enough for ground stabilization. Hence, it was recommended to use 20% of glass powder. The UCS results have generally a tendency to decrease with increasing the glass powder content. However, the ageing effect reported that the UCS data increase with increasing the curing time.

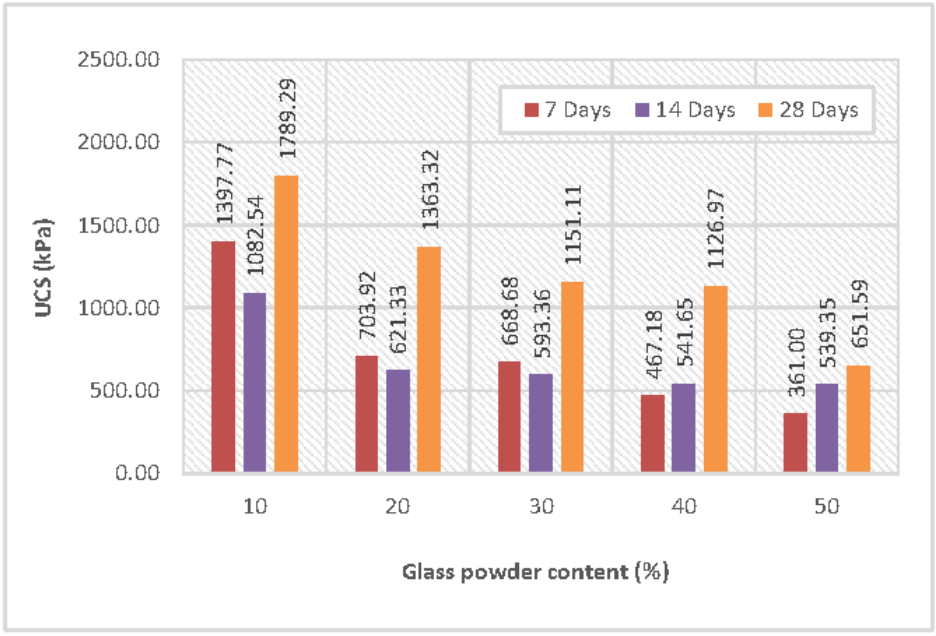

Fig. 11. UCS results of Group D vs glass powder Content and ageing.

3.5 Effect of Ageing

The impact of ageing on the percentage of glass fiber was examined and depicted in Fig. 12. Glass fiber content was varied between 0.5, 1, 1.5, 2, and 2.5% by fixing the cement content at 8%, glass fiber length of 6 mm, glass powder content of 20%, and curing times at 7, 14, and 28 days. The maximum UCS statistics were discovered once more at 1% of glass fiber content, which corresponds with Section 3.2's findings. ACI 230.1R-09 [16] states that a soil-cement strength of approximately 1200 kPa is sufficient for soil-cement stabilization. It was then discovered that 1% glass fiber content was the optimum amount. However, the ageing effect reported that the UCS data increase with increasing the curing time.

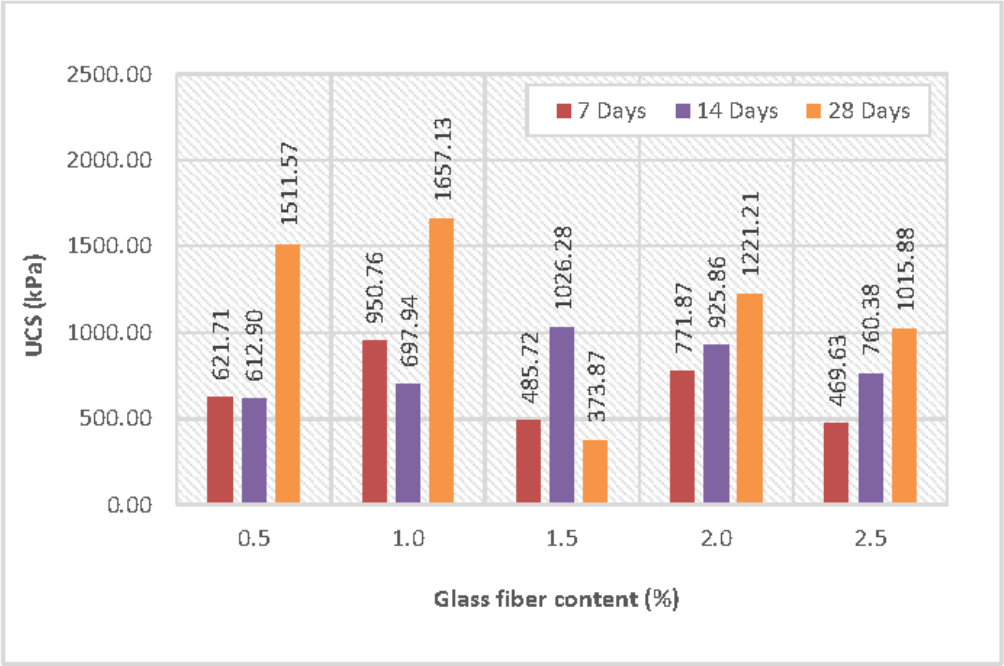

Fig. 12. UCS results of Group D vs glass fiber content and ageing.

3.6 Microscopy Image Analysis

Microscopic images can be used to investigate the glass fiber-matrix interface interaction mechanism, as shown in Fig. 13. The composition of the glass fiber surface, the combination of glass powder and the cement-sand matrix, the hydration products, and the different interfaces within the composite material are all revealed by the microstructure. Enhancing the bond strength between the glass powder and the cement-sand matrix as well as the glass fiber itself is largely dependent on the inclusion of a modest amount of glass fiber content. The peculiar crimped shape of the glass fiber and the existence of hydration products are the main causes of this increased binding strength. The hydration products form a strong bond with the glass fiber surface, effectively anchoring the fiber within the matrix. Additionally, the crimped shape of the glass fiber provides mechanical interlocking within the matrix, further improving the overall strength and durability of the composite material.

As a result, the inclusion of glass fibers leads to a significant enhancement in the compressive strength behavior of the composite material, making it a valuable addition for applications requiring high strength and durability.

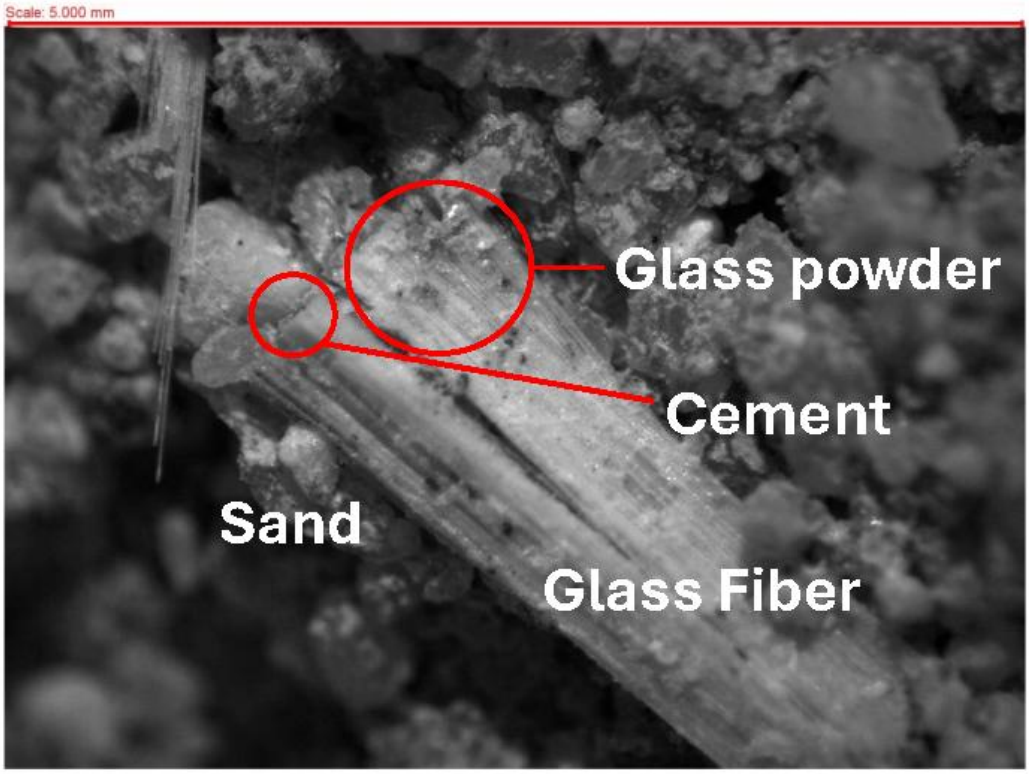

Fig. 13. Microscopic image of the glass fiber surface on reinforced stabilized sand with cement and glass powder.

4 Conclusions

This research was tested on compacted cement sand samples, varying glass fiber content at 0.5%, 1.0%, 1.5%, 2.0% and 2.5% by volume and varying glass fiber lengths of 3, 6 and 12 mm. The OPC content were used at 2%, 4%, 6%, 8% and 10% by weight. The glass powder was added at 10%, 20%, 30% 40% and 50% replacement of cement. Subsequently, the compacted cement samples were cured for 7, 14 and 28days to investigate the aging effect of the green construction materials. The investigation revealed the following:

- It was discovered because the unconfined compressive strength (UCS) increases with the amount of OPC cement used. Nonetheless, the ACI specifies a minimum strength of roughly 1200 kPa for the soil-cement in ground stabilization. For the purpose of creating the new compacted cement sand, it was advised to employ 8% cement content.

- It was observed that increasing the fiber content increased the UCS strength trend. However, the study discovered that it was in excellent accord with the ACI 230.1R-09

and reached its peak at 1.0%. Since the soft material is added to the soil-cement matrix, increasing the fiber content does not result in an increase in strength. The use of 1.0% glass fiber content was proposed.

- Due to the fact of their greater bonding on the surface, it was discovered that UCS strength rose as fiber length grew. The glass fiber length of 12 mm was showed the highest UCS strength. As a result, using glass fiber lengths between 6 and 12 mm was advised in order to comply with ACI 230.1R-09.

- The UCS strength tends to decrease as the glass powder content increases when glass power is substituted into the cement mixing process. Due to the fact that the hydration reaction involves a less quantity of cement. UCS strength is primarily influenced by the curing time. The effect on aging shows that UCS strength increases with longer curing times. Since the UCS strength satisfies ACI 230.1R-09 requirements, it was advised to apply 20% of glass powder after 28 days.

- Microscopic image confirmed hydration products form a strong bond with the glass fiber surface, effectively fastening the glass fiber within the cement sand matrix and improving the overall UCS strength and durability of this new green eco-friendly material.

Acknowledgement

This research was funded by National Science, Research and Innovation Fund (NSRF), and King Mongkut' s University of Technology North Bangkok with Contract no. KMUTNB-FF-66-33.

Conflicts of Interest

The authors declare no conflict of interest.

References

1. Castro-Alonso, M. J., Montañez-Hernandez, L. E., Sanchez-Muñoz, M. A., Macias Franco, M. R., Narayanasamy, R. and Balagurusamy, N.: Microbially induced calcium carbonate precipitation (MICP) and its potential in bioconcrete: microbiological and molecular concepts. Frontiers in Materials 6, 1-15 (2019).
2. Suyambulingam, I., Rangappa S. M. and Siengchin, S.: Advanced Materials and Technologies for Engineering Applications. Applied Science and Engineering Progress 16(3), 1-5, (2023).

3. Palaniappan, S. K., Singh, M. K., Rangappa S. M. and Siengchin, S.: Eco-friendly Biocomposites: A Step Towards Achieving Sustainable Development Goals. Compositesm17(4), 1-3 (2023).
4. Phiri, R., Rangappa, S. M., Siengchin, S. and Marinkovic, D.:Agro-waste natural fiber sample preparation techniques for bio-composites development: methodological insights. Facta Universitatis, Series: Mechanical Engineering 21(4), 631-656 (2023).
5. Petcherdchoo, A., Pochalard, S., Piriyakul, K. :Use of bender element tests for determining shear modulus of fly-ash and cement admixed Bangkok clay with considering unconfined compressive strength. Case Studies in Construction Materials 18, 1-13 (2023).
6. Pochalard, S., Wungsumpow, C. and Piriyakul, K.,: Strength development in cement and fly ash admixed Bangkok clay with considering shear wave velocity. Proceeding of the 21st Southeast Asian Geotechnical Conference and 4th AGSSEA Conference (SEAGC-AGSSEA 2023), pp.1-6, Bangkok (2023).
7. Eurostat Homepage, https://ec.europa.eu/eurostat/statistics-explained/index.php/Municipal_waste_statistics#Municipal_waste_ generation, last accessed 2023/12/10.
8. Iamchaturapatr, J., Piriyakul, K., Ketklin, T., Di Emidio, G. and Petcherdchoo, A.: Sandy soil improvement using MICP-based urease enzymatic acceleration method monitored by real-time system. Advances in Materials Science and Engineering, 1-12 (2021).
9. Iamchaturapatr, J., Piriyakul, K. and Petcherdchoo, A.: Characteristics of sandy soil treated using EICP-based urease enzymatic acceleration method and natural hemp fibers. Case Studies in Construction Materials 16, 1-13 (2022).
10. Iamchaturapatr, J., Piriyakul, K. and Petcherdchoo, A.: Use of a piezoelectric bender element for the determination of initial and final setting times of metakaolin geopolymer pastes, with applications to laterite soils. Sensors 22(3), 1-17 (2022).
11. Siengchin, S.: A review on lightweight materials for defence applications: A present and future developments. Defence Technology, 1-17 (2023).
12. Kumar, D., Rex, L. K., Sethuraman, V. S., Gokulnath, V.and Saravanan, B.: High performance glass fiber reinforced concrete. Materials Today: Proceedings 33, 784-788 (2020).
13. Wungsumpow, C., Pochalard, S., Killian B. and Piriyakul, K.:Flexural Strength Properties of Compacted Cement - Fly Ash from Municipal Solid Waste - Polypropylene Fiber Sand. Proceeding of the 21st Southeast Asian Geotechnical Conference and 4th AGSSEA Conference (SEAGC-AGSSEA 2023), pp.1-6, Bangkok (2023).
14. ASTM D1633–17, Standard Test Methods for Compressive Strength of Molded Soil-Cement Cylinders.
15. ASTM D698-12E1, Standard Test Methods for Laboratory Compaction Characteristics of Soil Using Standard Effort.
16. ACI 230.1R- 09, American Concrete Institute, Report on Soil Cement.

VITA

Name	Mr.Chalermpon Wungsumpow
Thesis Title	Industrial and Biological Wastes Compacted Cement Structures for Green Construction
Major Field	Construction Engineering Technology

Biography

My name is Chalermpon Wungsumpow, you can call me "Dream". I am a 32-year-old. In my free time, I enjoy hiking, restoring cars as a hobby, and exploring the forest by walking. I am a researcher at King Mongkut's University of Technology North Bangkok (KMUTNB), and research for KMUTNB Techno Park in terms of conservative energy and environmental technology. I would to talk about my educational background and work experience. I graduated with a bachelor's degree from Kasetsart University, Faculty of Science, a Bachelor of Science (BSc Earth Science), and a Master's degree from King Mongkut's University of Technology Thonburi, The Joint Graduate School of Energy and Environment, Master of Philosophy (M.Phil) Environmental Technology. I have been an assistant researcher since 2017 and specialize in geophysics in fieldwork by using Electrical resistivity tomography (ERT) in landfill mining. Worked as assistant of researchers such as consultants or senior projects. My duty is to support and explore with them to do the geophysics survey and landfill mining by using ERT and Waste-to-energy (WtE) technology for example, a job at Tham Luang–Khun Nam Nang Non Forest Park in Pong Pha Sub-District, Mae Sai District, Chiang Rai Province, Thailand to applied the resistivity survey and geology survey on Tham Luang cave to rescue 12 boys and coach soccer team. Before becoming a researcher, I worked for an applied job associated with geophysical and environmental technology (Waste-to-energy): geophysics techniques, technical survey, mineral exploration, and landfill mining with reclamation. I am interested in the environmental field, and I can perform equipment preparation (i.e. cable design and excavation planning), operation, survey line design, and data acquisition, as well as data processing. In addition, I have published several academic papers, including research in the fields of geophysical exploration, municipal solid waste management, alternative energy assessment, and green construction materials, which have been presented in both national and international journals and conferences. The published works include the following:

1. Enhancing landfill mining assessments: a dual-method approach using electrical resistivity and UAV photogrammetry at Buriram landfill – Published in

[Journal of Material Cycles and Waste Management, 2025]

2. Improving Mechanical Behavior of Compacted Cement Sand Mixed with Glass Powder from Glass Industry and Glass Fiber for Green Construction Materials – Published in [International Conference on Eco-friendly Fibers and Polymeric Materials, 2024]
3. A Geophysical Approach to Assessing Landfill Mining Feasibility: The Buriram Landfill Experience – Published in [Proceedings of the Annual Conference of Japan Society of Material Cycles and Waste Management, 2024]
4. Flexural Strength Properties of Compacted Cement - Fly Ash from Municipal Solid Waste - Polypropylene Fiber Sand – Published in [The 21st Southeast Asian Geotechnical Conference and 4th AGSSEA Conference (SEAGC-AGSSEA 2023), 2023]
5. Improving Mechanical Properties of Compacted Cement Sand by using 4-Strand Braided Polyethylene Fiber – Published in [2nd International Conference on Sustainable Technologies, Energies and Materials, 2025]
6. Effect of Glass Fiber and Municipal Solid Waste Incineration on Bending Stress of Compacted Cement Sand – Published in [The Journal of Industrial Technology, 2024]